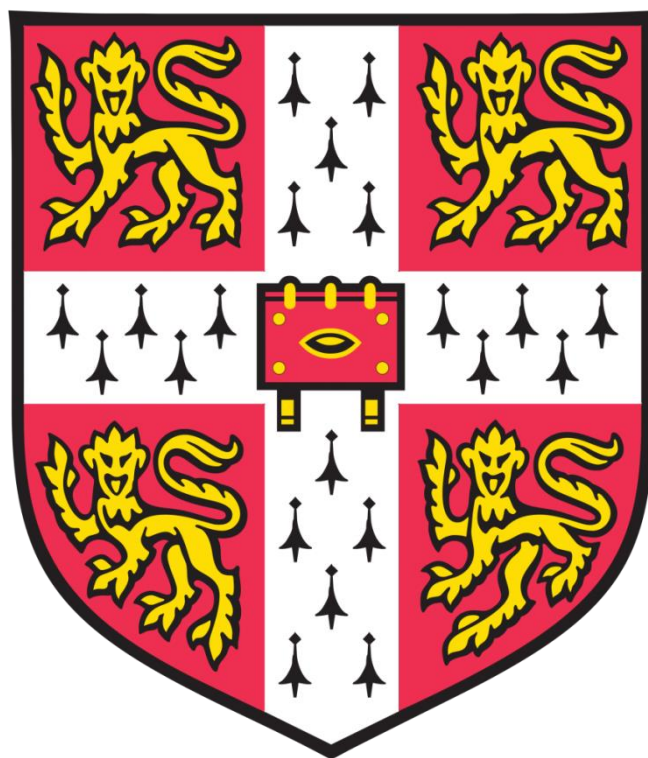


Coordination Cages for the Separation and Transportation of Molecular Cargo



Angela Beth Grommet

Pembroke College

University of Cambridge

December 2017

This dissertation is submitted for the degree of Doctor of Philosophy.

Declaration

This dissertation is an account of research carried out by the author at the Department of Chemistry, University of Cambridge between October 2013 and December 2017. Unless otherwise stated, either directly or by reference, the work described herein is the author's own. Results obtained through collaboration with other members of the Nitschke group are referenced directly in the text. Many of the results presented here have been published in peer-reviewed journals; original publications are referenced in the main text, and a list of publications is included. This work has not been submitted either in part or in whole for a degree or any other qualification at another university; the text does not exceed 60,000 words in length.

Angela B. Grommet

December 2017

Acknowledgments

First, I thank Prof Jonathan Nitschke for the opportunity to “lay a brick in the castle of knowledge” while conducting research in his group, thereby allowing me to fulfil my dream of studying supramolecular chemistry at the University of Cambridge. Thanks also for your unfailing patience and support as I struggled with post-concussion syndrome and tendonitis for two years.

I would also like to thank Dr Jeanne Bolliger for helping me find my feet as a new PhD student. Thank you, Jeanne, for seeing me when I was afraid to reach out for help – what would I have done if you hadn’t taken me under your dragon’s wing? Thanks also to my other collaborators and friends the Nitschke group – Lillian, Anna, Cally, Jesus, Edmundo, Jack, and Felix. Anna, thanks for Christmas dinners and waffles in the Market Square. Lillian, for countless giggles, mead, and candy bars. Cally, thanks for marrying a man who makes us tea while we work together at your kitchen table. And Felix, thanks for good times around the world at conferences. Thanks also to my students Ophelie and Zhichen for teaching *me* so much about chemistry. And, finally, thanks to all – Cally, Edmundo, Julia, and Felix – who helped me edit numerous drafts of my thesis and fellowship proposals.

Thanks to the Cambridge University Rambling Club, especially Pete, Savi, and Pierre, for keeping me grounded throughout my PhD. I will always treasure the 1000s of miles we blazed together through the British countryside. Thanks for being my adopted family here in Cambridge.

I thank my brothers Alex and John for being the first people with whom I began to explore the world. Thanks for good memories of the Water Place, of tree forts in the woods, of homemade bows and arrows, and of catching all manner of critters to raise in terrariums on the kitchen counter. Thanks to Megan and Grandma for being the very best cheerleaders. And finally, I thank my mother for fostering my love of learning. Thank you for nine years of homeschooling, for allowing me to explore my own interests, and for teaching me to value “the reason why”. Thanks for those countless times when you played hooky with us – when a walk in the backyard turned into a day of shopping for plants and working in the garden.

Summary

Name: Angela Beth Grommet

Title: Coordination Cages for the Separation and Transportation of Molecular Cargo

The first chapter of this thesis introduces the fundamental concepts governing the design and synthesis of supramolecular complexes. By illustrating the synthesis of several coordination cages reported in the literature, the principles underlying the construction of coordination cages by subcomponent self-assembly are elucidated. Ionic liquids are then proposed as solvents for cage systems; general methods for the preparation and synthesis of these solvents are described.

The second chapter explores the use of ionic liquids as solvents for existing coordination cages. Potential methods of characterising these cages in ionic liquids are discussed; cages are demonstrated to be stable and capable of encapsulating guests in these ionic environments; and systems in which cages have good solubility in ionic liquids are designed. Building upon these observations, a triphasic sorting system is presented such that each of three different host-guest complexes are soluble in only one of three immiscible liquid phases.

In contrast to the static triphasic system described in the second chapter, the third chapter explores directed phase transfer of coordination cages and their cargos from water, across a phase interface, and into an ionic liquid phase. The host-guest complex can then be recycled from the ionic liquid layer back into water after several additional steps. Furthermore, phase transfer of cationic cages is used to separate a mixture of cationic and anionic host-guest complexes.

In the fourth chapter, fully reversible phase transfer of coordination cages is developed. Using anion exchange to modulate the solubility of three different cationic cages, reversible transport between water and ethyl acetate is demonstrated. Sequential phase transfer can also be achieved such that, from a mixture of cubic (+16) and tetrahedral (+8) cages, the cubic cage transfers from water to ethyl acetate before the tetrahedral cage. This process is fully reversible; upon the addition of a hydrophilic anion, the tetrahedral cage returns from ethyl acetate to water before the cubic cage.

Publications

1. Aakeröy, C. B.; Grommet, A. B.; Desper, J. “Co-Crystal Screening of Diclofenac”, *Pharmaceutics* **2011**, *3*, 601–614.
2. Grommet, A. B.; Bolliger, J. L.; Browne, C.; Nitschke, J. R. “A Triphasic Sorting System: Coordination Cages in Ionic Liquids”, *Angew. Chem., Int. Ed.* **2015**, *54*, 15100-15104. Corresponds to the results presented in Chapter 2.
3. Grommet, A. B.; Nitschke, J. R. “Directed Phase Transfer of an Fe^{II}₄L₄ Cage and Encapsulated Cargo”, *J. Am. Chem. Soc.* **2017**, *139*, 2176-2179. Corresponds to the results presented in Chapter 3.
4. McConnell, A. J.; Aitchison, C. M.; Grommet, A. B.; Nitschke, J. R. “Subcomponent Exchange Transforms a Fe^{II}₄L₄ Cage from High- to Low-Spin, Switching Guest Release in a Two-Cage System”, *J. Am. Chem. Soc.* **2017**, *139*, 6294-6297.
5. Grommet, A. B.; Mosquera, J.; Guzman-Percastegui, E.; Bolliger, J. L.; Nitschke, J. R. “Reversible Transport of Coordination Cages by Anion Exchange”, *manuscript in preparation*. Corresponds to the results presented in Chapter 4.
6. McConnell, A. J.; Haynes, C. J. E.; Grommet, A. B.; Guilleme, J.; Aitchison, C. M.; Mikutis, S.; Nitschke, J. R. “Orthogonal Stimuli Trigger Self-Assembly and Phase Transfer of Fe^{II}₄L₄ Cages”, *manuscript in preparation*.

Abbreviations

CH ₃ CN	Acetonitrile
CD ₃ CN	Deuterated acetonitrile
H ₂ O	Water
D ₂ O	Deuterated water
CH ₂ Cl ₂	Dichloromethane
CD ₂ Cl ₂	Deuterated dichloromethane
CHCl ₃	Chloroform
CDCl ₃	Deuterated chloroform
CH ₃ OH	Methanol
CD ₃ OD	Deuterated methanol
(CD ₃) ₂ CO or acetone-d ₆	Deuterated acetone
EtOAc	Ethyl acetate
Et ₂ O	Diethyl ether
TFA	Trifluoroacetic acid
DSS	Dextran sulfate sodium salt
[A]	Anion
NH ₄ ⁺ or [NH ₄]	Ammonium
ⁿ Bu ₄ N ⁺ or [ⁿ Bu ₄ N]	Tetrabutylammonium
Me ₄ N ⁺ or [Me ₄ N]	Tetramethylammonium
NTf ₂ ⁻ or [NTf ₂]	Bis(trifluoromethanesulfonyl)imide (triflimide)
SO ₄ ²⁻ or [SO ₄]	Sulfate
BF ₄ ⁻ or [BF ₄]	Tetrafluoroborate
OTf ⁻ or [OTf]	Trifluoromethanesulfonate (triflate)
PF ₆ ⁻ or [PF ₆]	Hexafluorophosphate
EtOSO ₃ ⁻ or [EtOSO ₃]	Ethylsulfate
P _{6,6,6,14} ⁻ or [P _{6,6,6,14}]	Trihexyltetradecylphosphonium
BArF ₅ ⁻ or [BArF ₅]	Tetrakis(pentafluorophenyl)borate
BAr(CF ₃) ₂ ⁻ or [BAr(CF ₃) ₂]	Tetrakis[3,5-bis(trifluoromethyl)phenyl]borate
NMR	Nuclear Magnetic Resonance
COSY	Correlated Spectroscopy
DOSY	Diffusion Ordered Spectroscopy

<i>J</i>	Coupling constant
ppm	Parts per million
δ_{H}	^1H chemical shifts
δ_{C}	^{13}C chemical shifts
δ_{F}	^{19}F chemical shifts
s	Singlet
bs	Broad singlet
d	Doublet
dd	Doublet of doublets
t	Triplet
q	Quartet
m	Multiplet
bm	Broad multiplet
equiv	Equivalents
Hz	Hertz
ns	Number of scans
K	Kelvin
nm	Nanometre
mm	Millimetre
μL	Microlitre
μmol	Micromole
mL	Millilitre
mmol	Millimole
μM	Micromolar
mM	Millimolar
UV-Vis	Ultraviolet-Visible
Abs	Absorbance
λ	Wavelength
ESI-MS	Electrospray Ionisation Mass Spectrometry
EA	Elemental Analysis
[emim]	1-Ethyl-3-methylimidazolium
[hmim]	1-Hexyl-3-methylimidazolium
K_{a}	Affinity constant
1-FA	1-Fluoroadamantane

min

Minute

hr

Hour

Table of Contents

Declaration	i
Acknowledgments	ii
Abstract	iii
Publications	iv
Abbreviations	v
Chapter 1: Introduction	1
1.1 Supramolecular Chemistry and Molecular Flasks	1
1.2 Metal-Organic Supramolecular Architectures	2
1.3 Subcomponent Self-Assembly for the Synthesis of Coordination Cages	6
1.4 Size-Selective Guest Encapsulation in Molecular Flasks	9
1.5 The Role of Cage Counterions	16
1.6 Ionic Liquids	19
1.7 Aims	21
1.8 References	23
Chapter 2: A Triphasic Sorting System: Coordination Cages in Ionic Liquids	27
2.1 Introduction	27
2.2 Results and Discussion.....	29
2.2.1 Characterisation of coordination cages dissolved in neat ionic liquids.....	29
2.2.2 Comparison of guest binding in ionic liquids vs. organic solvents	32
2.2.3 Competitive guest binding within coordination cages in an ionic liquid	36
<i>Calculation of binding constants</i>	39
<i>A brief discussion on the kinetics and thermodynamics of this system</i>	41
2.2.4 Designing a triphasic sorting system	41
2.2.5 Characterisation of a triphasic sorting system	45
2.3 Conclusions	50
2.4 Experimental	51
2.4.1 General.....	51
2.4.2 Synthesis	52
<i>N2,N4,N6-Trimethyl-N2,N4,N6-tris(4-nitrophenyl)-1,3,5-triazine-2,4,6-triamine</i>	52
<i>N2,N4,N6-Tris(4-aminophenyl)-N2,N4,N6-trimethyl-1,3,5-triazine-2,4,6-triamine</i>	54
<i>Cage 2[OTf]</i>	55

<i>Cage [Me₄N]3</i>	56
<i>Cage 4[NTf₂]</i>	58
<i>Cage 5[NTf₂]</i>	58
<i>Trihexyltetradecylphosphonium triflimide ([P_{6,6,6,14}][NTf₂])</i>	61
<i>1-Ethyl-3-methylimidazolium triflimide ([emim][NTf₂])</i>	62
2.5 References	64
Chapter 3: Phase Transfer of an Fe^{II}L₄ Cage and Encapsulated Cargo	67
3.1 Introduction	67
3.2 Results and Discussion.....	68
3.2.1 Directed phase transfer of 1-fluoroadamantane \subset 1	68
3.2.2 Guest uptake kinetics of 1-fluoroadamantane \subset 1	70
<i>Control experiments in D₂O</i>	70
<i>Control experiments in [hmim][BF₄]</i>	72
<i>Control experiments in CD₃CN</i>	72
<i>Summary of control experiments</i>	75
3.2.3 Characterisation of 1-fluoroadamantane \subset 1 transport cycle	75
3.2.4 Tuning the properties of ionic liquids and coordination cages.....	86
3.2.5 Separation of 1-fluoroadamantane \subset 2 from 1-fluorobenzene \subset 3	88
3.3 Overview: Solubility of Coordination Cages in Ionic Liquids	95
3.4 Conclusions	97
3.5 Experimental	98
3.5.1 General.....	98
3.5.2 Synthesis.....	98
<i>Cage 1[SO₄]</i>	99
<i>1-Fluoroadamantane \subset 1[SO₄]</i>	100
<i>Cage 1[BF₄]</i>	102
<i>1-Fluoroadamantane \subset 2[SO₄]</i>	104
<i>1-Fluorobenzene \subset [Me₄N]3</i>	107
<i>1-Hexyl-3-methylimidazolium tetrafluoroborate ([hmim][BF₄])</i>	108
<i>1-Ethyl-3-methylimidazolium triflimide ([emim][NTf₂])</i>	110
3.5 References	113
Chapter 4: Reversible Phase Transfer of Cages by Anion Exchange	117
4.1 Introduction	117

4.2 Results and Discussion.....	119
4.2.1 Stability of cages 1 , 2 , and 3 in water and EtOAc.....	119
4.2.2 Determination of the minimum anion equivalents necessary for cage transport ..	119
4.2.3 Slice-selective ¹ H NMR to monitor phase transfer cycles	123
<i>A brief explanation of slice-selective NMR.....</i>	<i>123</i>
<i>General procedure</i>	<i>125</i>
<i>Phase transfer cycles: 1[SO₄] ⇌ 1[BAr(CF₃)₂]</i>	<i>128</i>
<i>Phase transfer cycles: 1[SO₄] ⇌ 1[BArF₅].....</i>	<i>129</i>
<i>Phase transfer cycles: 2[SO₄] ⇌ 2[BAr(CF₃)₂]</i>	<i>130</i>
<i>Phase transfer cycles: 2[SO₄] ⇌ 2[BArF₅].....</i>	<i>131</i>
<i>Phase transfer cycles: 3[SO₄] ⇌ 3[BAr(CF₃)₂]</i>	<i>132</i>
<i>Phase transfer cycles: 3[SO₄] ⇌ 3[BArF₅].....</i>	<i>133</i>
4.2.4 Sequential phase transfer of coordination cages.....	134
<i>Sequential phase transfer of cages 1 and 2</i>	<i>136</i>
<i>Sequential phase transfer of cages 1 and 3</i>	<i>137</i>
<i>Sequential phase transfer of cages 2 and 3</i>	<i>138</i>
4.3 Conclusions and Future Work.....	139
4.4 Experimental	140
4.4.1 General.....	140
4.4.2 Self-assembly of cages 1 , 2 , and 3	140
<i>Cage 1[SO₄] in D₂O.....</i>	<i>141</i>
<i>Cage 1[SO₄] in D₂O, with EtOAc layer.....</i>	<i>143</i>
<i>Cage 1[BArF₅] in EtOAc.....</i>	<i>144</i>
<i>Cage 2[SO₄] in D₂O.....</i>	<i>145</i>
<i>Cage 2[SO₄] in D₂O, with EtOAc layer.....</i>	<i>147</i>
<i>Cage 2[BArF₅] in EtOAc.....</i>	<i>148</i>
<i>Cage 3[SO₄] in D₂O.....</i>	<i>149</i>
<i>Cage 3[SO₄] in D₂O, with EtOAc layer.....</i>	<i>151</i>
<i>Cage 3[BArF₅] in EtOAc.....</i>	<i>152</i>
4.4.3 UV-Vis calibration data.....	153
<i>General procedure</i>	<i>153</i>
<i>Calibration of cage 1 in water.....</i>	<i>154</i>
<i>Calibration of cage 1 in EtOAc</i>	<i>155</i>

<i>Calibration of cage 2 in water</i>	156
<i>Calibration of cage 2 in EtOAc</i>	157
<i>Calibration of cage 3 in water</i>	158
<i>Calibration of cage 3 in EtOAc</i>	159
4.4.4 Stability of cages 1 , 2 , and 3 by UV-Vis	160
<i>Stability of cage 1</i>	160
<i>Stability of cage 2</i>	163
<i>Stability of cage 3</i>	166
4.4.5 Anion titrations	169
<i>Phase transfer: 1[SO₄] ⇌ 1[BAr(CF₃)₂]</i>	169
<i>Phase transfer: 1[SO₄] ⇌ 1[BArF₅]</i>	172
<i>Phase transfer: 2[SO₄] ⇌ 2[BAr(CF₃)₂]</i>	175
<i>Phase transfer: 2[SO₄] ⇌ 2[BArF₅]</i>	178
<i>Phase transfer: 3[SO₄] ⇌ 3[BAr(CF₃)₂]</i>	181
<i>Phase transfer: 3[SO₄] ⇌ 3[BArF₅]</i>	184
4.5 References	188

Chapter 1: Introduction

This chapter introduces the field of supramolecular chemistry and the design of large architectures within this conceptual regime. Particular emphasis is given to the role of subcomponent self-assembly for the construction of coordination cages. Likewise, attention is drawn to the selection of counteranions as an important design feature for functional cage[anion] systems. Finally, ionic liquids are briefly introduced as prospective solvents for coordination cages, and the aims of the research described within this thesis are outlined.

1.1 Supramolecular Chemistry and Molecular Flasks

Supramolecular chemistry is the study of complex architectures built from individual subcomponents held together *via* intermolecular interactions.¹ These interactions, which include dispersion forces, π -interactions, halogen bonding, and hydrogen bonding (all of which range between 2 – 40 kJ/mol), and coordinative bonds (60 – 200 kJ/mol), are weaker than covalent bonds (250 – 500 kJ/mol) and, as such, are inherently labile.² The reversibility of supramolecular interactions allows molecular recognition to govern the self-assembly of dynamic structures. Generally, the synthesis of a supramolecular complex is therefore a process in which molecular components assemble, disassemble, and reassemble until they equilibrate to the most thermodynamically stable structure.¹ Nevertheless, there is also considerable interest in supramolecular architectures that are governed by their assembly pathways instead of the free energy of their final structure.³ Instead of forming under thermodynamic control, these structures are kinetically trapped⁴ far from equilibrium and exist in a metastable regime. As this field continues to mature and become more sophisticated, intermolecular interactions have been exploited to construct pieces of supramolecular machinery such as catenanes (two molecular rings linked together by a mechanical bond),^{5,6} rotaxanes (a molecular wheel on a molecular axle),^{7,8} and molecular motors.⁹ For the design and synthesis of molecular machines, the 2016 Nobel Prize in Chemistry was shared by Sauvage, Stoddart and Feringa.

Supramolecular machinery, as defined above, is abundant in nature: from weak intermolecular forces arise the double helix of DNA, the intricate folding of proteins, the interactions between enzymes and their substrates, and much more. In the laboratory, however, host-guest

complexes of inorganic cations with crown ethers,¹⁰ cryptands,¹¹ and spherands¹² were the earliest examples of supramolecular chemistry (Figure 1.1). Favourable electrostatic interactions between these electron-rich molecular hosts and inorganic cations lead to the formation of supramolecular complexes. An entropic gain associated with the desolvation of the host's binding site likewise drives the equilibrium toward formation of the host-guest complex.¹³

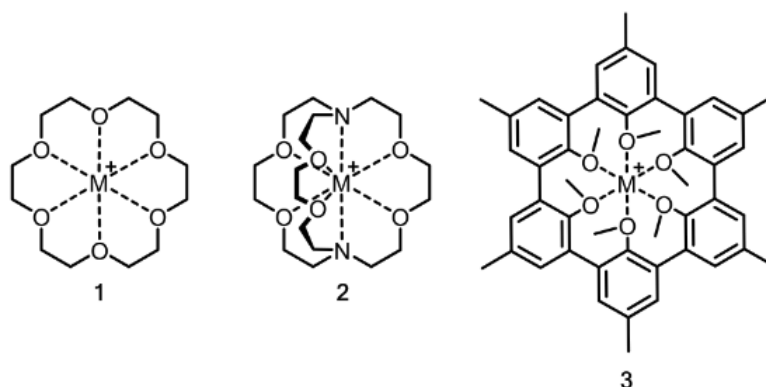


Figure 1.1 Supramolecular host-guest complexes: crown ether (1), cryptand (2), spherand (3).

This discovery, for which Lehn, Cram, and Pedersen shared the 1987 Nobel Prize in Chemistry, became the prelude to the development of other “molecular flasks”.¹⁴ Like macroscopic flasks, these structures act as containers and encapsulate ionic or neutral guest species. Unlike macroscopic flasks, however, molecular flasks are capable of influencing the chemistry of encapsulated guest molecules by stabilising reactive species and catalysing unfavourable reactions.¹⁵ As synthetic host molecules have become more sophisticated, a range of different molecular flasks have been developed. Cage-, cup-, or barrel-shaped organic container molecules include carcerands,¹⁶ cyclodextrins,¹⁷ calixarenes,¹⁸ pillararenes,¹⁹ and cucurbiturils.²⁰

1.2 Metal-Organic Supramolecular Architectures

While organic molecular flasks serve as excellent hosts for supramolecular host-guest complexes, they often require extensive synthesis. Alternatively, supramolecular molecular flasks can be designed such that coordination between ligands and transition metal cations causes the self-assembly of larger structures.²¹ As a feature of the geometry of the coordination

sphere around the metal cation, the directionality of binding between ligand and metal can be exploited to control the geometry of these supramolecular architectures. Likewise, the geometry of the ligand can serve as a second handle for controlling the outcome of self-assembly. The figure below illustrates how metals and ligands of varying geometries can be combined to produce a range of polyhedra, from simple trigonal bipyramidal and trigonal prismatic cages composed of two metal vertices and three organic ligands (M_2L_3) to more complex dodecahedral cages ($M_{20}L_{30}$).

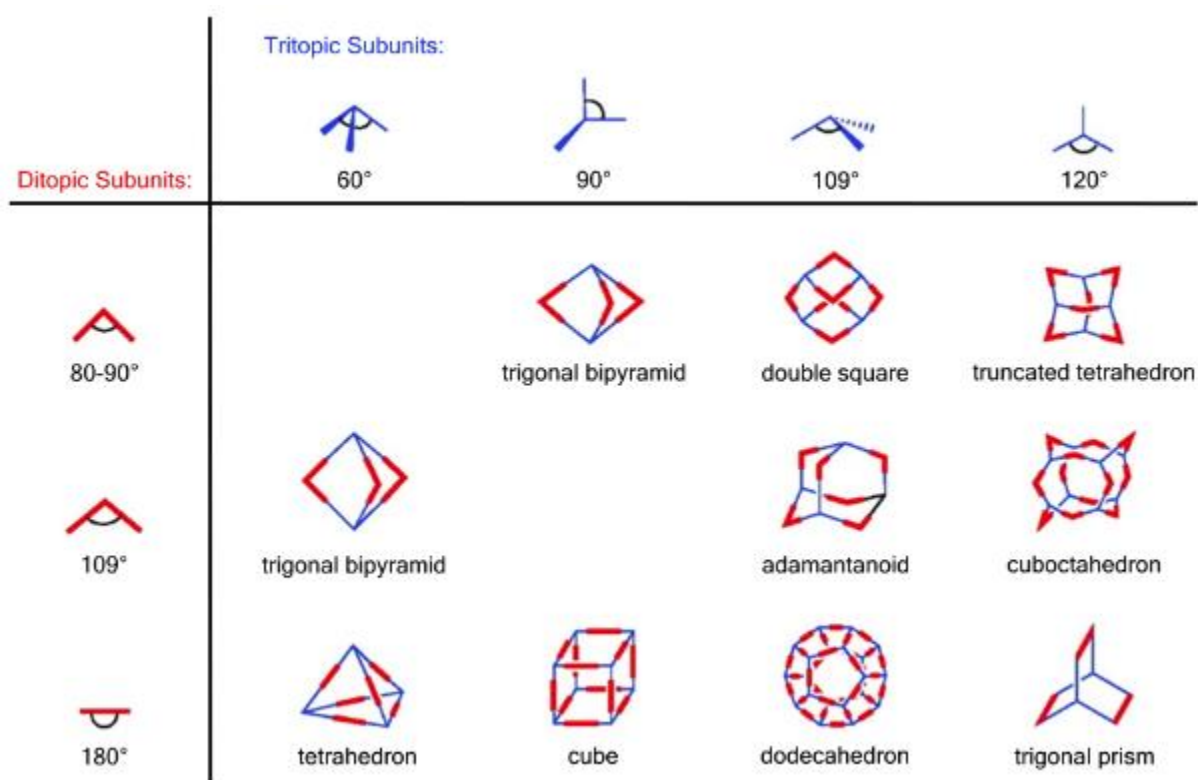


Figure 1.2 The design of supramolecular architectures through selection of ligand and transition metal geometries. Figure adapted from reference 2.

In the figure above, the tritopic and ditopic subunits can refer to either the metal or the ligand component. For example, Fujita has synthesised a truncated tetrahedron (Figure 1.3a) in which the square planar Pd^{II} vertices provide a ditopic subunit with an angle of approximately 90° .²² The threefold symmetric tripyridyl triazine ligand functions as the tritopic subunit, with a 120° angle between coordination sites. In this structure, bidentate ethylenediamine ligands occupy two of the four available coordination sites around Pd^{II} , effectively “capping” the corners by

forcing the planar, triazine-centred ligands to adopt 90° *cis* conformations around each metal centre.

Conversely, Raymond has synthesised a cage in which the octahedral coordination sphere of Fe^{III} functions as the tritopic subunit, enforcing a 60° angle between the edges of a tetrahedron (Figure 1.3b).²³ The twofold symmetric biscatechol ligand provides a linker between the metal vertices with an angle of 180° . Notably, both cages (truncated tetrahedron and tetrahedron) self-assemble, making their synthesis significantly more straightforward than molecular cages composed entirely of covalent bonds. Despite the dynamic nature of these cages, however, they have been shown to be highly stable and bind a range of different guests.^{23,24}

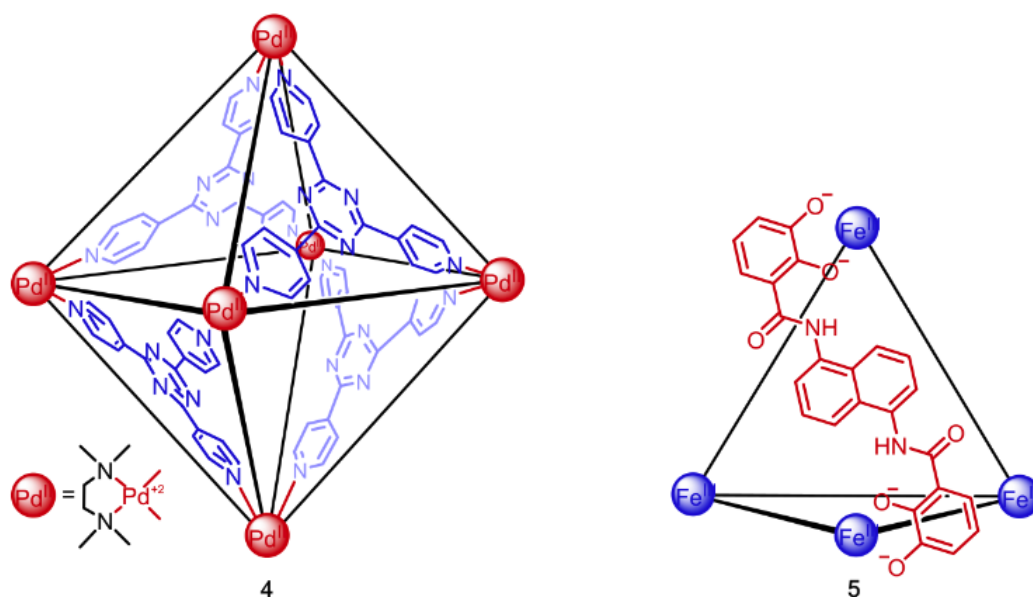


Figure 1.3 (Left) Self-assembled truncated tetrahedral coordination cage **4**. Figure adapted from reference 22. (Right) Self-assembled tetrahedral coordination cage **5**. Figure adapted from reference 23.

Components for the self-assembly of coordination cages are not limited to ditopic and tritopic units; incorporating fourfold and fivefold symmetric ligands into these structures enables the design of supramolecular architectures such as face-capped cubes and icosahedral cages, respectively.^{25,26} Furthermore, Fujita has demonstrated that finely tuning the angles of bent ditopic ligands can provide access to highly unusual polyhedra (Figure 1.4)²⁷ which, in some cases, result in exceptionally large coordination cages (Figure 1.5).²⁸

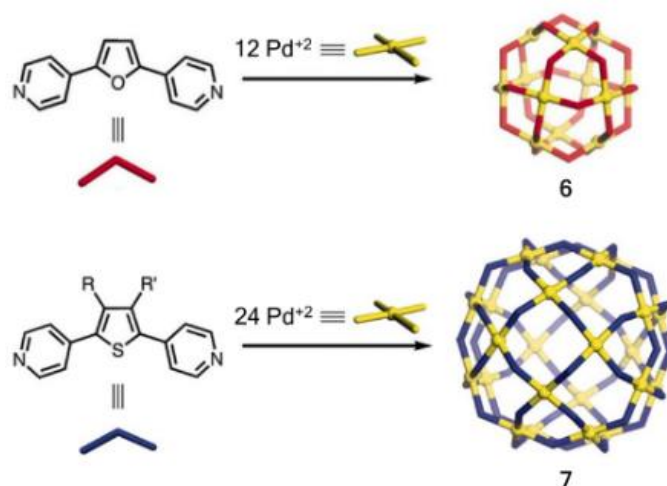


Figure 1.4 (Top) Synthesis of $M_{12}L_{24}$ coordination cage **6** from a bent furan ligand, 126.9° angle. (Bottom) Synthesis of $M_{24}L_{48}$ coordination cage **7** from a bent thiophene ligand, 149.3° angle. Figure from reference 27.

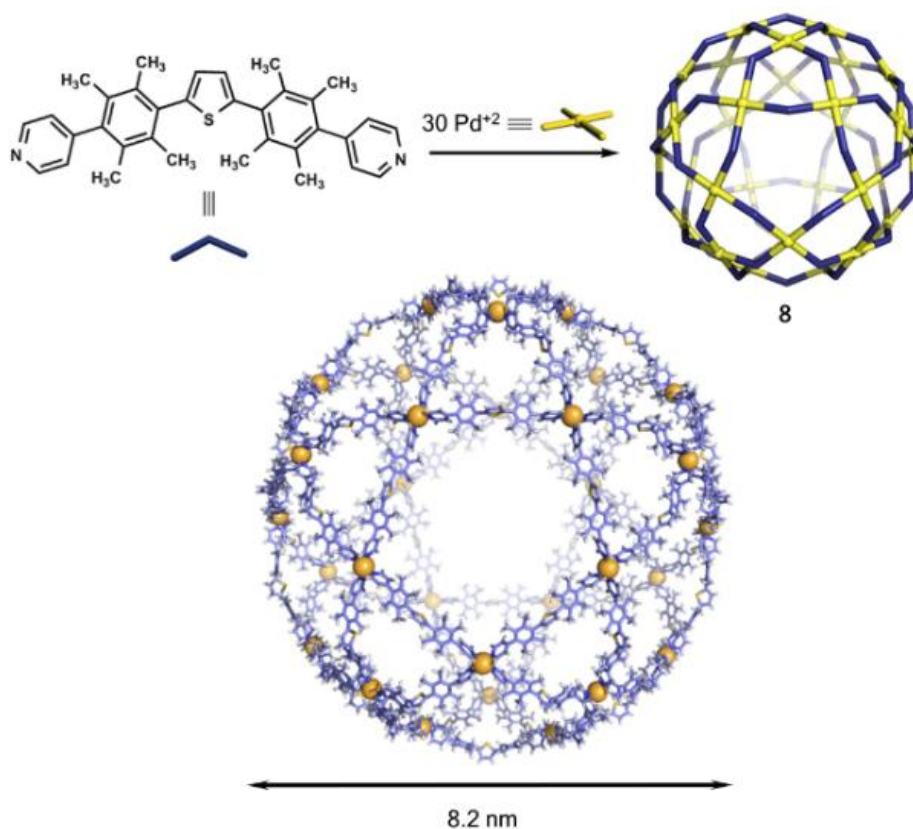


Figure 1.5 Synthesis of $M_{30}L_{60}$ icosidodecahedral coordination cage **8**. Figure adapted from reference 28.

In the structures above, Pd^{II} acts as a tetratopic component to bind four bent ditopic ligands in a square planar geometry. The bent furan ligand (Figure 1.4) has an angle of 126.9° between the two pyridine rings, resulting in cubo-octahedral $M_{12}L_{24}$ cage **6**. The bent thiophene ligand

(Figure 1.4) has an angle of 149.3° between the two pyridine rings, resulting in $M_{24}L_{48}$ rhombicuboctahedral cage **7**. Attempts by the Fujita group to gain access to structures larger than $M_{24}L_{48}$ by additional tuning of the ligand bend angle were limited, however, by the formation of kinetically trapped $M_{24}L_{48}$ or smaller coordination cages. Instead, tetramethylphenylene (Figure 1.5) was incorporated into the structure between the thiophene and pyridine groups to afford the bent ligand a small degree of flexibility, enabling the formation of $M_{30}L_{60}$ icosidodecahedral cage **8**, one of the largest reported coordination cages to date. The creation of this large supramolecular cage illustrates that, despite the dynamic nature of the intermolecular bonds of which this structure is composed, the thermodynamic product is stable enough to overcome the enormous entropic cost and electrostatic repulsion associated with assembling 90 components into a structure with an overall charge of +60.

1.3 Subcomponent Self-Assembly for the Synthesis of Coordination Cages

Conceptually related to supramolecular chemistry, dynamic covalent chemistry allows the reversible formation of covalent bonds.²⁹ While stronger than intermolecular interactions, dynamic covalent bonds are weaker than the corresponding covalent bonds. As such, dynamic covalent bonds can generally assemble, disassemble, and reassemble to form the most thermodynamically stable product. For example, imine bonds are formed from the condensation of aldehydes and primary amines and can readily hydrolyse under certain conditions.³⁰ Under conditions in which the reaction between amine and aldehyde is unfavourable, coordination with a transition metal cation can stabilise the imine bond. Specifically, the following figure demonstrates the mutual stabilisation of imine ligands and Cu^I cations in aqueous solution.³¹

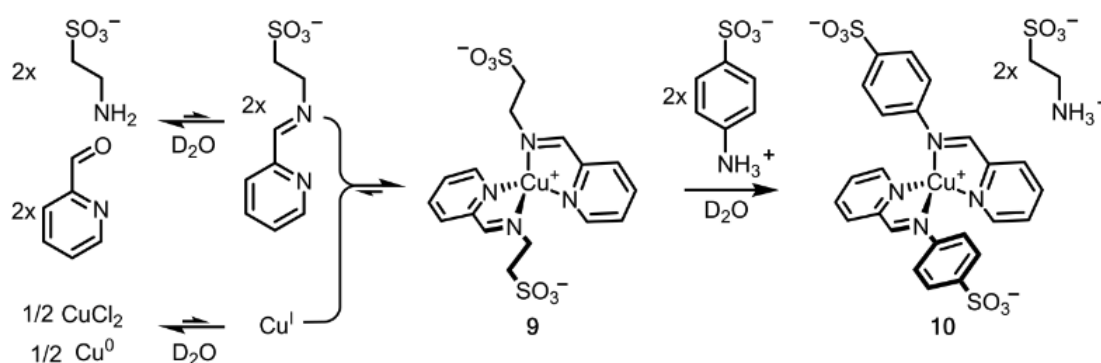


Figure 1.6 Mutual stabilisation of Cu^I cation and imine bonds. Figure adapted from reference 31.

While imine bonds are generally hydrolysed in the presence of water, and free aqueous Cu^{I} cations quickly convert to Cu^0 and Cu^{II} , each imine ligand is capable of donating two lone pairs of electrons to the Cu^{I} cation. The coordination between the imine ligand and Cu^{I} therefore drives the equilibrium to the right by rendering formation of the complex thermodynamically favourable. Furthermore, the dynamic nature of the resulting complex allows more strongly coordinating ligands to replace less energetically compatible ligands.

A synthetic strategy termed “subcomponent self-assembly” combines principles from both dynamic covalent chemistry and supramolecular chemistry. Figure 1.7, for instance, illustrates the subcomponent self-assembly of a tetrahedral coordination cage:³² aldehyde and amine subcomponents react to form an organic ligand (dynamic covalent chemistry) that coordinates to metal cations to self-assemble into a tetrahedral coordination cage (supramolecular chemistry).

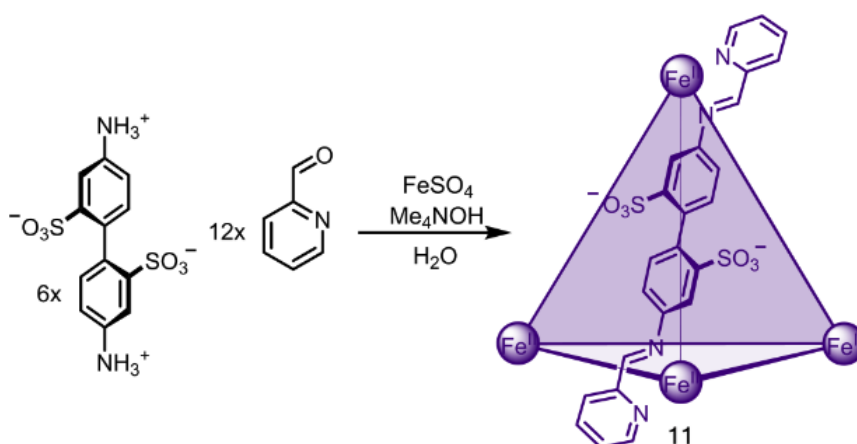


Figure 1.7 Self-assembly of sulfonated tetrahedral coordination cage **11**. Figure adapted from reference 32.

More specifically, tetramethyl ammonium hydroxide serves as a base to deprotonate and activate the diamine ligand, which in turn reacts to form imine bonds with two equivalents of 2-formylpyridine. The resulting *bis*-bidentate ligand coordinates to and is stabilised by the Fe^{II} corners. Cage **11** has an overall charge of -4 , with four equivalents of the counterion Me_4N^+ balancing the charge. Cage **11** is capable of binding a range of small neutral and anionic guest molecules. Notably, the cage has been shown to bind and stabilise white phosphorus (P_4),³³ a material that generally reacts violently with oxygen. A more thorough discussion of the host-guest chemistry of cage **11** can be found in Chapter 1.4.

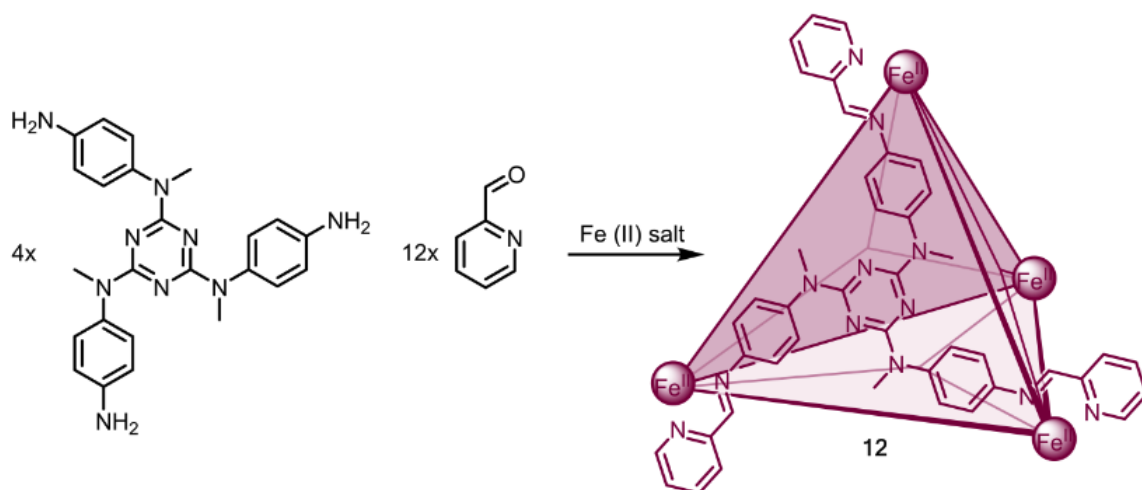


Figure 1.8 Self-assembly of face-capped tetrahedral coordination cage **12**. Figure adapted from reference 34.

Using subcomponent self-assembly as a design strategy allows a modular approach to the synthesis of coordination cages. For example, substituting a threefold symmetric triamine ligand for the linear diamine used in Figure 1.8 results in a larger face-capped tetrahedral coordination cage.³⁴ In Figure 1.8, the triazine-centred triamine ligand reacts to form imine bonds with three equivalents of 2-formylpyridine, forming a new *tris*-bidentate ligand that coordinates to and is stabilised by the Fe^{II} vertices. The resulting cationic cage has an overall charge of +8.

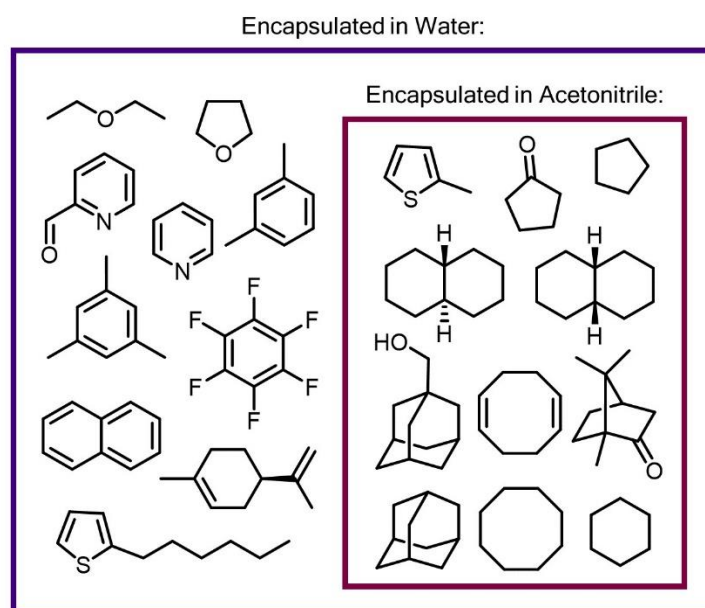


Figure 1.9 Guest molecules encapsulated by cage **12** in acetonitrile (inner box) or water (outer box). Figure adapted from reference 34.

The initial report of cationic cage **12** included the observation that this cage is soluble in either water or acetonitrile, depending on the identity of the counteranions.³⁴ When synthesised with iron (II) sulfate, cage **12**[SO₄] is soluble in water. Alternatively, synthesis with iron (II) triflate results in cage **12**[OTf], which is soluble in acetonitrile. The cage also demonstrates solvent-dependent guest-binding selectivity, binding aromatic and aliphatic guests in water while binding only aliphatic guests in acetonitrile (Figure 1.9). The binding constants associated with encapsulation of guests in cage **11** were universally higher in water than in acetonitrile. These patterns arise from the difference in magnitude of the solvophobic driving forces intrinsic to water or acetonitrile. In water, the hydrophobic effect drives the encapsulation of hydrophobic guests (*i.e.* both the aliphatic and the aromatic guests depicted in Figure 1.9) into the hydrophobic cavity of the cage. In acetonitrile, however, the aromatic guests from Figure 1.9 are well solubilised; there is thus no solvophobic driving force for guest encapsulation.

Further application of subcomponent self-assembly to the synthesis of coordination cages has produced supramolecular architectures with a range of geometries: from tetrahedrons^{35,36} and cubes^{37,38} to pentagonal prisms³⁹ and icosahedrons.⁴⁰ Likewise, these cages encompass an extensive range of cavity volumes and guest-binding properties. Within the body of this thesis, subcomponent self-assembly is crucial for the modular design of cages for increasingly sophisticated guest separation and transportation systems.

1.4 Size-Selective Guest Encapsulation in Molecular Flasks

Perhaps the most interesting applications of coordination cages and molecular flasks in general involve the ability of these structures to encapsulate molecular cargo. While the guest binding abilities of cages **11** and **12** have briefly been introduced above, this section will further address the subtleties associated with the size complementarity necessary between molecular flasks and their guest molecules. Intuitively, molecular flasks with larger internal volumes are able to encapsulate larger classes of guests than molecular flasks with relatively small cavities. As will be discussed below, however, small changes in the volume occupied by guest molecules can have drastic effects on their binding constants within a given capsule. Conversely, small changes in the volume of the cage cavity can have drastic effects on the size of guest molecules able to be encapsulated.

Many of the first investigations of guest binding in molecular flasks were performed by Rebek, who specialises in the synthesis of twofold symmetric organic ligands that self-assemble *via* hydrogen bonding into organic capsules.⁴¹ As seen in Figure 1.10, each ligand contains complementary hydrogen bonding donors and acceptors;⁴² two of these ligands thus curve around one another in a C-shape to form a structure analogous to a softball, in which two pieces are leather are stitched together.

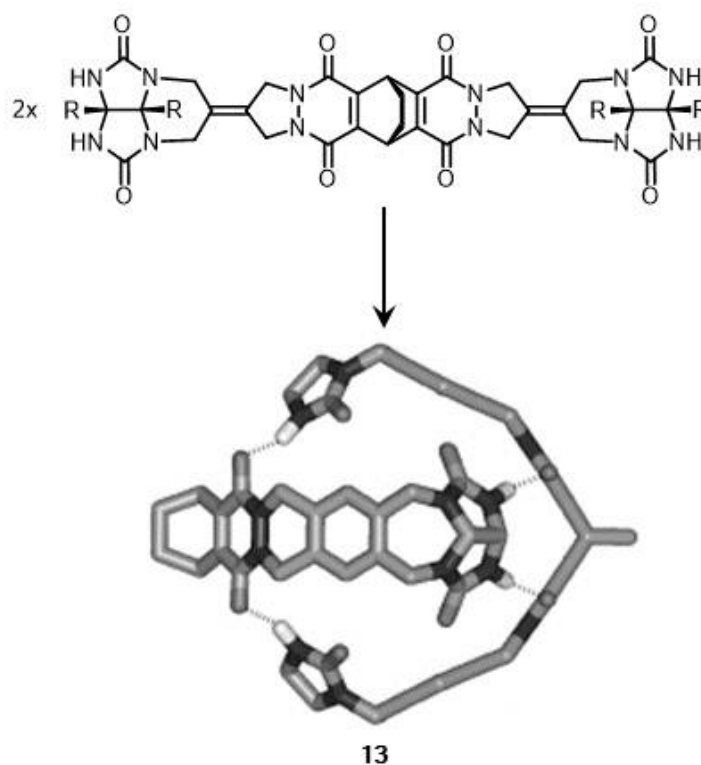


Figure 1.10 Assembly of two ligands *via* hydrogen bonding into softball-shaped molecular capsule **13**. Figure adapted from references 41 and 42.

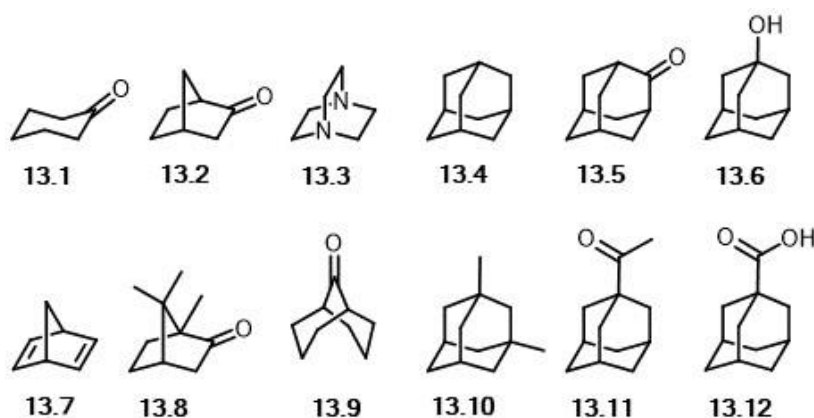


Figure 1.11 Guest molecules encapsulated in capsule **13**. Figure adapted from reference 42.

The volume of the cavity within the resulting capsule **13** measures 225 \AA^3 , and the capsule is soluble in organic solvents such as chloroform, *p*-xylene, and benzene. The table below summarises the binding constants for a range of guests (Figure 1.11) within capsule **13** as compared to guest volume and packing coefficient (*i.e.* the ratio between the van der Waals volume of the guest and the volume of the cavity in capsule **13**). The guests in Table 1.1 are arranged according to increasing volume; in general, the binding constant first increases then decreases as guest volume increases. The most strongly bound guests have a packing coefficient equivalent to 0.55 ± 0.09 .

Guest **13.8** constitutes an exception to this general rule. Despite having a large packing coefficient within capsule **13** (0.71), this guest has a relatively high binding constant (910 kJ / mol). Because guest **13.8** contains both hydrogen bonding donor and acceptor groups, the authors hypothesise that this guest is stabilised within the capsule *via* highly favourable hydrogen bonding interactions with the capsule's ligands.

Table 1.1 Binding constants, volume, and packing coefficients for guest molecules encapsulated by capsule **13**.

Data taken from reference 42.

Guest:	Binding Constant (kJ / mol):	Guest Volume (\AA^3):	Packing Coefficient:
13.7	12	97	0.43
13.3	500	102	0.45
13.1	1700	103	0.46
13.2	1800	110	0.49
13.4	3800	125	0.56
13.5	5.2×10^5	132	0.59
13.6	5.2×10^5	135	0.60
13.9	510	142	0.63
13.12	130	154	0.68
13.10	0	154	0.68
13.8	910	160	0.71
13.11	0	181	0.80

From this data, Rebek's "55% Rule" was thus established – this principle continues to give a good first approximation of appropriate guest size for cages of all sizes. The validity of the "55% Rule" has also been established for cubic M_8L_{12} coordination cage **14**, which has a calculated volume of 407 \AA^3 (Figure 1.12).⁴³ A series of cyclic aliphatic ketones, with the

number of carbons (N_C) in each ring increasing from $N_C = 5$ to $N_C = 14$, were used to probe guest volume *vs.* binding strength in water. Because all these guests have the same polar functional group, they only differ in their flexibility and total volume. Assuming that the interactions between each ketone and the cage are comparable, the difference in free energy associated with the formation of each host-guest complex should result only from the volume and the total hydrophobic surface area of each guest.

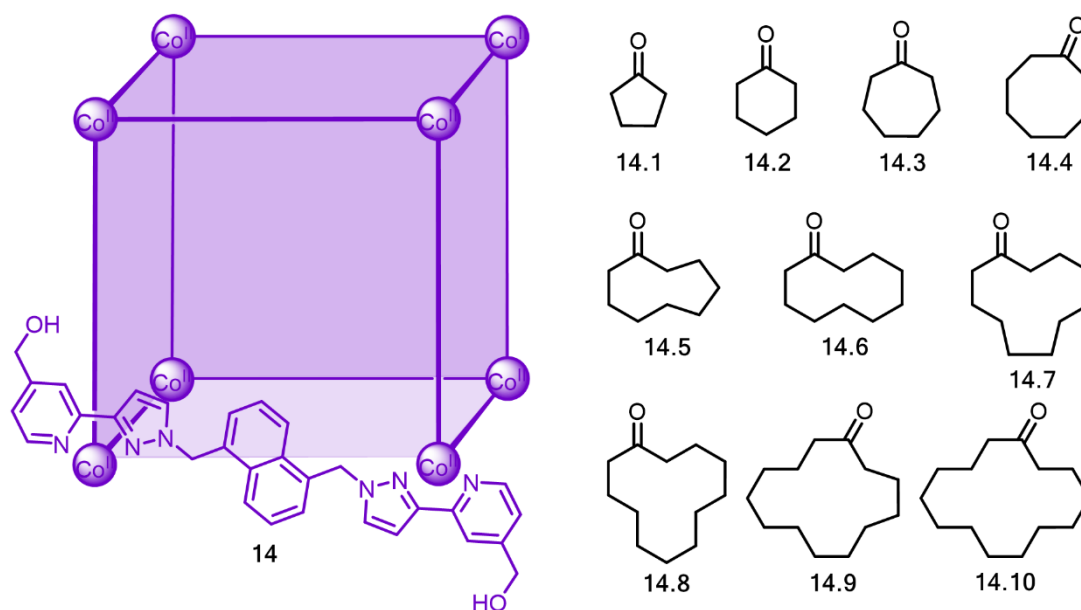


Figure 1.12 Cage **14** and guest molecules. Figure adapted from reference 43.

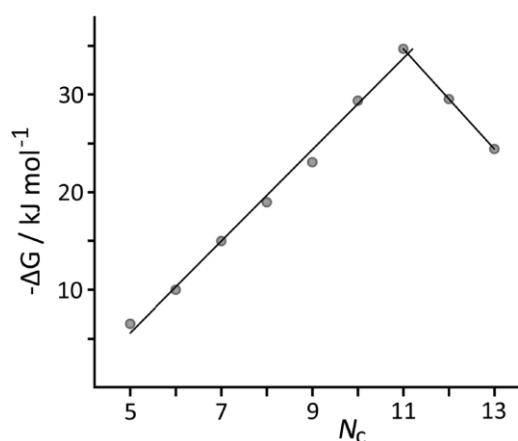


Figure 1.13 Decrease in free energy associated with guest **14** *vs.* number of carbons in the cyclic ketone ring. Figure taken from reference 43.

The graph above (Figure 1.13) plots the binding strength of guests 14.1 – 14.9 against the number of carbon atoms in the ring. Guest 14.10 was too insoluble in water for the authors to obtain an accurate affinity constant. As the ring size increases, $-\Delta G$ increases linearly until $N_C = 11$ (guest 14.7), then decreases linearly for data points $N_C = 12$ (guest 14.8) and $N_C = 13$ (guest 14.9). Guest 14.7, with $N_C = 11$, was calculated to have a volume of 205 \AA^3 or 50% of the volume of the cage cavity; this value falls within the $55 \pm 9\%$ range described by Rebek as being the optimal fit between host and guest.

Small differences between the volume of different guests have significant effects on the guests' affinities for a cage; likewise, small changes in cage volume can also have a significant impact on guest binding. When the organic subcomponents that form cage **11** (introduced in Chapter 1.3) are combined with CoSO_4 instead FeSO_4 , cage **15** is self-assembled.⁴⁴ Because the $\text{Co}^{\text{II}}\text{-L}$ bonds are longer in cage **15** ($13.04(4) \text{ \AA}$) than the $\text{Fe}^{\text{II}}\text{-L}$ bonds in cage **11** ($12.837(1) \text{ \AA}$), the internal volume of cage **15** ($149 - 153 \text{ \AA}^3$) is larger than cage **11** ($118(1) \text{ \AA}^3$). As a result, cage **15** is capable of binding larger guests than cage **11** (Table 1.2). While benzene can be encapsulated by either cage **11** or cage **15**, for instance, toluene only binds inside cage **15**. Significantly, very precise control over guest encapsulation can be achieved using cage **11** and cage **15**. While both cages encapsulate cyclohexane, cyclooctane is only encapsulated by cage **15**, and neither cage encapsulates cyclodecane. Similarly, *n*-pentane can be encapsulated by both cages; *n*-hexane is only encapsulated by cage **15**; and *n*-heptane is not encapsulated by either cage. Remarkably, this result indicates that cages **11** and **15** can distinguish between aliphatic chains on the single carbon level.

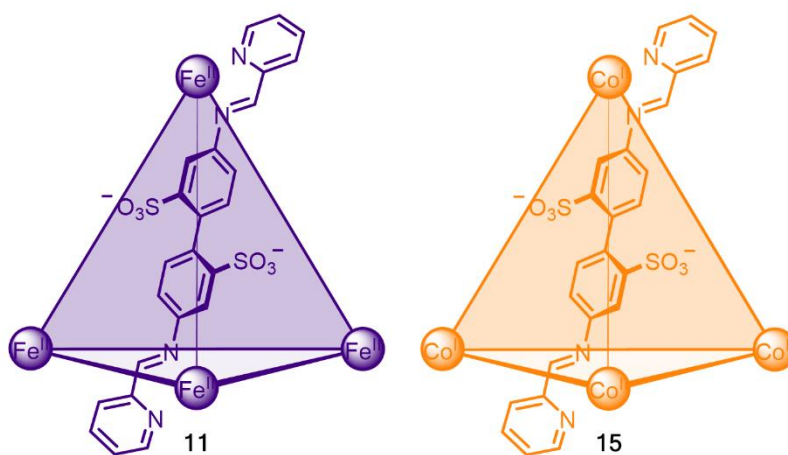


Figure 1.14 Isostructural cages **11** and **15** have different guest binding properties. Figure adapted from reference 44.

Table 1.2 Comparison of guest encapsulation by cages **11** and **15**. Data taken from reference 44.

Guest:	Guest Volume (Å ³):	Encapsulation in Cage 11:	Encapsulation in Cage 15:
CH ₂ Cl ₂	60.9	yes	yes
CHCl ₃	74.7	yes	yes
CCl ₄	88.7	yes	yes
CBr ₄	108.0	yes	yes
cyclopentane	70.7	yes	yes
cyclohexane	111.5	yes	yes
methylcyclopentane	113.1	yes	yes
benzene	99.5	yes	yes
<i>n</i> -pentane	106.5	partial	yes
tetrachloroethylene	101.8	partial	yes
cycloheptane	129.1	no	yes
cyclooctane	146.5	no	yes
methylcyclohexane	129.7	no	yes
<i>n</i> -hexane	124.9	no	yes
2,3-dimethylbutane	123.6	no	yes
toluene	117.4	no	yes
cyclodecane	182.7	no	no
<i>n</i> -heptane	143.1	no	no
<i>n</i> -octane	161.9	no	no
naphthalene	151.0	no	no

Similarly to tetrahedral cages **11** and **15**, octahedral M₆L₄ cages **16**, **17**, **18**, and **19** are isostructural, with sequentially more bulky phenanthroline capping ligands coordinated to the Pd^{II} vertices.⁴⁵ These bulky phenanthroline ligands decrease the bite angle between the threefold symmetric tripyridine ligands that bind to the other two coordination sites on each Pd^{II} metal centre. By decreasing the angle between the faces of the octahedron, the internal cage cavity is likewise decreased. The additional mesityl groups on cage **19**, for instance, shrink the cage cavity by 20% with respect to unmodified cage **16**.

As previously observed with tetrahedral cages **11** and **15**, their difference in internal volume lends these four cages different guest binding preferences. Unlike in the previous example, however, restricting the size of the octahedral cage cavity allows greater guest diversity. Cage **16**, with the largest internal volume of the four cages, also has the largest windows – none of the neutral tetraphenyl guests listed in Table 1.3 are encapsulated by cage **16**, because all of them are small enough to pass easily through the cage's pores. When methyl groups are

appended to the phenanthroline capping ligands (cage **17**), the smaller cavity and smaller pores enable the cage to weakly encapsulate neutral tetraphenyl guests in which the central atom, M, is C, Si, Ge, or Sn (Table 1.3). When the methyl groups from cage **17** are substituted for more bulky *m*-xylenyl groups (cage **18**), the cage cavity is constricted even further, and all four guests are bound more tightly. Notably, the inclusion yields for guests binding in cages **18** and **19** are comparable, indicating the additional methyl groups incorporated onto the phenanthrolines in cage **19** have no significant impact on the cavity size.

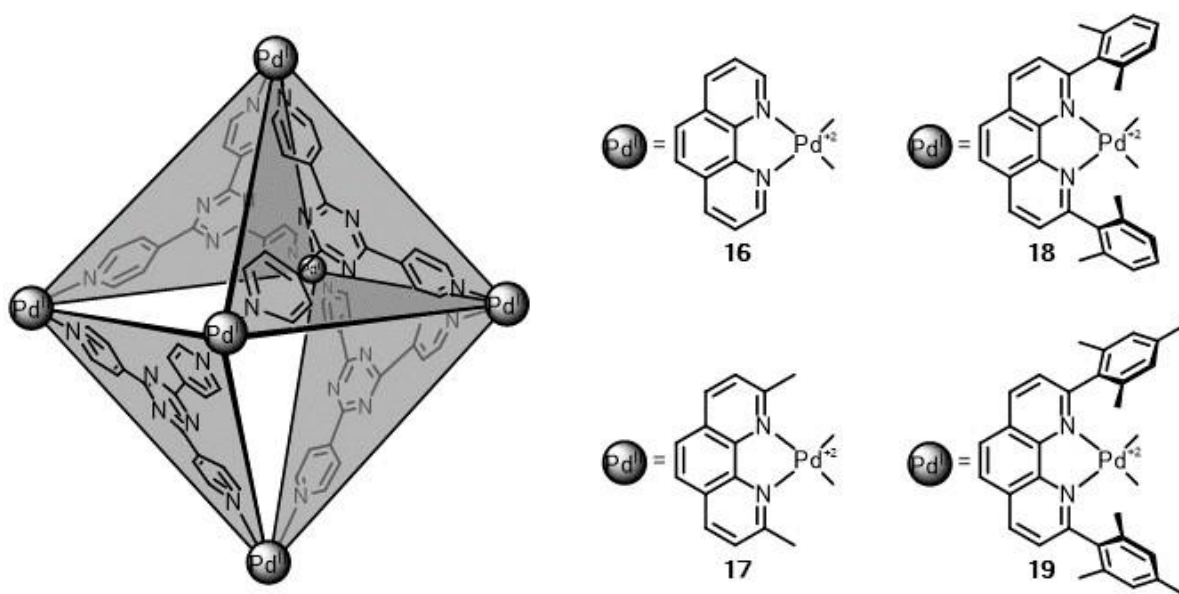
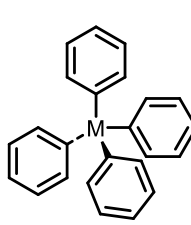


Figure 1.15 Cages **16**, **17**, **18**, and **19**. Figure adapted from reference 45.

Table 1.3 Summary of guests, guest volumes, and inclusion yields for cages **16**, **17**, **18**, and **19**. Data taken from reference 45.



Guest:	Guest Volume (Å ³):	Inclusion Yield (%):			
		Cage 16	Cage 17	Cage 18	Cage 19
M = C	361.50	0	11	55	56
M = Si	374.46	0	11	76	75
M = Ge	382.73	0	12	40	43
M = Sn	393.75	0	18	39	38
M = B ⁻	355.28	>99	>99	>99	>99
M = P ⁺	378.30	0	0	0	0

In addition to the neutral tetraphenyl guests (M = C, Si, Ge, or Sn), the authors also introduced anionic tetraphenyl guest (M = B⁻) with comparable size and shape to the neutral guest

analogues. This anionic guest was incorporated with quantitative inclusion yields into all four cages. This illustrates that size and shape are not the only variables important in the selectivity of cages for different guests; in this case, highly favourable electrostatic interactions between the positively charged cages and the negatively charged guest result in inclusion complexes with high binding affinities. Conversely, the authors combined a cationic tetraphenyl guest ($M = P^+$) with the cages but saw no guest encapsulation because of the repulsion between the positively charged species.

1.5 The Role of Cage Counterions

While the choice of ligand and transition metal components are generally of first consideration in the design of a coordination cage, the counterions used to balance the charge of the cage have a significant impact on the properties of the resulting system. As described in Chapter 1.3, cage **12**[SO₄] is soluble in water while cage **12**[OTf] is soluble in acetonitrile. Indeed, water soluble cationic coordination cages are generally synthesised with sulfate or nitrate;^{22,36,46} cationic coordination cages that are soluble in organic solvents such as acetonitrile or chloroform generally have more hydrophobic anions (*e.g.* triflate, triflimide, tetrafluoroborate, hexafluorophosphate) to balance their charge.⁴⁷⁻⁴⁹ Although the way in which these counterions interact with the cage is not well understood, they clearly have a significant impact on the solubility of the cage[anion] complex.

A growing body of literature supports the idea that anions may remain closely associated with cationic cages in solution in certain cases. For example, Ward has designed and synthesised a coordination cage in which *bis*-bidentate pyrazolyl-pyridine ligands with a naphthalene linker coordinates to Co^{II} vertices to form a cubic structure.⁵⁰ The ligands are appended with hydroxyl groups, which renders the resulting cage soluble in water and able to encapsulate a range of small molecules. Upon encapsulation in cage **14**, the reaction of benzisoxazole with hydroxide to form the 2-cyanophenolate anion is catalysed. While the rate of this ring-opening reaction normally increases as the solution becomes more basic, the rate of the cage-catalysed reaction remains constant throughout the pH range 8.5 – 11.4. From this observation, the authors conclude that hydroxide ions must be closely associated with the cage windows by ion-pairing; the proposed mechanism is shown in Figure 1.16.

The close association of hydroxide in the windows of the cage increases the effective molarity of hydroxide ions, essentially increasing the local basicity around the encapsulated guest. After the reaction between benzisoxazole and hydroxide, the resulting hydrophilic, anionic product exits the cage; the empty cage is then free to bind another equivalent of benzisoxazole. The addition of a large excess of lithium chloride allows chloride to competitively associate in the windows of the cage, lowering the effective molarity of hydroxide anions and completely suppressing catalysis.

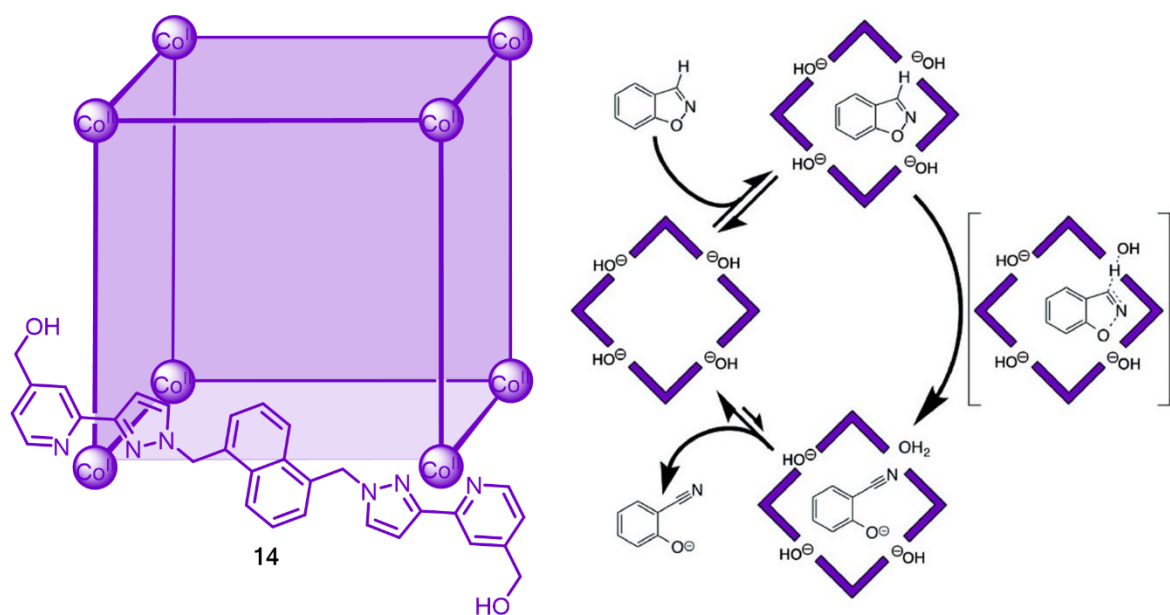


Figure 1.16 (Left) M_8L_{12} cubic coordination cage **14**. (Right) Proposed mechanism for the Kemp elimination from benzisoxazole to the 2-cyanophenolate anion. Figure adapted from reference 50.

Similar interactions between a cage and its counterions have been observed in acetonitrile, in which tetraphenylborate anions bind to coordination cage **20** peripherally within the windows (Figure 1.17).⁵¹ 1D selective ¹H NOESY experiments demonstrate NOE correlations between protons from the tetraphenylborate anion (X = H) and the phenylene, imine, and phenanthroline protons from the cage. Likewise, the ¹H-¹⁹F HOESY spectrum indicates NOE interactions between the fluorine from the tetraphenylborate anion (X = F) and the phenanthroline protons from the cage. No NOE interactions such as the ones observed would be possible if the tetraphenylborate anion was bound internally. Significantly, the peripheral binding of this anion enables internal binding of neutral and anionic guest molecules. Furthermore, the anion enables the self-assembly of the Cd^{II} analogue of **20** by acting as a peripheral template for the cage.

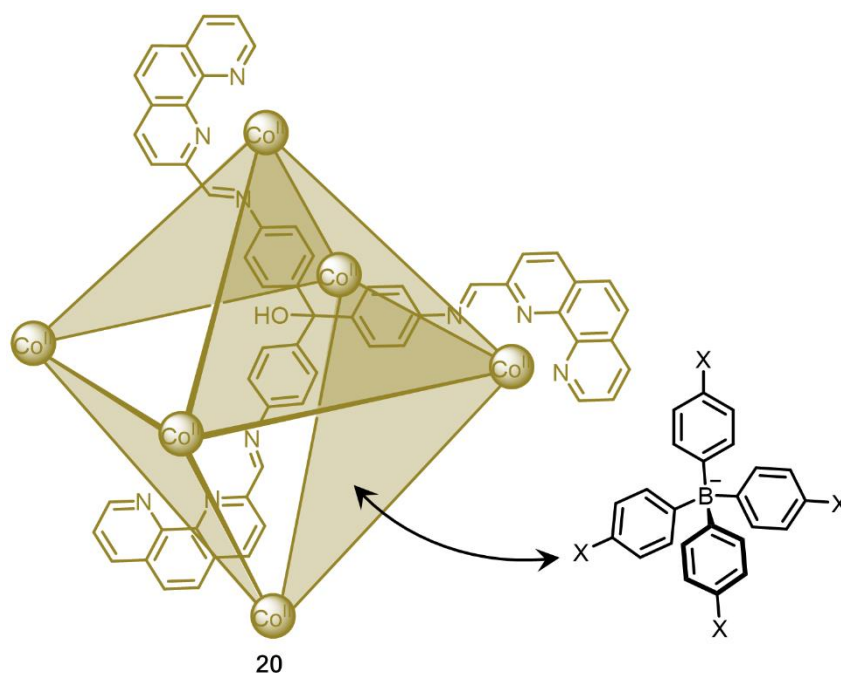


Figure 1.17 Tetraphenylborate anion binding in the windows of octahedral coordination cage **20**. Figure adapted from reference 51.

In the two examples above, interactions between anions and coordination cages could be deduced either indirectly, by observing the impact of an anion on the rate of catalysis within a cage, or directly, by measuring NOE correlations between anion and coordination cage. While these methods may not be extensible to all cage[anion] systems, the two studies described here illustrate that anions are indeed capable of interacting with the external faces of cationic coordination cages in ways that impact their functionality and structure. As such, counteranions are clearly an important component in the design of functional systems of coordination cages.

A recent study, published after the results in Chapters 2 and 3 of this thesis were reported, further demonstrates how counterions can drastically alter the solubility preferences of coordination cages.⁵² The authors investigated a range of previously-reported $\text{Fe}^{\text{II}}\text{L}_4$ and $\text{Fe}^{\text{II}}\text{L}_6$ cages, which had been assumed to be soluble only in organic solvents – the tritopic and tetratopic subcomponents from which these cages self-assemble are insoluble in water. After exchanging the hydrophobic triflate cage counteranions for sulfate, these cages were rendered soluble in water and were observed to remain stable in aqueous solutions for months. Due to the enhanced solvophobic driving force for guest encapsulation in water, these cages bound guests which were not encapsulated by their counterparts in organic solvents. Significantly, these guests include biologically relevant molecules such as caffeine, estradiol, and

testosterone. After exchanging sulfate back to triflate, the cages can be redissolved in the original organic solvent. This process is demonstrated in Figure 1.18. While there is no evidence that the sulfate anions are closely associated with the cages in this report, and the cages and counterions may exist in solution as solvated ion pairs, there is nevertheless a strong correlation between the physicochemical properties of the coordination cages and the identity of their counterions.

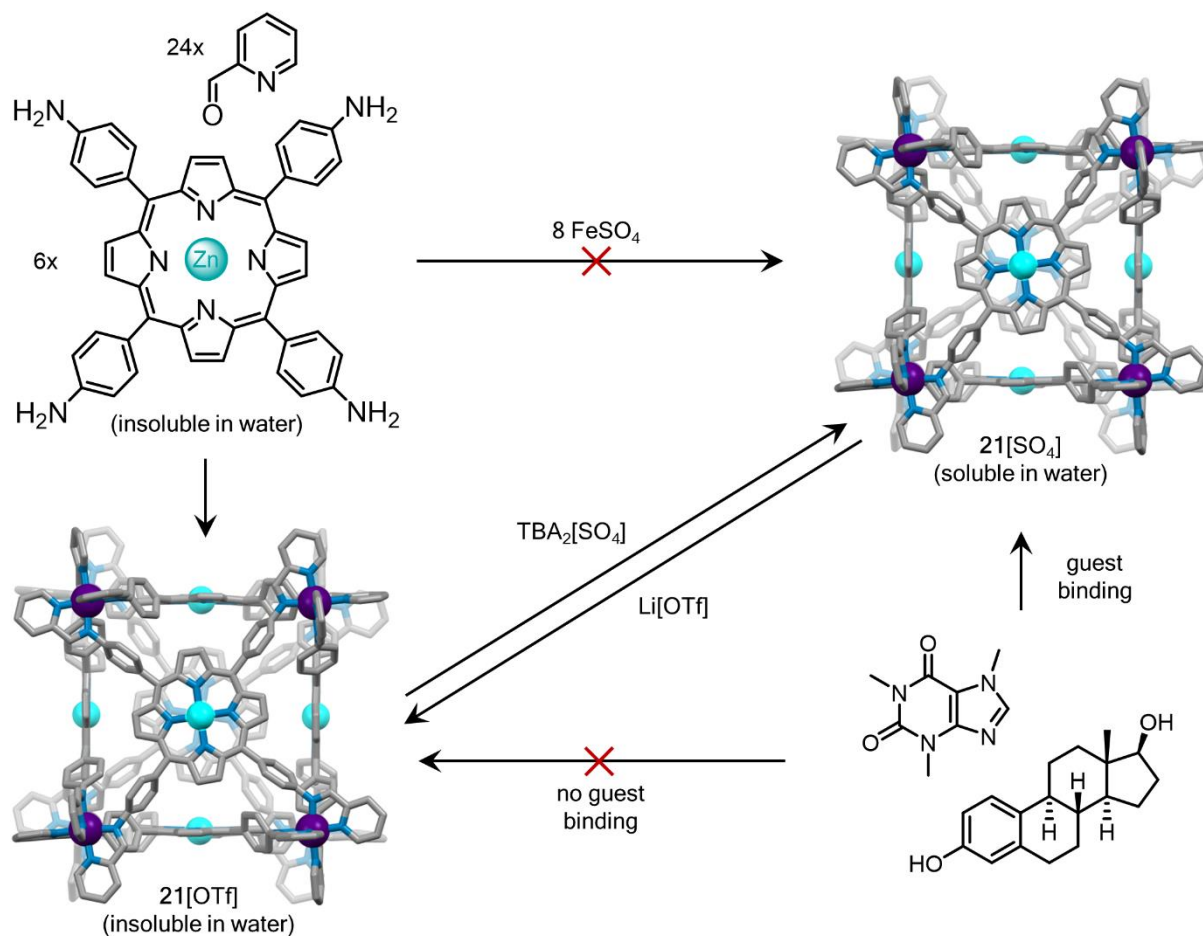


Figure 1.18 Solubility and guest binding preferences of cage **21** are strongly dependent on the identity of the counteranion. Figure adapted from reference 52.

1.6 Ionic Liquids

Ionic liquids are salts with melting points below 100 °C and are generally composed of small organic cations and inorganic anions.⁵³ Of particular interest are ionic liquids that are molten at room temperature. With negligible vapour pressure and high thermal stability, ionic liquids

have become an increasingly common alternative to traditional organic solvents. By selecting different cations and anions, the polarity of ionic liquids can be readily tuned, a feature which has earned these materials the moniker “designer solvents.”⁵³ Hydrophobic ionic liquids can be designed, for example, by pairing cations from Figure 1.19⁵⁴ with hydrophobic anions such as triflimide.⁵⁵ Conversely, hydrophilic ionic liquids can be designed by pairing any cation with a chloride or bromide anion.⁵⁶ Ionic liquids with intermediate hydrophobicity can be synthesised with tetrafluoroborate or hexafluorophosphate; the length of the alkyl chain on the cation can be modulated to further tune the polarity of the ionic liquid.^{55,56} Furthermore, mutually immiscible ionic liquids can be designed such that the anions are identical, but the cations have markedly different sizes.⁵⁷

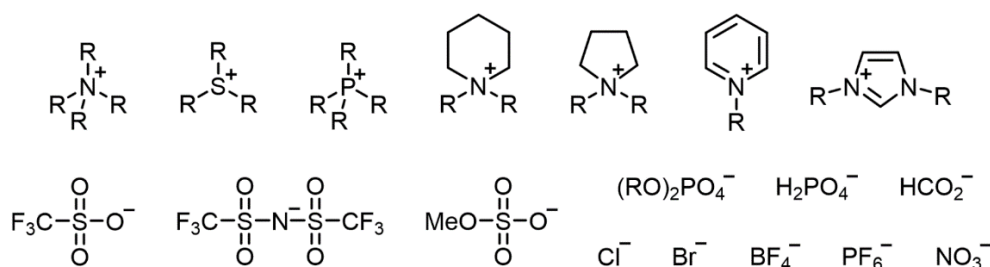


Figure 1.19 Common cations and anions used in the design of ionic liquids. Figure adapted from reference 54.

The tunability of ionic liquids is facilitated by their straightforward synthesis, which can generally be accomplished in one or two steps. Phosphonium, ammonium, or imidazolium halide ionic liquids, for example, are formed by quaternisation of phosphanes, amines, or imidazoles, respectively, with alkylating agents.⁵⁸ The anion from the resulting ionic liquid, which depends on the alkylating agent, can then be exchanged for a different anion. Figure 1.20 further illustrates this process for imidazolium ionic liquids.

Step I immediately provides access to a variety of imidazolium ionic liquids, with different length alkyl chains and different anions. Methyl imidazolium can react with ethyl triflate, for example, to form 1-ethyl-3-methylimidazolium triflate ([emim][OTf]);⁵⁹ methyl imidazolium can also react with chlorobutane to form 1-butyl-3-methylimidazolium chloride ([bmim][Cl]).⁶⁰ When Step I results in a halide salt, the anion can be exchanged via two pathways. In Step IIa, a Lewis acid such as aluminium chloride (AlCl_3) can be added to $[\text{R}'\text{Rim}][\text{Cl}]$ to form $[\text{R}'\text{Rim}][\text{AlCl}_4]$ and $[\text{R}'\text{Rim}][\text{Al}_2\text{Cl}_7]$.⁶¹ In Step IIb, a metal salt such as lithium triflimide can be combined with $[\text{R}'\text{Rim}][\text{X}]$ to form $[\text{R}'\text{Rim}][\text{NTf}_2]$.⁶² Because

triflimide ionic liquids are generally hydrophobic, they can be washed with water to remove residual lithium halide salts. Alternatively, a Brønsted acid such as fluoroboric acid can be reacted with $[R'Rim][X]$ to form an ionic liquid with the tetrafluoroborate anion, $[R'Rim][BF_4]$;⁶³ the resulting strong acid $H[X]$ can then be evaporated off. Finally, ion exchange resins can be used to exchange the halide anion from $[R'Rim][X]$ for other halide anions, tetrafluoroborate, hexafluorophosphate, thiocyanate, and more.⁶⁴

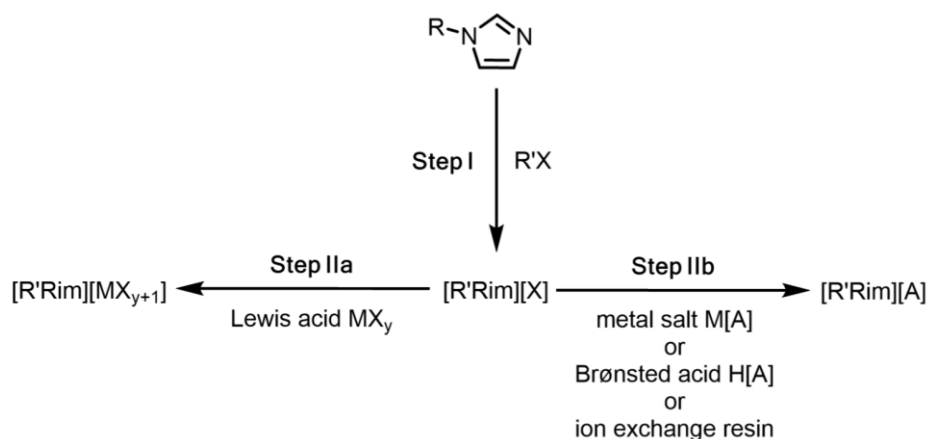


Figure 1.20 Synthesis pathways for imidazolium ionic liquids. Figure adapted from reference 58.

Because ionic liquids span the entire spectrum of polarity, they have been demonstrated to be good solvents for a range of different molecules. In addition to dissolving small organic, inorganic, and organometallic compounds, ionic liquids have also been used to solubilise polymers,⁶⁵ enzymes,⁶⁶ and carbon nanotubes.⁶⁷ Despite interest in the chemistry of ionic liquids, however, studies from a supramolecular perspective remain scarce. Thus far, ionic liquids have been used as solvents for cucurbiturils,^{68–70} calixarenes,^{71–75} and pillararenes;⁷⁶ furthermore, these organic molecular flasks can form host-guest complexes with imidazolium ionic liquids.

1.7 Aims

In this chapter, the fundamental concepts governing the design and synthesis of supramolecular complexes have been introduced. The strategy of subcomponent self-assembly has been used to illustrate the synthesis of several previously-reported coordination cages, and ionic liquids have been proposed as solvents for cage systems. Chapter 1.4 describes several coordination

cages that exhibit high selectivity for guests based on the size of the guest and/or the size of the host cavity. This feature renders coordination cages an attractive alternative to current separations technologies. Currently, the energy required to separate chemicals comprises 10-15% of global consumption.^{77,78} Energy-intensive processes such as distillation are responsible for 80% of the energy used for chemical separations. The three projects presented in the following chapters thus converge around the aim of developing strategies to use coordination cages for performing size-selective chemical separations with minimal energy input. Ultimately, we anticipate that techniques and materials similar to those described in the following chapters may provide energy-efficient alternatives to thermal separations. We imagine different cages selectively encapsulating, compartmentalizing, and transporting hydrocarbons of different sizes, in complementary fashion to the means by which different fractions are separated by boiling point through distillation.

The second chapter of this thesis⁷⁹ explores the use of ionic liquids as solvents for existing coordination cages. Potential methods of characterising these cages in ionic liquids are discussed; cages are demonstrated to be stable and capable of encapsulating guests in these highly ionic environments; and systems in which cages have good solubility in ionic liquids are designed. Using these observations, a *triphasic sorting system* is designed such that each of three different host-guest complexes is soluble in only one of three immiscible liquid phases.

While Chapter 2 achieves separation of host-guest complexes through static confinement in different liquid phases, Chapter 3⁸⁰ illustrates *dynamic transport* of an encapsulated cargo across a phase boundary, from water into an ionic liquid layer. The host-guest complex can be recycled back to water after several additional steps. Within a mixture of two cages and their respective cargoes, cationic cages are demonstrated to undergo selective phase transfer while anionic cages remain in the water layer. The cationic and anionic host-guest complexes are thus separated.

Because several steps are required to recycle the cage in Chapter 3, we explore *reversible transport* of coordination cages within the fourth chapter. Using anion exchange to modulate the solubility of three different cationic cages, we demonstrate reversible transport between water and ethyl acetate. Furthermore, sequential phase transfer of individual cationic cages from among mixtures is achieved.

1.8 References

- (1) Lehn, J.-M. *Chem. Soc. Rev.* **2007**, *36* (2), 151.
- (2) Chakrabarty, R.; Mukherjee, P. S.; Stang, P. J. *Chem. Rev.* **2011**, *111* (11), 6810.
- (3) Korevaar, P. A.; George, S. J.; Markvoort, A. J.; Smulders, M. M. J.; Hilbers, P. A. J.; Schenning, A. P. H. J.; De Greef, T. F. A.; Meijer, E. W. *Nature* **2012**, *481*, 492.
- (4) Dichtel, W. R.; Miljanić, O. Š.; Zhang, W.; Spruell, J. M.; Patel, K.; Aprahamian, I.; Heath, J. R.; Stoddart, J. F. *Acc. Chem. Res.* **2008**, *41* (12), 1750.
- (5) Champin, B.; Mobian, P.; Sauvage, J.-P. *Chem. Soc. Rev.* **2007**, *36* (2), 358.
- (6) Sauvage, J.-P. *Acc. Chem. Res.* **1998**, *31* (10), 611.
- (7) Amabilino, D. B.; Stoddart, J. F. *Chem. Rev.* **1995**, *95* (8), 2725.
- (8) Balzani, V.; Gomez-Lopez, M.; Stoddart, J. F. *Acc. Chem. Res.* **1998**, *31* (7), 405.
- (9) Browne, W. R.; Feringa, B. L. *Nat. Nanotechnol.* **2006**, *1* (1), 25.
- (10) Pedersen, C. J. *Angew. Chem. Int. Ed.* **1988**, *27*, 1021.
- (11) Lehn, J.-M. *Angew. Chem. Int. Ed.* **1988**, *27*, 89.
- (12) Cram, D. J. *Angew. Chem. Int. Ed.* **1988**, *27*, 1009.
- (13) Leung, D. H.; Bergman, R. G.; Raymond, K. N. *J. Am. Chem. Soc.* **2008**, *130* (9), 2798.
- (14) Yoshizawa, M.; Klosterman, J. K.; Fujita, M. *Angew. Chem. Int. Ed.* **2009**, *48* (19), 3418.
- (15) Hooley, R. J.; Rebek, J. *Chem. Biol.* **2009**, *16* (3), 255.
- (16) Cram, D. J. *Science* **1987**, *240*, 760.
- (17) Crini, G. *Chem. Rev.* **2014**, *114* (21), 10940.
- (18) Shinkai, S. *Tetrahedron* **1993**, *49* (40), 8933.
- (19) Cragg, P. J. *Supramol. Chem.* **2010**, *45* (8), 1.
- (20) Kim, K.; Selvapalam, N.; Ko, Y. H.; Park, K. M.; Kim, D.; Kim, J. *Chem. Soc. Rev.* **2007**, *36* (2), 267.
- (21) Seidel, S. R.; Stang, P. J. *Acc. Chem. Res.* **2002**, *35* (11), 972.
- (22) Fujita, M.; Oguro, D.; Miyazawa, M.; Oka, H.; Yamaguchi, K.; Ogura, K. *Nature* **1995**, *378*, 469.
- (23) Caulder, D. L.; Powers, R. E.; Parac, T. N.; Raymond, K. N. *Angew. Chem. Int. Ed.* **1998**, *37*, 1840.
- (24) Yoshizawa, M.; Tamura, M.; Fujita, M. *J. Am. Chem. Soc.* **2004**, *126* (22), 6846.
- (25) Meng, W.; Breiner, B.; Rissanen, K.; Thoburn, J. D.; Clegg, J. K.; Nitschke, J. R.

- Angew. Chem. Int. Ed.* **2011**, *50* (15), 3479.
- (26) Pasquale, S.; Sattin, S.; Escudero-Adán, E. C.; Martínez-Belmonte, M.; De Mendoza, J. *Nat. Commun.* **2012**, *3*.
- (27) Sun, Q.; Iwasa, J.; Ogawa, D.; Ishido, Y.; Sato, S.; Ozeki, T.; Sei, Y.; Yamaguchi, K.; Fujita, M. *Science* **2009**, *328*, 1144.
- (28) Fujita, D.; Ueda, Y.; Sato, S.; Yokoyama, H.; Mizuno, N.; Kumasaka, T.; Fujita, M. *Chem* **2016**, *1* (1), 91.
- (29) Rowan, S. J.; Cantrill, S. J.; Cousins, G. R. L.; Sanders, J. K. M.; Stoddart, J. F. *Angew. Chem. Int. Ed.* **2002**, *41*, 898.
- (30) Belowich, M. E.; Stoddart, J. F. *Chem. Soc. Rev.* **2012**, *41* (6), 2003.
- (31) Nitschke, J. R. *Angew. Chem. Int. Ed.* **2004**, *43* (23), 3073.
- (32) Mal, P.; Schultz, D.; Beyeh, K.; Rissanen, K.; Nitschke, J. R. *Angew. Chem. Int. Ed.* **2008**, *47*, 8297.
- (33) Mal, P.; Breiner, B.; Rissanen, K.; Nitschke, J. R. *Science* **2009**, *324*, 1697.
- (34) Bolliger, J. L.; Ronson, T. K.; Ogawa, M.; Nitschke, J. R. *J. Am. Chem. Soc.* **2014**, *136* (41), 14545.
- (35) Frischmann, P. D.; Kunz, V.; Würthner, F. *Angew. Chem. Int. Ed.* **2015**, *54*, 7285.
- (36) Yi, S.; Brega, V.; Captain, B.; Kaifer, A. E. *Chem. Commun.* **2012**, *48* (83), 10295.
- (37) Zhou, X. P.; Wu, Y.; Li, D. *J. Am. Chem. Soc.* **2013**, *135* (43), 16062.
- (38) Struch, N.; Bannwarth, C.; Ronson, T. K.; Lorenz, Y.; Mienert, B.; Wagner, N.; Engeser, M.; Bill, E.; Puttreddy, R.; Rissanen, K.; Beck, J.; Grimme, S.; Nitschke, J. R.; Lützen, A. *Angew. Chem. Int. Ed.* **2017**, *56*, 4930.
- (39) Riddell, I. A.; Smulders, M. M. J.; Clegg, J. K.; Hristova, Y. R.; Breiner, B.; Thoburn, J. D.; Nitschke, J. R. *Nat. Chem.* **2012**, *4* (9), 751.
- (40) Bilbeisi, R. A.; Ronson, T. K.; Nitschke, J. R. *Angew. Chem. Int. Ed.* **2013**, *52*, 9027.
- (41) Hof, F.; Craig, S. L.; Nuckolls, C.; Rebek, Jr., J. *Angew. Chem. Int. Ed.* **2002**, *41*, 1488.
- (42) Mecozzi, S.; Rebek, J. *Chem. Eur. J.* **1998**, *4* (6), 1016.
- (43) Turega, S.; Whitehead, M.; Hall, B. R.; Meijer, A. J. H. M.; Hunter, C. A.; Ward, M. D. *Inorg. Chem.* **2013**, *52* (2), 1122.
- (44) Ronson, T. K.; Giri, C.; Kodiah Beyeh, N.; Minkkinen, A.; Topič, F.; Holstein, J. J.; Rissanen, K.; Nitschke, J. R. *Chem. Eur. J.* **2013**, *19* (10), 3374.
- (45) Fang, Y.; Murase, T.; Sato, S.; Fujita, M. *J. Am. Chem. Soc.* **2013**, *135* (2), 613.
- (46) Zhang, D.; Ronson, T. K.; Mosquera, J.; Martinez, A.; Guy, L.; Nitschke, J. R. *J. Am.*

- Chem. Soc.* **2017**, *139*, 6574.
- (47) Bonakdarzadeh, P.; Topić, F.; Kalenius, E.; Bhowmik, S.; Sato, S.; Groessl, M.; Knochenmuss, R.; Rissanen, K. *Inorg. Chem.* **2015**, *54* (12), 6055.
- (48) Freye, S.; Michel, R.; Stalke, D.; Pawliczek, M.; Frauendorf, H.; Clever, G. H. *J. Am. Chem. Soc.* **2013**, *135* (23), 8476.
- (49) Zhang, J.; Miller, P. W.; Nieuwenhuyzen, M.; James, S. L. *Chem. Eur. J.* **2006**, *12* (9), 2448.
- (50) Ward, M. D.; Hunter, C. A.; Williams, N. H. *Chem. Lett.* **2017**, *46* (1), 2.
- (51) Rizzuto, F. J.; Wu, W. Y.; Ronson, T. K.; Nitschke, J. R. *Angew. Chem. Int. Ed.* **2016**, *55* (28), 7866.
- (52) Percástegui, E. G.; Mosquera, J.; Nitschke, J. R. *Angew. Chem. Int. Ed.* **2017**, *56* (31), 9136.
- (53) Freemantle, M. *Introduction to Ionic Liquids*; 2011.
- (54) Freudenmann, D.; Wolf, S.; Wolff, M.; Feldmann, C. *Angew. Chem. Int. Ed.* **2011**, *50*, 11050.
- (55) Huddleston, J. G.; Visser, A. E.; Reichert, W. M.; Willauer, H. D.; Broker, G. A.; Rogers, R. D. *Green Chem.* **2001**, *3* (4), 156.
- (56) Stockmann, T. J.; Guterman, R.; Ragogna, P. J.; Ding, Z. *Langmuir* **2016**, *32* (49), 12966.
- (57) Arce, A.; Earle, M. J.; Katdare, S. P.; Rodríguez, H.; Seddon, K. R. *Chem. Commun.* **2006**, *2* (24), 2548.
- (58) Wasserscheid, P.; Keim, W. *Angew. Chem. Int. Ed.* **2000**, *39* (21), 3772.
- (59) McCune, J. A.; He, P.; Petkovic, M.; Coleman, F.; Estager, J.; Holbrey, J. D.; Seddon, K. R.; Swadźba-Kwaśny, M. *Phys. Chem. Chem. Phys.* **2014**, *16* (42), 23233.
- (60) Varma, R. S.; Namboodiri, V. V. *Chem. Commun.* **2001**, 643.
- (61) Laali, K. K.; Gettewert, V. J. *J. Org. Chem.* **2001**, *66* (1), 35.
- (62) Dhanalakshmi, K.; Vaultier, M. *Tetrahedron* **2003**, *59* (50), 9907.
- (63) Li, W.; Dai, S.; Li, D.; Zhang, Q.; Fan, H.; Zhang, T.; Zhang, Z. *Synthesis* **2016**, *49* (5), 1065.
- (64) Dinarès, I.; Garcia de Miguel, C.; Ibáñez, A.; Mesquida, N.; Alcalde, E. *Green Chem.* **2009**, *11* (10), 1507.
- (65) Winterton, N. *J. Mater. Chem.* **2006**, *16* (44), 4281.
- (66) Zhao, H. *J. Chem. Technol. Biotechnol.* **2010**, *85* (7), 891.
- (67) Polo-Luque, M. L.; Simonet, B. M.; Valcárcel, M. *TrAC, Trends Anal. Chem.* **2013**,

- 47, 99.
- (68) Buaki-Sogo, M.; Alvaro, M.; Garcia, H. *Tetrahedron* **2012**, 68 (22), 4296.
- (69) Liu, L.; Zhao, N.; Scherman, O. A. *Chem. Commun.* **2008**, 1070.
- (70) Montes-Navajas, P.; Corma, A.; Garcia, H. *J. Mol. Catal. A Chem.* **2008**, 279 (2), 165.
- (71) Fowler, D. A.; Atwood, J. L.; Baker, G. A. *Chem. Commun.* **2013**, 49 (18), 1802.
- (72) Fowler, D. A.; Teat, S. J.; Baker, G. A.; Atwood, J. L. *Chem. Commun.* **2012**, 48 (43), 5262.
- (73) Pandey, S.; Ali, M.; Kamath, G.; Pandey, S.; Baker, S. N.; Baker, G. A. *Anal. Bioanal. Chem.* **2012**, 403 (8), 2361.
- (74) Wintgens, V.; Amiel, C.; Biczók, L.; Miskolczy, Z.; Megyesi, M. *Thermochim. Acta* **2012**, 548, 76.
- (75) Wintgens, V.; Biczók, L.; Miskolczy, Z. *Thermochim. Acta* **2011**, 523, 227.
- (76) Dong, S.; Zheng, B.; Yao, Y.; Han, C.; Yuan, J.; Antonietti, M.; Huang, F. *Adv. Mater.* **2013**, 25 (47), 6864.
- (77) Sholl, D. S.; Lively, R. P. *Nature* **2016**, 532 (7600), 435.
- (78) Lively, R. P.; Sholl, D. S. *Nat. Mater.* **2017**, 16 (3), 276.
- (79) Grommet, A. B.; Bolliger, J. L.; Browne, C.; Nitschke, J. R. *Angew. Chem. Int. Ed.* **2015**, 54, 15100.
- (80) Grommet, A. B.; Nitschke, J. R. *J. Am. Chem. Soc.* **2017**, 139, 2176.

Chapter 2:

A Triphasic Sorting System: Coordination Cages in Ionic Liquids

Host–guest chemistry is generally carried out either in water or in organic solvents. To investigate the utility of alternative solvents, three different coordination cages were dissolved in neat ionic liquids in this chapter.¹ By using ¹⁹F NMR spectroscopy to monitor the presence of free and bound guest molecules, all three cages were demonstrated to be stable and capable of encapsulating guests in ionic solution. Different cages were found to preferentially dissolve in different phases, allowing for the design of a triphasic sorting system. Within this system, three coordination cages, namely Fe₄L₆ [Me₄N]3, Fe₈L₁₂ 4[NTf₂], and Fe₄L₄ 5[NTf₂], each segregated into a distinct layer. Upon the addition of a mixture of three different guests, each cage (in each separate layer) selectively bound its preferred guest.

2.1 Introduction

Designing new functionality into supramolecular cage systems can be accomplished *via* two different routes: by building a cage with a cavity of specific size,^{2–4} shape,^{5,6} or chemical functionality;^{7,8} or by changing the environmental conditions that govern guest binding.^{4,9–12} The first method may require considerable synthetic effort,^{13–15} whereas the second requires only variation of the reaction temperature or solvent. Guest binding is enhanced, for example, in a solvent in which the guest is poorly solvated.¹⁶ Whereas extensive solution-based host-guest investigations have been carried out either in water^{17–22} or in organic solvents,^{23–25} far fewer studies have involved a third class of solvents – ionic liquids.

Uniquely, Dagueuet and Dyson have demonstrated that a Ni^{II} coordination cage²⁶ can be dissolved in a range of ionic liquids.²⁷ Because the cage shown in Figure 2.1 required templation by chloride in methanol, the host-guest complex chloride **1** was selected to measure the solvation of chloride in a range of ionic liquids. Extraction of the chloride from the cage upon solvation in the ionic liquids led to cage decomposition, which was followed by UV-Vis spectroscopy. The ionic liquids analysed all contained triflimide as the anion, since the authors assumed chloride solvation to be dependent on the identity of the cation.

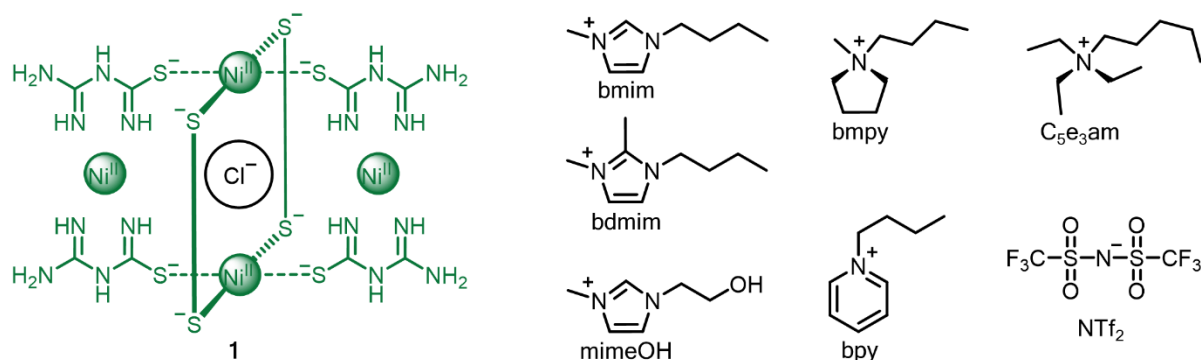


Figure 2.1 A Ni^{II} coordination cage, which has been dissolved in a range of different ionic liquids, [cation][NTf₂]. Figure adapted from reference 27.

The authors did not address the possibility that decomposition of cage could have been the result of factors other than loss of chloride, such as competitive interactions from the ionic liquids. Neither did they investigate characterisation methods other than UV-Vis spectroscopy to monitor cage stability in the ionic liquid. Nevertheless, this example of a Ni^{II} cage dissolved in ionic liquids suggests latent potential in exploiting ionic liquids as solvents for coordination cages. The modularity of ionic liquids, coupled with the modularity of coordination cages synthesised *via* subcomponent self-assembly, would enable considerable control over the design of supramolecular systems.

This chapter introduces the concept of using different coordination cages in multiple ionic liquid phases simultaneously. Three cages are shown to be stable and capable of encapsulating guests in imidazolium and phosphonium ionic liquids, allowing us to selectively dissolve cages in specific phases and bind specific guests within hosts. We present a triphasic system (consisting of water and two mutually immiscible, hydrophobic ionic liquids)²⁸ in which each of three different cages is soluble in only one layer. Upon the addition of three different guests, each cage selectively encapsulates the guest to which it binds most favourably, influencing the composition of each layer.

2.2 Results and Discussion

2.2.1 Characterisation of coordination cages dissolved in neat ionic liquids

Neat, nondeuterated ionic liquids were used in this study, rendering the characterisation of coordination cages in these solvents nontrivial. While mass spectrometry (MS) can be done on neat ionic liquids, large m/z peaks from the ionic liquid swamp the spectrum, thereby precluding the use of MS for characterisation.²⁹ Similarly, ^1H NMR signals from the ionic liquid saturate the detector, decrease the sensitivity of NMR experiments, and therefore frustrate attempts to observe cage peaks. ^1H NMR peaks from imidazolium ionic liquids occur throughout the spectral range, overlapping with potential cage peaks and rendering the use of selective pulses for solvent suppression futile. Conversely, ^1H peaks from phosphonium ionic liquids are displayed in the aliphatic region and aromatic peaks from cages could hypothetically be observed. Observable cage peaks, however, were too broad to be used for characterisation. This broadening is likely due to the high viscosity of the ionic solution. Likewise, using ^1H DOSY to separate ionic liquid signals from solute signals is not feasible – as observed by Giernoth,³⁰ the diffusion coefficients of the ionic liquid and large solutes are too similar.

The use of ^{19}F NMR, however, proved to be a fruitful method for the characterisation of host-guest complexes of cages in ionic liquid solution, with fluorinated guests reporting the presence of the cage. When a fluorinated prospective guest molecule was dissolved in an ionic liquid, its characteristic spectrum was observed by ^{19}F NMR. If this spectrum remained unchanged after the addition of a cage, we inferred no complexation to have occurred. In this case, the cage might not be stable in the ionic liquid. Or the cage could be intact, but there may be no driving force for encapsulation; the prospective guest might be too large, for instance. A significant change in the ^{19}F chemical shifts of the guest, however, would be consistent with guest encapsulation in fast exchange on the NMR timescale, allowing us to conclude that the cage is intact and functional.³¹ The observation of an additional set of ^{19}F guest peaks would indicate the presence of both free and encapsulated guests in slow exchange, also confirming guest binding within a stable cage.³²

To probe the stability of coordination cages in ionic liquids, a solution of cage **2**[OTf]³³ (3.3 mM) in 1-ethyl-3-methylimidazolium ethylsulfate ([emim][EtOSO₃]) was prepared (Figure 2.2a). Initially, two signals were observed by ^{19}F NMR (Figure 2.3a), corresponding to free and

encapsulated triflate, the counterion for cage **2**[OTf]. After 1,3,5-trifluorobenzene (5 equiv) was added to a solution of **2**[OTf] in [emim][EtOSO₃] and the mixture was stirred for 1 week at 298 K (Figure 2.2b), three signals were observed by ¹⁹F NMR (Figure 2.3b). Signals corresponding to free triflate and free 1,3,5-trifluorobenzene were observed at the same chemical shift values in the presence and absence of the cage. We therefore attributed the new peak to 1,3,5-trifluorobenzene within **2**[OTf], in slow exchange with free 1,3,5-trifluorobenzene on the NMR timescale.

We also attempted using ¹⁹F DOSY NMR to distinguish encapsulated from free fluorinated guests. In all cases, however, the encapsulated guest peaks lacked the intensity to be observed by DOSY after measuring 16 increments of 1600 scans each.

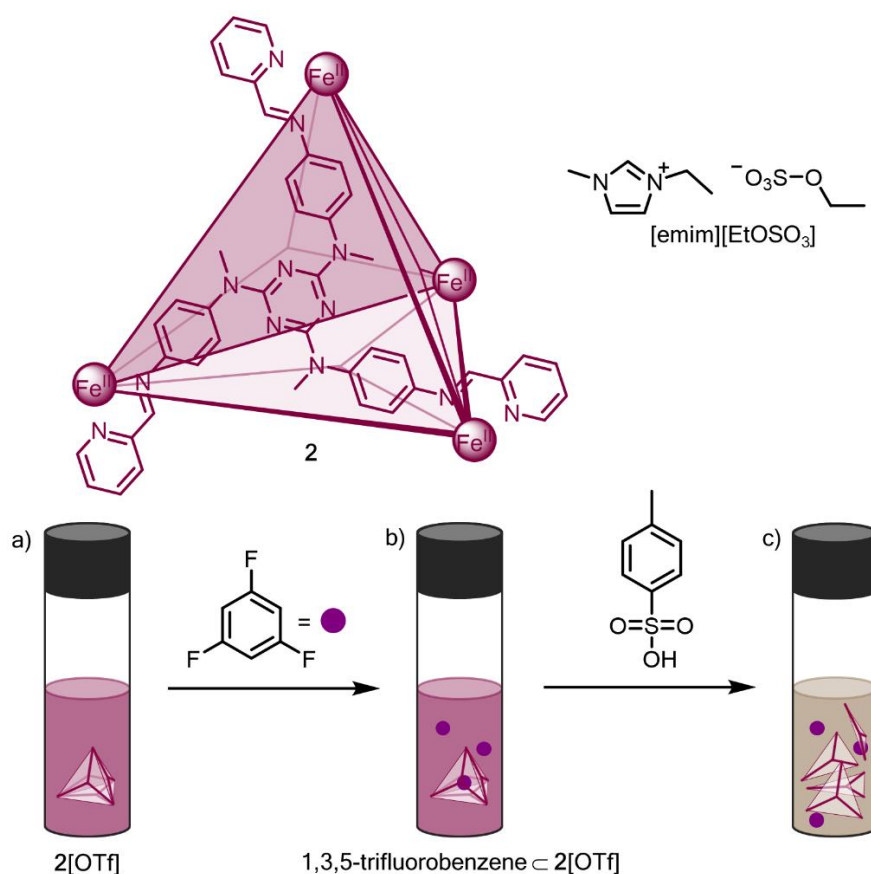


Figure 2.2 a) Cage **2**[OTf] was observed to dissolve in the ionic liquid [emim][EtOSO₃]. b) 1,3,5-Trifluorobenzene was observed to bind within cage **2**[OTf] by ¹⁹F NMR. c) 1,3,5-Trifluorobenzene was released from “unlocked” **2**[OTf] following the addition of *p*-toluenesulfonic acid. Figure adapted from reference 1.

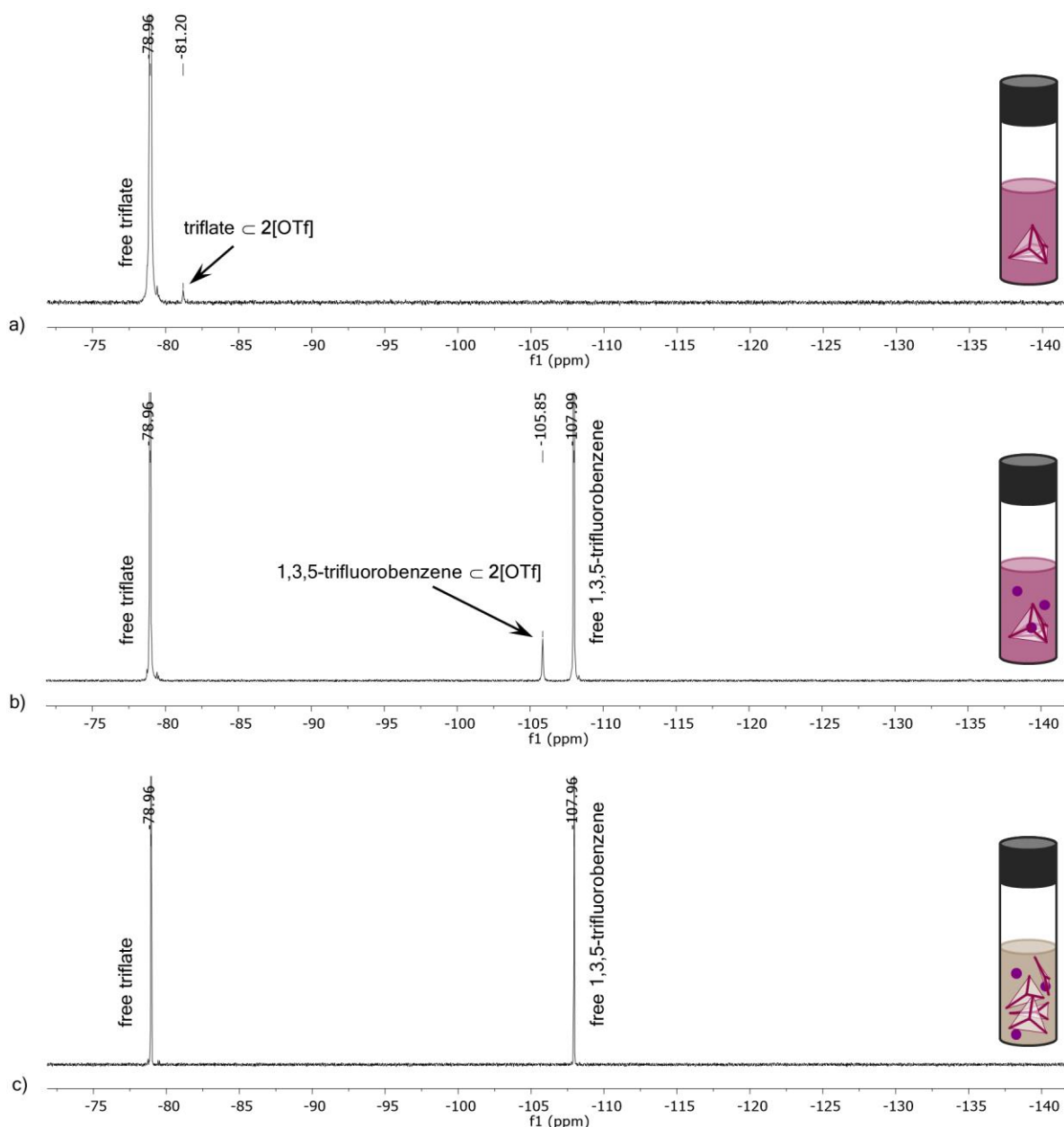


Figure 2.3 a) A 3.3 mM solution of cage $2[\text{OTf}]$ dissolved in $[\text{emim}][\text{EtOSO}_3]$. $^{19}\text{F}\{^1\text{H}\}$ NMR (471 MHz, referenced to triflate): $\delta_{\text{F}} = -78.96$ (free triflate, counterion for cage $2[\text{OTf}]$), -81.20 (triflate $\subset 2[\text{OTf}]$). b) Solution from a) after the addition of 1,3,5-trifluorobenzene (5 equiv) and stirring for 1 week. $^{19}\text{F}\{^1\text{H}\}$ NMR (471 MHz, referenced to triflate): $\delta_{\text{F}} = -78.96$ (free triflate), -105.85 (1,3,5-trifluorobenzene $\subset 2[\text{OTf}]$), -107.99 (free 1,3,5-trifluorobenzene). c) Solution from b) after the addition of *p*-toluenesulfonic acid (10 equiv) and stirring for 24 hours. $^{19}\text{F}\{^1\text{H}\}$ NMR (471 MHz, referenced to triflate): $\delta_{\text{F}} = -78.96$ (free triflate), -107.96 (free 1,3,5-trifluorobenzene).

As previously reported, Fe^{II} tetrahedral cages can be “unlocked” by adding *p*-toluenesulfonic acid, resulting in guest release.³⁴ We inferred that cage $2[\text{OTf}]$ should also be “unlockable” in an ionic liquid. Since a cage must first be “locked” in order to be “unlocked”, success would

further confirm that the cage remains intact and functional in the ionic liquid. *p*-Toluenesulfonic acid (10 equiv) was thus added to a solution of 1,3,5-trifluorobenzene \subset **2**[OTf] in [emim][EtOSO₃]. After stirring at 298 K for 24 hours, the purple solution was observed to turn brown (Figure 2.2c), and the ¹⁹F NMR peak assigned to encapsulated 1,3,5-trifluorobenzene disappeared (Figure 2.3c). The signals from triflate and free 1,3,5-trifluorobenzene, however, remained unchanged. The disappearance of the ¹⁹F peak at -105.85 ppm suggested that cage **2**[OTf] had indeed “unlocked” to release encapsulated 1,3,5-trifluorobenzene. A ¹H NMR spectrum of the sample after the colour change confirmed that the ionic liquid had not decomposed.

2.2.2 Comparison of guest binding in ionic liquids vs. organic solvents

In this section, we demonstrate the similarity between ¹⁹F NMR and UV-Vis spectra of comparable host-guest complexes in acetonitrile and [emim][EtOSO₃]. We note the similarity between the host-guest chemistry of cage **2**[OTf] in acetonitrile and in [emim][EtOSO₃]. Since cage **2**[OTf] has been studied extensively in acetonitrile,³³ these data help to corroborate our claim that host-guest chemistry in [emim][EtOSO₃] proceeds as observed in other solvents.

As seen below, the shift for triflate (the counterion for cage **2**[OTf]) in acetonitrile (-78.32 ppm; Figure 2.4a) is very similar to triflate in [emim][EtOSO₃] (-78.96 ppm; Figure 2.4b). Likewise, the shifts for encapsulated (-105.08 ppm) and free (-108.42 ppm) 1,3,5-trifluorobenzene in CD₃CN are nearly identical to the comparable peaks in [emim][EtOSO₃] (-105.86 ppm and -107.99 ppm, respectively). The binding constant for 1,3,5-trifluorobenzene \subset **2**[OTf], however, was calculated to be stronger in the ionic liquid (80 M⁻¹) than in acetonitrile (14 M⁻¹) (see Chapter 2.2.3, Tables 2.1 and 2.2 for calculations).

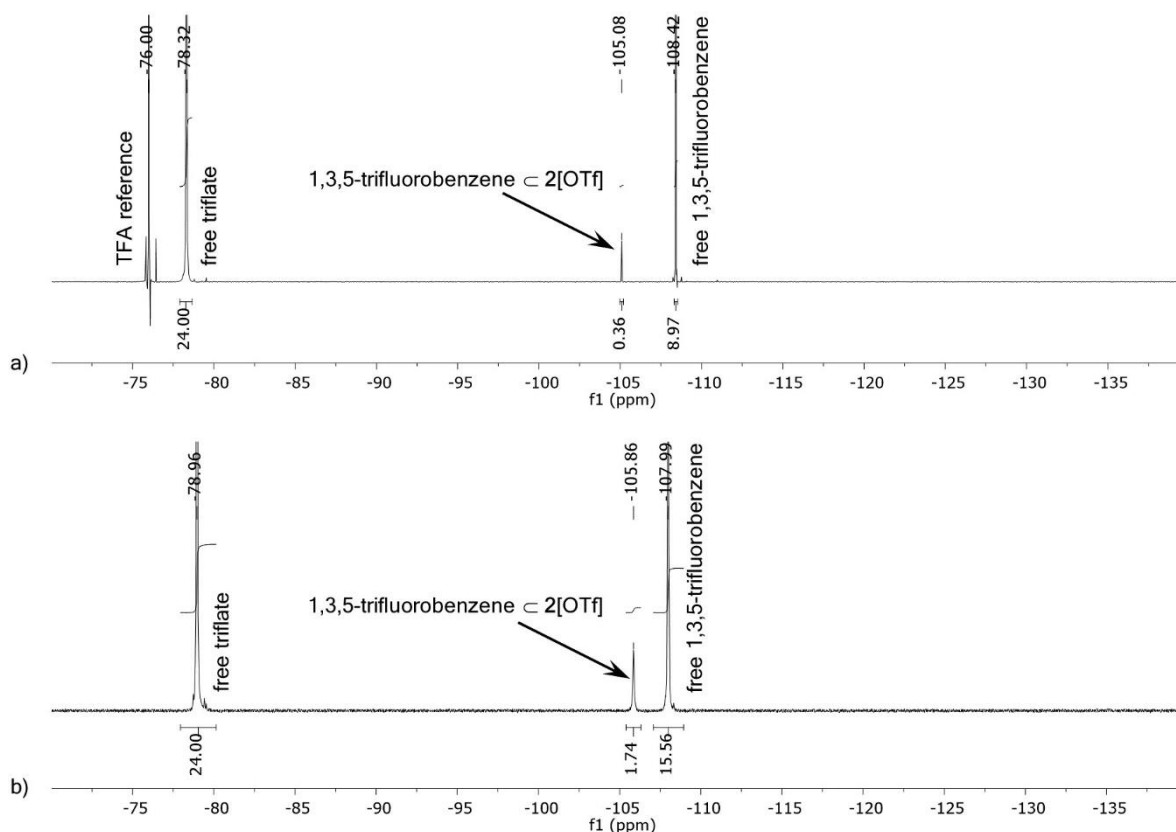


Figure 2.4 a) ^{19}F NMR of 1,3,5-trifluorobenzene (5 equiv) in a solution of cage **2**[OTf] in CD_3CN (3.3 mM). $^{19}\text{F}\{^1\text{H}\}$ NMR (471 MHz, referenced to TFA in an acetone- d_6 capillary): $\delta_{\text{F}} = -78.32$ (free triflate, counterion for cage **2**[OTf]), -105.08 (1,3,5-trifluorobenzene \subset **2**[OTf]), -108.42 (free 1-fluoroadamantane). b) ^{19}F NMR of 1,3,5-trifluorobenzene (5 equiv) in a solution of cage **2**[OTf] in [emim][EtOSO₃] (3.3 mM). $^{19}\text{F}\{^1\text{H}\}$ NMR (471 MHz, referenced to triflate): $\delta_{\text{F}} = -78.96$ (free triflate, counterion for cage **2**[OTf]), -105.86 (1,3,5-trifluorobenzene \subset **2**[OTf]), -107.99 (free 1,3,5-trifluorobenzene).

As seen in Figure 2.5, the shifts for encapsulated (-119.85 ppm) and free (-126.95 ppm) 1-fluoroadamantane in CD_3CN are nearly identical to the comparable peaks in [emim][EtOSO₃] (-120.80 ppm and -127.46 ppm, respectively). In acetonitrile, nearly 100% of cage **2**[OTf] bound 1-fluoroadamantane; in the ionic liquid, approximately 80% of cage **2**[OTf] bound 1-fluoroadamantane. In both solvents, 1-fluoroadamantane was encapsulated by cage **2**[OTf] more strongly than 1,3,5-trifluorobenzene.

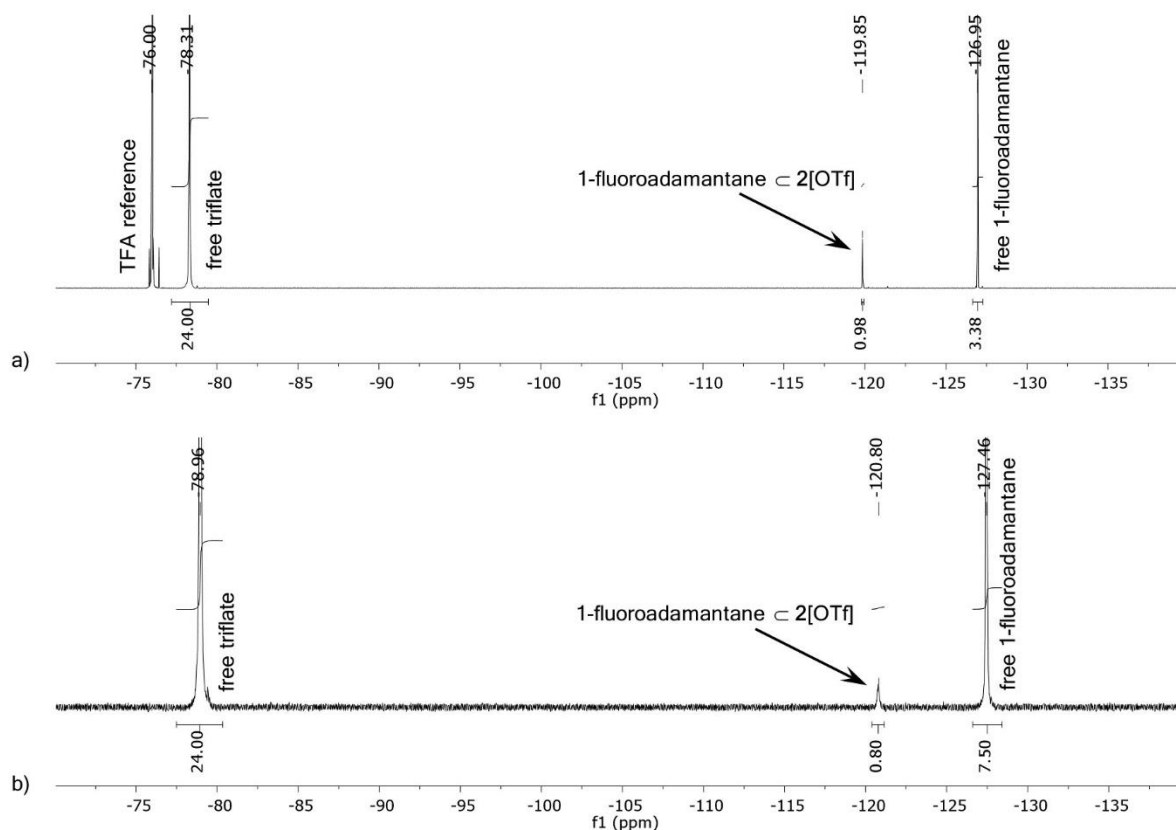


Figure 2.5 a) ^{19}F NMR of 1-fluoroadamantane (5 equiv) in a solution of cage **2**[OTf] in CD_3CN (3.3 mM). $^{19}\text{F}\{^1\text{H}\}$ NMR (471 MHz, referenced to TFA in an acetone- d_6 capillary): $\delta_{\text{F}} = -78.31$ (free triflate, counterion for cage **2**[OTf]), -119.85 (1-fluoroadamantane \subset **2**[OTf]), -126.95 (free 1-fluoroadamantane). b) ^{19}F NMR of 1-fluoroadamantane (5 equiv) in a solution of cage **2**[OTf] in $[\text{emim}][\text{EtOSO}_3]$ (3.3 mM). $^{19}\text{F}\{^1\text{H}\}$ NMR (471 MHz, referenced to triflate): $\delta_{\text{F}} = -78.96$ (free triflate, counterion for cage **2**[OTf]), -120.80 (1-fluoroadamantane \subset **2**[OTf]), -127.46 (free 1-fluoroadamantane).

Additionally, UV-Vis spectrophotometry was used to analyse samples of 1-fluoroadamantane \subset **2**[OTf] in $[\text{emim}][\text{EtOSO}_3]$ and in acetonitrile (Figures 2.6 and 2.7). In each solvent, samples containing the only the guest, both the guest and cage, or only the cage were compared.

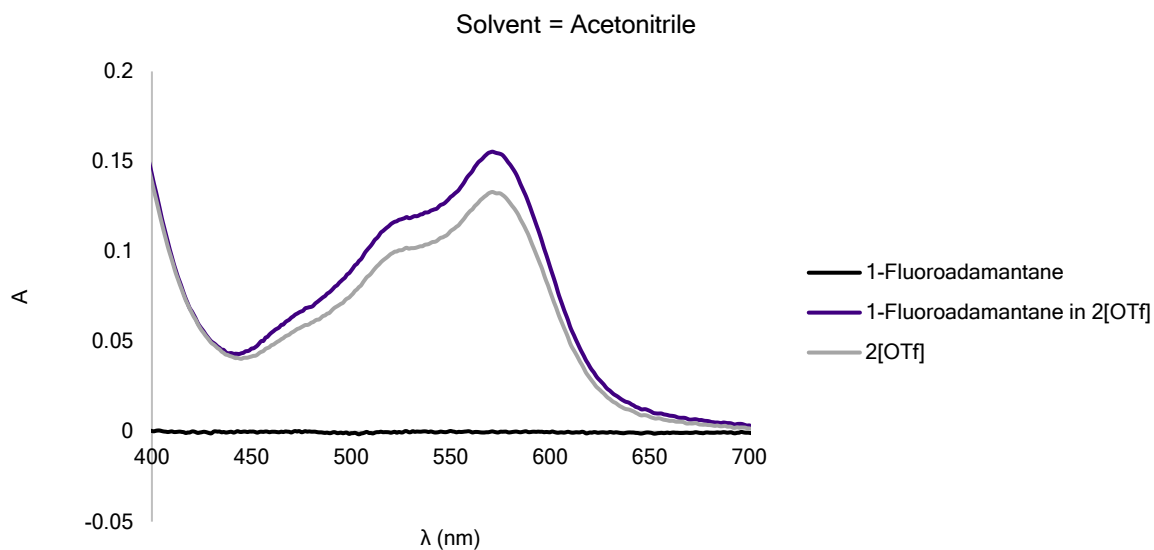


Figure 2.6 UV-Vis spectrum of 1-fluoroadamantane, 1-fluoroadamantane \subset 2[OTf], and cage 2[OTf] in acetonitrile.

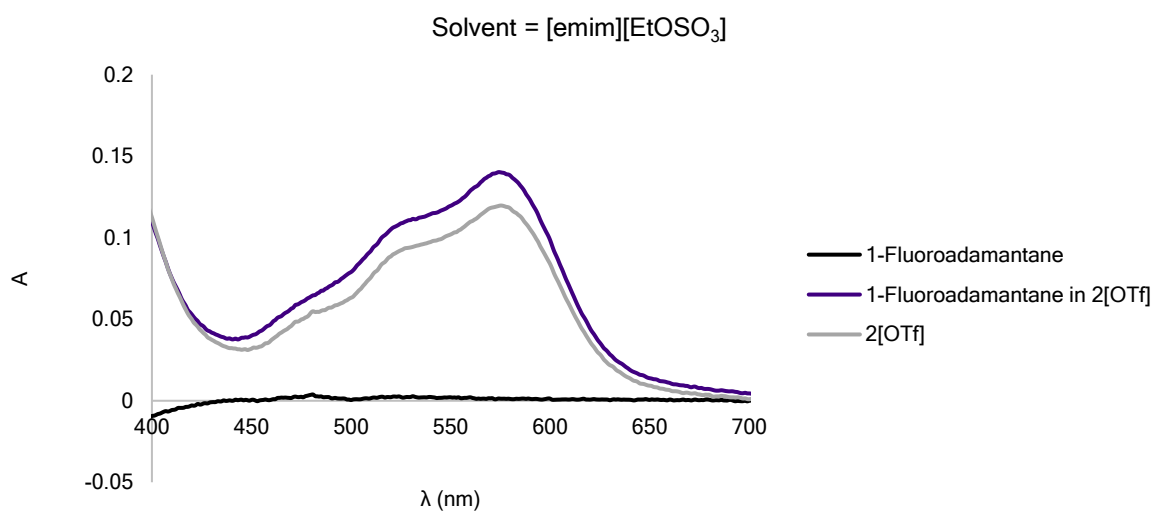


Figure 2.7 UV-Vis spectrum of 1-fluoroadamantane, 1-fluoroadamantane \subset 2[OTf], and cage 2[OTf] in [emim][EtOSO₃].

Upon guest encapsulation, no shift in the MLCT band was observed in acetonitrile or the ionic liquid. UV-Vis spectrophotometry cannot, therefore, be used to measure the binding constants of these host-guest systems. The maximum absorbance of cage 2[OTf] in [emim][EtOSO₃] ($\lambda_{\text{max}} = 574$ nm), however, is close to that of cage 2[OTf] in acetonitrile ($\lambda_{\text{max}} = 571$ nm); the 3 nm difference likely solvent-dependent. Furthermore, the characteristic shape of the UV-Vis

spectrum by the cage in [emim][EtOSO₃] is indistinguishable from the spectrum in acetonitrile. Taken together with the ¹⁹F NMR data presented above, this UV-Vis data serves as further evidence that cage **2**[OTf] persists and behaves similarly in both acetonitrile and [emim][EtOSO₃].

2.2.3 Competitive guest binding within coordination cages in an ionic liquid

In water and acetonitrile, strongly binding guests have been shown to displace weakly binding guests within coordination cages.^{35,36} Competition experiments carried out using a cage in ionic liquid solution were undertaken in order to further probe whether guest encapsulation proceeds similarly in ionic liquids as in water and organic solvents. Two fluorinated guests, 1,3,5-trifluorobenzene and 1-fluoroadamantane, were added to separate solutions of cage **2**[OTf] dissolved in [emim][EtOSO₃]. After one week, the binding constants of the two guests were determined by integrating the ¹⁹F NMR signals from the free and encapsulated species (see the end of this section for calculations). 1-Fluoroadamantane ($K_a = 160 \text{ M}^{-1}$) was observed to bind more strongly than 1,3,5-trifluorobenzene ($K_a = 80 \text{ M}^{-1}$), which in turn bound more strongly than triflate ($K_a = 4.4 \text{ M}^{-1}$), the counterion for **2**[OTf] (Figures 2.8, 2.9, and 2.10). No significant change to the ¹⁹F NMR spectrum was observed after an additional week, indicating that equilibrium had been attained (see the end of this section for a short discussion on the kinetics and thermodynamics of this system).

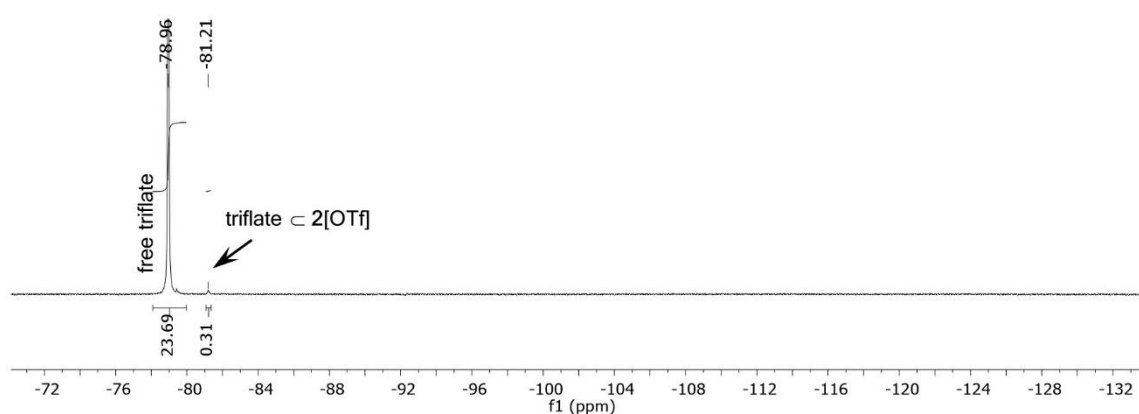


Figure 2.8 ¹⁹F NMR of a solution of cage **2**[OTf] in [emim][EtOSO₃] (3.3 mM). ¹⁹F{¹H} NMR (471 MHz, referenced to triflate): $\delta_F = -78.96$ (free triflate, counterion for cage **2**[OTf]), -81.21 (triflate \subset **2**[OTf]).

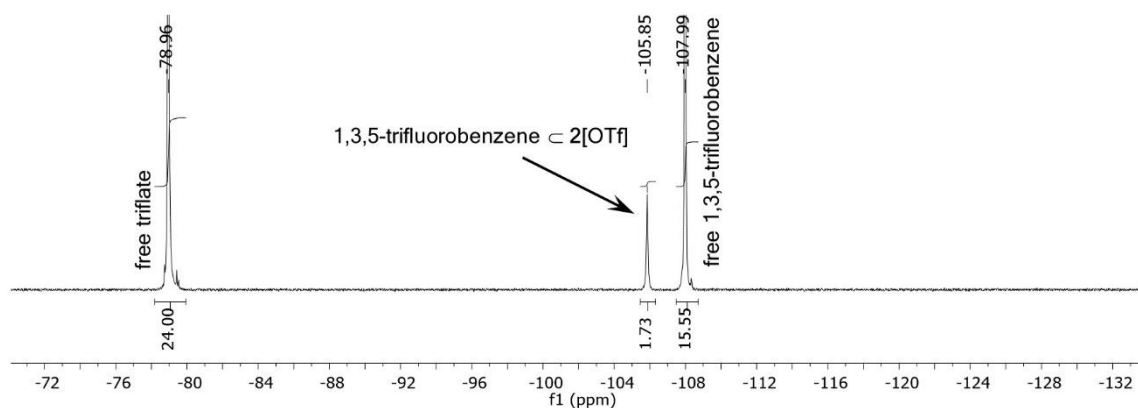


Figure 2.9 ^{19}F NMR of 1,3,5-trifluorobenzene (5 equiv) in a solution of cage **2**[OTf] in [emim][EtOSO₃] (3.3 mM). $^{19}\text{F}\{^1\text{H}\}$ NMR (471 MHz, referenced to triflate): $\delta_{\text{F}} = -78.96$ (free triflate, counterion for cage **2**[OTf]), -105.85 (1,3,5-trifluorobenzene \subset **2**[OTf]), -107.99 (free 1,3,5-trifluorobenzene).

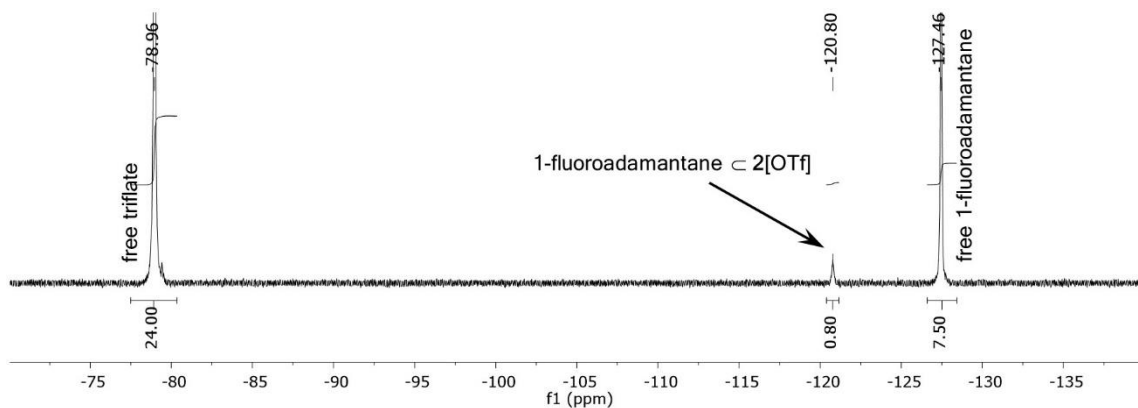


Figure 2.10 ^{19}F NMR of 1-fluoroadamantane (5 equiv) in a solution of cage **2**[OTf] in [emim][EtOSO₃] (3.3 mM). $^{19}\text{F}\{^1\text{H}\}$ NMR (471 MHz, referenced to triflate): $\delta_{\text{F}} = -78.96$ (free triflate, counterion for cage **2**[OTf]), -120.80 (1-fluoroadamantane \subset **2**[OTf]), -127.46 (free 1-fluoroadamantane).

Based on these affinity differentials, we designed a sequence of guest exchanges involving **2**[OTf] dissolved in [emim][EtOSO₃] (Figure 2.11).

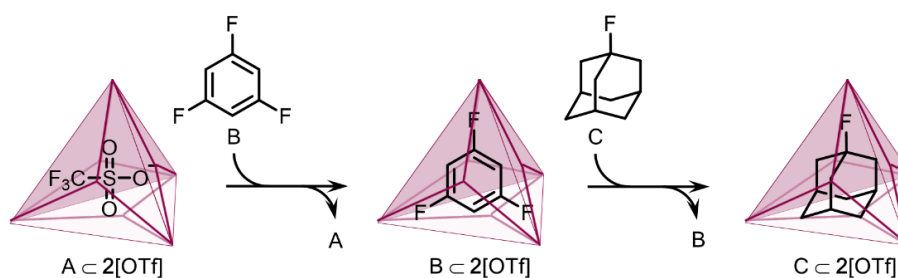


Figure 2.11 Selective guest exchange within **2**[OTf] dissolved in [emim][EtOSO₃], based upon affinity differentials. Figure adapted from reference 1.

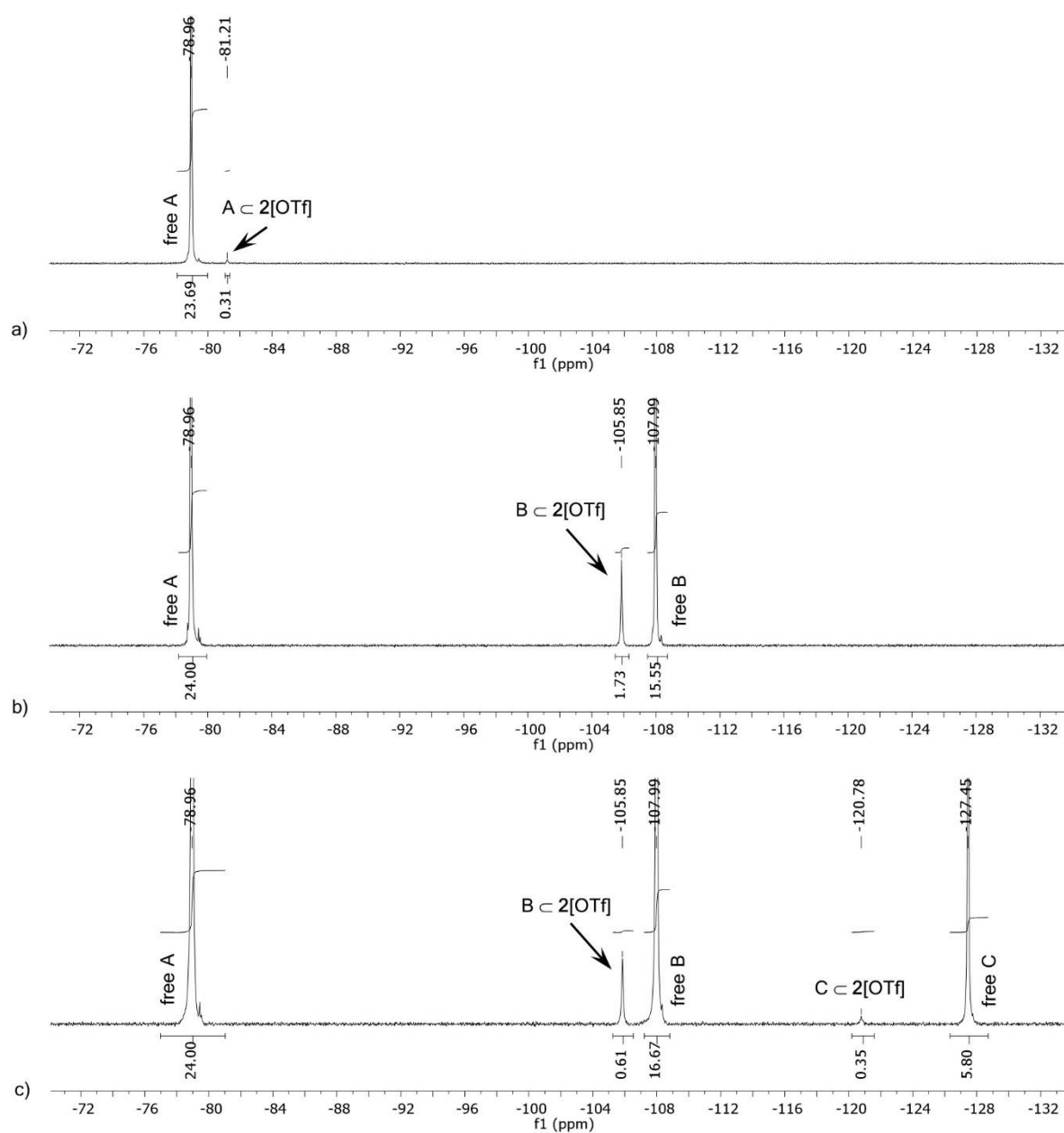


Figure 2.12 a) 3.3 mM solution of cage **2**[OTf] dissolved in [emim][EtOSO₃]. $^{19}\text{F}\{^1\text{H}\}$ NMR (471 MHz, referenced to triflate): $\delta_{\text{F}} = -78.96$ (23.69F, free triflate, counterion for cage **2**[OTf]), -81.21 (0.31F, triflate \subset **2**[OTf]). b) Solution from a) after the addition of 1,3,5-trifluorobenzene (5 equiv) and stirring for 1 week. $^{19}\text{F}\{^1\text{H}\}$ NMR (471 MHz, referenced to triflate): $\delta_{\text{F}} = -78.96$ (24.00F, free triflate), -105.85 (1.73F, 1,3,5-trifluorobenzene \subset **2**[OTf]), -107.99 (15.55F, free 1,3,5-trifluorobenzene). c) Solution from b) after the addition of 1-fluoroadamantane (5 equiv) and stirring for 1 week. $^{19}\text{F}\{^1\text{H}\}$ NMR (471 MHz, referenced to triflate): $\delta_{\text{F}} = -78.96$ (24.00F, free triflate), -105.85 (0.61F, 1,3,5-trifluorobenzene \subset **2**[OTf]), -107.99 (16.67F, free 1,3,5-trifluorobenzene), -120.78 (0.35F, 1-fluoroadamantane cage **2**[OTf]), 127.45 (5.80F, free 1-fluoroadamantane).

Initially, ^{19}F NMR signals for both free and encapsulated triflate were observed (Figure 2.12a). After the addition of 1,3,5-trifluorobenzene (5 equiv), the signal for encapsulated triflate

disappeared and was replaced by peaks assigned to free and encapsulated 1,3,5-trifluorobenzene (Figure 2.12b), indicating that 1,3,5-trifluorobenzene had replaced bound triflate. Following the addition of 1-fluoroadamantane (5 equiv), the peak for encapsulated 1,3,5-trifluorobenzene diminished in intensity and peaks assigned to free and encapsulated 1-fluoroadamantane appeared (Figure 2.12c). Using the free triflate signal as a point of comparison, the proportion of cage 2[OTf] binding 1,3,5-trifluorobenzene was determined to be 58% before and 20% after the addition of 1-fluoroadamantane (see below for calculations). The decrease in the proportion of cage binding 1,3,5-trifluorobenzene indicated that 1-fluoroadamantane displaced the more weakly binding 1,3,5-trifluorobenzene, as anticipated based upon their binding constants.

Calculation of binding constants

Binding constants were calculated using the following equation.

$$K_a = \frac{[XA]}{[X][A]} \quad \text{Equation 2.1}$$

[XA] is the molar concentration of the host-guest complex; [X] is the molar concentration of the empty cage; and [A] is the molar concentration of the free guest. From a known amount of cage sample, the moles of cage and the moles of triflate were calculated. After calculating the moles of triflate, the triflate peak(s) were used as the standard for further integration. By integrating the free and encapsulated guest peaks and factoring in the number of fluorine atoms per mole of guest, the moles of free guest (A) and the moles of host-guest complex (XA) could be determined. Subtracting the moles of host-guest complex from the moles of cage in the initial sample gives the moles of empty cage (X), Table 2.1. A known volume of solvent was also used, which allowed the calculation of [A], [XA], and [X] from A, XA, and X respectively.

Table 2.1 Calculation of binding constants of guest 2[OTf] in [emim][EtOSO₃]

Guest:	Integral of Triflate:	F from Triflate (mol):	F per Guest:	Integral of Encapsulated Guest:	XA (mol):	Integral of Free Guest:	A (mol):	X (mol):	Volume (L):	K _a :
Triflate	24	3.95x10 ⁻⁵	3	0.31	1.70x10 ⁻⁷	23.69	1.30x10 ⁻⁵	1.48x10 ⁻⁶	0.0005	4.4
1,3,5-Trifluorobenzene	24	3.95x10 ⁻⁵	3	1.73	9.50x10 ⁻⁷	15.55	8.53x10 ⁻⁶	6.97x10 ⁻⁷	0.0005	80
1-Fluoroadamantane	24	3.95x10 ⁻⁵	1	0.80	1.32x10 ⁻⁶	7.50	1.23x10 ⁻⁵	3.30x10 ⁻⁷	0.0005	160

Table 2.2 Calculation of binding constants of guest 2[OTf] in acetonitrile

Guest:	Integral of Triflate:	F from Triflate (mol):	F per Guest:	Integral of Encapsulated Guest:	XA (mol):	Integral of Free Guest:	A (mol):	X (mol):	Volume (L):	K _a :
1,3,5-Trifluorobenzene	24	3.95x10 ⁻⁵	3	0.36	1.98x10 ⁻⁷	8.97	4.92x10 ⁻⁶	1.45x10 ⁻⁶	0.0005	14
1-Fluoroadamantane	24	3.95x10 ⁻⁵	1	0.98	1.61x10 ⁻⁶	3.38	5.57x10 ⁻⁶	3.29x10 ⁻⁸	0.0005	4400

A brief discussion on the kinetics and thermodynamics of this system

We observed that equilibration of host-guest complexes in [emim][EtOSO₃] required more time than in acetonitrile, in which three days were required to approach equilibrium of guests with 2[OTf]. The samples of Figures 2.8, 2.9, and 2.10 were stirred for one week prior to ¹⁹F NMR analysis. No significant change to their ¹⁹F NMR spectra were observed after an additional week. This observation is consistent with host-guest equilibration having occurred. We infer that the high viscosity of the ionic liquid solvent slows the kinetics of guest exchange substantially with respect to prior observations in less viscous solvents.

Based on the binding constants of 1,3,5-trifluorobenzene ($K_a = 80 \text{ M}^{-1}$) and 1-fluoroadamantane ($K_a = 160 \text{ M}^{-1}$) in [emim][EtOSO₃], we would expect the ratio of encapsulated 1-fluoroadamantane to encapsulated 1,3,5-trifluorobenzene to be around 1.9:1 in Figure 2.12c. While the proportion of cage 2[OTf] binding 1,3,5-trifluorobenzene was determined to be 20% after the addition of 1-fluoroadamantane, however, only 35% of all cages bound the more strongly-binding 1-fluoroadamantane guest (ratio of 1.8:1). This suggests that the state analysed in Figure 2.12c had not reached thermodynamic equilibrium after one week of stirring – a timescale which had previously been determined to suffice for the equilibration of samples containing a single guest. We therefore infer that the presence of encapsulated 1,3,5-trifluorobenzene decreases the observed rate at which 1-fluoroadamantane is bound and equilibration is achieved.

2.2.4 Designing a triphasic sorting system

The properties of ionic liquids, such as their polarity and hydrophobicity, can be tuned through the choice of the cation and anion, each of which contribute different characteristics to the bulk liquid.²⁸ Ionic liquids can thus be designed to dissolve different solutes selectively and be rendered mutually miscible or immiscible. In concert with coordination cages, complex phase-sorting behaviour may thus be engineered. In this triphasic system, the triflimide anions in trihexyltetradecylphosphonium triflimide ([P_{6,6,6,14}][NTf₂]) and 1-ethyl-3-methylimidazolium triflimide ([emim][NTf₂]) render these ionic liquids hydrophobic. The large, lipophilic phosphonium and small, more polar imidazolium cations do not associate strongly with each other, making the two ionic liquids mutually immiscible. Together with water, these two ionic liquids form a triphasic system.

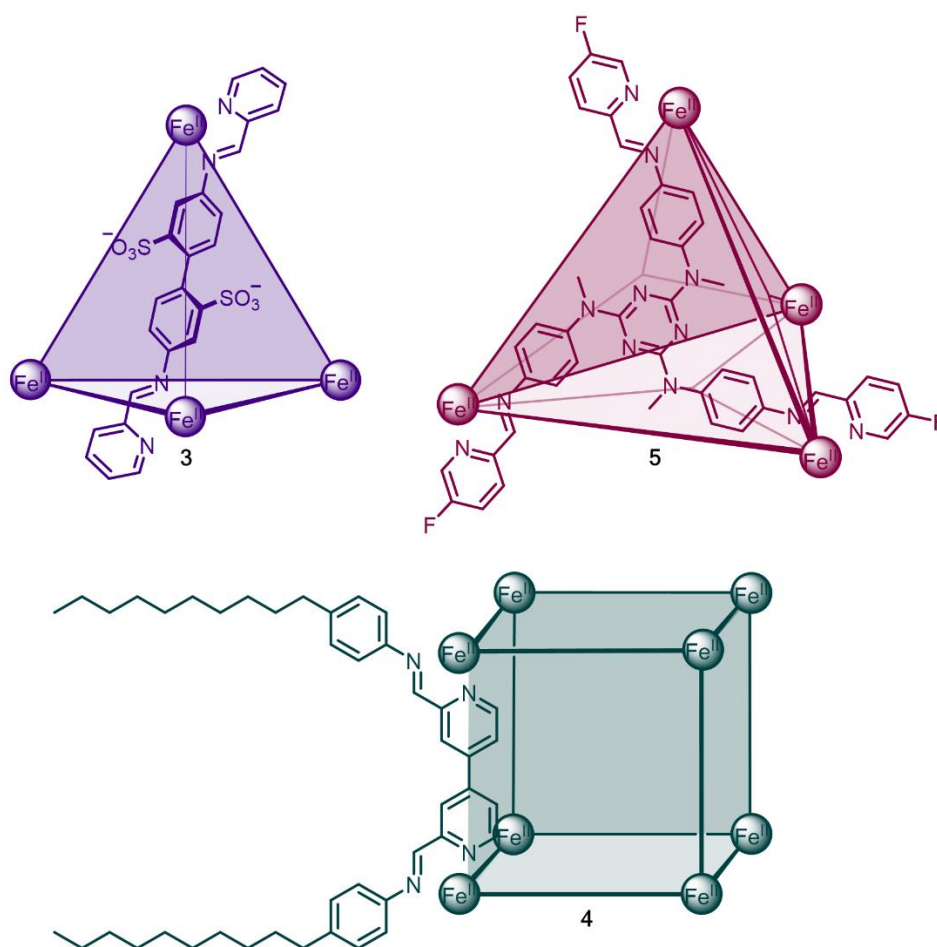


Figure 2.13 Coordination cages **3**, **4**, and **5** as designed for incorporation into a triphasic sorting system. Figure adapted from reference 1.

Cage [Me₄N]**3**³⁴ (Figure 2.13) bears twelve sulfonate groups, rendering this cage highly soluble in water and insoluble in the two hydrophobic ionic liquid layers. Cage **4**[NTf₂]³⁷ (Figure 2.13) is decorated with 24 decyl chains, making it lipophilic and insoluble in water. Although [emim][NTf₂] is hydrophobic, it is also relatively polar – a combination of properties unique to ionic liquids.³⁸ Therefore, only [P_{6,6,6,14}][NTf₂] offers a suitably lipophilic solvent for cage **4**[NTf₂].

Selecting a cage that dissolves readily in [emim][NTf₂] required a nuanced approach. Cages **2**[OTf] and **2**[NTf₂] are only sparingly soluble in [emim][NTf₂], despite having good solubility in the similar ionic liquid, [emim][EtOSO₃]. Since the only difference between these two ionic liquids is their anion, we hypothesised that the more fluoruous environment in [emim][NTf₂] contributed to the poor solubility of cages **2**[OTf] and **2**[NTf₂]. We therefore incorporated

twelve fluorine atoms into the periphery of cage **5**[NTf₂] by employing 5-fluoro-2-formylpyridine as a subcomponent instead of the parent 2-formylpyridine used in the preparation of **2**[OTf] and **2**[NTf₂] (Figure 1.8). This change resulted in a marked increase in the solubility of the cage in [emim][NTf₂], and cage **5**[NTf₂] was therefore used in the sorting system.



Figure 2.14 Equal volumes (0.5 mL) of water (top layer), [P_{6,6,6,14}][NTf₂] (middle layer), and [emim][NTf₂] (bottom layer) were added to each vial. Each vial was shaken vigorously for 10 seconds and allowed to settle before the photo was taken. a) Cage [Me₄N]**3** was soluble only in water. b) Cage **4**[NTf₂] was soluble only in [P_{6,6,6,14}][NTf₂]. c) Cage **5**[NTf₂] was soluble only in [emim][NTf₂]. Figure taken from reference 1.

As seen in Figure 2.14, the affinity of each cage ([Me₄N]**3**, **4**[NTf₂], and **5**[NTf₂]) for its designated layer was visually conspicuous. Each of three vials were filled with 0.5 mL of each phase (water, [P_{6,6,6,14}][NTf₂] and [emim][NTf₂]); and solid samples of cage [Me₄N]**3**, **4**[NTf₂], and **5**[NTf₂] were added to the first, second, and third vials, respectively. After the addition of cage, all vials were shaken vigorously and the phases were allowed to settle. Cage [Me₄N]**3** was thus observed to be soluble only in water (Figure 2.14; left vial), whereas cage **4**[NTf₂] dissolved only in [P_{6,6,6,14}][NTf₂] (Figure 2.14; centre vial), and cage **5**[NTf₂] only in [emim][NTf₂] (Figure 2.14; right vial).

By considering the partially overlapping guest-binding preferences of the three cages in Figure 2.13, we were able to bring about a situation wherein each host bound a single guest selectively in its respective phase. Many of the guests bound by cage [Me₄N]**3** can also be encapsulated by cage **5**[NTf₂]. In water, benzene binds strongly to [Me₄N]**3** and weakly to the fluorine-free analogue of **5**[NTf₂] (cage **2**[NTf₂]).^{33,39} We therefore selected 1-fluorobenzene as a guest for [Me₄N]**3**. Cage **4**[NTf₂] has been previously shown to encapsulate 9-acetylanthracene in

cyclohexane.³⁷ Since a fluorinated guest is required for this experiment, 9-trifluoroacetylanthracene was chosen as a guest for cage **4**[NTf₂]. This guest is too large to bind inside [Me₄N]**3** or **5**[NTf₂] and therefore can only be encapsulated by **4**[NTf₂]. Cage **2**[OTf] has been previously shown to encapsulate adamantane with high affinity in acetonitrile;³³ 1-fluoroadamantane was therefore selected as a guest for cage **5**[NTf₂].

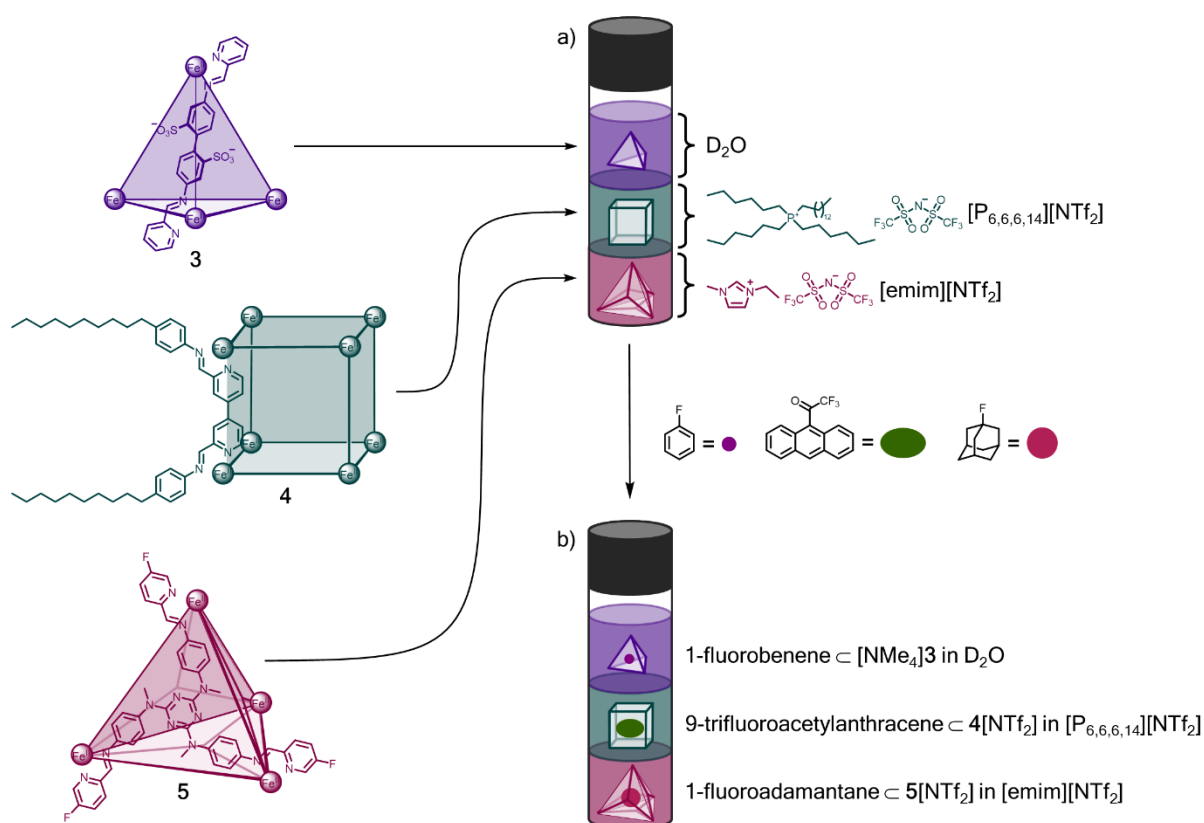


Figure 2.15 Within a triphasic system, cages [Me₄N]**3**, **4**[NTf₂] and **5**[NTf₂] were observed to partition selectively into D₂O, [P_{6,6,6,14}][NTf₂], and [emim][NTf₂], and to bind selectively 1-fluorobenzene, 9-trifluoroacetylanthracene, and 1-fluoroadamantane, respectively. Figure adapted from reference 1.

To a triphasic mixture of cage [Me₄N]**3** in water (5.0 mM), cage **4**[NTf₂] in [P_{6,6,6,14}][NTf₂] (1.5 mM), and cage **5**[NTf₂] in [emim][NTf₂] (1.5 mM), 30 equiv each (relative to [Me₄N]**3**, **4**[NTf₂] or **5**[NTf₂]) of 1-fluorobenzene, 9-trifluoroacetylanthracene, and 1-fluoroadamantane were added. The mixture was stirred for 2 weeks at 298 K. A control experiment, in which identical amounts of the three phases and guests were present, but no cages, was set up and stirred in parallel. The layers were then allowed to separate, and each layer was isolated for analysis by ¹⁹F NMR.

2.2.5 Characterisation of a triphasic sorting system

While the three layers (water, $[P_{6,6,6,14}][NTf_2]$, and $[emim][NTf_2]$) are mutually immiscible, they have some degree of mutual solubility. It has been shown that alkyl imidazolium ionic liquids with triflimide anions form micelles in aqueous solution above a certain critical concentration.⁴⁰ As seen in Figure 2.16, a triflimide peak with the same chemical shift as $[emim][NTf_2]$ was observed in the ^{19}F NMR spectrum of the water layer – we therefore infer that the bottom layer of our experiment formed $[emim][NTf_2]$ micelles in the water layer.

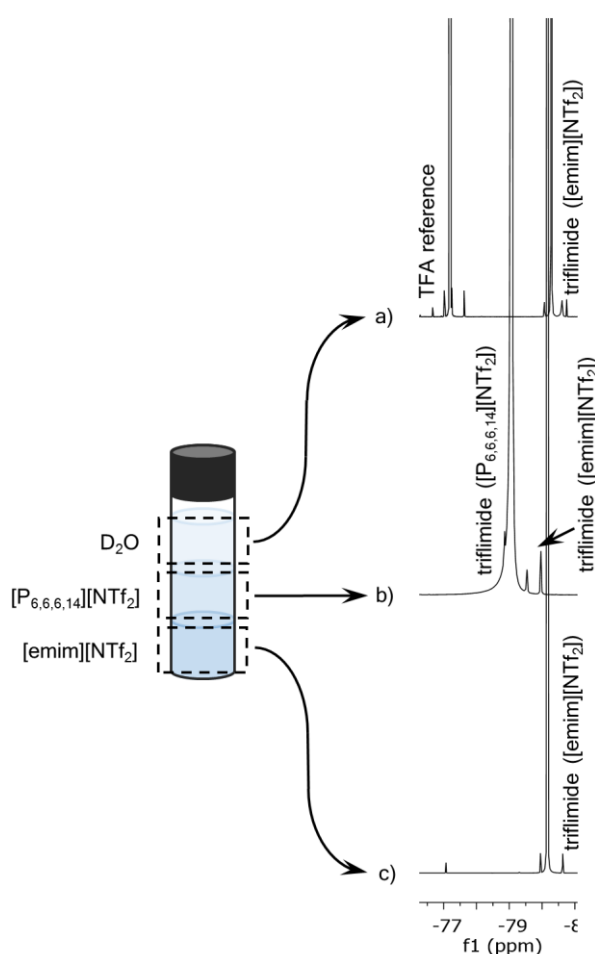


Figure 2.16 a) ^{19}F NMR of top layer (D_2O) of no cages / 3 phases / 3 guests control experiment; triflimide region. See Figure 2.18a for full spectrum. b) ^{19}F NMR of middle layer ($[P_{6,6,6,14}][NTf_2]$) of no cages / 3 phases / 3 guests control experiment; triflimide region. See Figure 2.19a for full spectrum. c) ^{19}F NMR of bottom layer ($[emim][NTf_2]$) of no cages / 3 phases / 3 guests control experiment. See Figure 2.20a for full spectrum.

Additionally, the two ionic liquid layers were difficult to separate entirely, as they interacted strongly with the sides of the glass vials and glass pipettes used for this experiment. As a result,

small droplets from the bottom layer were observed in the final “isolated” middle layer. These small droplets behaved similarly as the micelles discussed above, resulting in ^{19}F signals from [emim][NTf₂] in the NMR spectrum for the [P_{6,6,6,14}][NTf₂] layer.

Within the triphasic system with cages in each layer, a ^{19}F NMR peak was observed for encapsulated 1-fluorobenzene \subset [Me₄N]**3** in the top D₂O layer (Figure 2.17a). No peaks were observed for any free guests in water because all three guests were preferentially soluble in the ionic liquid layers. In the middle layer (**4**[NTf₂] in [P_{6,6,6,14}][NTf₂]), ^{19}F NMR peaks were observed for encapsulated 9-trifluoroacetylanthracene, free 9-trifluoroacetylanthracene, free triflimide, free 1-fluorobenzene, and free 1-fluoroadamantane (Figure 2.17b). In the bottom layer (**5**[NTf₂] in [emim][NTf₂]), ^{19}F NMR peaks were observed for 1-fluoroadamantane \subset **5**[NTf₂], free 9-trifluoroacetylanthracene, free triflimide, free 1-fluorobenzene, and free 1-fluoroadamantane (Figure 2.17c). The cage in each layer thus encapsulated the guest that it was previously observed to bind most strongly.

A peak with the same chemical shift as free 1-fluorobenzene in [emim][NTf₂] was observed in the water layer (Figure 2.17a) and the [P_{6,6,6,14}][NTf₂] layer (Figure 2.17b). We therefore infer that these peaks result from 1-fluorobenzene dissolved in the [emim][NTf₂] micelles present in the water phase and from small droplets of [emim][NTf₂] present in the [P_{6,6,6,14}][NTf₂] layer.

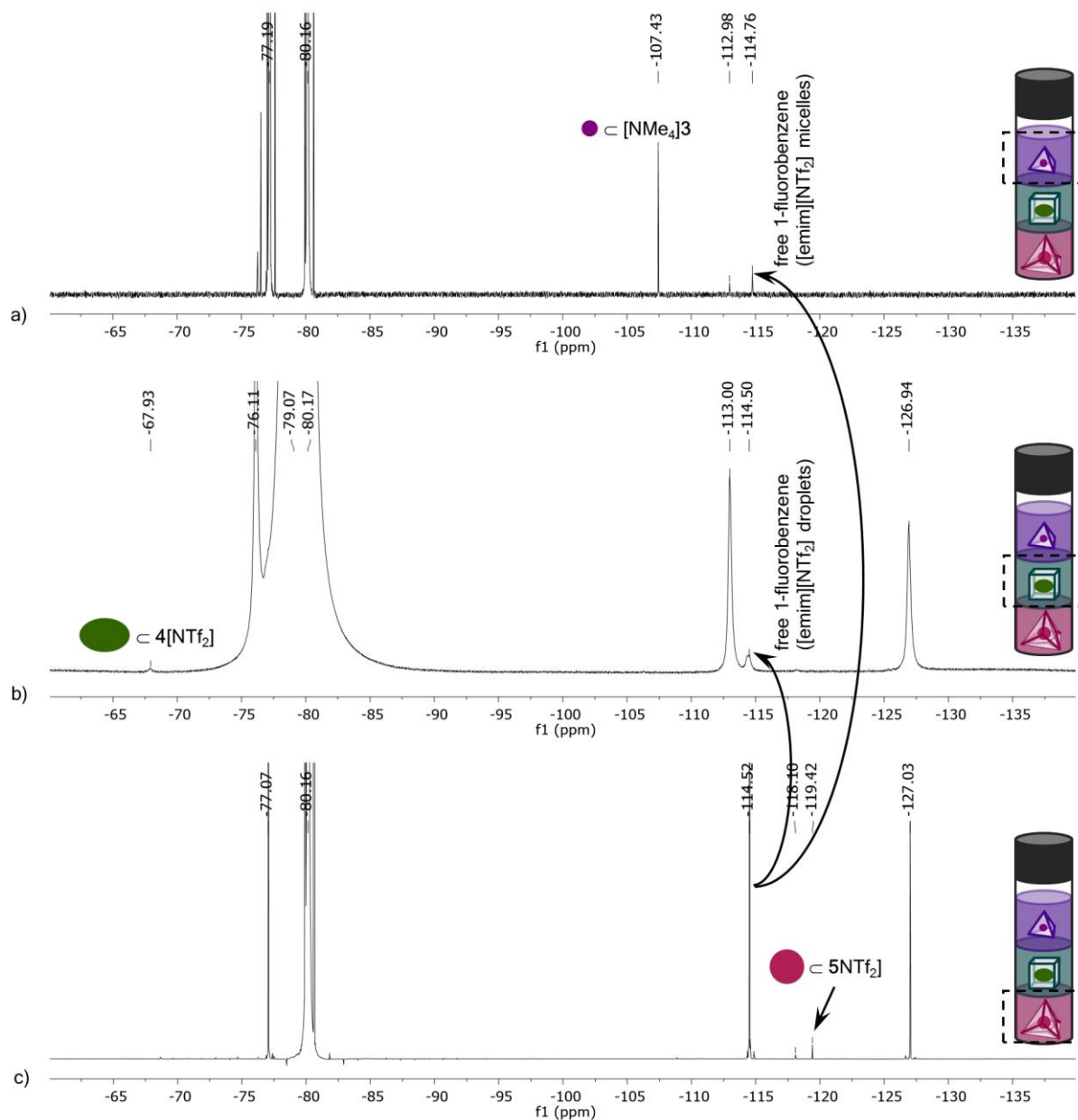


Figure 2.17 a) ^{19}F NMR of top layer (D_2O) of 3 cages / 3 phases / 3 guests experiment. See Figure 2.18b for chemical shifts. b) ^{19}F NMR of middle layer ($[\text{P}_{4,4,4,16}][\text{NTf}_2]$) of 3 cages / 3 phases / 3 guests experiment. See Figure 2.19b for chemical shifts. c) ^{19}F NMR of bottom layer ($[\text{emim}][\text{NTf}_2]$) of 3 cages / 3 phases / 3 guests experiment. See Figure 2.20b for chemical shifts.

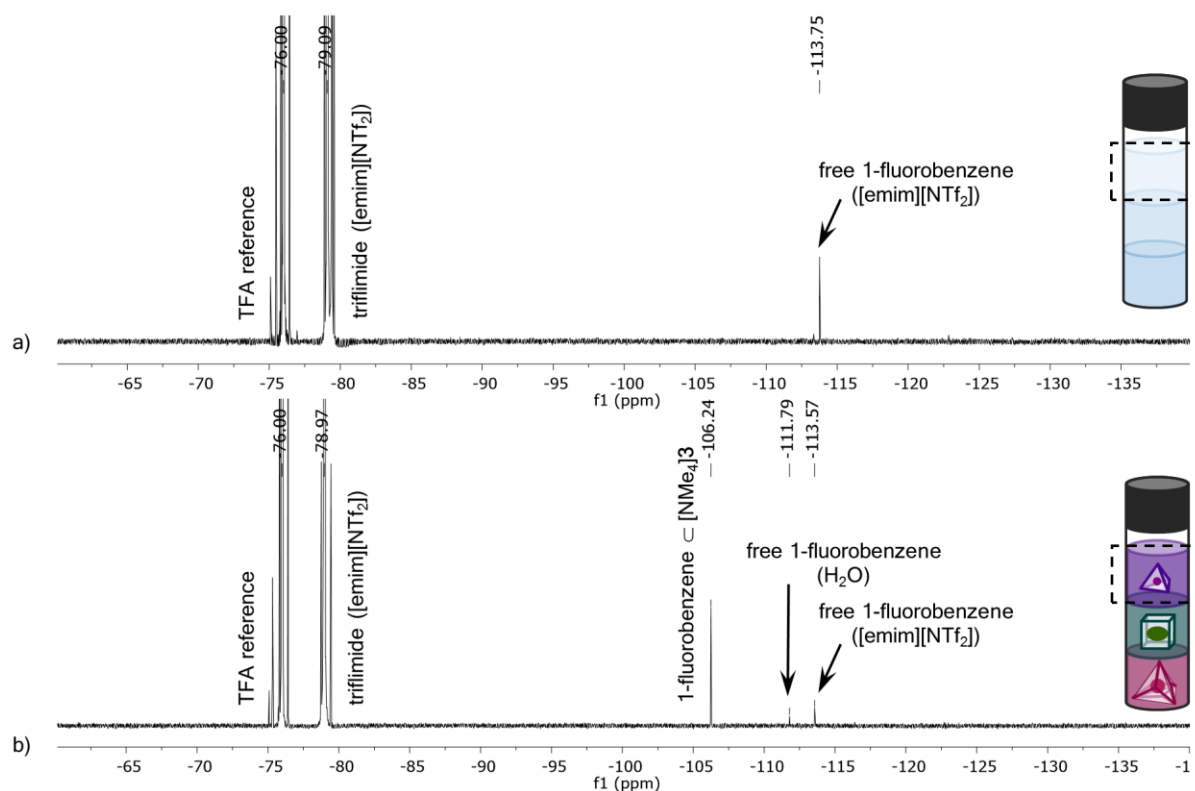


Figure 2.18 a) ^{19}F NMR of top layer (D_2O) of control experiment (no cages / 3 phases / 3 guests). $^{19}\text{F}\{^1\text{H}\}$ NMR (471 MHz, referenced to TFA in an acetone- d_6 capillary): $\delta_{\text{F}} = -79.09$ (triflimide from $[\text{emim}][\text{NTf}_2]$), -113.75 (free 1-fluorobenzene from $[\text{emim}][\text{NTf}_2]$). b) ^{19}F NMR of top layer (D_2O) of 3 cages / 3 phases / 3 guests experiment. 5.0 mM solution of cage $[\text{Me}_4\text{N}]\mathbf{3}$. $^{19}\text{F}\{^1\text{H}\}$ NMR (471 MHz, referenced to TFA in an acetone- d_6 capillary): $\delta_{\text{F}} = -78.97$ (triflimide from $[\text{emim}][\text{NTf}_2]$), -106.24 (1-fluorobenzene $\subset [\text{Me}_4\text{N}]\mathbf{3}$), -111.79 (free 1-fluorobenzene in water), -113.57 (free 1-fluorobenzene from $[\text{emim}][\text{NTf}_2]$).

Immediately after being separated from the two ionic liquid layers, the water layer was analysed by ^{19}F NMR. The peak from free 1-fluorobenzene in water at -111.79 ppm in Figure 2.18b did not occur in this initial spectrum. Since there was a significant quantity of $[\text{emim}][\text{NTf}_2]$ in the water layer (in the form of micelles or very small droplets), the water layer was allowed to settle for several days. The water layer was then pipetted off and analysed again by ^{19}F NMR. During this time, however, the water layer was allowed to begin equilibrating in the absence of the ionic liquid layers, and a small portion of the encapsulated guest left the cage. In the presence of the ionic liquid layers, free 1-fluorobenzene is preferentially dissolved in $[\text{P}_{6,6,6,14}][\text{NTf}_2]$ and $[\text{emim}][\text{NTf}_2]$. When added to water (without other phases present), it occurs at -111.79 ppm.

As discussed above, free 1-fluorobenzene dissolved in [emim][NTf₂] was present as small droplets in [P_{6,6,6,14}][NTf₂]. Consequently, a ¹⁹F signal from free 1-fluorobenzene in [emim][NTf₂] can be observed in the NMR spectrum of the middle layer.

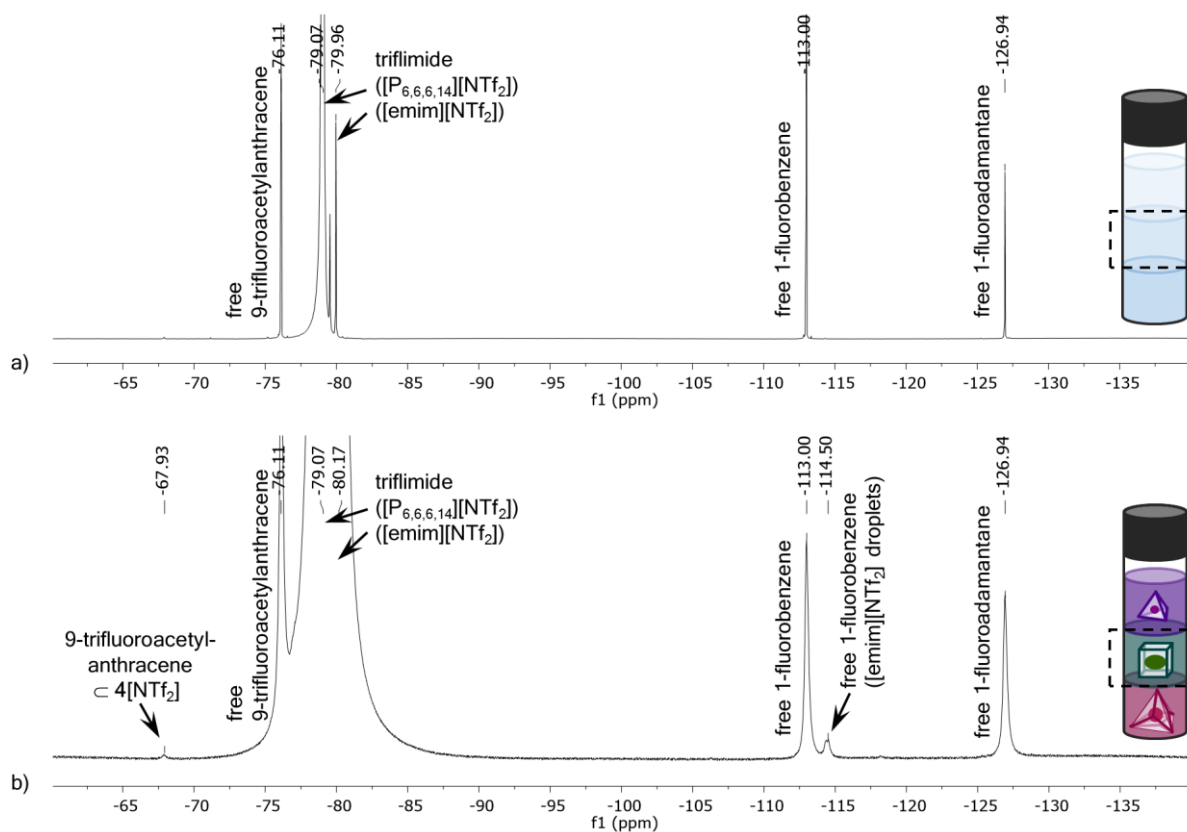


Figure 2.19 a) ¹⁹F NMR of middle layer ([P_{6,6,6,14}][NTf₂]) of control experiment (no cages / 3 phases / 3 guests). ¹⁹F{¹H} NMR (471 MHz, referenced to triflimide from [P_{6,6,6,14}][NTf₂]): δ_F = -76.11 (free 9-trifluoroacetylanthracene), -79.07 (free triflimide from [P_{6,6,6,14}][NTf₂]), -79.96 (free triflimide from [emim][NTf₂]), -113.00 (free 1-fluorobenzene in [P_{6,6,6,14}][NTf₂]), -126.94 (free 1-fluoroadamantane). b) ¹⁹F NMR of middle layer ([P_{6,6,6,14}][NTf₂]) of 3 cages / 3 phases / 3 guests experiment. 1.5 mM solution of cage **4**[NTf₂]. ¹⁹F{¹H} NMR (471 MHz, referenced to triflimide from [P_{6,6,6,14}][NTf₂]): δ_F = -67.93 (9-trifluoroacetyl-anthracene c **4**[NTf₂]), -76.11 (free 9-trifluoroacetylanthracene), -79.07 (free triflimide from [P_{6,6,6,14}][NTf₂]), -80.17 (free triflimide from [emim][NTf₂]), -113.00 (free 1-fluorobenzene in [P_{6,6,6,14}][NTf₂]), -114.50 (free 1-fluorobenzene in [emim][NTf₂]), -126.94 (free 1-fluoroadamantane).

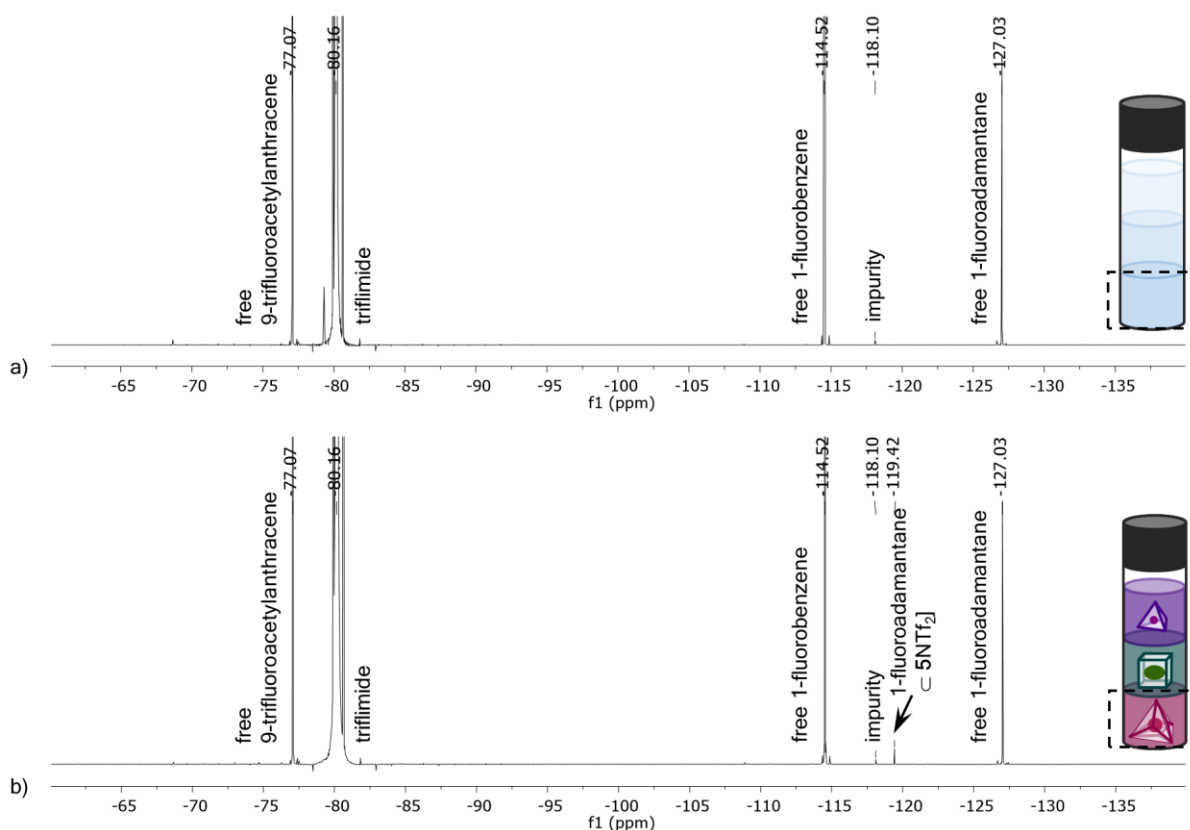


Figure 2.20 a) ^{19}F NMR of bottom layer ($[\text{emim}][\text{NTf}_2]$) of control experiment (no cages / 3 phases / 3 guests). $^{19}\text{F}\{^1\text{H}\}$ NMR (471 MHz, referenced to triflimide from $[\text{emim}][\text{NTf}_2]$): $\delta_{\text{F}} = -77.07$ (free 9-trifluoroacetylanthracene), -80.16 (free triflimide), -114.52 (free 1-fluorobenzene), -118.10 (unknown impurity, originating from the ionic liquid), -127.03 (free 1-fluoroadamantane). b) ^{19}F NMR of bottom layer ($[\text{emim}][\text{NTf}_2]$) of 3 cages / 3 phases / 3 guests experiment. 1.5 mM solution of cage **5** $[\text{NTf}_2]$. $^{19}\text{F}\{^1\text{H}\}$ NMR (471 MHz, referenced to triflimide from $[\text{emim}][\text{NTf}_2]$): $\delta_{\text{F}} = -77.07$ (free 9-trifluoroacetylanthracene), -80.16 (free triflimide), -114.52 (free 1-fluorobenzene), -118.10 (unknown impurity, originating from the ionic liquid), -119.42 (1-fluoroadamantane \subset **5** $[\text{NTf}_2]$), -127.03 (free 1-fluoroadamantane).

In the ^{19}F NMR spectra of the $[\text{emim}][\text{NTf}_2]$ layer above, an impurity that originates from the ionic liquid can be seen at -118.10 ppm.

2.3 Conclusions

In this chapter, ionic liquids have been demonstrated to be versatile solvents for coordination cages. Cage **2** $[\text{OTf}]$ was shown to be soluble, stable, and capable of encapsulating guests in $[\text{emim}][\text{EtOSO}_3]$; host-guest complexes were monitored by ^{19}F NMR. In a series of competition experiments in which cage **2** $[\text{OTf}]$ was dissolved in $[\text{emim}][\text{EtOSO}_3]$, bound triflate was displaced by 1,3,5-trifluorobenzene, and bound 1,3,5-trifluorobenzene was

displaced by 1-fluoroadamantane. Likewise, cage **4**[NTf] was observed to bind 9-trifluoroacetylanthracene in [P_{6,6,6,14}][NTf₂], and **5**[NTf] was observed to bind 1-fluoroadamantane in [emim][NTf₂]. This enabled the design of a triphasic sorting system in which each of three different coordination cages ([Me₄N]**3**, **4**[NTf₂], and **5**[NTf₂]) partitioned selectively into three different liquid phases (water, [P_{6,6,6,14}][NTf₂], and [emim][NTf₂], respectively). Upon the addition of a mixture of three different guests, each cage (in each separate layer) selectively bound 1-fluorobenzene, 9-trifluoroacetylanthracene, or 1-fluoroadamantane, respectively.

This study thus establishes the functionality of guest-binding coordination cages in ionic liquid phases, which have become an increasingly-used alternative to traditional organic solvents,⁴¹ with potential applications in fields as diverse as catalysis,^{42–44} cellulose processing,^{45–47} CO₂ sequestration,⁴⁸ and extraction.⁴⁹ This work adds to the toolbox of complex self-assembled systems^{50–56} by extending the preparation of such systems into new solvents. The triphasic system described here appears extensible, for example, to fluoruous phases. Given the selective guest binding here observed, new applications are envisaged in chemical separations or new phase-transfer catalysis.

2.4 Experimental

2.4.1 General

Reagents and solvents were purchased and used as supplied unless otherwise noted. Water and acetonitrile for cage syntheses were degassed by 3–4 evacuation/N₂ fill cycles prior to use. ¹H NMR spectra were all recorded either at 500 MHz on a Bruker AVC-500 spectrometer with an ATM BB probe or at 400 MHz on a Bruker AVC-400 spectrometer with a QNP probe. ¹³C{¹H} NMR spectra were recorded at 100 MHz on a Bruker AVC-400 spectrometer with a QNP probe. ¹⁹F{¹H} NMR spectra were recorded either at 471 MHz on a Bruker AVC-500 spectrometer with an ATM BB probe or at 376 MHz on a Bruker AVC-400 spectrometer with a QNP probe. ¹H chemical shifts (δ_H) are expressed in parts per million (ppm) and reported relative to the resonance of the residual protons of CDCl₃ (δ_H = 7.26 ppm), CD₃CN (δ_H = 1.94 ppm), or CD₃OD (δ_H = 3.31 ppm) or relative to the internal standard acetone (δ_H = 2.22 ppm) for samples in D₂O. ¹³C chemical shifts (δ_C) are expressed in ppm and reported relative to the resonance of the carbons in CDCl₃ (δ_C = 77.16 ppm) or CD₃OD (δ_C = 49.00 ppm). In organic

solvents and water, ^{19}F chemical shifts (δ_{F}) are reported relative the external standard (contained in a coaxial capillary) trifluoroacetic acid in $(\text{CD}_3)_2\text{CO}$ ($\delta_{\text{F}} = -76.00$ ppm). In neat ionic liquids, ^{19}F chemical shifts are reported relative to the internal standard triflate in [emim][EtOSO₃] ($\delta_{\text{F}} = -78.96$ ppm) or to triflimide in CD_3CN ($\delta_{\text{F}} = -79.33$ ppm), [P_{6,6,6,14}][NTf₂] ($\delta_{\text{F}} = -79.07$ ppm), and [emim][NTf₂] ($\delta_{\text{F}} = -80.16$ ppm). NMR experiments in neat ionic liquids were locked to D₂O contained in a coaxial capillary. All measurements were carried out at 298 K unless stated differently. Abbreviations used in the description of NMR data are as follows: bs, broad singlet; s, singlet; d, doublet; t, triplet; q, quartet; m, multiplet. Coupling constants (J) are given in Hz. Elemental analysis were performed on a Exeter Analytical CE-440 Analyzer at the University of Cambridge, Department of Chemistry, U.K. Low-resolution electrospray ionisation mass spectra (ESI-MS) were obtained on a Micromass Quattro LC, infused from a Harvard Syringe Pump at a rate of 10 μL per minute.

2.4.2 Synthesis

N2,N4,N6-Trimethyl-N2,N4,N6-tris(4-nitrophenyl)-1,3,5-triazine-2,4,6-triamine

Cyanuric chloride (0.369 g, 2.00 mmol), N-methyl-4-nitroaniline (1.07 g, 7.00 mmol), and dioxane (10 mL) were combined in a microwave vial. The reaction mixture was microwaved for 20 minutes at 120 °C. The resulting off-white solid was washed with water (100 mL), methanol (300 mL), and diethyl ether (70 mL) to give the desired product in 78% yield (0.832 g, 1.57 mmol). ^1H and ^{13}C NMR signal matched the values reported in the literature.³³ ^1H NMR (500 MHz, CD_2Cl_2): $\delta_{\text{H}} = 8.14$ (d, $J = 9.1$ Hz, 6H, H_a), 7.50 (d, $J = 9.1$ Hz, 6H, H_b), 3.47 (s, 9H, H_c). $^{13}\text{C}\{^1\text{H}\}$ NMR (125 MHz, CD_2Cl_2): $\delta_{\text{C}} = 165.5, 150.6, 144.5, 126.3, 124.0, 37.3$.

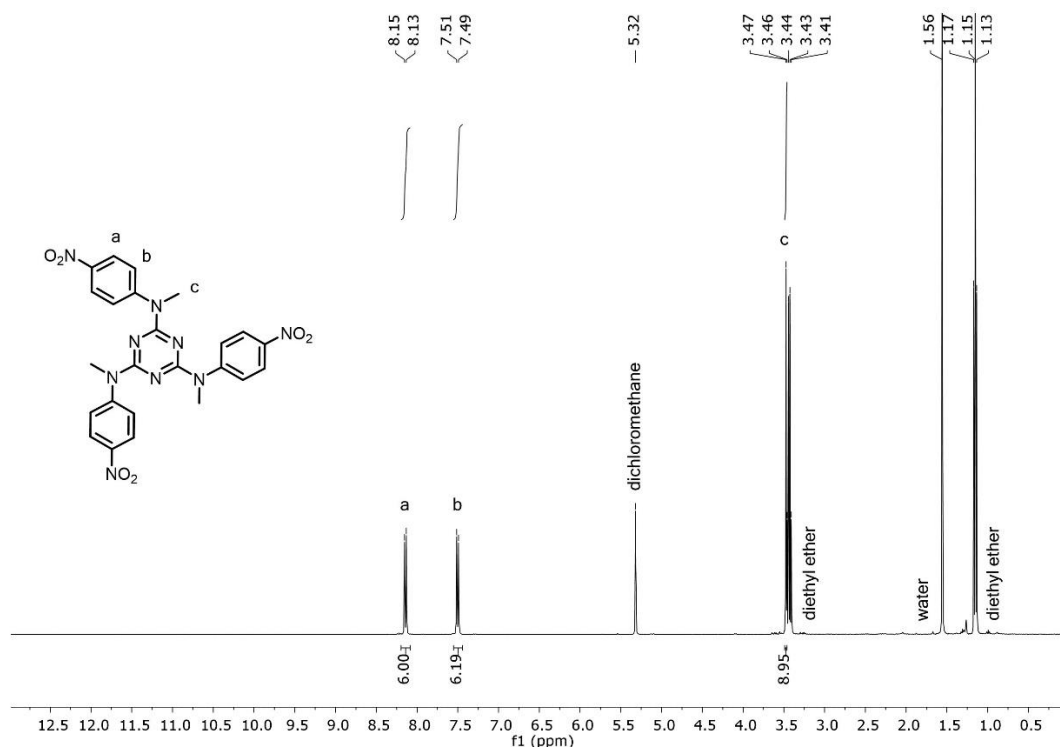


Figure 2.21 ¹H NMR spectrum of N₂,N₄,N₆-trimethyl-N₂,N₄,N₆-tris(4-nitrophenyl)-1,3,5-triazine-2,4,6-triamine in CD₂Cl₂.

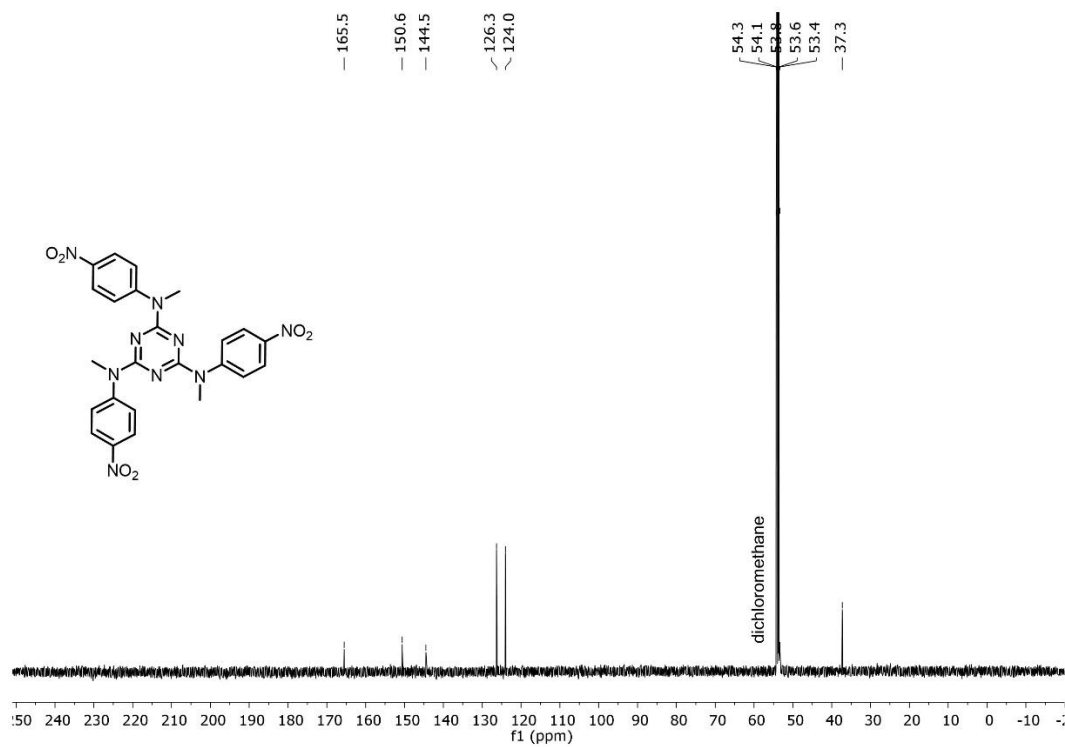


Figure 2.22 ¹³C NMR spectrum of N₂,N₄,N₆-trimethyl-N₂,N₄,N₆-tris(4-nitrophenyl)-1,3,5-triazine-2,4,6-triamine in CD₂Cl₂.

N2,N4,N6-Tris(4-aminophenyl)-N2,N4,N6-trimethyl-1,3,5-triazine-2,4,6-triamine

This compound was synthesised according to a procedure previously described in the literature.

^1H and ^{13}C NMR signals matched the literature values.³³ ^1H NMR (500 MHz, CD_2Cl_2): $\delta_{\text{H}} = 7.03$ (d, $J = 8.5$ Hz, 6H, H_c), 6.58 (d, $J = 8.5$ Hz, 6H, H_b), 3.64 (bs, 6H, H_a), 3.28 (s, 9H, H_d).

$^{13}\text{C}\{^1\text{H}\}$ NMR (125 MHz, CD_2Cl_2): $\delta_{\text{C}} = 166.0, 144.2, 136.6, 127.6, 114.8, 37.5$.

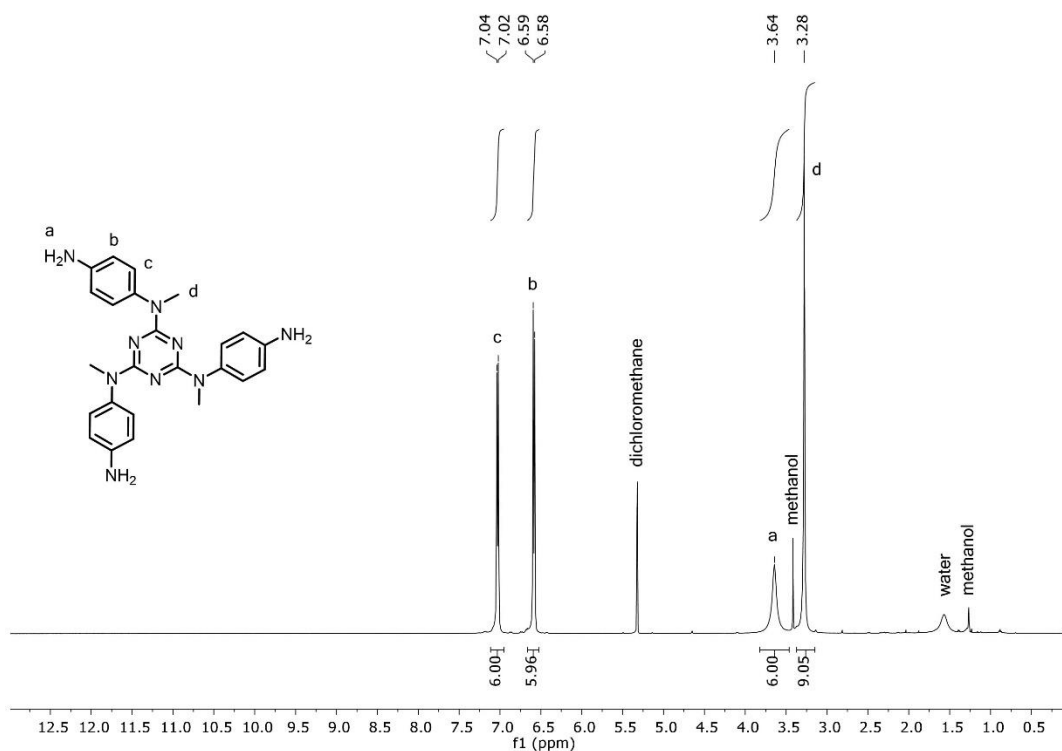


Figure 2.23 ^1H NMR spectrum of *N2,N4,N6-tris(4-aminophenyl)-N2,N4,N6-trimethyl-1,3,5-triazine-2,4,6-triamine* in CD_2Cl_2 .

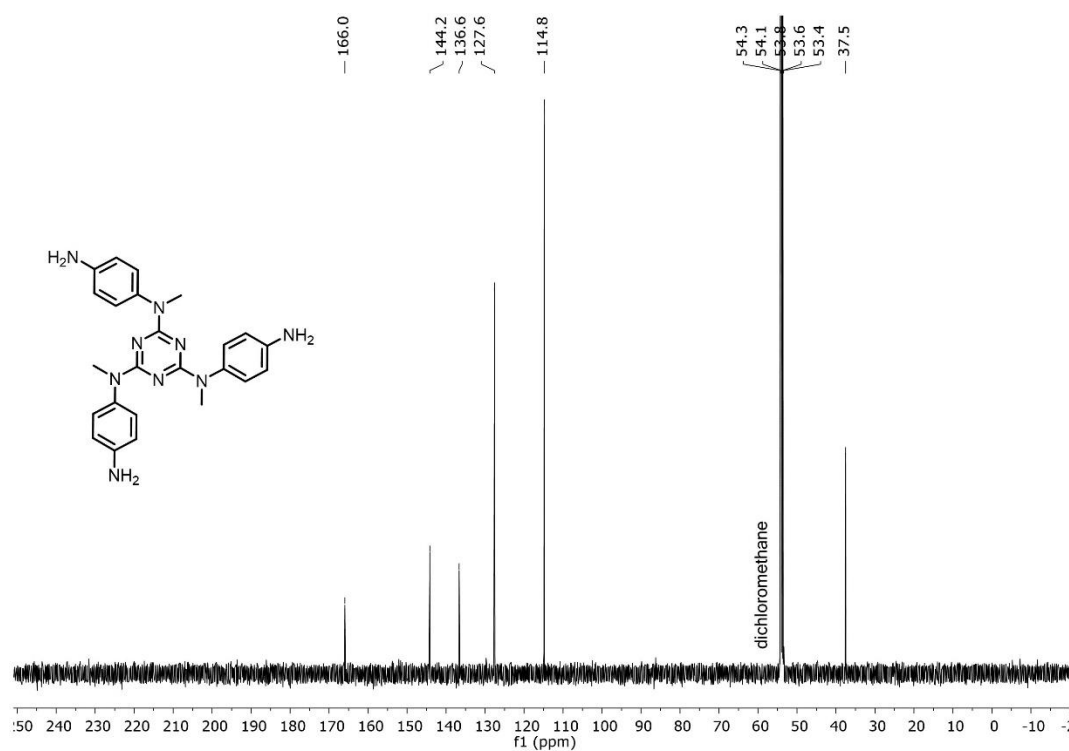


Figure 2.24 ¹³C NMR spectrum of N₂,N₄,N₆-tris(4-aminophenyl)-N₂,N₄,N₆-trimethyl-1,3,5-triazine-2,4,6-triamine in CD₂Cl₂.

Cage 2[OTf]

This cage was synthesised by modifying a procedure previously described in the literature.³³ N₂,N₄,N₆-Tris(4-aminophenyl)-N₂,N₄,N₆-trimethyl-1,3,5-triazine-2,4,6-triamine (0.176 g, 0.4 mmol), 2-formylpyridine (114.15 μL, 1.2 mmol), and iron (II) triflate (0.142 g, 0.4 mmol) were combined in acetonitrile (30 mL). The reaction mixture was then degassed by three evacuation/N₂ fill cycles and stirred at 298 K for 24 hours, during which the solution became deep purple. The product, cage 2[OTf], was precipitated by adding diethyl ether to the solution and isolated by filtration (0.420 g, 0.0987 mmol, 98.7%). ¹H NMR signals matched the values reported in the literature.³³ ¹H NMR (400 MHz, CD₃CN, referenced to acetonitrile): δ_H = 8.90 (s, 12H, H_e), 8.54 (d, J = 7.7 Hz, 12H, H_d), 8.39 (unresolved dd, 12H, H_c), 7.74 (unresolved dd, 12H, H_b), 7.41-7.37 (m, 36H, H_a, H_g), 5.08 (bs, 24H, H_f), 3.41 (s, 36H, H_h).

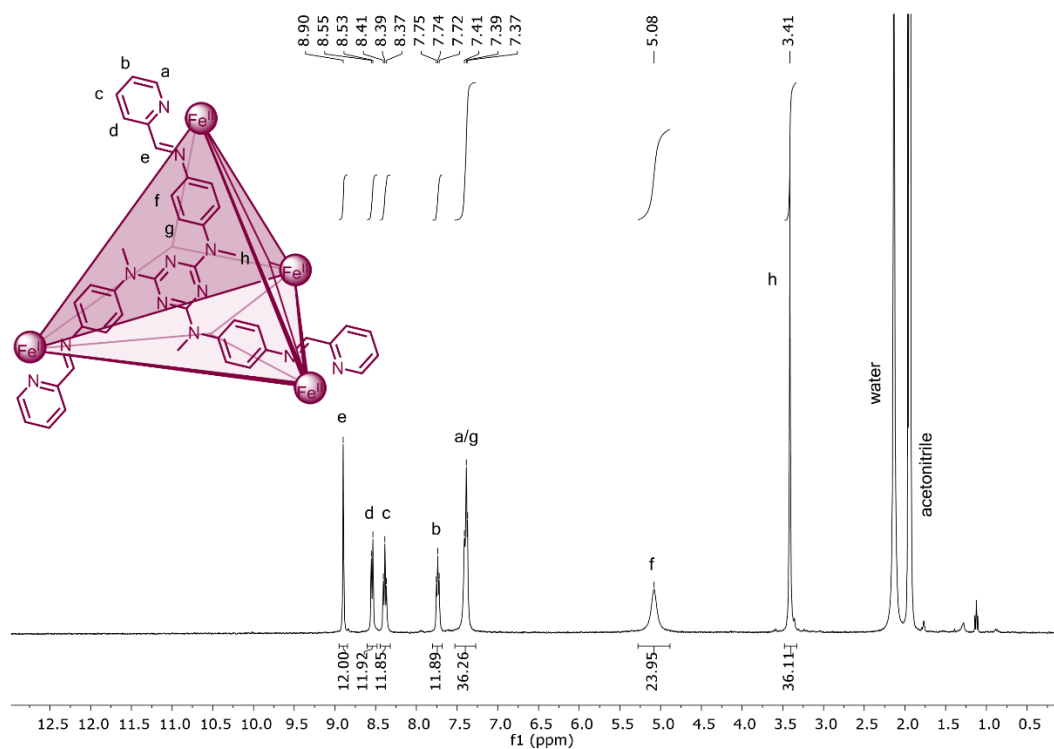


Figure 2.25 ^1H NMR spectrum of $2[\text{OTf}]$ in CD_3CN .

Cage $[\text{Me}_4\text{N}]\mathbf{3}$

This cage was prepared according to a procedure previously described in the literature. ^1H and ^{13}C NMR signals matched the literature values.³⁴ ^1H NMR (400 MHz, D_2O , referenced to acetone): $\delta_{\text{H}} = 9.31$ (s, 12H), 8.69 (d, $J = 6.9$ Hz, 12H), 8.39 (t, $J = 6.9$ Hz, 12H), 7.75 (t, $J = 4.3$ Hz, 12H), 7.52 (d, $J = 4.3$ Hz, 12H), 7.13 (unresolved d, 12H), 6.43 (s, 12H), 5.82 (unresolved d, 12H), 3.18 (s, 48H).

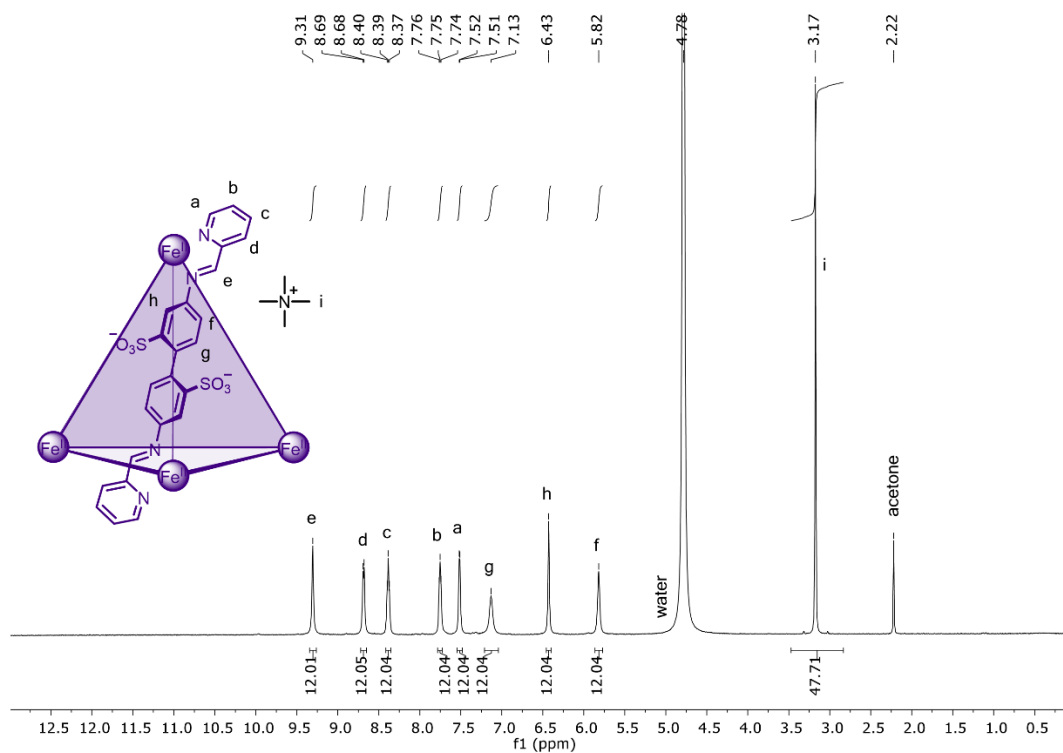


Figure 2.26 ¹H NMR spectrum of [Me₄N]3 in D₂O.

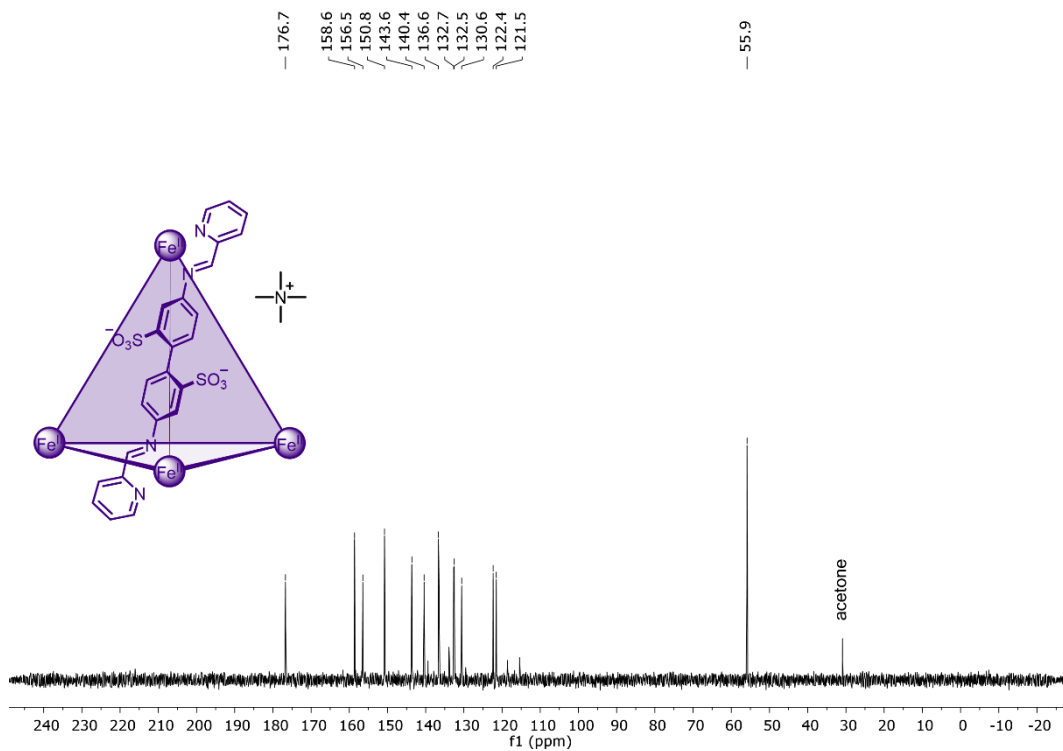


Figure 2.27 ¹³C NMR spectrum of [Me₄N]3 in D₂O.

Cage 4[NTf₂]

This cage was synthesised by Dr Colm Browne according to a procedure described previously in the literature. ¹H and ¹³C NMR signals matched the values reported in the literature.¹ ¹H NMR (500 MHz, CD₃CN, referenced to acetonitrile): δ_H = 9.41 (d, J = 1.5 Hz, 1H), 8.92 (s, 1H), 8.57 (dd, J = 2 Hz, J = 2 Hz, 1H), 7.16 (d, J = 7.5 Hz, 1H), 7.003 (d, J = 10.5 Hz, 2H), 5.49 (d, J = 10.5 Hz, 2H), 2.37 (s, 3H), 1.61 (s, 18H), 1.35 (s, 10H), 1.28 (s, 19H), 0.89 (s, 7H), 0.09 (s, 4H). ¹³C NMR (500 MHz, CD₃CN, reference to acetonitrile): δ_C = 174.7, 159.0, 156.5, 148.3, 144.3, 140.3, 131.9, 126.5, 122.9, 119.2, 32.9, 30.5, 29.5, 23.2, 22.9, 14.2.

Cage 5[NTf₂]

N2,N4,N6-Tris(4-aminophenyl)-N2,N4,N6-trimethyl-1,3,5-triazine-2,4,6-triamine (17.66 mg, 0.04 mmol), 5-fluoro-2-formylpyridine (15.01 mg, 0.12 mmol), and iron (II) triflimide (28.25 mg, 0.04 mmol) were combined in acetonitrile (5 mL). The reaction mixture was then degassed by three evacuation/N₂ fill cycles and stirred at 298 K for 24 hours, during which the solution became deep red. The resulting product, cage **5**[NTf₂], was precipitated from the solution with diethyl ether and isolated by filtration. The spectroscopic data presented below suggest that cage **5**[NTf₂] partially encapsulates its counterion triflimide, which is in slow exchange on the NMR timescale with unbound triflimide. ¹H NMR (400 MHz, CD₃CN, referenced to acetonitrile): δ_H = 8.81 (s, 12H, empty cage, H_e), 8.77 (s, full cage, H_{e'}), 8.57 (dd, J = 5.1 Hz, J = 3.7 Hz, 12H, empty cage, H_d), 8.53 (dd, J = 4.8 Hz, J = 3.2 Hz, full cage, H_{d'}), 8.20 (m, 12H, empty cage, H_c), 7.48 (d, J = 7.7 Hz, full cage, H_g), 7.44 (s, 12H, empty cage, H_a), 7.38 (d, J = 8.8 Hz, 24H, empty cage, H_g), 5.15 (d, J = 8.8 Hz, full cage, H_f), 5.07 (bs, 24H, empty cage, H_f), 3.39 (s, 36H, empty cage, H_h), 3.31 (s, full cage, H_{h'}). ¹⁹F{¹H} NMR (376 MHz, CD₃CN, referenced to triflimide): δ_F = -74.24 (F_i, encapsulated triflimide), -79.33 (F_i, free triflimide), -112.44 (F_b, empty cage), -112.85 (F_b, full cage). ESI-MS: m/z: {[**4**]}⁺⁸ = 409.2, {[**4**] + NTf₂}⁺⁷ = 507.7, {[**4**] + 2NTf₂}⁺⁶ = 639.1, {[**4**] + 3NTf₂}⁺⁵ = 822.9, {[**4**] + 4NTf₂}⁺⁴ = 1098.7.

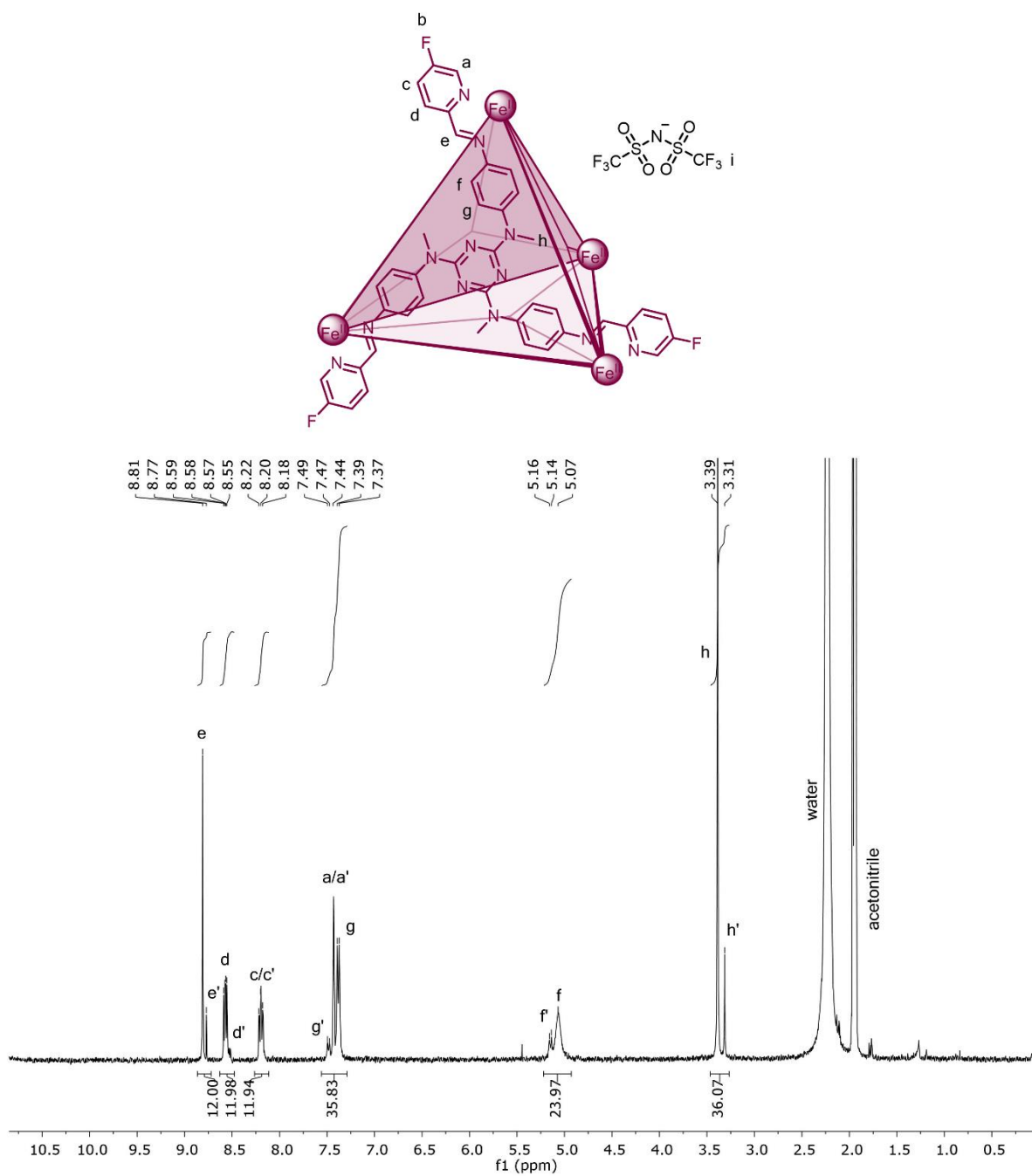


Figure 2.28 ¹H NMR spectrum of 4[NTf₂] in CD₃CN.

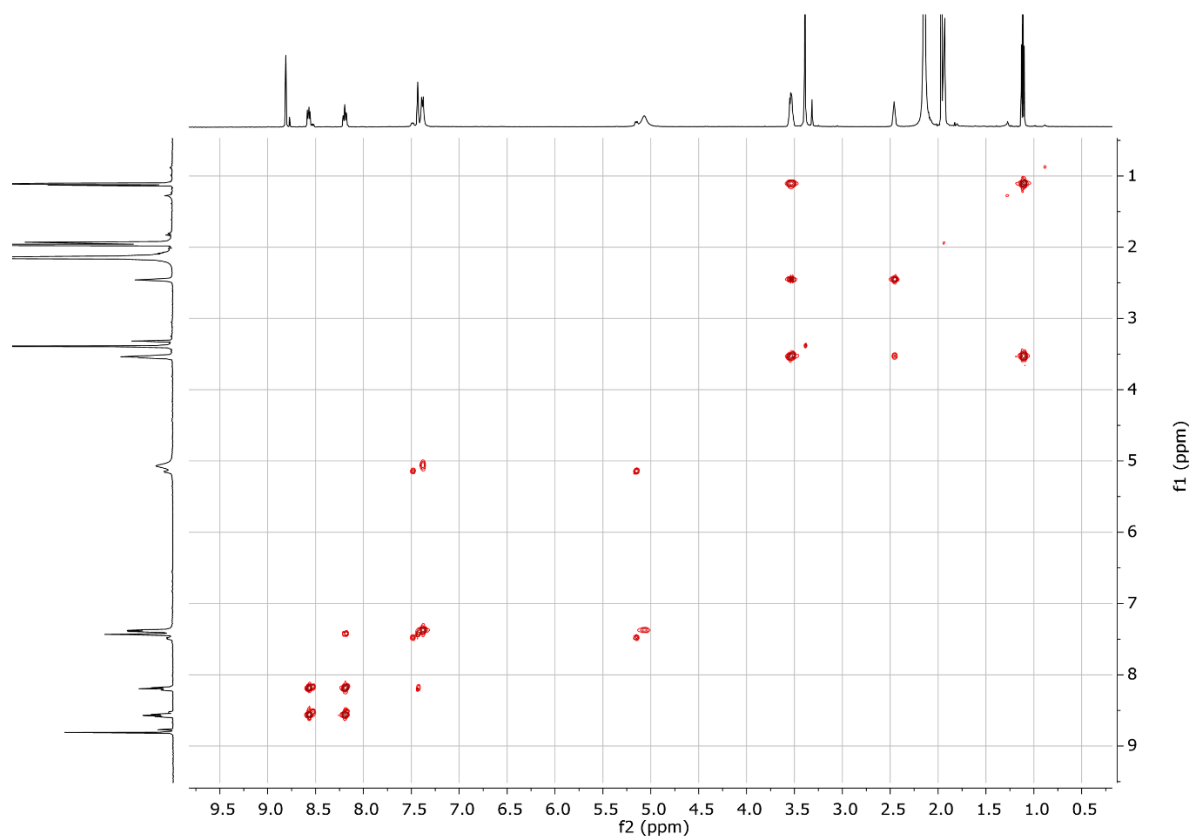


Figure 2.29 ^1H COSY NMR spectrum of $4[\text{NTf}_2]$ in CD_3CN .

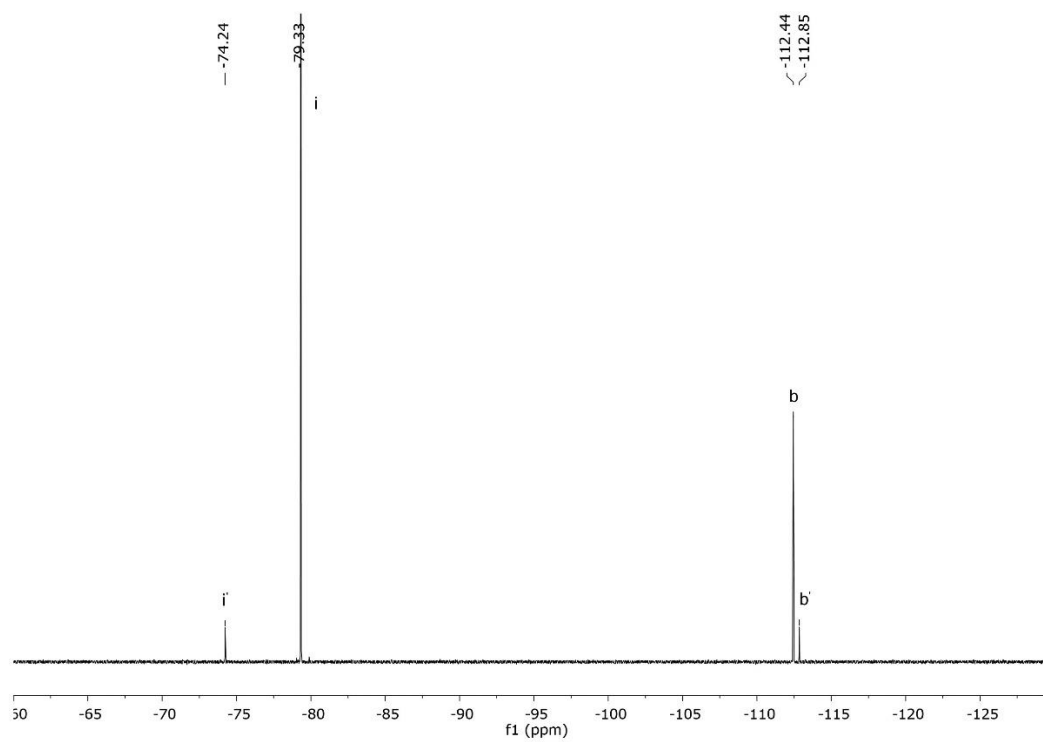


Figure 2.30 ^{19}F NMR spectrum of $4[\text{NTf}_2]$ in CD_3CN .

Trihexyltetradecylphosphonium triflimide ($[P_{6,6,6,14}][NTf_2]$)

This ionic liquid was synthesised by modifying a previously described procedure.⁵⁷ Trihexyltetradecylphosphonium chloride (10.0 g, 19.3 mmol) was dissolved in water (10 mL). Separately, lithium triflimide (6.63 g, 23.1 mmol) was dissolved in water (5 mL). The aqueous solution of lithium triflimide was added dropwise to the aqueous solution of trihexyltetradecylphosphonium chloride while stirring at 298 K, and the reaction mixture was stirred for 24 hours. The product, trihexyltetradecylphosphonium triflimide, formed as an opaque white layer. This layer was extracted into DCM (10 mL), and the organic layer was washed with water until no chloride was detected in the aqueous wash using aqueous silver nitrate solution. ^1H and ^{13}C NMR signals are in agreement with the values reported in the literature.⁵⁷ ^1H NMR (400 MHz, CDCl_3 , referenced to chloroform): $\delta_{\text{H}} = 2.05\text{--}2.13$ (m, 8H, $\text{H}_{\text{a}1\text{--}4}$), 1.47 (m, 16H, $\text{H}_{\text{b}1\text{--}8}$), 1.25–1.32 (m, 32H, $\text{H}_{\text{c}1\text{--}16}$), 0.89–0.91 (m, 12H, $\text{H}_{\text{d}1\text{--}4}$). $^{13}\text{C}\{^1\text{H}\}$ NMR (100 MHz, CDCl_3 , referenced to chloroform): $\delta_{\text{C}} = 119.9, 31.9, 30.6, 30.4, 30.2, 29.68, 29.65, 29.61, 29.5, 29.4, 29.3, 28.8, 22.7, 22.3, 21.49, 21.45, 21.4, 18.8, 18.4, 14.1, 13.8$. Elemental analysis (%) calcd for $\text{C}_{34}\text{H}_{68}\text{F}_6\text{NO}_4\text{PS}_2$: C, 53.45; H, 8.97; N, 1.83; P, 4.05; Cl, 0.00; found: C, 53.54; H, 9.13; N, 1.82; P, 3.51; Cl, 0.02.

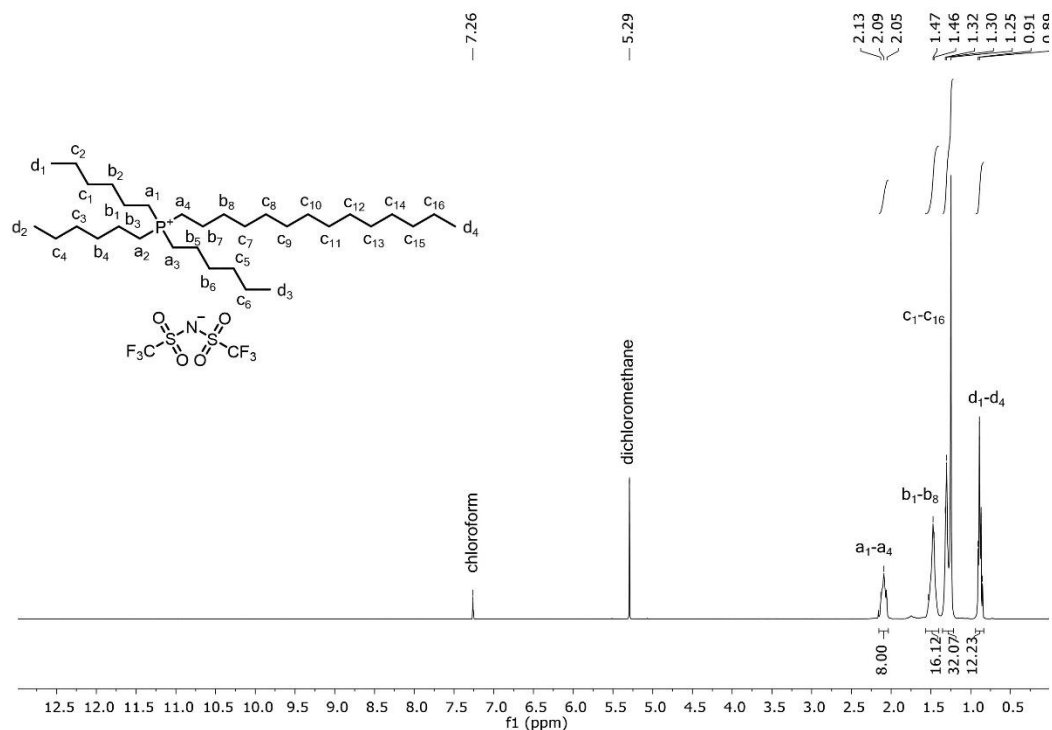


Figure 2.31 ^1H NMR spectrum of $[P_{6,6,6,14}][\text{NTf}]$ in CDCl_3 .

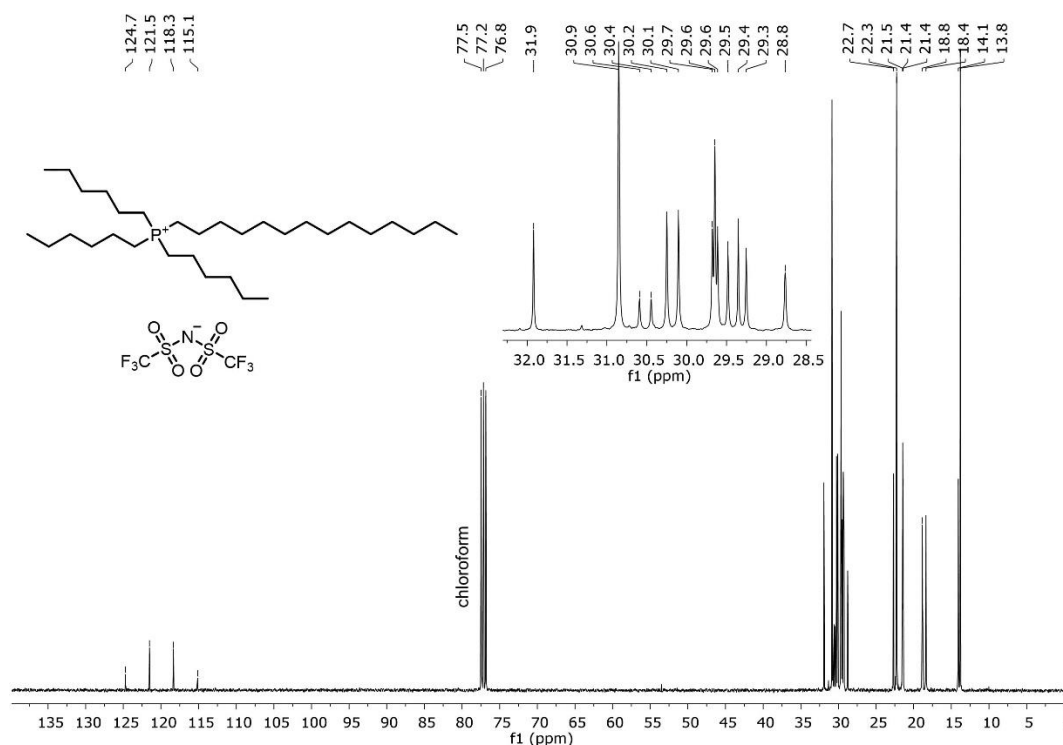


Figure 2.32 ^{13}C NMR spectrum of $[\text{P}_{6,6,6,14}][\text{NTf}]$ in CDCl_3 .

1-Ethyl-3-methylimidazolium triflimide ($[\text{emim}][\text{NTf}_2]$)

This ionic liquid was synthesised by modifying a previously described procedure.⁵⁸ 3-Ethyl-1-methylimidazolium ethyl sulfate (5.00 g, 21.2 mmol) was dissolved in water (5 mL). Separately, lithium triflimide (7.28 g, 25.4 mmol) was dissolved in water (5 mL). The aqueous solution of lithium triflimide was added dropwise to the aqueous solution of 3-ethyl-1-methylimidazolium ethyl sulfate while stirring at 298 K, and the reaction mixture was stirred for 24 hours. The product, 3-ethyl-1-methylimidazolium triflimide, formed as a separate, colourless layer and was washed with water until no chloride was detected in the aqueous wash using aqueous silver nitrate solution. ^1H and ^{13}C NMR signals are in agreement with the values reported in the literature.⁵⁹ ^1H NMR (400 MHz, CD_3OD , referenced to methanol): $\delta_{\text{H}} = 8.84$ (s, 1H, H_b), 7.60 (s, 1H, H_d), 7.52 (s, 1H, H_c), 4.25 (q, $J = 7.4$ Hz, 2H, H_e), 3.91 (s, 3H, H_a), 1.52 (t, $J = 7.4$ Hz, 3H, H_f). $^{13}\text{C}\{^1\text{H}\}$ NMR (100 MHz, CD_3OD , referenced to methanol): $\delta_{\text{C}} = 137.1, 124.8, 123.1, 121.0, 45.9, 36.4, 15.3$. Elemental analysis (%) calcd for $\text{C}_8\text{H}_{11}\text{F}_6\text{N}_3\text{O}_4\text{S}_2$: C, 24.56; H, 2.83; N, 10.74, Cl, 0.00; found: C, 24.59; H, 2.76; N, 10.67; Cl, <0.004.

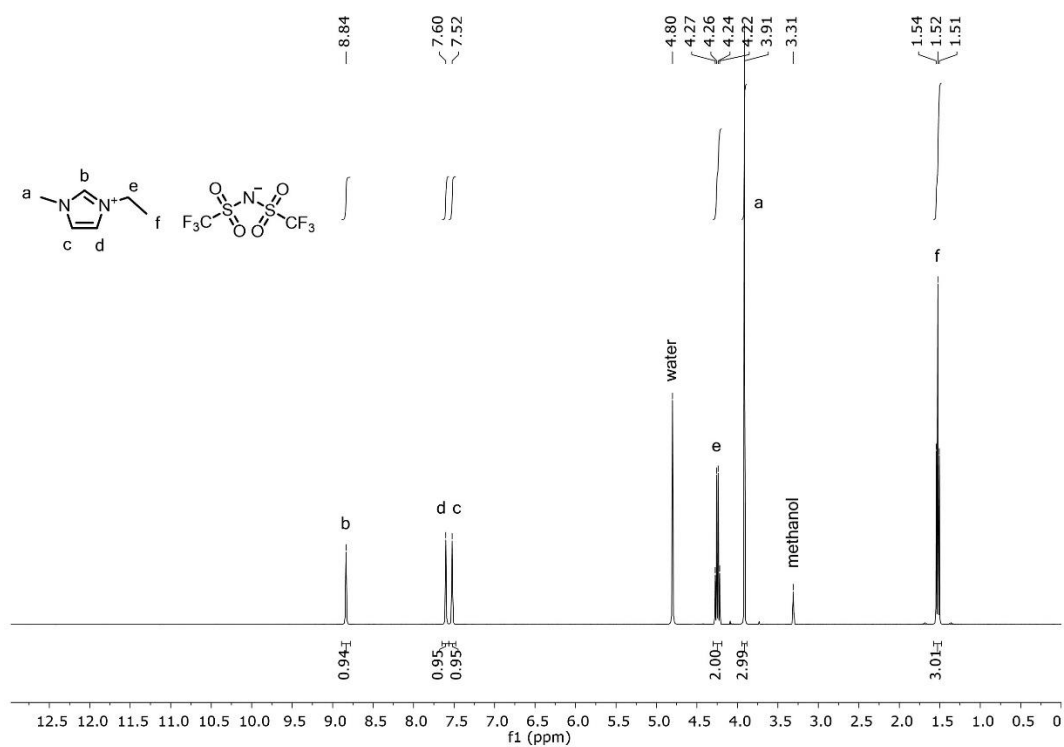


Figure 2.33 ¹H NMR spectrum of [emim][NTf] in CD₃OD.

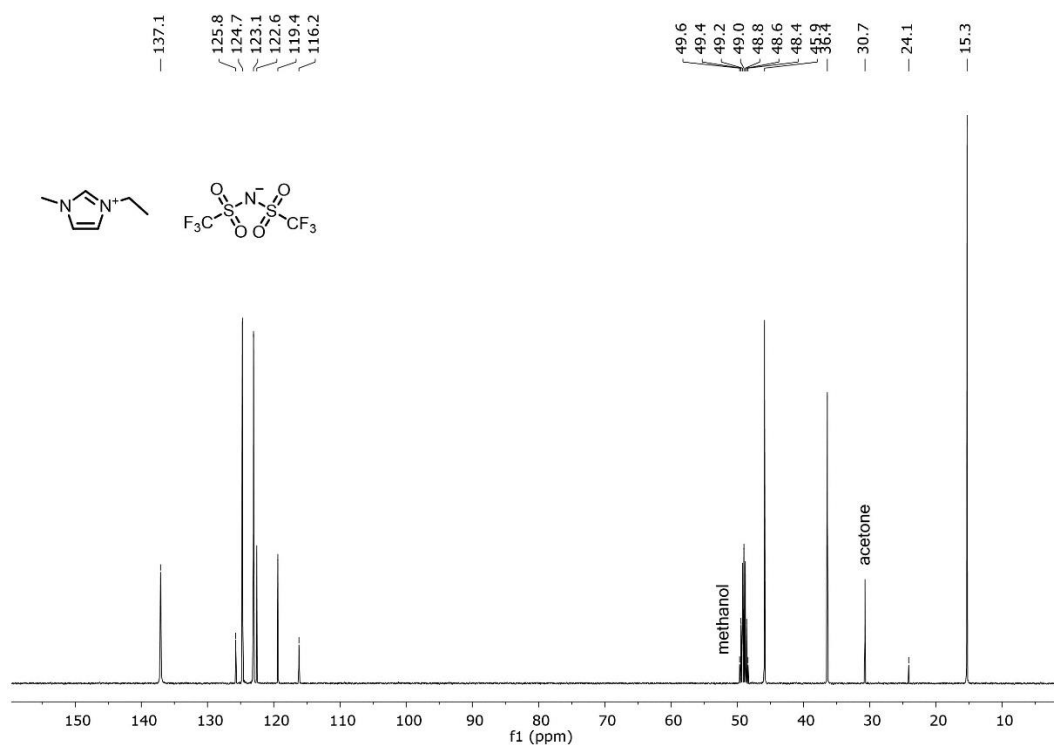


Figure 2.34 ¹³C NMR spectrum of [emim][NTf] in CD₃OD.

2.5 References

- (1) Grommet, A. B.; Bolliger, J. L.; Browne, C.; Nitschke, J. R. *Angew. Chem. Int. Ed.* **2015**, *54*, 15100.
- (2) Fang, Y.; Murase, T.; Sato, S.; Fujita, M. *J. Am. Chem. Soc.* **2013**, *135* (2), 613.
- (3) Schalley, C. A.; Lützen, A.; Albrecht, M. *Chem. Eur. J.* **2004**, *10* (5), 1072.
- (4) Tiefenbacher, K.; Zhang, K. Da; Ajami, D.; Rebek, J. *J. Phys. Org. Chem.* **2015**, *28* (3), 187.
- (5) Turega, S.; Cullen, W.; Whitehead, M.; Hunter, C. A.; Ward, M. D. *J. Am. Chem. Soc.* **2014**, *136* (23), 8475.
- (6) Schneider, M. W.; Opper, I. M.; Griffin, A.; Mastalerz, M. *Angew. Chem. Int. Ed.* **2013**, *52* (13), 3611.
- (7) García-Simón, C.; Gramage-Doria, R.; Raoufmoghaddam, S.; Parella, T.; Costas, M.; Ribas, X.; Reek, J. N. H. *J. Am. Chem. Soc.* **2015**, *137* (7), 2680.
- (8) Han, M.; Michel, R.; He, B.; Chen, Y.-S.; Stalke, D.; John, M.; Clever, G. H. *Angew. Chem. Int. Ed.* **2013**, *52* (4), 1319.
- (9) Mugridge, J. S.; Zahl, A.; Van Eldik, R.; Bergman, R. G.; Raymond, K. N. *J. Am. Chem. Soc.* **2013**, *135* (11), 4299.
- (10) Stephenson, A.; Argent, S. P.; Riis-Johannessen, T.; Tidmarsh, I. S.; Ward, M. D. *J. Am. Chem. Soc.* **2011**, *133* (4), 858.
- (11) Whitehead, M.; Turega, S.; Stephenson, A.; Hunter, C. A.; Ward, M. D. *Chem. Sci.* **2013**, *4* (7), 2744.
- (12) Dumele, O.; Trapp, N.; Diederich, F. *Angew. Chem. Int. Ed.* **2015**, *54* (42), 12339.
- (13) Gale, P. A. *Acc. Chem. Res.* **2006**, *39* (7), 465.
- (14) Hay, B. P.; Firman, T. K.; Moyer, B. A. *J. Am. Chem. Soc.* **2005**, *127* (6), 1810.
- (15) Lavigne, J. J.; Anslyn, E. V. *Angew. Chem. Int. Ed.* **2001**, *40* (17), 3118.
- (16) Leung, D. H.; Bergman, R. G.; Raymond, K. N. *J. Am. Chem. Soc.* **2008**, *130* (9), 2798.
- (17) Moyer, B. A.; Custelcean, R.; Hay, B. P.; Sessler, J. L.; Bowman-James, K.; Day, V. W.; Kang, S.-O. *Inorg. Chem.* **2013**, *52* (7), 3473.
- (18) Ruan, Y.; Dalkılıç, E.; Peterson, P. W.; Pandit, A.; Dastan, A.; Brown, J. D.; Polen, S. M.; Hadad, C. M.; Badjić, J. D. *Chem. – A Eur. J.* **2014**, *20* (15), 4251.
- (19) Ryan, S. T. J.; Del Barrio, J.; Ghosh, I.; Biedermann, F.; Lazar, A. I.; Lan, Y.; Coulston, R. J.; Nau, W. M.; Scherman, O. A. *J. Am. Chem. Soc.* **2014**, *136* (25), 9053.

- (20) Sawada, T.; Hisada, H.; Fujita, M. *J. Am. Chem. Soc.* **2014**, *136* (12), 4449.
- (21) Sawada, T.; Yoshizawa, M.; Sato, S.; Fujita, M. *Nat. Chem.* **2009**, *1* (1), 53.
- (22) Symmers, P. R.; Burke, M. J.; August, D. P.; Thomson, P. I. T.; Nichol, G. S.; Warren, M. R.; Campbell, C. J.; Lusby, P. J. *Chem. Sci.* **2015**, *6* (1), 756.
- (23) Bruns, C. J.; Fujita, D.; Hoshino, M.; Sato, S.; Stoddart, J. F.; Fujita, M. *J. Am. Chem. Soc.* **2014**, *136* (34), 12027.
- (24) Galán, A.; Gil-Ramírez, G.; Ballester, P. *Org. Lett.* **2013**, *15* (19), 4976.
- (25) Liu, T.; Liu, Y.; Xuan, W.; Cui, Y. *Angew. Chem. Int. Ed.* **2010**, *49* (24), 4121.
- (26) Diaz, P.; Mingos, D. M. P.; Vilar, R.; White, A. J. P.; Williams, D. J. *Inorg. Chem.* **2004**, *43* (24), 7597.
- (27) Daguinet, C.; Dyson, P. J. *Inorg. Chem.* **2007**, *46* (2), 403.
- (28) Arce, A.; Earle, M. J.; Katdare, S. P.; Rodríguez, H.; Seddon, K. R. *Chem. Commun.* **2006**, *2* (24), 2548.
- (29) Jackson, G. P.; Duckworth, D. C. *Chem. Commun.* **2004**, *10* (5), 522.
- (30) Giernoth, R.; Bankmann, D. *Eur. J. Org. Chem.* **2005**, No. 21, 4529.
- (31) Hall, B. R.; Manck, L. E.; Tidmarsh, I. S.; Stephenson, A.; Taylor, B. F.; Blaikie, E. J.; Griend, D. A. Vander; Ward, M. D. *Dalt. Trans.* **2011**, *40* (45), 12132.
- (32) Shimizu, K. D.; Rebek, J. *Proc. Natl. Acad. Sci.* **1995**, *92* (26), 12403.
- (33) Bolliger, J. L.; Ronson, T. K.; Ogawa, M.; Nitschke, J. R. *J. Am. Chem. Soc.* **2014**, *136* (41), 14545.
- (34) Mal, P.; Schultz, D.; Beyeh, K.; Rissanen, K.; Nitschke, J. R. *Angew. Chem. Int. Ed.* **2008**, *47*, 8297.
- (35) Ma, S. C.; Smulders, M. M. J.; Hristova, Y. R.; Clegg, J. K.; Ronson, T. K.; Zarra, S.; Nitschke, J. R. *J. Am. Chem. Soc.* **2013**, *135* (15), 5678.
- (36) Smulders, M. M. J.; Nitschke, J. R. *Chem. Sci.* **2012**, *3* (3), 785.
- (37) Browne, C.; Brenet, S.; Clegg, J. K.; Nitschke, J. R. *Angew. Chem. Int. Ed.* **2013**, *52* (7), 1944.
- (38) Fukaya, Y.; Ohno, H. *Phys. Chem. Chem. Phys.* **2013**, *15* (11), 4066.
- (39) Smulders, M. M. J.; Zarra, S.; Nitschke, J. R. *J. Am. Chem. Soc.* **2013**, *135* (18), 7039.
- (40) Heintz, A.; Lehmann, J. K.; Kozlova, S. A.; Balantseva, E. V.; Bazyleva, A. B.; Ondo, D. *Fluid Phase Equilib.* **2010**, *294* (1–2), 187.
- (41) Seddon, K. R. *Nat. Mater.* **2003**, *2* (6), 363.
- (42) Kumar, R.; Saima; Shard, A.; Andhare, N. H.; Richa; Sinha, A. K. *Angew. Chem. Int. Ed.* **2015**, *54* (3), 828.

- (43) Steinrück, H.-P.; Wasserscheid, P. *Catal. Letters* **2015**, *145* (1), 380.
- (44) Wasserscheid, P.; Keim, W. *Angew. Chem. Int. Ed.* **2000**, *39* (21), 3772.
- (45) Song, J. L.; Fan, H. L.; Ma, J.; Han, B. X. *Green Chem.* **2013**, *15* (10), 2619.
- (46) Barber, P. S.; Griggs, C. S.; Gurau, G.; Liu, Z.; Li, S.; Li, Z.; Lu, X.; Zhang, S.; Rogers, R. D. *Angew. Chem. Int. Ed.* **2013**, *52* (47), 12350.
- (47) George, A.; Brandt, A.; Tran, K.; Zahari, S. M. S. N. S.; Klein-Marcuschamer, D.; Sun, N.; Sathitsuksanoh, N.; Shi, J.; Stavila, V.; Parthasarathi, R.; Singh, S.; Holmes, B. M.; Welton, T.; Simmons, B. A.; Hallett, J. P. *Green Chem.* **2015**, *17* (3), 1728.
- (48) Brennecke, J. E.; Gurkan, B. E. *J. Phys. Chem. Lett.* **2010**, *1* (24), 3459.
- (49) Sun, X. Q.; Luo, H. M.; Dai, S. *Chem. Rev.* **2012**, *112* (4), 2100.
- (50) Beves, J. E.; Blight, B. A.; Campbell, C. J.; Leigh, D. A.; McBurney, R. T. *Angew. Chem. Int. Ed.* **2011**, *50* (40), 9260.
- (51) Chifotides, H. T.; Dunbar, K. R. *Acc. Chem. Res.* **2013**, *46* (4), 894.
- (52) Dhers, S.; Feltham, H. L. C.; Brooker, S. *Coord. Chem. Rev.* **2015**, *296*, 24.
- (53) Huang, Z.; Yang, L.; Liu, Y.; Wang, Z.; Scherman, O. A.; Zhang, X. *Angew. Chem. Int. Ed.* **2014**, *53* (21), 5351.
- (54) Weissman, H.; Rybtchinski, B. *Curr. Opin. Colloid Interface Sci.* **2012**, *17* (6), 330.
- (55) Wong, K. M. C.; Chan, M. M. Y.; Yam, V. W. W. *Adv. Mater.* **2014**, *26* (31), 5558.
- (56) Zhang, Z.; Kim, D. S.; Lin, C.-Y.; Zhang, H.; Lammer, A. D.; Lynch, V. M.; Popov, I.; Miljanić, O. Š.; Anslyn, E. V.; Sessler, J. L. *J. Am. Chem. Soc.* **2015**.
- (57) Vander Hoogerstraete, T.; Blockx, J.; Decoster, H.; Binnemans, K. *Chem. Eur. J.* **2015**, *21* (33), 11757.
- (58) Shimojo, K.; Nakashima, K.; Kamiya, N.; Goto, M. *Biomacromolecules* **2006**, *7*, 2.
- (59) Dubois, P.; Marchand, G.; Fouillet, Y.; Berthier, J.; Douki, T.; Hassine, F.; Gmouh, S.; Vaultier, M. *Anal. Chem.* **2006**, *78* (14), 4909.

Chapter 3:

Phase Transfer of an Fe^{II}₄L₄ Cage and Encapsulated Cargo

*Supramolecular capsules can now be prepared with a wide range of volumes and geometries. Consequently, many of these capsules encapsulate guests selectively by size and shape, an important design feature for separations. To successfully address practical separations problems, however, a guest cannot simply be isolated from its environment; the molecular cargo must be removed to a separate physical space. Here we demonstrate that an Fe^{II}₄L₄ coordination cage **1** can transport a cargo spontaneously and quantitatively from water across a phase boundary and into an ionic liquid layer. This process is triggered by an anion exchange from **1**[SO₄] to **1**[BF₄]. Upon undergoing a second anion exchange, from **1**[BF₄] to **1**[SO₄], the cage – together with its encapsulated guest – can then be manipulated back into a water layer. Furthermore, we demonstrate the selective phase transfer of cationic cages to separate a mixture of two cages and their respective cargos. We envisage that supramolecular technologies based upon these concepts could ultimately be employed to carry out separations of industrially relevant compounds.*

3.1 Introduction

This chapter¹ explores the idea of using coordination cages to transport guests across a phase boundary, with the ultimate aim of addressing practical separations problems. Because these cages are not charge neutral,^{2–7} they derive properties from both cation and anion. Counterions have previously been shown to play a significant role in the stability,^{8–11} shape,^{12–22} solubility,²³ and other physicochemical properties^{24,25} of coordination cages. We further demonstrate in this work that exchanging cage counterions can drive spontaneous and quantitative transport of cages from water across a phase boundary and into an ionic liquid.^{26–28} In an advance over cation transport driven by anionic phase transfer catalysts,^{29,30} our strategy allows the simultaneous transfer of selectively-bound guest molecules. To the best of our knowledge, this work constitutes the first example of the directed transport of cages and their cargoes between two liquid phases.

As discussed in Chapter 1, when cage **1** (Figure 3.1) is prepared as the SO₄²⁻ salt, the complex is soluble in water. Paired with fluorinated anions (triflate or BF₄⁻), however, **1** becomes

insoluble in water.²³ This feature allows the design of a system in which cationic cage **1** can be transported between liquid phases, as shown in Figure 3.1. Having demonstrated in Chapter 2 that coordination cages can be soluble and stable in ionic liquids,²³ we now utilise the hydrophobic ionic liquid 1-hexyl-3-methylimidazolium tetrafluoroborate ([hmim][BF₄])^{31,32} as both a salt to supply BF₄⁻ anions and as a solvent to act as a receiving phase for **1**[BF₄]. Furthermore, by exchanging the BF₄⁻ counterion for SO₄²⁻, we can ultimately manipulate cage **1** back into its original aqueous environment.

3.2 Results and Discussion

3.2.1 Directed phase transfer of 1-fluoroadamantane \subset **1**

Because the solubility of cage **1** in different solvents is largely dependent on the counteranion, exchanging the anion from sulfate to a more hydrophobic anion can switch the solvent preference and thus trigger directed phase transfer. In the transport cycle proposed in Figure 3.1, cage **1**[SO₄] initially resides in water (Figure 3.1a). Upon the addition of hydrophobic [hmim][BF₄], an ionic liquid layer forms beneath the existing water layer (Figure 3.1b). Upon shaking, the cage undergoes anion exchange from cage **1**[SO₄] to **1**[BF₄] – this process is driven by the partitioning of cage **1**[BF₄] into the ionic liquid layer (Figure 3.1c) and leaves the water layer colourless. To manipulate cage **1** back into water, a second anion exchange is required to convert cage **1**[BF₄] back into **1**[SO₄]. Because no amount of sulfate added to water layer can counterbalance the amount of tetrafluoroborate present in the ionic liquid, **1**[BF₄] is then isolated from the ionic liquid layer. This can be done by adding ethyl acetate to the water/ionic liquid biphasic system; the ethyl acetate is miscible with [hmim][BF₄] and lowers the solubility of **1**[BF₄] in the organic/ionic liquid layer, precipitating the cage from solution (Figure 3.1d). Precipitated cage **1**[BF₄] can then be isolated *via* filtration and redissolved in acetonitrile, as shown in Figure 3.1e. After cage **1**[BF₄] is dissolved in acetonitrile, tetrabutylammonium sulfate can be added to convert cage **1**[BF₄] back into **1**[SO₄]. Anion exchange causes the cage to precipitate from solution (Figure 3.1f); precipitated cage **1**[SO₄] can then be isolated *via* filtration and redissolved in water (Figure 3.1a). This final step thus closes the transport cycle of cage **1** from water, to an ionic liquid, and finally back to water.

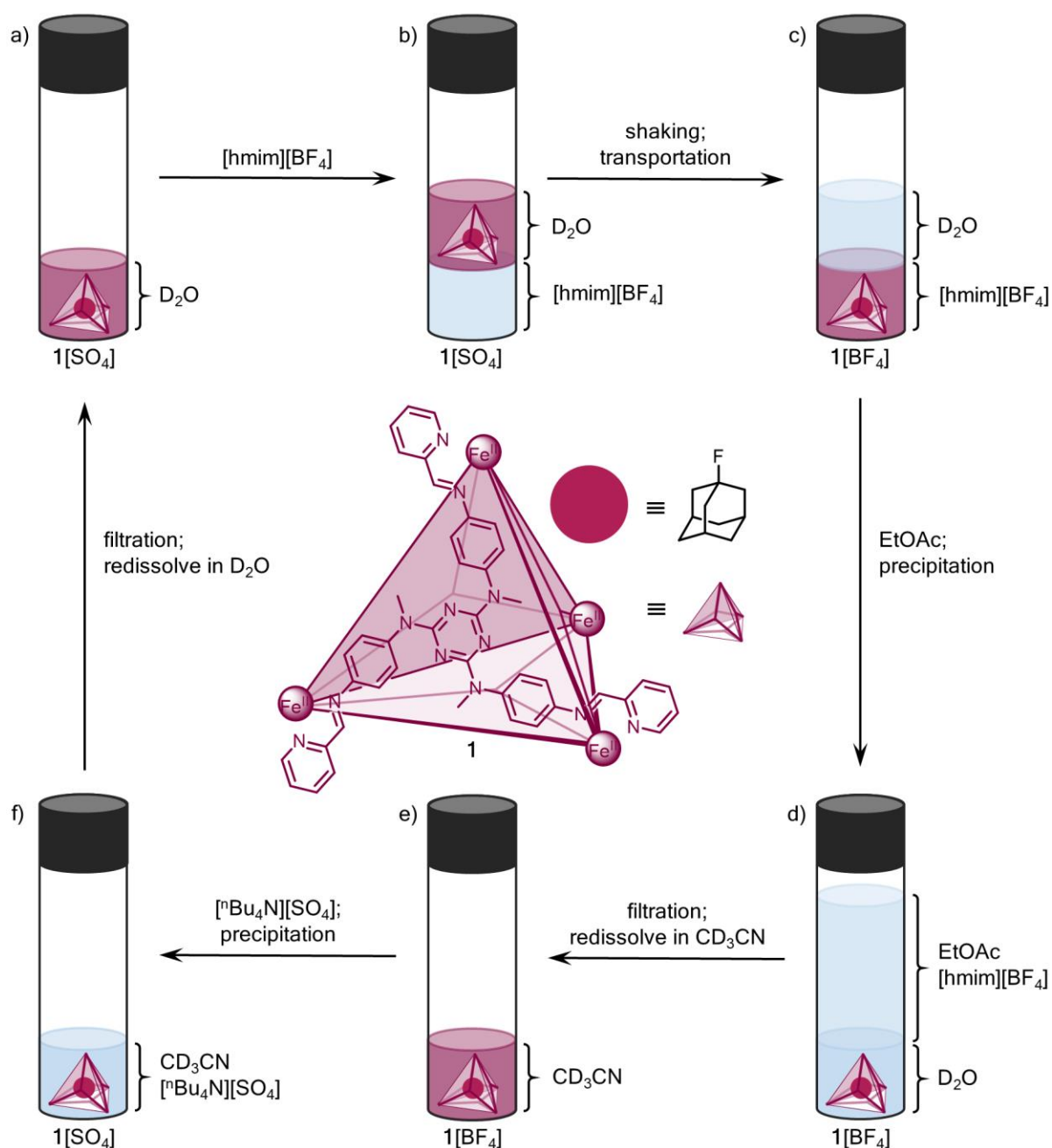


Figure 3.1 a) 1-Fluoroadamantane \subset $\mathbf{1}[\text{SO}_4]$ dissolved in water. b) Addition of $[\text{hmim}][\text{BF}_4]$. c) Upon shaking, 1-fluoroadamantane \subset $\mathbf{1}$ transferred from the water to the ionic liquid layer. d) Upon addition of EtOAc, 1-fluoroadamantane \subset $\mathbf{1}[\text{BF}_4]$ was filtered off and redissolved in CD_3CN . e) Upon addition of $[\text{nBu}_4\text{N}][\text{SO}_4]$, 1-fluoroadamantane \subset $\mathbf{1}[\text{SO}_4]$ precipitated. f) Solid 1-fluoroadamantane \subset $\mathbf{1}[\text{SO}_4]$ was filtered off and redissolved in water, completing the cycle.

The execution of this proposed transport cycle is further discussed in Chapter 3.2.3. Our use of non-deuterated $[\text{hmim}][\text{BF}_4]$ in this study, however, renders challenging the use of ^1H NMR techniques to observe cage peaks in ionic solution (see Chapter 2.2.1 for further discussion).

We therefore used ¹⁹F NMR to track an encapsulated, fluorinated guest as the host-guest complex moved between different liquid phases. The guest was chosen to be 1-fluoroadamantane because it binds strongly and exchanges slowly within cage **1** in water, [hmim][BF₄], and acetonitrile. Control experiments justifying our use of 1-fluoroadamantane ⊂ **1** as a handle for characterisation through the counteranion exchange cycle are presented in the following section (Chapter 3.2.2).

3.2.2 Guest uptake kinetics of 1-fluoroadamantane ⊂ **1**

Adamantane has previously been shown to equilibrate slowly with cage **1**, requiring two weeks in water and three days in acetonitrile. The host-guest complex 1-fluoroadamantane ⊂ **1** was therefore chosen as a handle by which to monitor every step in the transport cycle; in addition to being observable by ¹H NMR in D₂O and CD₃CN, ¹⁹F NMR can be used to observe encapsulated 1-fluoroadamantane in [hmim][BF₄]. Similarly to adamantane, 1-fluoroadamantane ⊂ **1** was observed to require two weeks of equilibration in water and three days of equilibration in acetonitrile. We therefore hypothesised that the ¹⁹F NMR signal corresponding to 1-fluoroadamantane ⊂ **1** in the transport cycle would primarily result from a stable host-guest complex that has remained intact throughout the cycle. The experiments described in this section serve as controls by which we demonstrate that the signal from 1-fluoroadamantane ⊂ **1** is not likely to result from decomposed cage that had re-assembled and re-encapsulated 1-fluoroadamantane. Specifically, we tracked the ¹⁹F NMR signal from 1-fluoroadamantane ⊂ **1** during the self-assembly of **1** around 1-fluoroadamantane and the encapsulation of 1-fluoroadamantane within pre-formed **1**. When applicable, these control experiments were performed in D₂O, [hmim][BF₄], and CD₃CN.

To quantitatively measure the rate at which 1-fluoroadamantane was encapsulated by **1** throughout this chapter section, the integrals from the 1-fluoroadamantane fluorine signals were calculated against an internal concentration reference. The reference used was a coaxial capillary containing TFA in (CD₃)₂CO.

Control experiments in D₂O

The self-assembly of cage **1**[SO₄] around 1-fluoroadamantane in D₂O was monitored according to the following procedure: in a glovebox, N₂,N₄,N₆-tris(4-aminophenyl)-N₂,N₄,N₆-

trimethyl-1,3,5-triazine-2,4,6-triamine (1.77 mg, 4.00×10^{-3} mmol), iron (II) sulfate heptahydrate (1.11 mg, 4.00×10^{-3} mmol), and 1-fluoroadamantane (2.31 mg, 15.0×10^{-3} mmol) were combined with D₂O (0.5 mL) in a J Young NMR tube with an internal reference (TFA in a (CD₃)₂CO capillary). 2-Formylpyridine (1.14 μ L, 12.0×10^{-3} mmol) was then added to the reaction mixture, and the NMR tube was briefly shaken. The first ¹⁹F NMR spectrum was recorded 15 minutes after the addition of 2-formylpyridine, and subsequent spectra were measured every 5 minutes. Table 3.1 lists the integrals for the ¹⁹F NMR signals attributed to 1-fluoroadamantane encapsulated in cage **1** (1-FA \subset **1**), and free 1-fluoroadamantane (Free 1-FA), as calibrated against the internal concentration reference (TFA in an acetone-d₆ capillary).

Table 3.1 Summary of ¹⁹F NMR integrals for the self-assembly of cage **1**[SO₄] around 1-fluoroadamantane in water.

Time (hrs):	1-FA \subset 1 :	Free 1-FA:
0:15	0.00	0.00
0:20	0.00	0.00
0:35	0.00	0.00
0:40	0.00	0.00
0:45	0.00	0.00
0:50	0.00	0.00
0:55	0.00	0.00
1.00	0.00	0.00

The information presented in Table 3.1 illustrates that no encapsulation of 1-fluoroadamantane by self-assembled **1**[SO₄] was observed within the first hour of the subcomponents being combined. The assembly of **1**[SO₄] in water requires the presence of acetonitrile (generally a 1 : 1 ratio of water : acetonitrile)²³ to solubilise the triamine subcomponent (Figure 1.8); the lack of ¹⁹F NMR signals from 1-fluoroadamantane \subset **1** thus suggests that cage **1**[SO₄] failed to assemble in water in the absence of acetonitrile.

Encapsulation of 1-fluoroadamantane in preassembled cage **1**[SO₄] in water was monitored according to the following procedure: a stock solution of **1**[SO₄] in D₂O (2.0 mM, 0.5 mL) was combined with 1-fluoroadamantane (2.50 mg, 16.2×10^{-3} mmol) in an NMR tube with an internal concentration reference (TFA in a (CD₃)₂CO capillary). The first ¹⁹F NMR spectrum was recorded 20 minutes after cage **1**[SO₄] was combined with 1-fluoroadamantane. Table 3.2

lists the integrals for the ¹⁹F NMR signals attributed to 1-fluoroadamantane encapsulated in cage **1** (1-FA ⊂ **1**), and free 1-fluoroadamantane (Free 1-FA), as calibrated against the internal concentration reference (TFA in an acetone-d₆ capillary).

Table 3.2 Summary of ¹⁹F NMR integrals for encapsulation of 1-fluoroadamantane into cage **1**[SO₄] in water.

Time (hrs):	1-FA ⊂ 1 :	Free 1-FA:
0:20	0.00	0.00
1:20	0.00	0.00
3:20	0.02	0.00
5:50	0.10	0.00
23:20	0.36	0.00
46:50	0.54	0.00
70:50	0.59	0.00

The information presented in Table 3.2 above illustrate that no significant encapsulation of 1-fluoroadamantane by cage **1**[SO₄] was observed within the first three hours after cage **1**[SO₄] was combined with 1-fluoroadamantane.

Control experiments in [hmim][BF₄]

Immediately after transport from the water layer, the concentration of **1**[BF₄] in [hmim][BF₄] is approximately 2.0 mM. This concentration is significantly greater than the maximum solubility of cage **1**[BF₄] in this ionic liquid; cage **1**[BF₄] thus precipitates out of this supersaturated solution over several days. Because cage **1**[BF₄] is poorly soluble in [hmim][BF₄], the cage cannot be self-assembled in this solvent. The control experiments described above are therefore rendered unnecessary in this solvent.

Control experiments in CD₃CN

The self-assembly of cage **1**[SO₄] around 1-fluoroadamantane in CD₃CN was monitored according to the following procedure: in a glovebox, N₂,N₄,N₆-tris(4-aminophenyl)-N₂,N₄,N₆-trimethyl-1,3,5-triazine-2,4,6-triamine (1.77 mg, 4.00 × 10⁻³ mmol), iron (II) tetrafluoroborate hexahydrate (1.35 mg, 4.00 × 10⁻³ mmol), and 1-fluoroadamantane (0.15 mg, 1.0 × 10⁻³ mmol) were combined with CD₃CN (0.5 mL) in a J Young NMR tube with an internal reference (TFA in a (CD₃)₂CO capillary). 2-Formylpyridine (1.14 μL, 12.0 × 10⁻³ mmol) was

then added to the reaction mixture, and the NMR tube was briefly shaken. The encapsulation of 1-fluoroadamantane by **1**[BF₄] was monitored by ¹⁹F NMR over the following hour. The first ¹⁹F NMR spectrum was recorded 15 minutes after the addition of 2-formylpyridine, and subsequent spectra were measured every 5 minutes (Figure 3.2). Table 3.3 lists the integrals for the ¹⁹F NMR signals attributed to 1-fluoroadamantane encapsulated in cage **1** (1-FA ⊂ **1**), and free 1-fluoroadamantane (Free 1-FA), as calibrated against the internal concentration reference (TFA in an acetone-d₆ capillary).

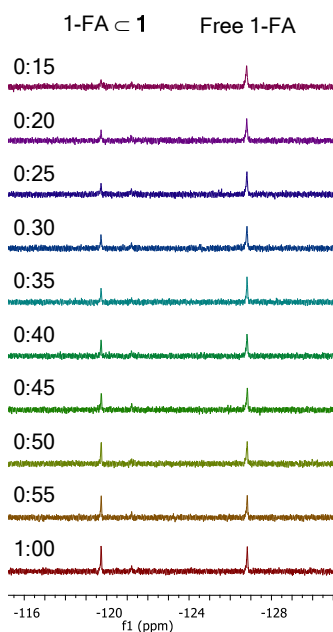


Figure 3.2 ¹⁹F{¹H} NMR (471 MHz, CD₃CN, referenced to TFA in a (CD₃)₂CO capillary) tracking the self-assembly of **1**[BF₄] around 1-fluoroadamantane.

Table 3.3 Summary of ¹⁹F NMR integrals for the self-assembly of cage **1**[BF₄] around 1-fluoroadamantane in acetonitrile.

Time (hrs):	1-FA ⊂ 1 :	Free 1-FA:
0:15	0.14	0.86
0:20	0.21	0.79
0:25	0.29	0.71
0:30	0.30	0.70
0:35	0.31	0.69
0:40	0.34	0.66
0:45	0.37	0.63
0:50	0.40	0.60
0:55	0.41	0.59
1:00	0.45	0.55

The information presented in Table 3.3 illustrates that, in fact, a significant amount of **1**[BF₄] self-assembles around 1-fluoroadamantane within the first hour of the subcomponents being combined. For the step of the transport cycle in which precipitated 1-fluoroadamantane ⊂ **1**[BF₄] is redissolved in acetonitrile (Figure 3.1e), the possibility that the ¹⁹F NMR signal from 1-fluoroadamantane ⊂ **1** results from decomposed cage that has re-assembled and re-encapsulated 1-fluoroadamantane cannot be entirely eliminated.

Encapsulation of 1-fluoroadamantane in preassembled cage **1**[BF₄] in acetonitrile was monitored according to the following procedure: a stock solution of **1**[BF₄] in CD₃CN (2.0 mM, 0.5 mL) was combined with 1-fluoroadamantane (2.31 mg, 15.0 × 10⁻³ mmol) in an NMR tube with an internal concentration reference (TFA in in a (CD₃)₂CO capillary). The first ¹⁹F NMR spectrum was recorded 15 minutes after cage **1**[BF₄] was combined with 1-fluoroadamantane. Table 3.4 lists the integrals for the ¹⁹F NMR signals attributed to 1-fluoroadamantane encapsulated in cage **1** (1-FA ⊂ **1**), and free 1-fluoroadamantane (Free 1-FA), as calibrated against the internal concentration reference (TFA in an acetone-d₆ capillary).

Table 3.4 Summary of ¹⁹F NMR integrals for encapsulation of 1-fluoroadamantane into cage **1**[BF₄] in acetonitrile.

Time (hrs):	1-FA ⊂ 1 :	Free 1-FA:
0:15	-0.01	6.60
0:45	0.01	6.76
1:45	0.12	6.76
3:45	0.21	6.79
21:15	0.54	6.75
51:15	0.62	6.64
76:15	0.60	6.39
193:30	0.59	6.45

The information presented in Table 3.4 above illustrate that no significant encapsulation of 1-fluoroadamantane by **1**[BF₄] was observed within the first 45 min after cage **1**[BF₄] was combined with 1-fluoroadamantane.

Summary of control experiments

In water, no measurable uptake of 1-fluoroadamantane was observed by ¹⁹F NMR within the first three hours after adding the guest – these results hold true for both control experiments (self-assembly of **1**[SO₄] around 1-fluoroadamantane; addition of 1-fluoroadamantane to preassembled **1**[SO₄]). By comparison, each step in the transport cycle presented in Figure 3.1 takes less than 15 min to complete. Because 1-fluoroadamantane ⊂ **1** equilibrates slowly, and because 1-fluoroadamantane is poorly soluble in water, any free 1-fluoroadamantane peaks in the ¹⁹F NMR may therefore be inferred to result from release of the encapsulated guest upon decomposition of the cage. Furthermore, cage **1**[BF₄] does not assemble in [hmim][BF₄], so any ¹⁹F signals from 1-fluoroadamantane ⊂ **1**[BF₄] in the ionic liquid must necessarily originate from a stable (not decomposed and reassembled) host-guest complex. In acetonitrile, no measurable uptake of guest was observed by ¹⁹F NMR within the first 45 min after guest addition when 1-fluoroadamantane was added to preassembled **1**[BF₄]. When **1**[BF₄] was allowed to self-assemble around 1-fluoroadamantane in acetonitrile, however, an ¹⁹F NMR signal corresponding to 1-fluoroadamantane ⊂ **1**[BF₄] (approximately 14% inclusion yield) was observed after 15 min, the timescale on which each step of the transport cycle can be performed. These results indicate that the encapsulated 1-fluoroadamantane peak in the ¹⁹F NMR spectrum cannot necessarily be inferred to correspond to a stable host-guest complex. If the yield of this transport cycle step is greater than 14%, however, we can assume that the difference between the observed inclusion and the inclusion yield from the control experiment is the lower limit of the true yield of stable 1-fluoroadamantane ⊂ **1**[BF₄] after being precipitated out of the ionic liquid and redissolved in acetonitrile.

3.2.3 Characterisation of 1-fluoroadamantane ⊂ **1 transport cycle**

An aqueous solution of **1**[SO₄] (2.0 mM) was allowed to equilibrate with 1-fluoroadamantane (15 equiv) for two weeks at 298 K. The resulting solution was then filtered to remove any unencapsulated, non-dissolved 1-fluoroadamantane (Figure 3.1a) and was analysed by ¹⁹F NMR to give the spectrum shown in Figure 3.3.

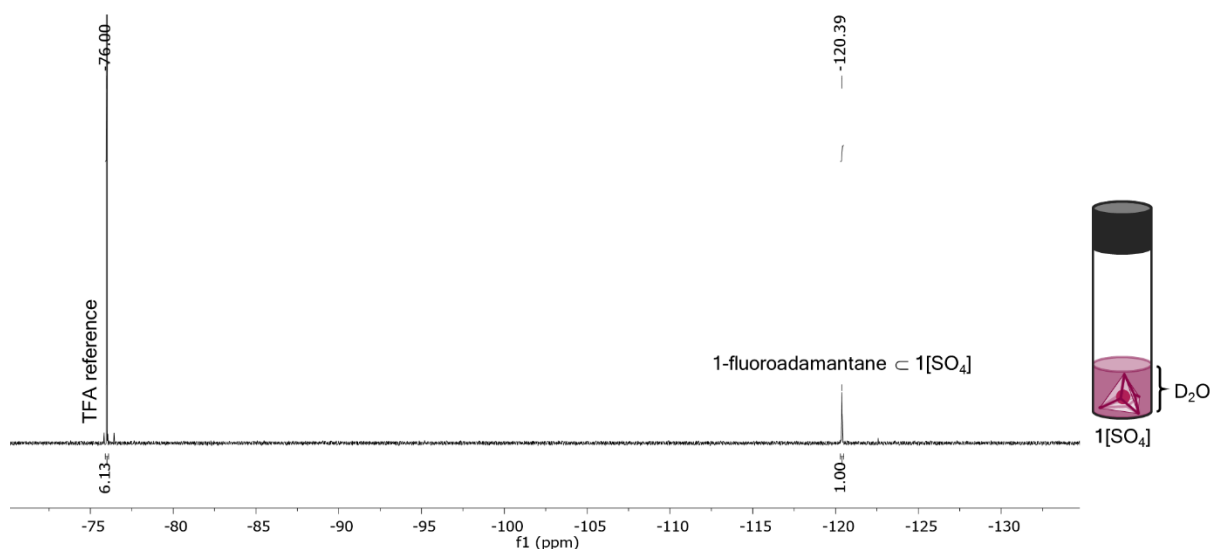


Figure 3.3 2.0 mM solution of 1-fluoroadamantane c **1**[SO₄] dissolved in D₂O. ¹⁹F{¹H} NMR (471 MHz, D₂O, referenced to TFA in a (CD₃)₂CO capillary): δ_F = -76.00 (TFA reference), -120.39 (encapsulated 1-fluoroadamantane).

In the spectrum above, the integration of the ¹⁹F NMR peak corresponding to 1-fluoroadamantane c **1**[SO₄] was set to 1. Because the same reference capillary and same NMR tube were used to analyse each step of the transport cycle, the integral for the reference peak determined above was used to measure the change in the abundance of the encapsulated 1-fluoroadamantane species throughout.

Upon the addition of hydrophobic [hmim][BF₄] (1.0 mL) to 1-fluoroadamantane c **1**[SO₄] in water (2.0 mM, 1.0 mL), an ionic liquid layer was observed to form beneath the existing water layer (Figure 3.4). Because cage **1**[BF₄] is insoluble in water, the cage rapidly underwent anion exchange from **1**[SO₄] to **1**[BF₄], with **1**[BF₄] partitioning into the ionic liquid layer upon shaking, leaving the water layer colourless.

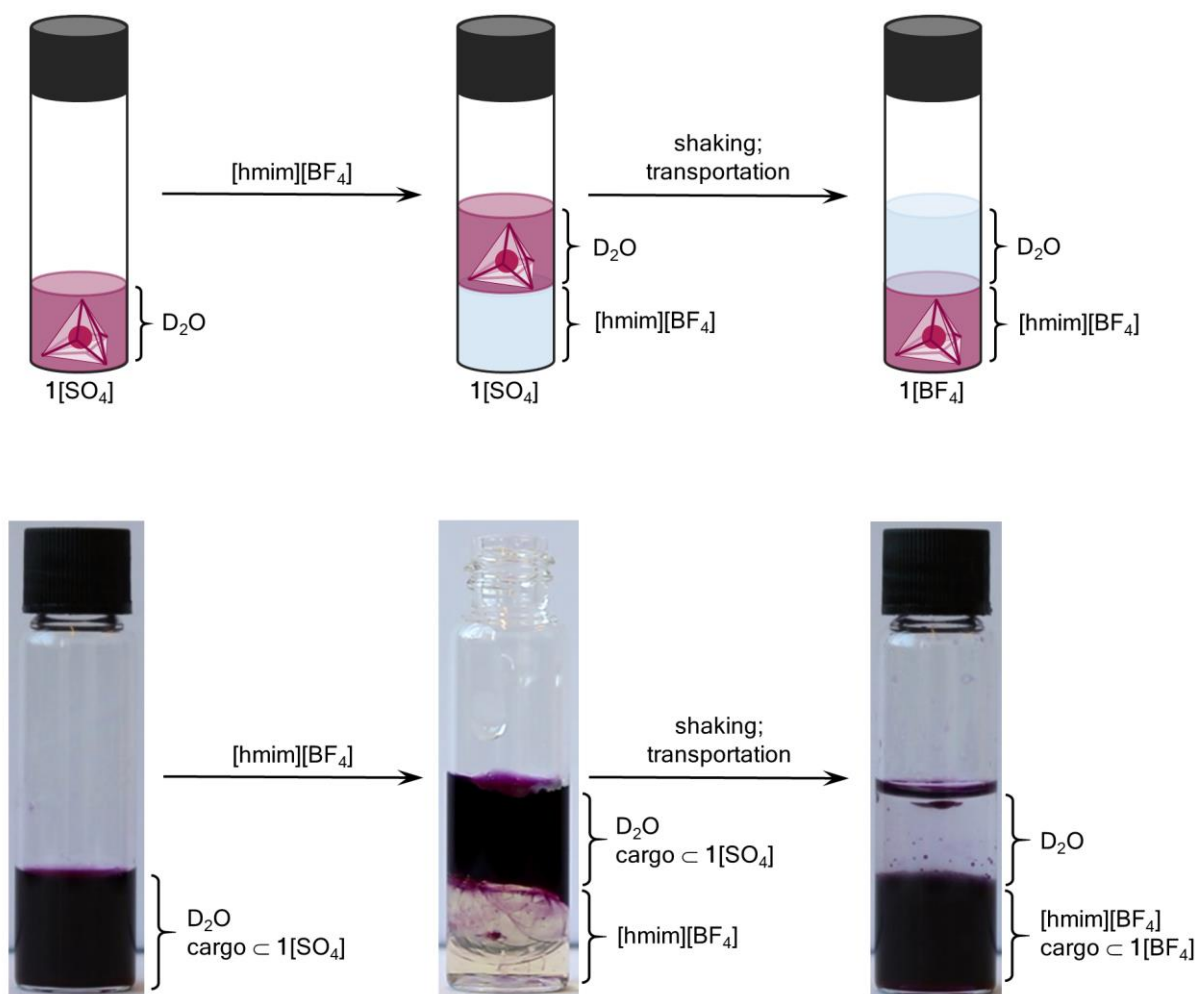


Figure 3.4 (Top) Cartoon representation of the anion exchange from 1-fluoroadamantane $\subset 1[\text{SO}_4]$ to 1-fluoroadamantane $\subset 1[\text{BF}_4]$, resulting in the phase transfer from water to the ionic liquid $[\text{hmim}][\text{BF}_4]$. (Bottom) Photographs of the experiments corresponding to the cartoons immediately above.

The following two NMR spectra were taken of the water layer after 1-fluoroadamantane $\subset 1[\text{SO}_4]$ was transported into the ionic liquid layer upon addition of $[\text{hmim}][\text{BF}_4]$. While water and $[\text{hmim}][\text{BF}_4]$ are mutually immiscible, they have some degree of mutual solubility. Consequently, peaks from the ionic liquid were observed in the ^1H and ^{19}F NMR spectra of the water layer (Figures 3.5 and 3.6, respectively) after the anion exchange from $1[\text{SO}_4]$ to $1[\text{BF}_4]$ and subsequent transport to the ionic liquid layer.

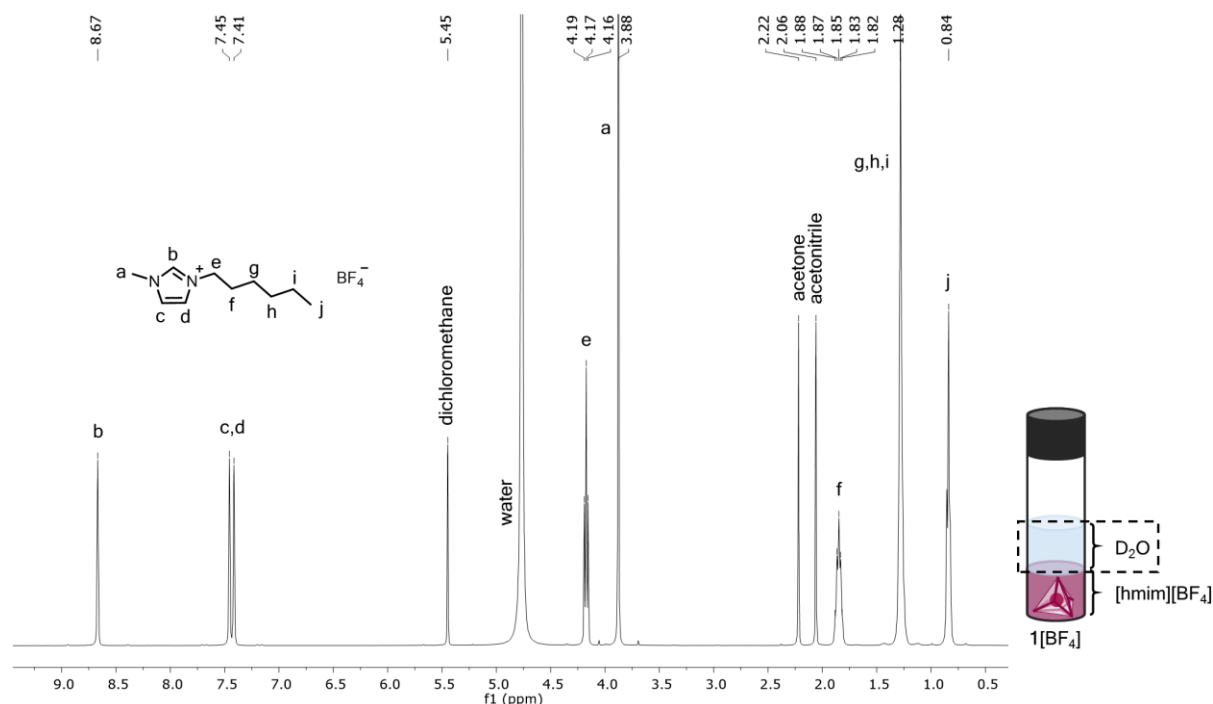


Figure 3.5 ¹H NMR spectrum of the water layer after 1-fluoroadamantane **1** was transported to the [hmim][BF₄] layer. ¹H NMR (500 MHz, D₂O): δ_H = 8.67 (s, H_b), 7.45 (s, H_d), 7.41 (s, H_c), 4.17 (t, *J* = 7.1 Hz, H_e), 3.88 (s, H_a), 1.85 (m, H_f), 1.28 (bs, H_{g,hi}), 0.84 (m, H_j).

In the ¹H NMR spectrum above, no peaks from 1-fluoroadamantane **1** can be detected, even after zooming into the baseline in the aromatic region of the spectrum. This indicates that no cage remained in the water layer after transport to [hmim][BF₄].

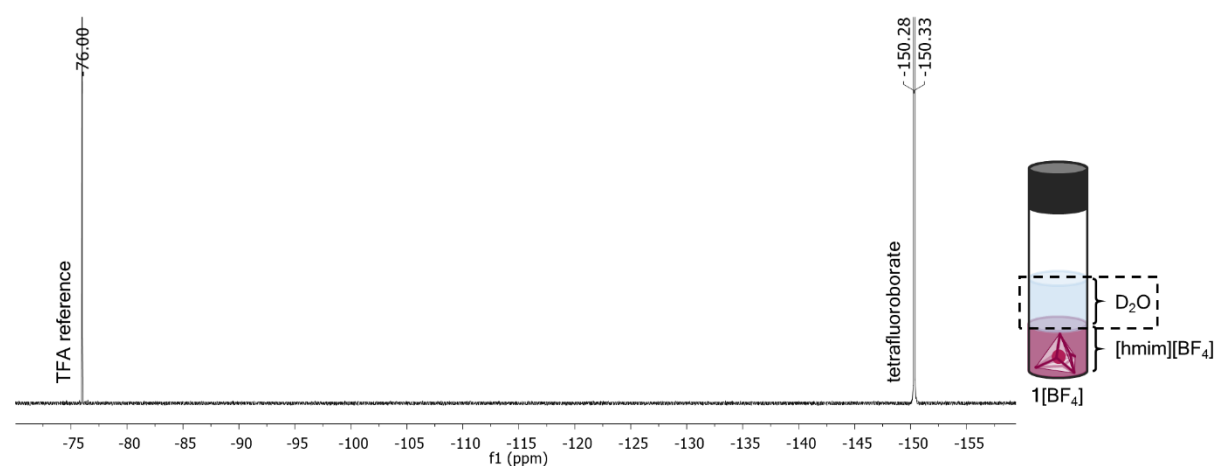


Figure 3.6 ¹⁹F NMR spectrum of the water layer after 1-fluoroadamantane **1** was transported to the [hmim][BF₄] layer. ¹⁹F{¹H} NMR (471 MHz, D₂O, referenced to TFA in a (CD₃)₂CO capillary): δ_F = -76.00 (TFA), -150.28 and -150.33 (BF₄⁻ from [hmim][BF₄] dissolved in water).

Likewise, in the ¹⁹F NMR spectrum above, no peaks from 1-fluoroadamantane **1** can be detected. The ¹H and ¹⁹F NMR spectra of the residual D₂O layer are thus in agreement: no 1-fluoroadamantane **1** remained in this layer after transport to the ionic liquid.

In the ionic liquid layer of the same experiment, the presence of a ¹⁹F NMR (Figure 3.7) signal from free 1-fluoroadamantane (-126.71 ppm) indicated that a small portion of cage decomposed upon being transferred from the water into the ionic liquid layer. Nevertheless, 97% of 1-fluoroadamantane **1** (-120.79 ppm) remained intact throughout the transport from D₂O to [hmim][BF₄]. This value was calculated using the same integral for the TFA reference peak as in the ¹⁹F NMR spectrum in Figure 3.3, the area underneath the signal corresponding to 1-fluoroadamantane **1** was found to be 0.97. In the same ¹⁹F NMR spectrum, the signals marked with an asterisk are due to impurities originating in [hmim][BF₄].

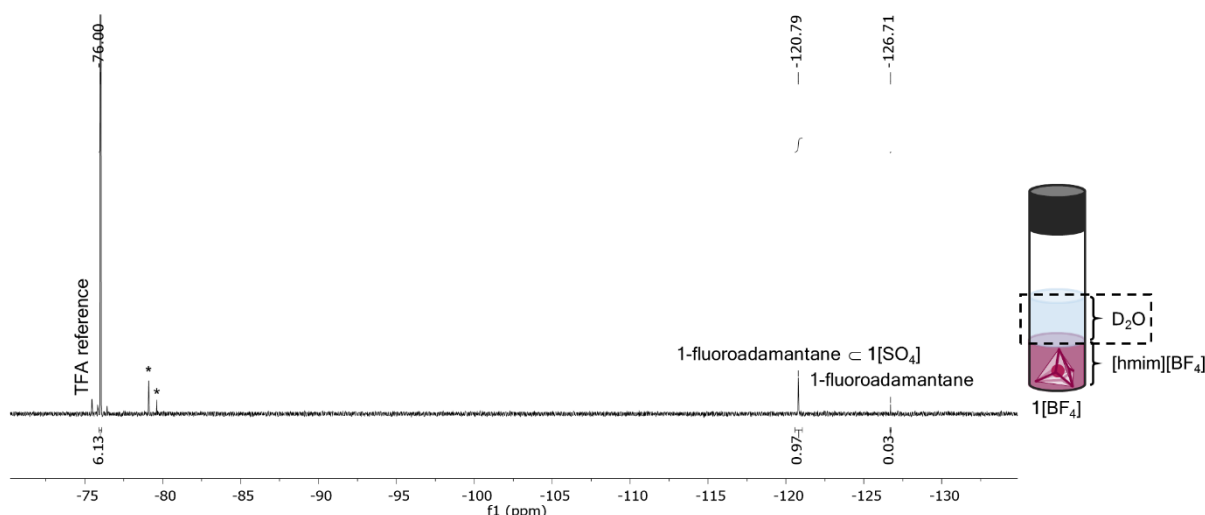


Figure 3.7 The ionic liquid layer after 1-fluoroadamantane **1** was transported to [hmim][BF₄]. ¹⁹F{¹H} NMR (471 MHz, neat, locked and referenced to TFA in a (CD₃)₂CO capillary): δ_F = -76.00 (TFA), -120.79 (1-fluoroadamantane **1**), -127.78 (free 1-fluoroadamantane), -149.81 and -149.86 (BF₄⁻ from [hmim][BF₄]; not shown).

The stability of cage **1** throughout transport from D₂O to [hmim][BF₄] was further confirmed by UV-Vis spectroscopy. Previously, we have shown that no shift in the MLCT band of this cage can be observed upon guest encapsulation, and we have found the maximum absorbance of the triflate adduct of cage **1** to be 571 nm in acetonitrile and 574 nm in the ionic liquid 1-ethyl-3-methylimidazolium ethylsulfate (Chapter 2.2.2). In the absence of ¹H NMR data, UV-

Vis was therefore chosen as a complementary technique to compare the stability of cage **1** before and after transport from the water layer to [hmim][BF₄] (Figures 3.8 and 3.9, respectively). The spectrum of cage **1**[SO₄] in water (0.5 mL, 0.25 mM) is shown below:

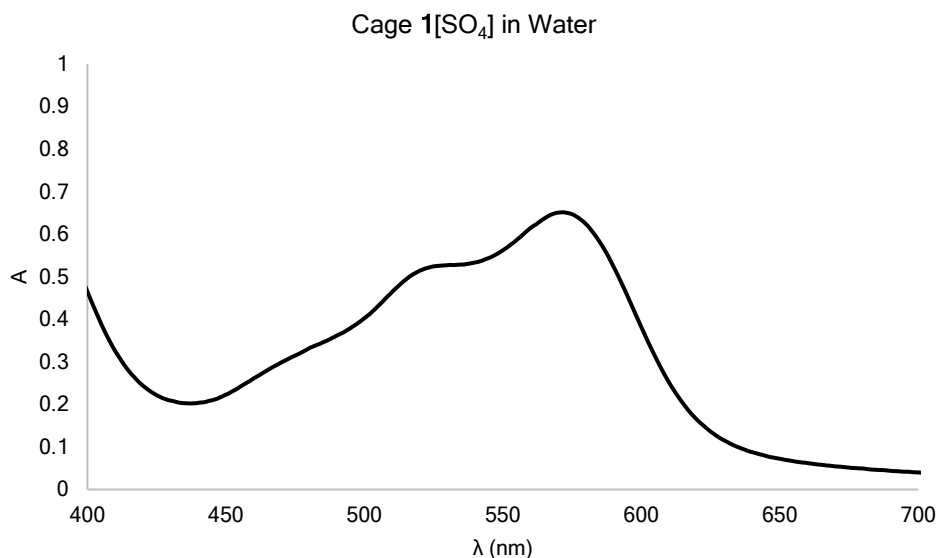


Figure 3.8 UV-Vis spectrum of cage **1**[SO₄] (6.25×10^{-2} mM) in water.

The sample analysed in Figure 3.8 was then added to [hmim][BF₄] (0.3 mL), and the cage was transported to the ionic liquid upon shaking. The spectrum of cage **1**[BF₄] in [hmim][BF₄] (Figure 3.9) was taken immediately after being shaken.

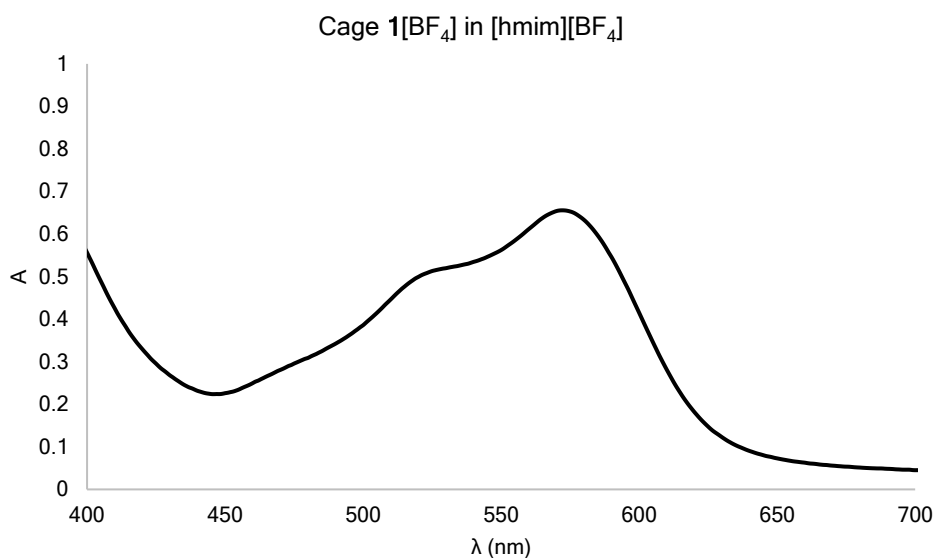


Figure 3.9 UV-Vis spectrum of cage **1**[BF₄] (6.25×10^{-2} mM) in [hmim][BF₄].

The characteristic shape of the UV-Vis spectrum by the cage in [hmim][BF₄] is indistinguishable from the spectrum in water. In both spectra, the maximum absorbance of cage **1** is 572 nm, comparable to the values previously measured in acetonitrile and 1-ethyl-3-methylimidazolium ethylsulfate (Chapter 2.2.2). Taken together with the ¹⁹F NMR data presented above, this UV-Vis data serves as further evidence that cage **1** persists throughout the transportation from water to [hmim][BF₄].

To manipulate cage **1** back into water, a second anion exchange – to convert **1**[BF₄] back into **1**[SO₄] – is required. Before this conversion may be accomplished, however, **1**[BF₄] must be isolated from the ionic liquid layer. This was done by adding ethyl acetate (10 mL) to the water/ionic liquid biphasic system. The ethyl acetate mixed with [hmim][BF₄], thus lowering the solubility of **1**[BF₄] in the organic/ionic liquid layer, and caused it to precipitate from solution (Figure 3.10). Precipitated cage **1**[BF₄] was then isolated *via* filtration, washed thoroughly with ethyl acetate (18 × 5 mL) to remove residual ionic liquid, and redissolved in CD₃CN (1.0 mL).

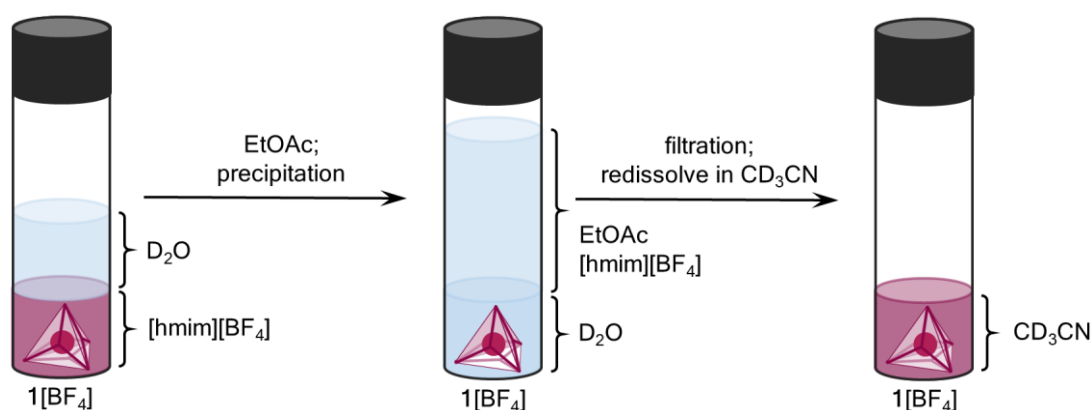


Figure 3.10 Isolation of 1-fluoroadamantane cation **1**[BF₄] from [hmim][BF₄] by precipitation with ethyl acetate; filtration of precipitated 1-fluoroadamantane cation **1**[BF₄]; redissolution in acetonitrile.

The ¹⁹F NMR spectrum of 1-fluoroadamantane cation **1**[BF₄] in CD₃CN showed a signal for encapsulated 1-fluoroadamantane at -120.17 ppm, and no peak for free 1-fluoroadamantane was observed.

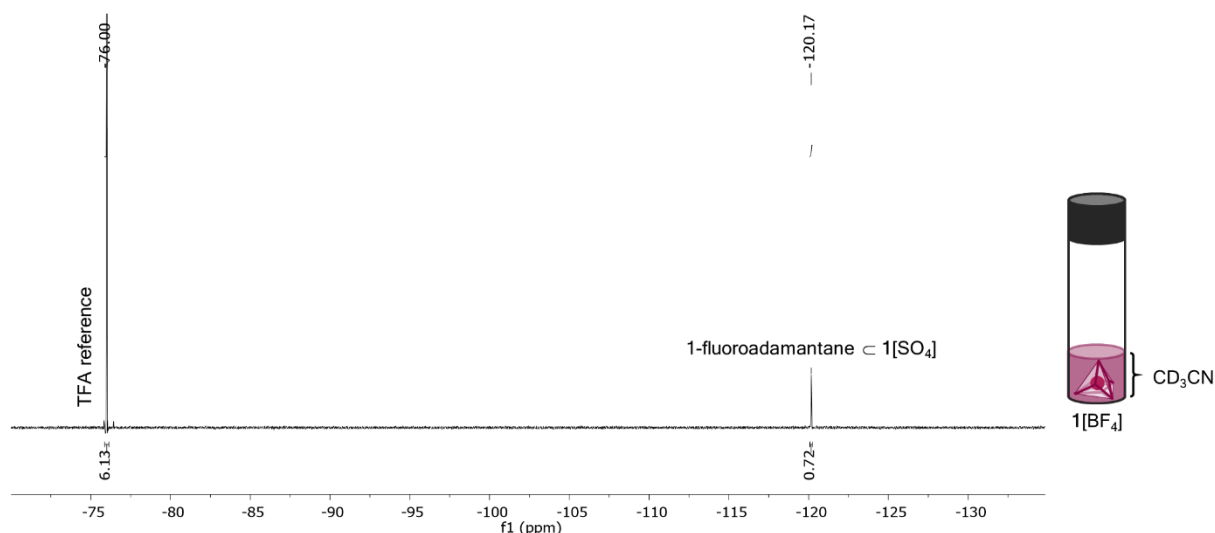


Figure 3.11 ^{19}F NMR spectrum of 1-fluoroadamantane c $\mathbf{1}[\text{BF}_4]$ after being precipitated out of $[\text{hmim}][\text{BF}_4]$ by ethyl acetate and redissolved in CD_3CN . $^{19}\text{F}\{^1\text{H}\}$ NMR (471 MHz, CD_3CN , referenced to TFA in a $(\text{CD}_3)_2\text{CO}$ capillary): $\delta_{\text{F}} = -76.00$ (TFA), -120.17 (1-fluoroadamantane c $\mathbf{1}$), -150.26 and -150.31 (BF_4^- ; counterion for cage $\mathbf{1}$, $[\text{hmim}][\text{BF}_4]$; not shown).

Using the same integral for the TFA reference peak as in the ^{19}F NMR spectrum in Figure 3.3, the area underneath the signal corresponding to 1-fluoroadamantane c $\mathbf{1}$ was found to be 0.72. This value divided by the integral from 1-fluoroadamantane c $\mathbf{1}$ in the previous step (0.97; Figure 3.7) gave the yield (74%) of intact cage after precipitation from $[\text{hmim}][\text{BF}_4]$ with ethyl acetate and redissolving in CD_3CN .

In the ^1H NMR spectrum (Figure 3.12), residual peaks from the ionic liquid, ethyl acetate, diethyl ether, and acetone can be found in addition to the peaks from 1-fluoroadamantane c $\mathbf{1}[\text{BF}_4]$. The small peaks marked with an asterisk in the figure below are attributed to encapsulated 1-fluoroadamantane and aliphatic protons on the hexyl chain of $[\text{hmim}][\text{BF}_4]$.

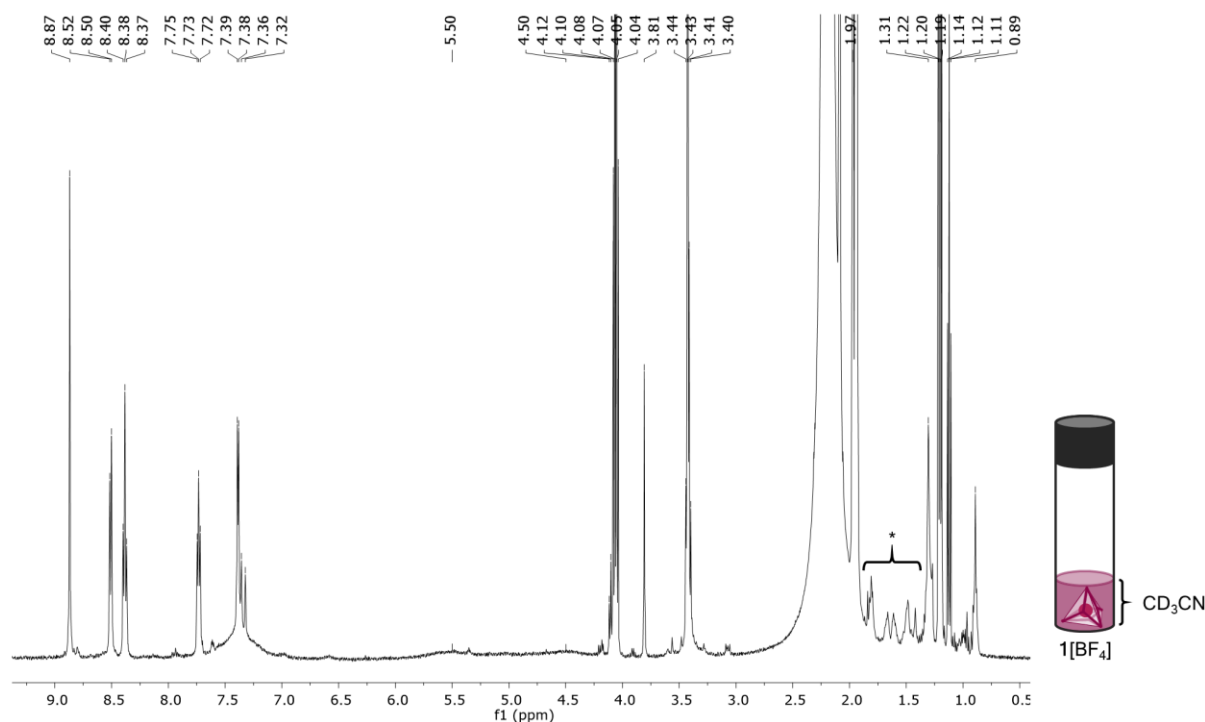


Figure 3.12 ^1H NMR spectrum of 1-fluoroadamantane $\text{c} \mathbf{1}[\text{BF}_4]$ after being precipitated out of $[\text{hmim}][\text{BF}_4]$ by ethyl acetate and redissolved in CD_3CN . ^1H NMR (500 MHz, CD_3CN): $\delta_{\text{H}} = 8.87$ (s, $\mathbf{1}[\text{BF}_4]$), 8.51 (d, $J = 7.7$ Hz, $\mathbf{1}[\text{BF}_4]$), 8.38 (t, $J = 7.7$ Hz, $\mathbf{1}[\text{BF}_4]$), 7.73 (t, $J = 6.8$ Hz, $\mathbf{1}[\text{BF}_4]$), 7.39 (d, $J = 5.5$ Hz, $\mathbf{1}[\text{BF}_4]$), 7.36 (s, $[\text{hmim}][\text{BF}_4]$), 7.32 (s, $[\text{hmim}][\text{BF}_4]$), 7.58-7.04 (bs, $\mathbf{1}[\text{BF}_4]$), 5.50 (bs, $\mathbf{1}[\text{BF}_4]$), 4.50 (bs, $\mathbf{1}[\text{BF}_4]$), 4.10 (t, $J = 7.3$ Hz, $[\text{hmim}][\text{BF}_4]$), 4.06 (q, $J = 7.1$ Hz, ethyl acetate), 3.81 (s, $[\text{hmim}][\text{BF}_4]$), 3.43 (s, $\mathbf{1}[\text{BF}_4]$), 2.19 (bs, water), 3.42 (q, $J = 7.0$ Hz, diethyl ether), 2.09 (s, acetone), 1.97 (s, ethyl acetate), 1.20 (t, $J = 7.1$ Hz, ethyl acetate), 1.31 (m, $[\text{hmim}][\text{BF}_4]$), 1.12 (t, $J = 7.0$ Hz, diethyl ether), 0.89 (unresolved t, $[\text{hmim}][\text{BF}_4]$).

After $\mathbf{1}[\text{BF}_4]$ was dissolved in acetonitrile, acetonitrile-soluble tetrabutylammonium sulfate was added (50% in water, 4.8 equiv) to convert $\mathbf{1}[\text{BF}_4]$ back into $\mathbf{1}[\text{SO}_4]$. Anion exchange was driven by precipitation of 1-fluoroadamantane $\text{c} \mathbf{1}$ from solution (Figure 3.13). Precipitated 1-fluoroadamantane $\text{c} \mathbf{1}[\text{SO}_4]$ was then isolated *via* filtration, washed with diethyl ether (3×1 mL) to remove residual ionic liquid, and redissolved in water. This final step thus closes the transport cycle of $\mathbf{1}$ from water, to an ionic liquid, and finally back to water.

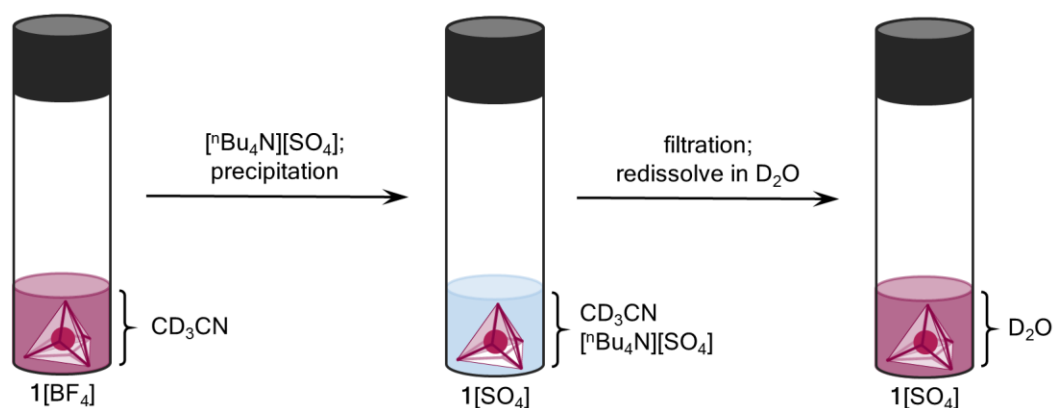


Figure 3.13 Anion exchange from 1-fluoroadamantane $\subset 1[\text{BF}_4]$ to 1-fluoroadamantane $\subset 1[\text{SO}_4]$, allowing the complex to be redissolved in water.

The ^{19}F NMR spectrum of 1-fluoroadamantane $\subset 1[\text{SO}_4]$ in D_2O showed a signal for encapsulated 1-fluoroadamantane at -120.42 ppm, and no peak for free 1-fluoroadamantane was observed.

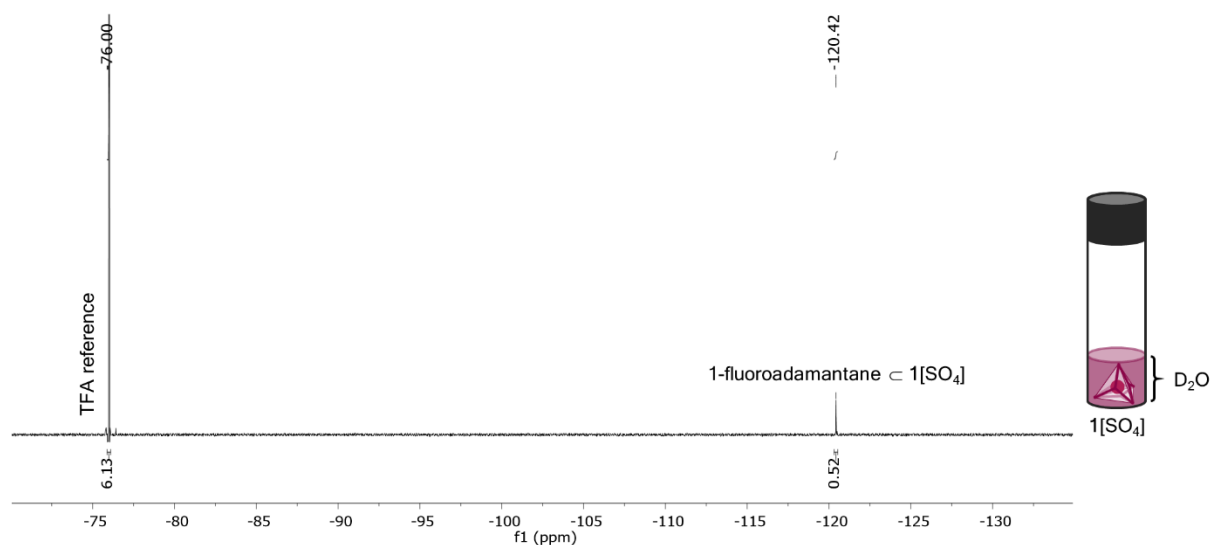


Figure 3.14 ^{19}F NMR analysis of 1-fluoroadamantane $\subset 1[\text{SO}_4]$ after being precipitated out of acetonitrile by [$n\text{Bu}_4\text{N}$][SO_4] and redissolved in D_2O . $^{19}\text{F}\{^1\text{H}\}$ NMR (471 MHz, D_2O , referenced to TFA in a $(\text{CD}_3)_2\text{CO}$ capillary): $\delta_{\text{F}} = -76.00$ (TFA), -120.42 (1-fluoroadamantane $\subset 1$).

Using the same integral for the TFA reference peak as in the ^{19}F NMR spectrum in Figure 3.3, the area underneath the signal corresponding to 1-fluoroadamantane $\subset 1$ was found to be 0.52. This value divided by the integral from 1-fluoroadamantane $\subset 1$ in the previous step (0.72;

Figure 3.11) gave the yield (72%) of intact cage after precipitation from CD₃CN with [nBu₄N][SO₄] and redissolving in D₂O.

In the ¹H NMR spectrum, residual peaks from the ionic liquids [hmim][BF₄] and [nBu₄N][SO₄] and the organic solvents ethyl acetate, acetonitrile, diethyl ether, and acetone can be found in addition to the peaks from 1-fluoroadamantane ⊂ **1**[BF₄].

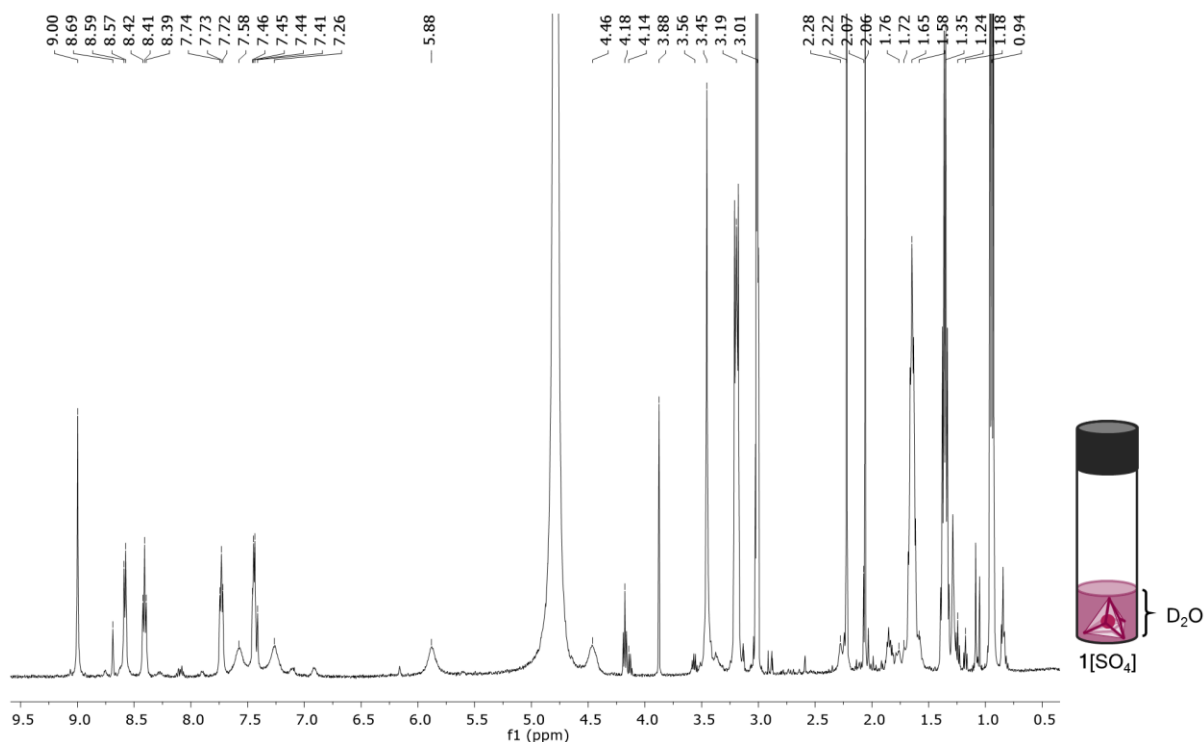


Figure 3.15 ¹H NMR analysis of 1-fluoroadamantane ⊂ **1**[SO₄] after being precipitated out of acetonitrile by [nBu₄N][SO₄] and redissolved in D₂O. ¹H NMR (500 MHz, D₂O): δ_H = 9.00 (s, **1**[SO₄]), 8.69 (s, [hmim][BF₄]), 8.58 (d, *J* = 7.6 Hz, **1**[SO₄]), 8.41 (t, *J* = 7.6 Hz, **1**[SO₄]), 7.73 (t, *J* = 6.5 Hz, **1**[SO₄]), 7.58 (bs, **1**[SO₄]), 7.46 (s, [hmim][BF₄]), 7.44 (d, *J* = 6.5 Hz, **1**[SO₄]), 7.41 (s, [hmim][BF₄]), 7.26 (bs, **1**[SO₄]), 5.88 (bs, **1**[SO₄]), 4.46 (bs, **1**[SO₄]), 4.18 (t, *J* = 7.1 Hz, [hmim][BF₄]), 4.14 (q, *J* = 7.2, ethyl acetate), 3.88 (s, [hmim][BF₄]), 3.56 (q, *J* = 7.1 Hz, diethyl ether), 3.45 (s, **1**[SO₄]), 3.19 (m, [nBu₄N][SO₄]), 3.01 (quin, *J* = 2.2 Hz, residual peak from TFA in a (CD₃)₂CO capillary), 2.28-1.58 (m, encapsulated 1-fluoroadamantane peaks), 2.22 (s, acetone), 2.07 (s, ethyl acetate), 2.06 (s, acetonitrile), 1.65 (m, [nBu₄N][SO₄]), 1.36 (m, [nBu₄N][SO₄]), 1.24 (t, *J* = 7.2 Hz, ethyl acetate), 1.17 (t, *J* = 7.1 Hz, diethyl ether), 0.94 (t, *J* = 7.4 Hz, [nBu₄N][SO₄]).

3.2.4 Tuning the properties of ionic liquids and coordination cages

The specific transport cycle outlined in Figure 3.1 is not the only possible manifestation of this concept; both the ionic liquid and the cage can be systematically modified. Since [hmim][BF₄] is known to be susceptible to hydrolysis, an ionic liquid that is more compatible with water can instead be chosen. 1-Ethyl-3-methylimidazolium triflimide ([emim][NTf₂]), for example, is a hydrophobic ionic liquid that is more stable to hydrolysis than [hmim][BF₄]. We have previously shown that [emim][NTf₂] is a good solvent for the fluorinated analogue of cage **1**, synthesised with fluorinated subcomponent **C** instead of **B** (Figure 3.16). This fluorinated cage cannot be used for transport between water and ionic liquid phase, however, because it is insoluble in water. Neither can **1** be transported into [emim][NTf₂] – it is insoluble in this ionic liquid and precipitated out of both phases upon anion exchange from **1**[SO₄] to **1**[NTf₂]. We found, however, that the physicochemical properties of the cage can be tuned by incorporating both **B** and **C**. Combining four equivalents of **A** with six equivalents each of subcomponents **B** and **C**, we obtained a mixture of cages **2**, which is soluble in both water and [emim][NTf₂]. The preparation of **2** thus highlights the utility of subcomponent self-assembly in preparing materials with tunable properties – solubility, in the present case. The library of cages **2**[SO₄] acted in concert to bind 1-fluoroadamantane and were readily transported together from water into the ionic liquid layer upon addition of [emim][NTf₂].

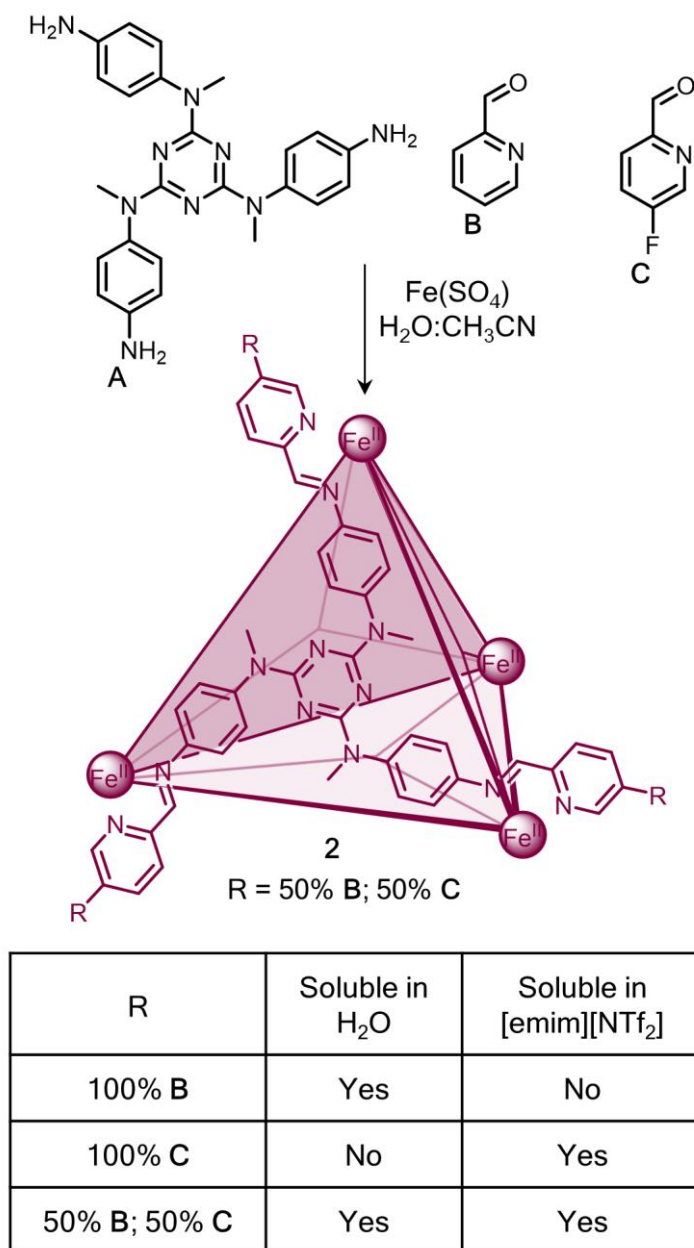


Figure 3.16 Cage **1** composed of 12 equivalents of **B** is soluble in water but insoluble in [emim][NTf₂]; an analogous cage composed of 12 equivalents of **C** is soluble in [emim][NTf₂] but insoluble in water; mixed cages **2**, prepared from 6 equivalents of **B** and 6 equivalents of **C** is soluble in both [emim][NTf₂] and water.

An aliquot of 1-fluoroadamantane \subset **2**[SO₄] in D₂O (2 mM, 0.3 mL) was filtered, and the following ¹⁹F NMR spectrum was recorded.

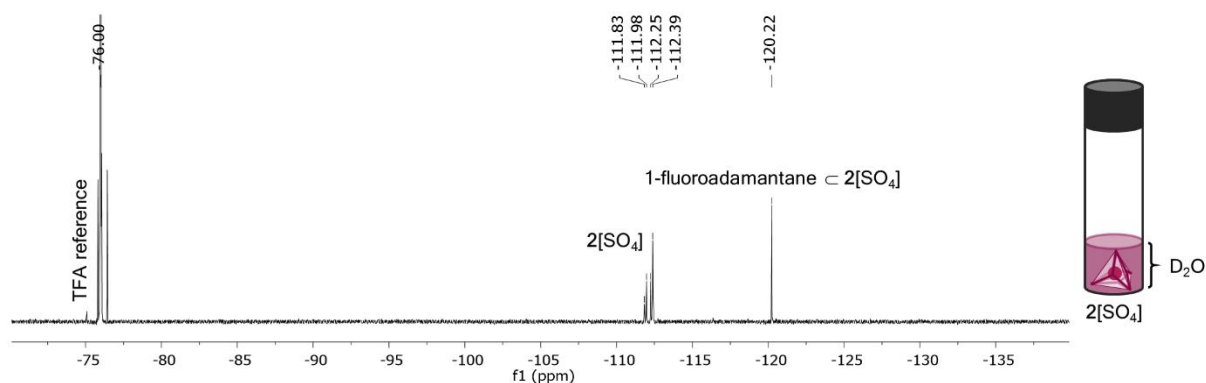


Figure 3.17 2.0 mM solution of 1-fluoroadamantane **c** 2[SO₄] dissolved in D₂O. ¹⁹F{¹H} NMR (471 MHz, D₂O, referenced to TFA in a (CD₃)₂CO capillary): ¹⁹F{¹H} NMR (471 MHz, D₂O, referenced to TFA in a (CD₃)₂CO capillary): δ_F = -76.00 (TFA), -111.83 (2[SO₄]), -111.98 (2[SO₄]), -112.25 (2[SO₄]), -112.39 (2[SO₄]), -120.22 (1-fluoroadamantane **c** 2[SO₄]).

Ionic liquid [emim][NTf₂] (0.3 mL) was added to the sample above; the complex 1-fluoroadamantane **c** 2 transferred to the ionic liquid layer upon shaking; and the following ¹⁹F NMR spectrum was recorded of the ionic liquid layer.

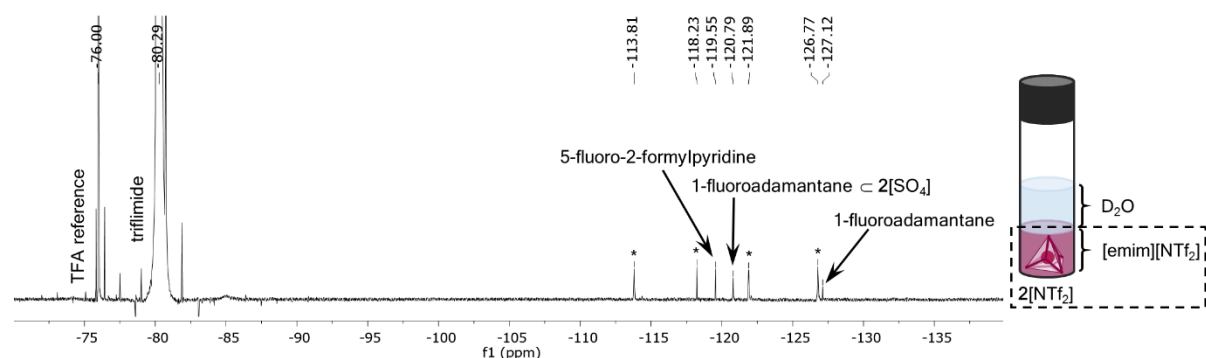


Figure 3.18 ¹⁹F NMR of 1-fluoroadamantane **c** 2[NTf₂] in [emim][NTf₂] layer after transport from D₂O. ¹⁹F{¹H} NMR (471 MHz, neat, locked and referenced to TFA in a (CD₃)₂CO capillary): δ_F = -76.00 (TFA), -80.29 (triflimide; anion from [emim][NTf₂]), -113.81 (impurity from [emim][NTf₂]), -118.23 (impurity from [emim][NTf₂]), -119.55 (5-fluoro-2-formylpyridine), -120.79 (1-fluoroadamantane **c** 2), -121.89 (impurity from [emim][NTf₂]), -126.77 (impurity from [emim][NTf₂]), -127.12 (free 1-fluoroadamantane).

3.2.5 Separation of 1-fluoroadamantane **c** 2 from 1-fluorobenzene **c** 3

The cycle described above (Figure 3.1) is enabled by counteranion exchange of a cationic coordination cage. If, however, a cage has an overall negative charge, transport from water to an ionic liquid would necessarily be driven by exchange of the cage's countercations. When

hydrophobic imidazolium ionic liquids [hmim][BF₄] or [emim][NTf₂] are added to an aqueous solution of anionic cage [Me₄N]**3** (Figure 3.19),³³ however, no transition from water to the ionic liquid is observed. While these ionic liquids are only slightly soluble in water, the combination of anionic cage and imidazolium cation yields a water-soluble salt. This feature allowed the design of the system in Figure 3.19, in which an aqueous mixture of two different cages (2[SO₄] and [Me₄N]**3**) were separated, thereby also separating a mixture of two different encapsulated guests.

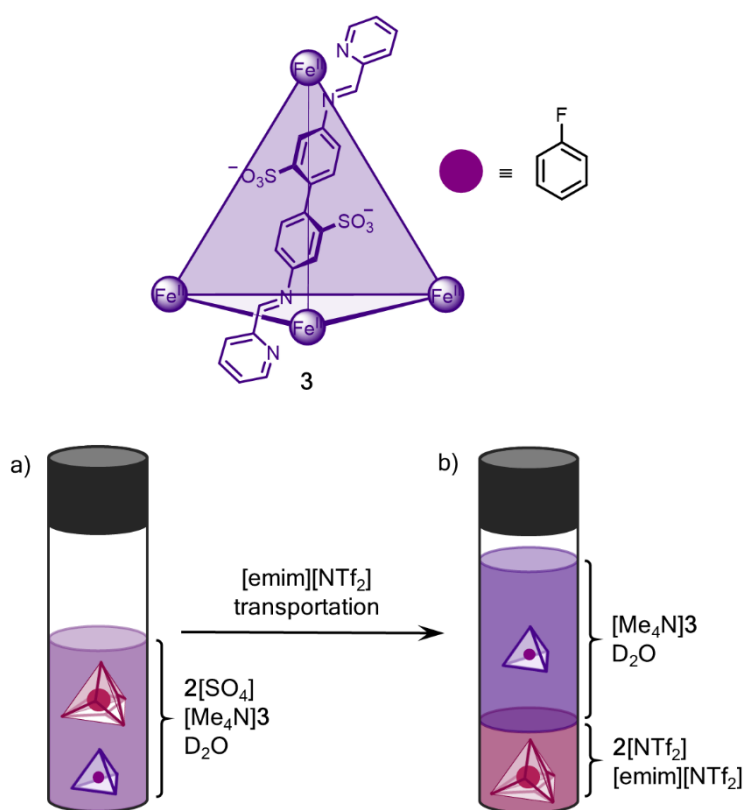


Figure 3.19 a) 1-Fluoroadamantane \subset 2[SO₄] and 1-fluorobenzene \subset [Me₄N]**3** dissolved in water. b) Upon the addition of [emim][NTf₂], 1-fluoroadamantane \subset **2** transferred from the water to the ionic liquid layer, whereas 1-fluorobenzene \subset [Me₄N]**3** remained dissolved in water.

Aliquots of 1-fluoroadamantane \subset 2[SO₄] (2 mM, 1 mL) in D₂O and 1-fluorobenzene \subset [Me₄N]**3** (2 mM, 1 mL) in D₂O were combined and filtered to remove suspended free 1-fluoroadamantane and precipitated cage. Due to the partial precipitation of each cage upon mixing, we know only that the concentration of each cage in solution is less than 1 mM. The ¹H NMR spectrum of the resulting solution can be found below (Figure 3.20c). For comparison,

the ¹H NMR spectra corresponding to 1-fluorobenzene ⊂ [Me₄N]3 in D₂O and 1-fluoroadamantane ⊂ 2[SO₄] in D₂O are also presented (Figures 3.20a and 3.20b, respectively).

Due to the number of components in solution together in this mixture (empty 2[SO₄], 1-fluoroadamantane ⊂ 2[SO₄], empty [Me₄N]3, 1-fluorobenzene ⊂ [Me₄N]3, free 1-fluorobenzene, and cage subcomponents), the ¹H NMR spectrum from the mixture has not been fully assigned. Comparison with the ¹H NMR spectra for 1-fluoroadamantane ⊂ 2[SO₄] and 1-fluorobenzene ⊂ [Me₄N]3 (the full assignments for which can be found in Chapter 3.4) was deemed sufficient for characterisation.

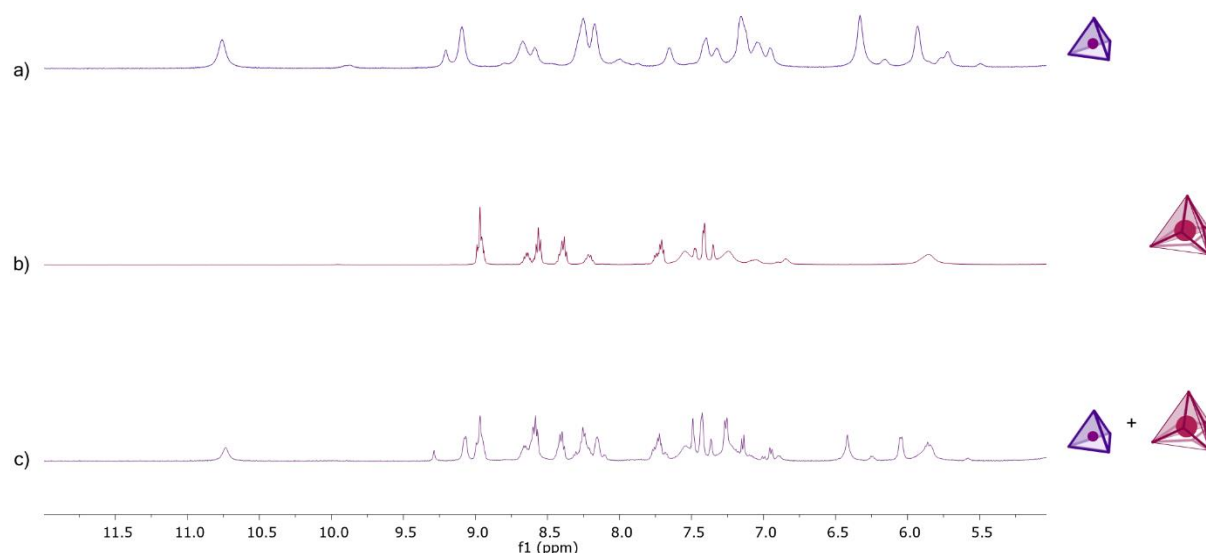


Figure 3.20 a) ¹H NMR (500 MHz, D₂O) of 1-fluorobenzene ⊂ [Me₄N]3. b) ¹H NMR (500 MHz, D₂O) of 1-fluoroadamantane ⊂ 2[SO₄]. c) ¹H NMR (500 MHz, D₂O) of a mixture of 1-fluoroadamantane ⊂ 2[SO₄] (<1 mM) and 1-fluorobenzene ⊂ [Me₄N]3 (<1 mM) in D₂O.

As anticipated, the spectrum presented in Figure 3.20c (from the mixture of each host-guest species) is a composite of the spectra from Figure 3.20a (1-fluorobenzene ⊂ [Me₄N]3) and Figure 3.20b (1-fluoroadamantane ⊂ 2[SO₄]). Likewise, the ¹⁹F NMR spectrum of the mixture, below, shows encapsulated 1-fluorobenzene, encapsulated 1-fluoroadamantane, and fluorine signals attributed to the cages 2[SO₄].

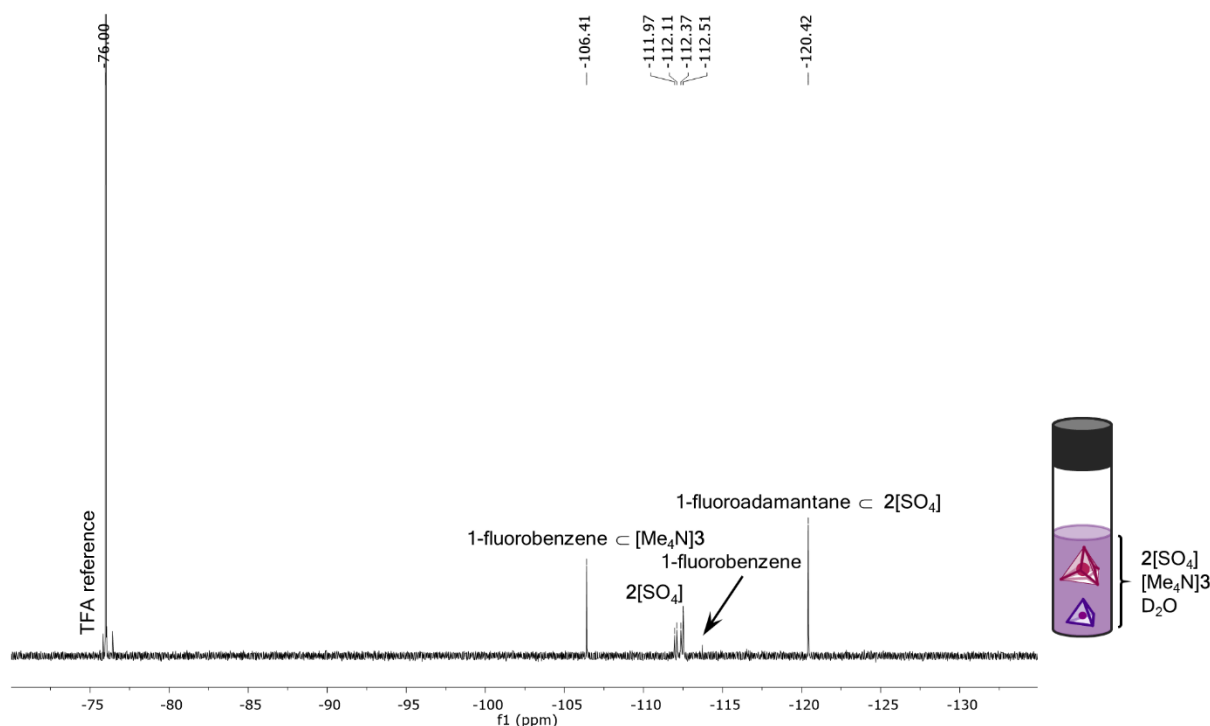


Figure 3.21 ^{19}F NMR analysis of a mixture of 1-fluoroadamantane \subset $2[\text{SO}_4]$ (<1 mM) and 1-fluorobenzene \subset $[\text{Me}_4\text{N}]\mathbf{3}$ (<1 mM) in D_2O . $^{19}\text{F}\{^1\text{H}\}$ NMR (471 MHz, D_2O , referenced to TFA in a $(\text{CD}_3)_2\text{CO}$ capillary): $\delta_{\text{F}} = -76.00$ (TFA), -106.41 (1-fluorobenzene \subset $[\text{Me}_4\text{N}]\mathbf{3}$), -111.97 ($2[\text{SO}_4]$), -112.11 ($2[\text{SO}_4]$), -112.37 ($2[\text{SO}_4]$), -112.51 ($2[\text{SO}_4]$), -120.42 (1-fluoroadamantane \subset $2[\text{SO}_4]$).

To this aqueous mixture of host-guest complexes, $[\text{emim}][\text{NTf}_2]$ (1.4 mL) was added, initiating the transport of 1-fluoroadamantane \subset $\mathbf{1}$ from the water to the ionic liquid layer (Figure 3.1b). By measuring the ^{19}F NMR spectra of the resulting water and ionic liquid layers, we observed clean separation of each cage into a different phase: 1-fluorobenzene \subset $[\text{Me}_4\text{N}]\mathbf{3}$ was found exclusively in the water layer, and 1-fluoroadamantane \subset $2[\text{NTf}_2]$ was found exclusively in the ionic liquid. No peak for encapsulated 1-fluoroadamantane was observed in the ^{19}F NMR of the water layer, wherein the ^{19}F NMR signal from 1-fluorobenzene \subset $[\text{Me}_4\text{N}]\mathbf{3}$ remained unchanged. Likewise, no peak for 1-fluorobenzene \subset $[\text{Me}_4\text{N}]\mathbf{3}$ was observed in the ionic liquid layer. Phase transfer of cationic cages $\mathbf{2}$ thus rendered straightforward the clean separation of two physicochemically similar host-guest complexes.

The following NMR spectra were taken of the water layer after 1-fluoroadamantane \subset $2[\text{SO}_4]$ was transported into $[\text{emim}][\text{NTf}_2]$, thereby isolating 1-fluorobenzene \subset $[\text{Me}_4\text{N}]\mathbf{3}$. While water and $[\text{emim}][\text{NTf}_2]$ are mutually immiscible, they have some degree of mutual solubility. Consequently, peaks from the ionic liquid were observed in the ^1H and ^{19}F NMR spectra of the

water layer (Figures 3.22b and 3.24, respectively) after the anion exchange from **1**[SO₄] to **1**[BF₄] and subsequent transport to the ionic liquid layer.

The ¹H NMR spectrum from the water layer has not been fully assigned due to the number of components in solution (empty [Me₄N]**3**, 1-fluorobenzene ⊂ [Me₄N]**3**, cage subcomponents, dissolved [emim][NTf₂], and [emim][NTf₂] droplets/micelles). Comparison with the ¹H NMR spectrum for 1-fluorobenzene ⊂ [Me₄N]**3** (the full assignment for which can be found in Chapter 3.5.2) has been deemed sufficient for characterisation.

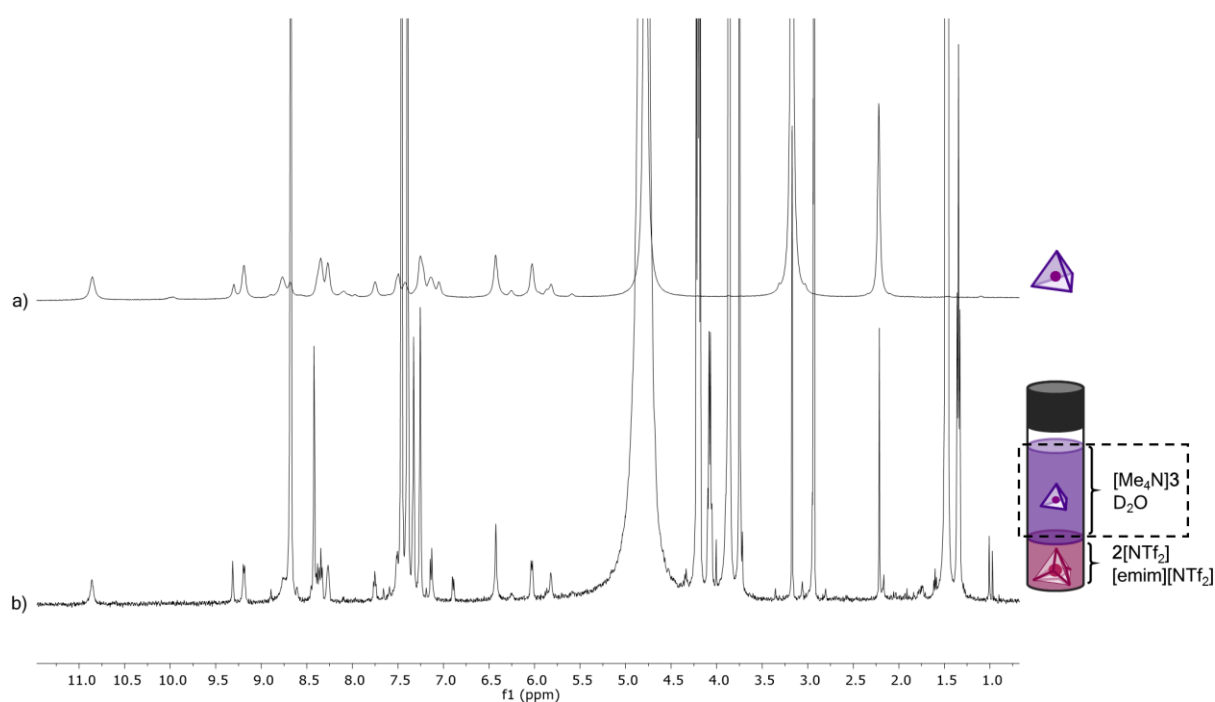


Figure 3.22 a) ¹H NMR (500 MHz, D₂O) of 1-fluorobenzene ⊂ [Me₄N]**3** in D₂O, as originally prepared. b) ¹H NMR (500 MHz, D₂O) of 1-fluorobenzene ⊂ [Me₄N]**3** in the water layer after transport of 1-fluoroadamantane ⊂ **2**[SO₄] from D₂O to [emim][NTf₂].

The spectrum in Figure 3.22b (from 1-fluorobenzene ⊂ [Me₄N]**3** after separation from 1-fluoroadamantane ⊂ **2**[SO₄]) has been zoomed in to show that the peaks in the baseline are identical to the ¹H NMR signals from Figure 3.22a (from 1-fluorobenzene ⊂ [Me₄N]**3** as originally prepared). The large signals found throughout the spectrum are due to the ionic liquid. The spectrum in Figure 3.22b has therefore been copied below, zoomed out so the [emim][NTf₂] peaks are better visualised. The major set of [emim][NTf₂] signals corresponds

to ionic liquid dissolved in the D_2O layer; the minor set of $[\text{emim}][\text{NTf}_2]$ signals corresponds to small droplets or micelles of the neat ionic liquid.

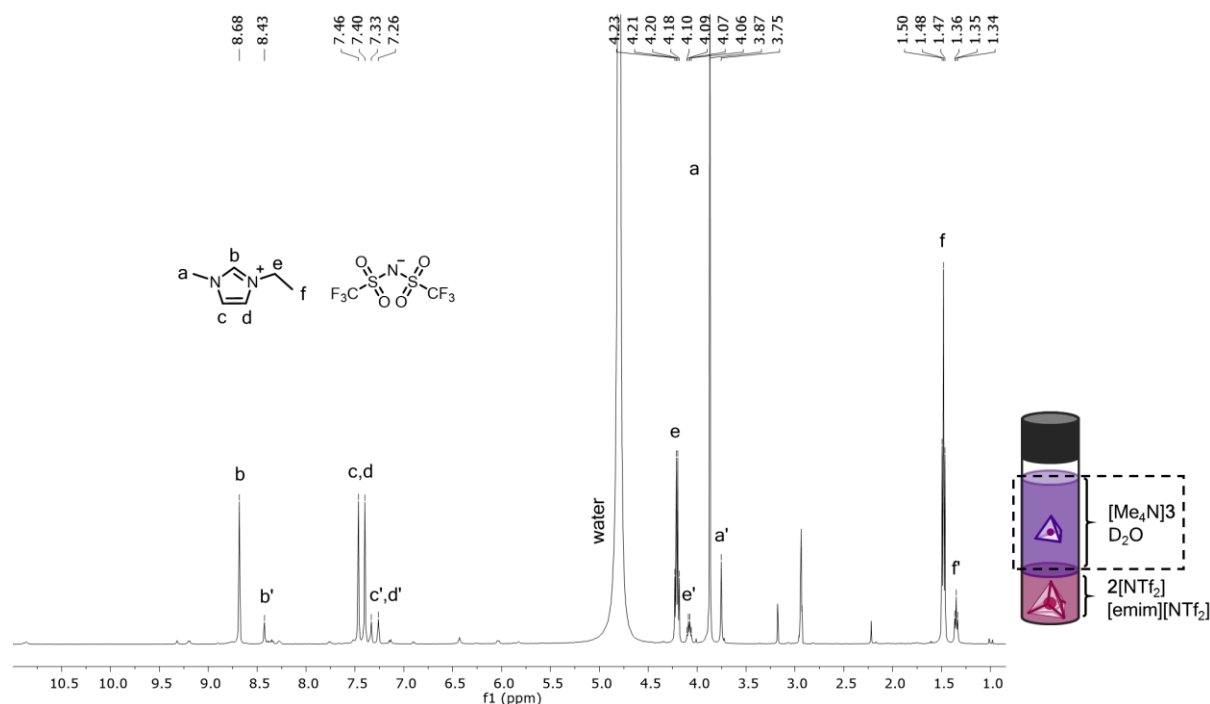


Figure 3.23 ^1H NMR of 1-fluorobenzene $\subset [\text{Me}_4\text{N}]^3$ in the water layer after transport of 1-fluoroadamantane $\subset \mathbf{2}$ from D_2O to $[\text{emim}][\text{NTf}_2]$. ^1H NMR (500 MHz, D_2O): $\delta_{\text{H}} = 8.68$ (s, H_b), 8.43 (s, $\text{H}_{b'}$), 7.46 (s, H_d), 7.40 (s, H_c), 7.33 (s, $\text{H}_{d'}$), 7.26 (s, H_c'), 4.21 (q, $J = 7.4$ Hz, H_e), 4.08 (q, $J = 7.2$ Hz, $\text{H}_{e'}$), 3.87 (s, H_a), 3.75 (s, H_a'), 1.48 (t, $J = 7.4$ Hz, H_f), 1.35 (t, $J = 7.2$ Hz, $\text{H}_{f'}$).

The ^{19}F NMR spectrum below of isolated 1-fluorobenzene $\subset [\text{Me}_4\text{N}]^3$ in water, shows encapsulated 1-fluorobenzene. The ^{19}F NMR signals from 1-fluoroadamantane $\subset \mathbf{2}[\text{SO}_4]$ are absent because 1-fluoroadamantane $\subset \mathbf{2}[\text{SO}_4]$ was transported out of the water layer and into the ionic liquid layer. As in the ^1H NMR spectrum above, the primary triflimide signal corresponds to ionic liquid dissolved in the D_2O layer; the lesser triflimide signal corresponds to small droplets or micelles of the neat ionic liquid.

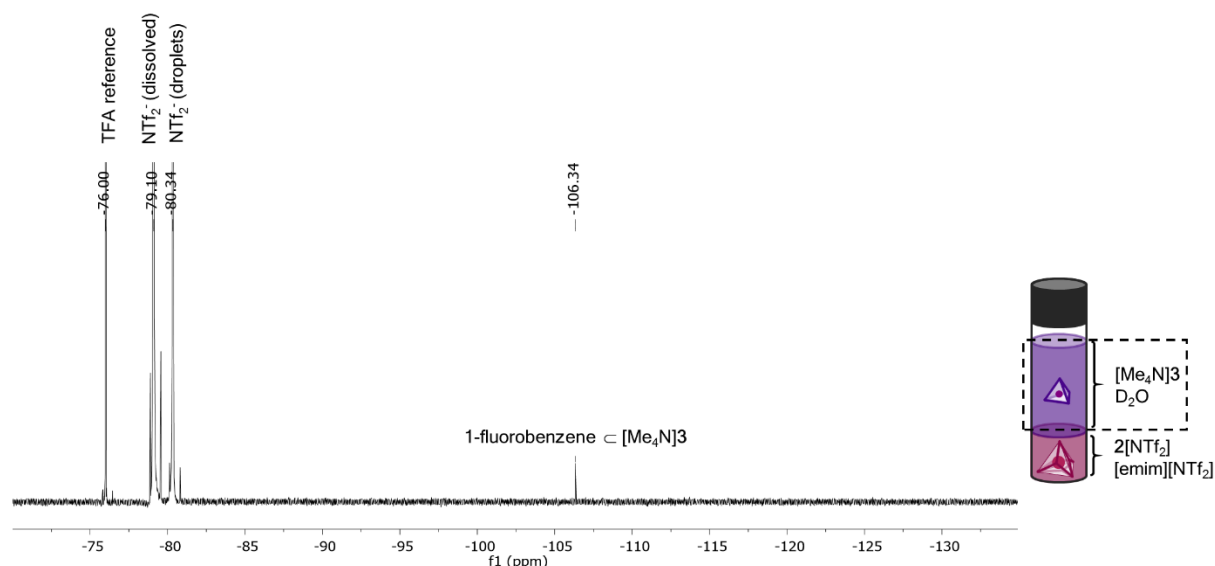


Figure 3.24 ^{19}F NMR analysis of 1-fluorobenzene \subset $[\text{Me}_4\text{N}]\mathbf{3}$ in the water layer after transport of 1-fluoroadamantane \subset $\mathbf{2}$ from D_2O to $[\text{emim}][\text{NTf}_2]$. $^{19}\text{F}\{^1\text{H}\}$ NMR (471 MHz, D_2O , referenced to TFA in a $(\text{CD}_3)_2\text{CO}$ capillary): $\delta_{\text{F}} = -76.00$ (TFA), -79.10 ($[\text{emim}][\text{NTf}_2]$ dissolved in D_2O), -80.34 (small droplets/micelles of $[\text{emim}][\text{NTf}_2]$ in D_2O), -106.34 (1-fluorobenzene \subset $[\text{Me}_4\text{N}]\mathbf{3}$).

The following ^{19}F NMR spectrum (Figure 3.25b) was taken of the ionic liquid layer after 1-fluoroadamantane \subset $\mathbf{2}[\text{SO}_4]$ was transported into $[\text{emim}][\text{NTf}_2]$, thereby separating cationic host-guest complex 1-fluoroadamantane \subset $\mathbf{2}[\text{SO}_4]$ from anionic 1-fluorobenzene \subset $[\text{Me}_4\text{N}]\mathbf{3}$. For comparison, the ^{19}F NMR spectrum of neat $[\text{emim}][\text{NTf}_2]$ is also included (Figure 3.25a). The ^{19}F signals at -113.86 ppm, -118.29 ppm, -121.94 ppm, and -126.83 ppm are impurities from the commercial lithium triflimide used in the preparation of $[\text{emim}][\text{NTf}_2]$. The ^{19}F NMR signals from 1-fluorobenzene \subset $[\text{Me}_4\text{N}]\mathbf{3}$ are absent because the host-guest complex 1-fluorobenzene \subset $[\text{Me}_4\text{N}]\mathbf{3}$ remained in the water layer when 1-fluoroadamantane \subset $\mathbf{2}[\text{SO}_4]$ was transported to the ionic liquid layer.

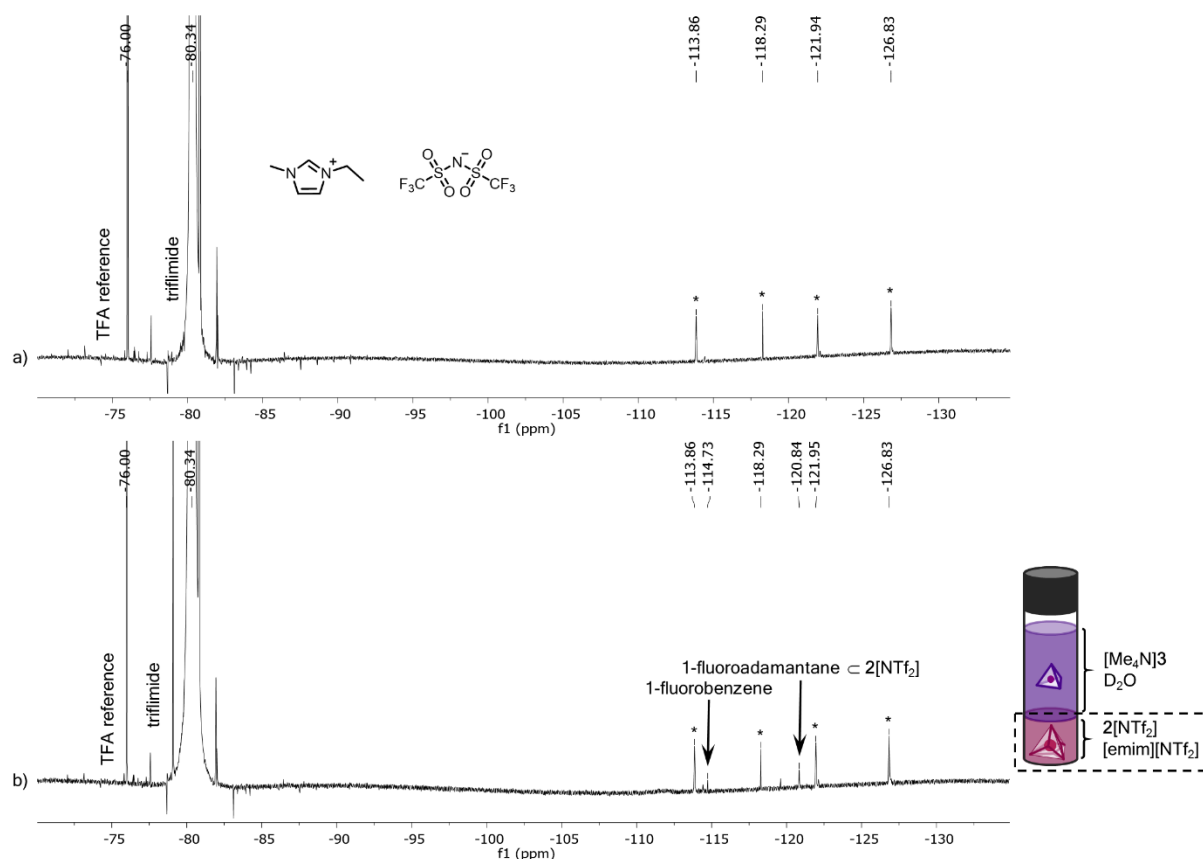


Figure 3.25 a) ¹⁹F NMR of neat [emim][NTf₂]. ¹⁹F{¹H} NMR (471 MHz, neat, locked and referenced to TFA in a (CD₃)₂CO capillary): δ_F = -76.00 (TFA), -80.34 (NTf₂⁻; anion from [emim][NTf₂]), -113.86 (impurity), -118.29 (impurity), -121.94 (impurity), -126.83 (impurity). b) ¹⁹F NMR of 1-fluoroadamantane c 2[NTf₂] in [emim][NTf₂] layer after transport from D₂O and separation from 1-fluorobenzene c [Me₄N]³⁺. ¹⁹F{¹H} NMR (471 MHz, neat, locked and referenced to TFA in a (CD₃)₂CO capillary): δ_F = -76.00 (TFA), -80.34 (NTf₂⁻; anion from [emim][NTf₂]), -113.86 (impurity from [emim][NTf₂]), -114.73 (free 1-fluorobenzene), -118.29 (impurity from [emim][NTf₂]), -120.84 (1-fluoroadamantane c 2), -121.95 (impurity from [emim][NTf₂]), -126.83 (impurity from [emim][NTf₂]).

3.3 Overview: Solubility of Coordination Cages in Ionic Liquids

In this section, the solubility trends observed for coordination cages and ionic liquids in Chapters 2 and 3 are briefly summarised. As seen in Figure 3.26, the hydrophobicity and polarity of ionic liquids can be tuned almost independently. The least hydrophobic ionic liquids are those with halide anions (*e.g.* [P_{6,6,6,14}][Cl], [hmim][Cl], [emim][Cl]) – these ionic liquids are fully miscible with water. Furthermore, they are not suitable solvents for the coordination cages used in this work; the chloride anions sequester Fe^{II} from the cages, causing decomposition. Among these three ionic liquids, the phosphonium ionic liquid ([P_{6,6,6,14}][Cl])

is least polar; the 1-ethyl-3-methyl imidazolium ionic liquid ([emim][NTf₂]) is most polar. When the anions of these two ionic liquids are exchanged for triflimide, the result are ionic liquids ([P_{6,6,6,14}][NTf₂] and [emim][NTf₂]) that are immiscible with water. The phosphonium ionic liquid remains, however, more lipophilic than the imidazolium ionic liquid. [P_{6,6,6,14}][NTf₂] is thus a good solvent for cage **4**.

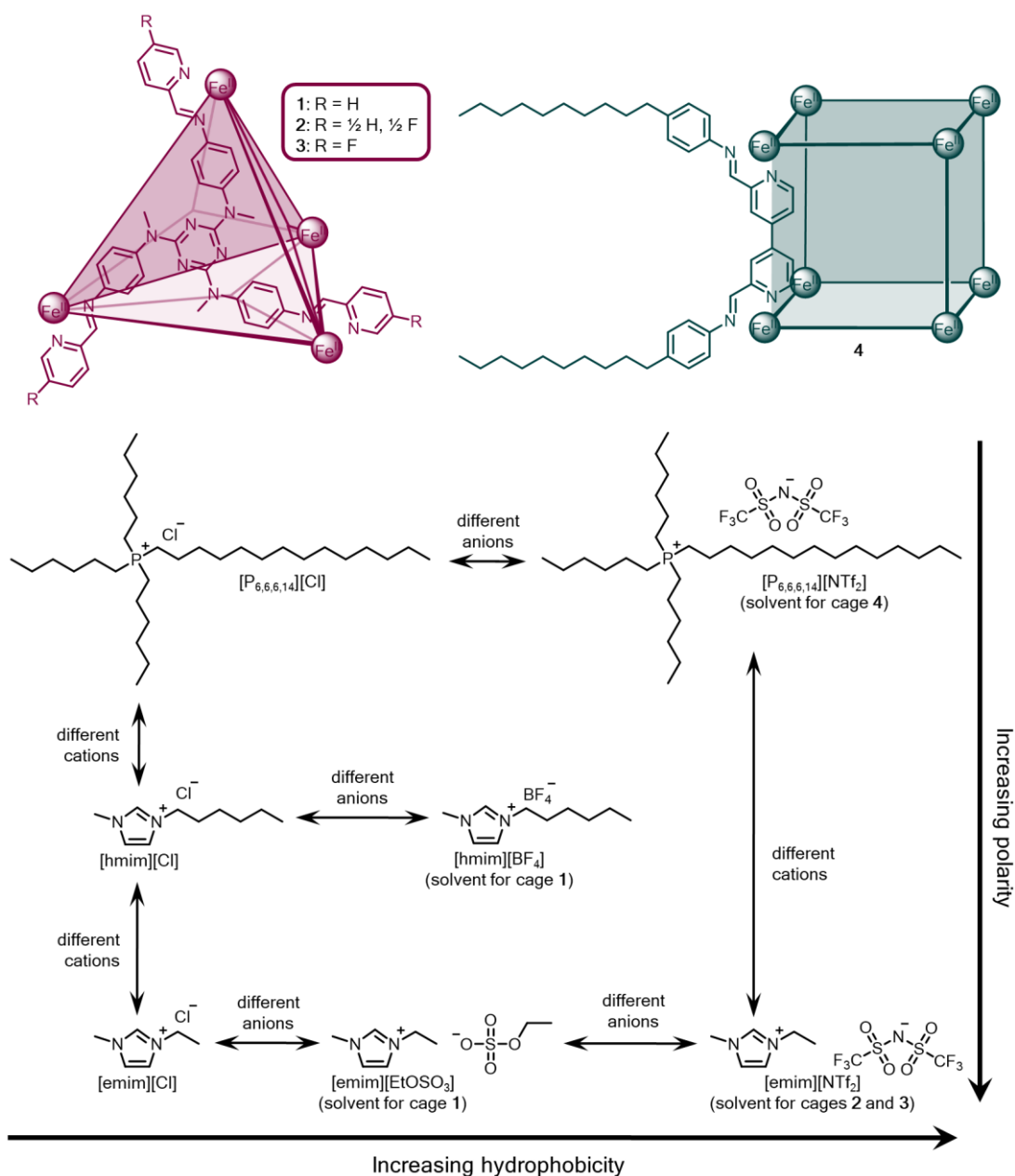


Figure 3.26 Solubility of coordination cages in ionic liquids. Doubled headed arrows denote structurally similar ionic liquids.

As discussed in Chapter 2, cage **1** is only sparingly soluble in [emim][NTf₂] – this incompatibility likely stems from the comparable size of the triflimide anion and the imidazolium cation, a feature which renders the environment in [emim][NTf₂] slightly fluoruous. Cages **2** and **3**, which are both fluorinated analogous of cage **1**, are thus soluble [emim][NTf₂]. Ionic liquids of intermediate polarity or hydrophobicity include [hmim][BF₄] and [emim][EtOSO₃]. While both ionic liquids are soluble in water, [emim][EtOSO₃] is fully miscible with water and [hmim][BF₄] is immiscible with water. This difference in miscibility is due both to the longer alkyl chain and more hydrophobic anion in [hmim][BF₄] than in [emim][EtOSO₃]. Both ionic liquids, however, are good solvents for cage **1**.

3.4 Conclusions

In this chapter, the phase transfer of 1-fluoroadamantane \subset **1** from water to an ionic liquid was triggered by anion exchange from cage **1**[SO₄] to **1**[BF₄]. To return the host-guest complex to water, 1-fluoroadamantane \subset **1** was precipitated out of the ionic liquid and redissolved in acetonitrile. A second anion exchange, from cage **1**[BF₄] to **1**[SO₄] was achieved by adding a sulfate salt to precipitate 1-fluoroadamantane \subset **1**[SO₄] out of acetonitrile; the host-guest complex was then isolated and redissolved in water. Anion exchange was then used to separate a mixture of cationic 1-fluoroadamantane \subset **1** and anionic 1-fluorobenzene \subset **3** by triggering the selective phase transfer of the cationic host-guest complex from water to an ionic liquid layer.

This study demonstrates that anion exchange is capable of driving the transport of cationic cages between two liquid phases. Such transport thus provides a new mechanism to separate physicochemically similar cages and cargoes. Added layers of complexity may be envisaged, involving the introduction of further solvent layers and cages with varying solvent preferences. This work thus adds to our understanding of how supramolecular capsules may contribute to solving practical separations problems.^{34–36} Ultimately, supramolecular capsules could provide an energy-efficient alternative to thermal separations,³⁷ with different cages selectively encapsulating hydrocarbons of different sizes,^{38–42} in complimentary fashion to the means by which different fractions are separated by boiling point through distillation.

3.5 Experimental

3.5.1 General

Reagents and solvents were purchased and used as supplied unless otherwise noted. H₂O and CH₃CN for cage syntheses were degassed by 3-4 evacuation/N₂ fill cycles prior to use. ¹H NMR spectra were recorded either at 500 MHz on a Bruker AVIII HD Smart Probe spectrometer, at 500 MHz on a Bruker DCH Cryoprobe spectrometer, or at 400 MHz on a Bruker Avance III HD Smart Probe spectrometer. ¹³C{¹H} NMR spectra were recorded at 125 MHz on a Bruker 500 MHz AVIII HD Smart Probe spectrometer, at 125 MHz on a Bruker 500 MHz DCH Cryoprobe spectrometer, or at 100 MHz on a Bruker 400 MHz Avance III HD Smart Probe spectrometer. ¹⁹F{¹H} NMR spectra were recorded at 471 MHz on a Bruker 500 MHz AVIII HD Smart Probe spectrometer or at 377 MHz on a Bruker 400 MHz Avance III HD Smart Probe spectrometer. ¹H chemical shifts (δ_H) are expressed in parts per million (ppm) and reported relative to the resonance of the residual protons of CDCl₃ (δ_H = 7.26 ppm), CD₂Cl₂ (δ_H = 5.32 ppm), CD₃CN (δ_H = 1.94 ppm), CD₃OD (δ_H = 3.31 ppm), or relative to the internal standard acetone (δ_H = 2.22 ppm) for samples in D₂O. ¹³C chemical shifts (δ_C) are expressed in ppm and reported relative to the resonance of the carbons in CDCl₃ (δ_C = 77.16 ppm), CD₂Cl₂ (δ_C = 53.84 ppm), CD₃CN (δ_C = 1.32 ppm), CD₃OD (δ_C = 49.00 ppm), or relative to the internal standard acetone (δ_C = 30.89 ppm) for samples in D₂O. ¹⁹F chemical shifts (δ_F) are expressed in ppm and are reported relative the external standard (contained in a coaxial capillary) trifluoroacetic acid in (CD₃)₂CO (δ_F = -76.00 ppm). NMR experiments in neat ionic liquids were locked to (CD₃)₂CO contained in a coaxial capillary. All measurements were carried out at 298 K. Abbreviations used in the description of NMR data are as follows: bs, broad singlet; s, singlet; d, doublet; t, triplet; q, quartet; m, multiplet. Coupling constants (*J*) are given in Hz. Elemental analysis were performed on a Exeter Analytical CE-440 Analyzer at the University of Cambridge, Department of Chemistry, U.K. UV-Vis spectra were taken on an Perkin Elmer Lambda 750 UV-Vis-NIR spectrophotometer.

3.5.2 Synthesis

The preparation and characterisation of precursor N₂,N₄,N₆-trimethyl-N₂,N₄,N₆-tris(4-nitrophenyl)-1,3,5-triazine-2,4,6-triamine, ligand N₂,N₄,N₆-tris(4-aminophenyl)-N₂,N₄,N₆-trimethyl-1,3,5-triazine-2,4,6-triamine, and cage [Me₄N]**3** were reported in Chapter 2.4.2.

Cage 1[SO₄]

This compound was synthesised according to a procedure previously described in the literature.²³ In a glovebox, N₂,N₄,N₆-tris(4-aminophenyl)-N₂,N₄,N₆-trimethyl-1,3,5-triazine-2,4,6-triamine (35.3 mg, 8.00 x 10⁻² mmol), 2-formylpyridine (22.8 μL, 24.0 x 10⁻² mmol), and iron (II) sulfate heptahydrate (22.2 mg, 8.00 x 10⁻² mmol) were combined with acetonitrile (5 mL) and water (5 mL). The resulting purple solution was stirred for 12 hours; the solvent was then removed, and the product was redissolved in D₂O (10 mL) to give a 2 mM stock solution. ¹H and ¹³C NMR signals matched the values reported in the literature.²³ ¹H NMR (500 MHz, D₂O, referenced to acetonitrile): δ_H = 9.02 (s, 12H, H_e), 8.61 (d, J = 7.8 Hz, 12H, H_d), 8.43 (t, J = 7.8 Hz, 12H, H_c), 7.76 (t, J = 6.7 Hz, 12H, H_b), 7.47 (d, J = 5.6 Hz, 12H, H_a), 7.44 (bs, 24H, H_g), 5.26 (bs, H_f), 3.47 and 3.46 (s, 36H, H_h from **1**[SO₄] and H_h from 2-formylpyridine ⊂ **1**[SO₄]). ¹³C{¹H} NMR (125 MHz, D₂O, referenced to acetonitrile): δ_C = 175.8, 165.3, 159.1, 156.7, 151.0 (encapsulated 2-formylpyridine), 147.2, 144.7, 140.7, 139.8 (encapsulated 2-formylpyridine), 131.9, 130.4, 126.2, 122.2, 38.6.

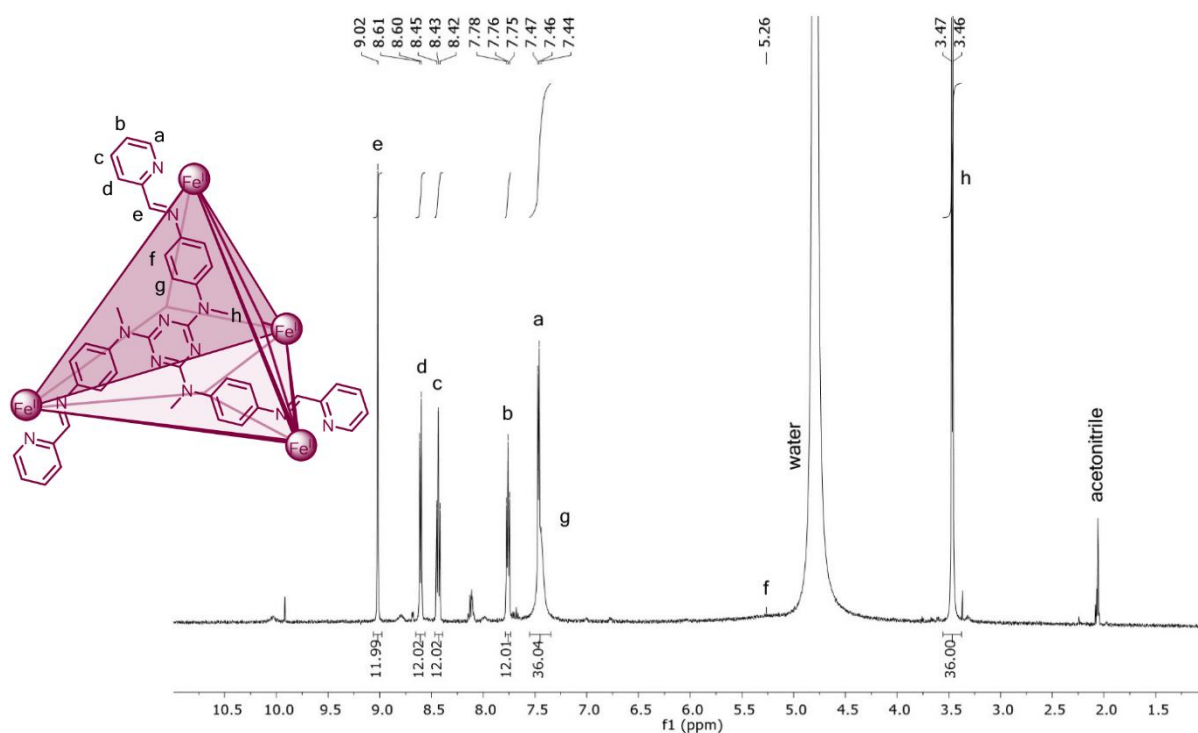


Figure 3.27 ¹H NMR spectrum of cage **1**[SO₄] in D₂O.

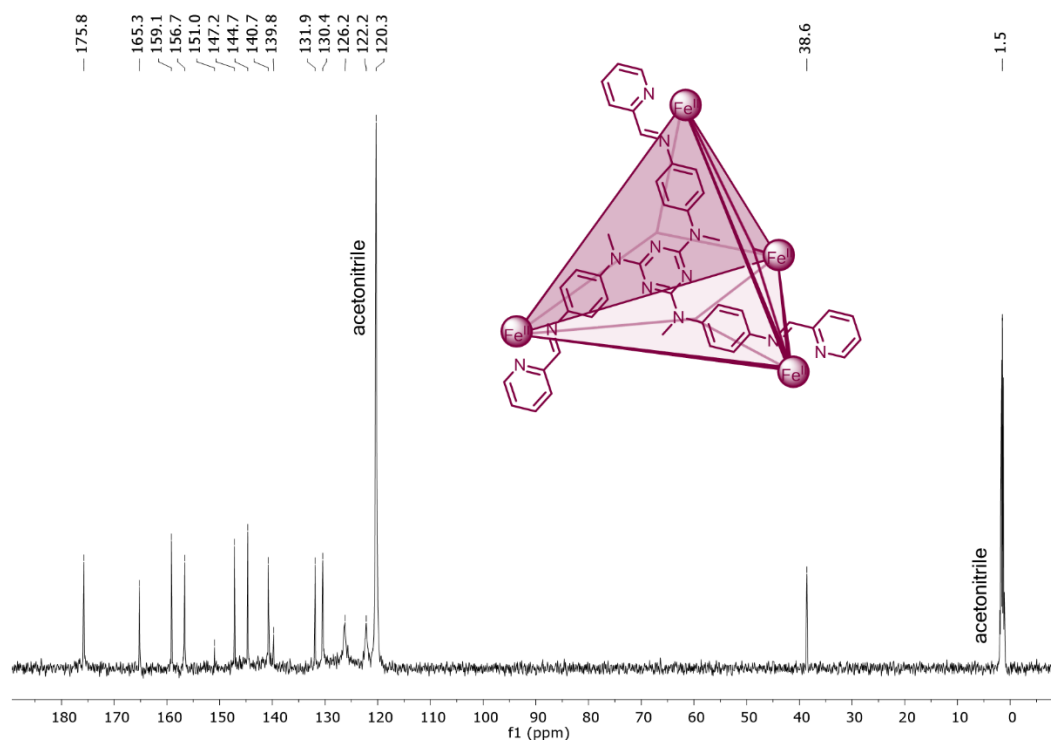


Figure 3.28 ^{13}C NMR spectrum of cage **1**[SO₄] in D₂O.

1-Fluoroadamantane \subset **1**[SO₄]

This compound was prepared by modifying a procedure previously described in the literature.²³ In a glovebox, 1-fluoroadamantane (46.3 mg, 30.0 \times 10⁻² mmol) was combined with the stock solution of **1**[SO₄] prepared above, and the resulting mixture was stirred for two weeks. ^1H and ^{13}C NMR signals were comparable to the values reported for adamantane \subset **1**[SO₄] in the literature.²³ ^1H NMR (500 MHz, D₂O, referenced to acetonitrile): δ_{H} = 9.00 (s, 12H, H_e), 8.58 (d, J = 7.7 Hz, 12H, H_d), 8.41 (t, J = 7.7 Hz, 12H, H_c), 7.74 (t, J = 6.6 Hz, 12H, H_b), 7.58 (bs, 12H, H_g), 7.44 (d, J = 5.4 Hz, 12H, H_a), 7.27 (bs, 12H, H_g), 5.88 (bs, 12H, H_f), 4.46 (bs, 12H, H_f), 3.46 (s, 36H, H_h), 2.28 (s, encapsulated 1-fluoroadamantane), 1.76 (m, encapsulated 1-fluoroadamantane), 1.72 (m, encapsulated 1-fluoroadamantane), 1.58 (m, encapsulated 1-fluoroadamantane). $^{13}\text{C}\{^1\text{H}\}$ NMR (125 MHz, D₂O, referenced to acetonitrile): δ_{C} = 175.4, 164.8, 158.7, 156.2, 146.9, 144.0, 140.3, 131.5, 130.0, 127.3, 125.0, 122.7, 120.7, 43.0 (encapsulated 1-fluoroadamantane), 38.3, 35.1 (encapsulated 1-fluoroadamantane), 31.8 (encapsulated 1-fluoroadamantane). $^{19}\text{F}\{^1\text{H}\}$ NMR (377 MHz, D₂O, referenced to TFA in a (CD₃)₂CO capillary): δ_{F} = -120.4 (encapsulated 1-fluoroadamantane).

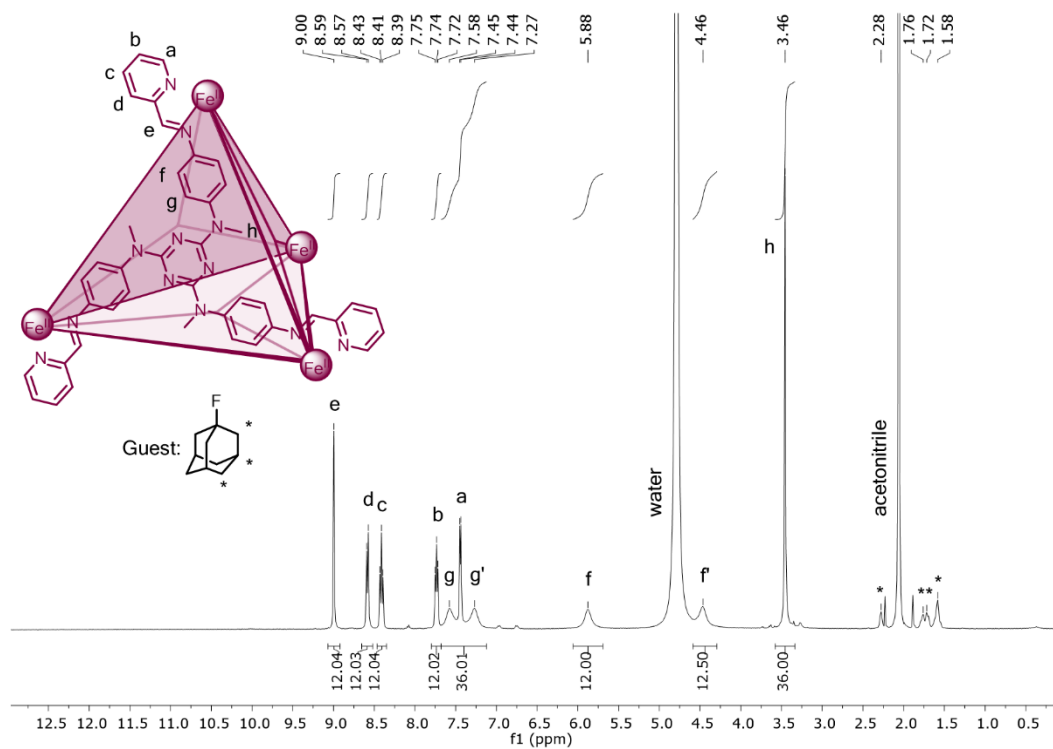


Figure 3.29 ¹H NMR spectrum of 1-fluoroadamantane c 1[SO₄] in D₂O.

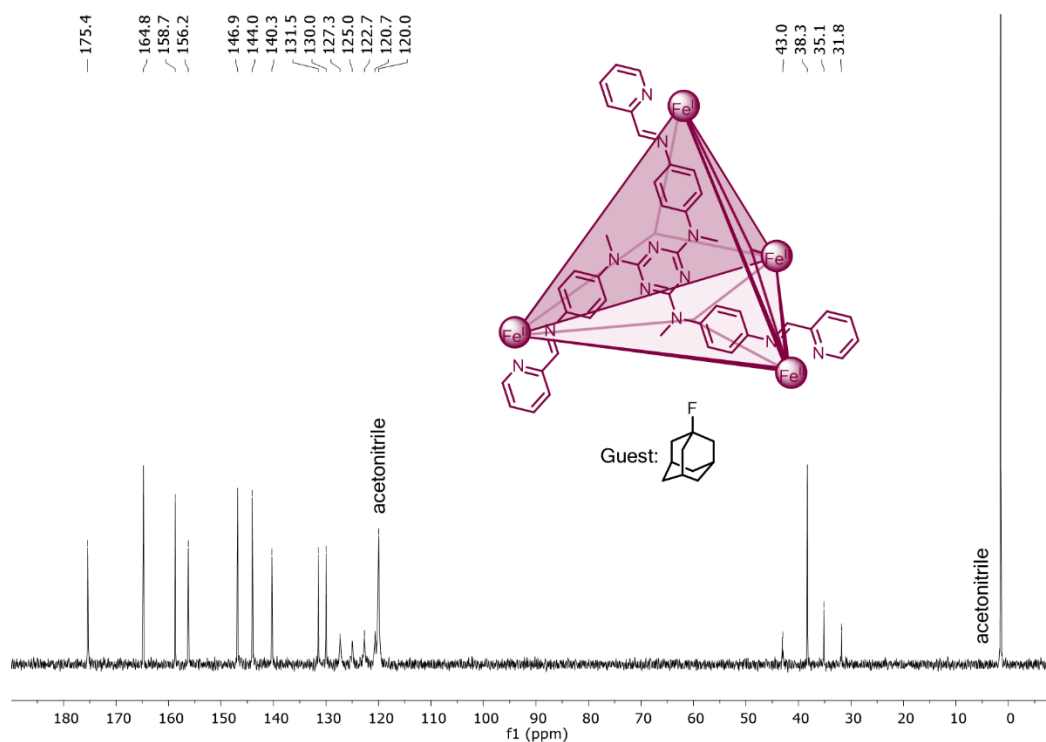


Figure 3.30 ¹³C NMR spectrum of 1-fluoroadamantane c 1[SO₄] in D₂O.

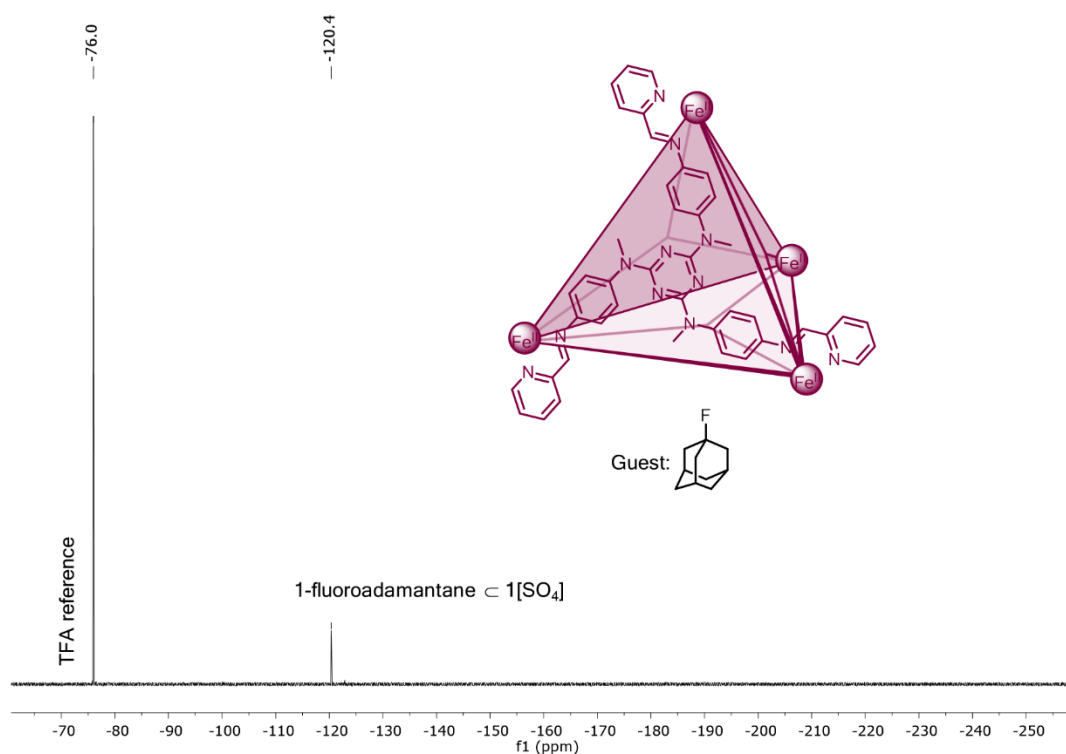


Figure 3.31 ¹⁹F NMR spectrum of 1-fluoroadamantane c 1[SO₄] in D₂O.

Cage 1[BF₄]

This compound was prepared by modifying a procedure previously described in the literature.²³ In a glovebox, N₂,N₄,N₆-tris(4-aminophenyl)-N₂,N₄,N₆-trimethyl-1,3,5-triazine-2,4,6-triamine (1.77 mg, 4.00 × 10⁻³ mmol), 2-formylpyridine (1.14 μL, 12.0 × 10⁻³ mmol), iron (II) tetrafluoroborate hexahydrate (1.35 mg, 4.00 × 10⁻³ mmol) were combined with CD₃CN (0.5 mL). The resulting purple solution was stirred for 12 hours at room temperature. ¹H and ¹³C NMR signals were comparable to the values reported for cage 1[OTf] in the literature.²³ ¹H NMR (500 MHz, CD₃CN): δ_H = 8.87 (s, 12H, H_e), 8.51 (d, *J* = 7.6 Hz, 12H, H_d), 8.38 (t, *J* = 7.8 Hz, 12H, H_c), 7.73 (t, *J* = 8.7 Hz, 12H, H_b), 7.44 (bs, 24H, H_g), 7.39 (d, *J* = 5.4 Hz, 12H, H_a), 5.09 (bs, 24H, H_f), 3.40 (s, 36H, H_h). ¹³C{¹H} NMR (125 MHz, CD₃CN): δ_C = 175.8, 165.1, 159.3, 156.7, 146.7, 144.9, 140.5, 131.8, 130.5, 126.4, 121.9, 38.2.

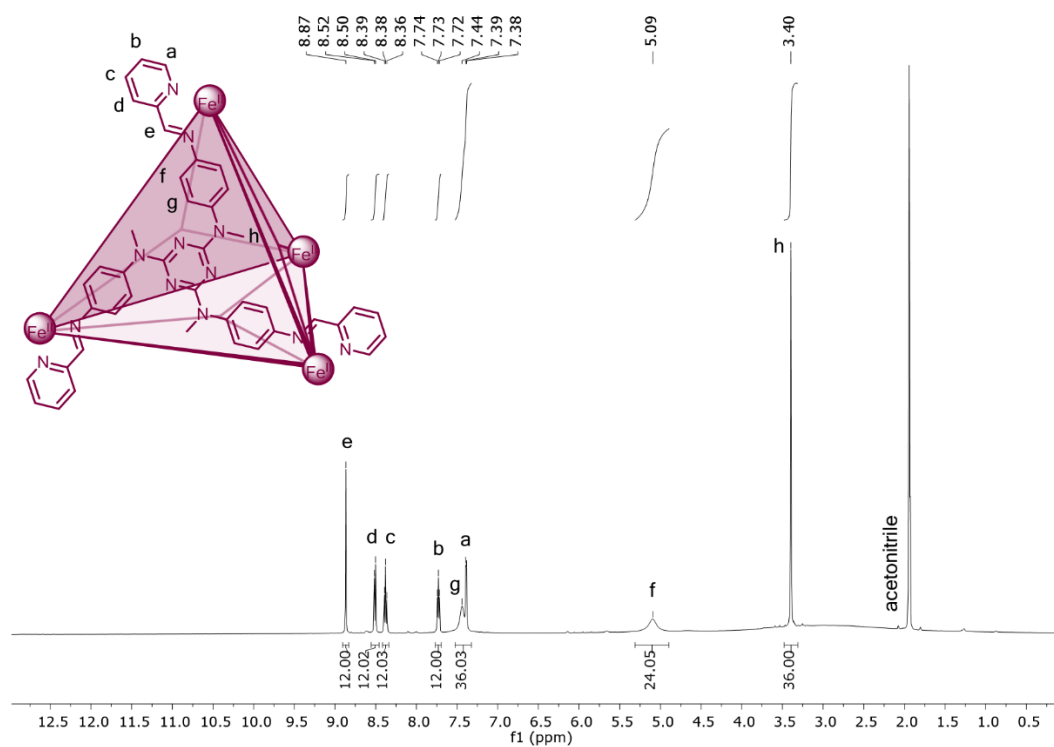


Figure 3.32 ¹H NMR spectrum of cage 1[BF₄] in CD₃CN.

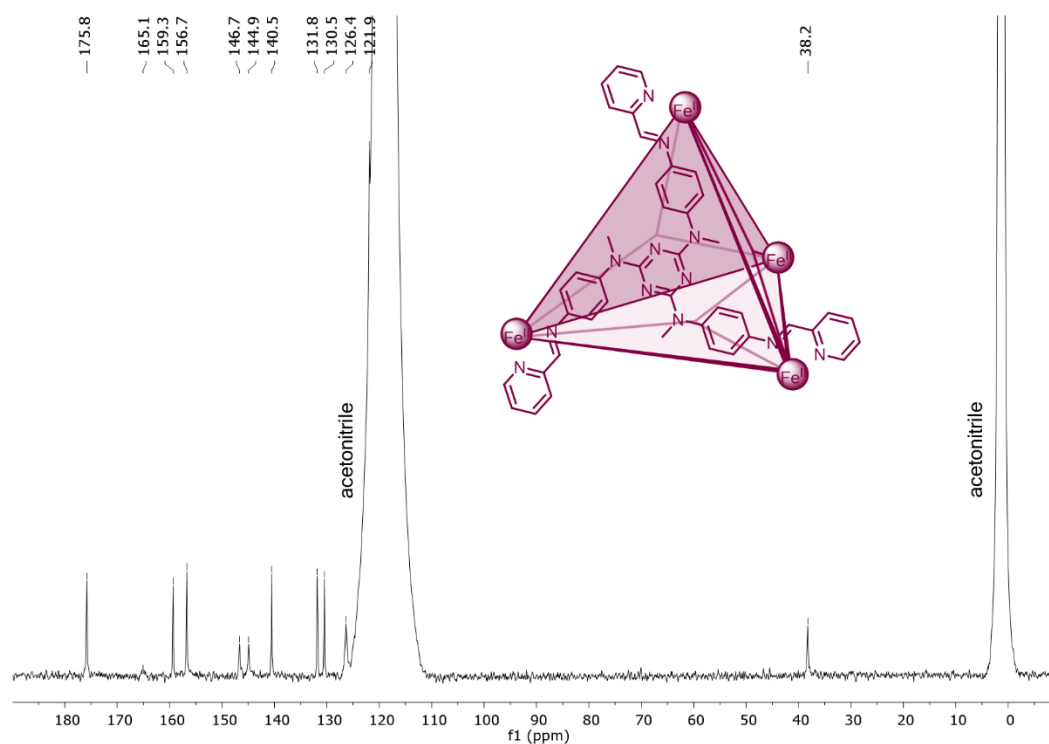


Figure 3.33 ¹³C NMR spectrum of cage 1[BF₄] in CD₃CN.

1-Fluoroadamantane \subset **2**[SO₄]

In a glovebox, N₂,N₄,N₆-tris(4-aminophenyl)-N₂,N₄,N₆-trimethyl-1,3,5-triazine-2,4,6-triamine (35.3 mg, 8.00 x 10⁻² mmol), 2-formylpyridine (11.3 μL, 11.9 x 10⁻² mmol), 5-fluoro-2-formylpyridine (14.9 mg, 11.9 x 10⁻² mmol), iron (II) sulfate heptahydrate (22.2 mg, 8.00 x 10⁻² mmol), and 1-fluoroadamantane (46.3 mg, 30.0 x 10⁻² mmol) were combined and stirred with CH₃CN (6.5 mL). As water (3.5 mL) was added dropwise, the solution turned dark red/purple. The resulting solution was stirred for 12 hours; the solvent was removed, and the product was redissolved in D₂O (10 mL). This stock solution (2 mM) was filtered before use.

¹H NMR (500 MHz, D₂O, referenced to acetonitrile): δ_H = 8.99 (m, H_{e,e',i,i'}), 8.67 (m, H_{l,l'}), 8.59 (m, H_{d,d'}), 8.42 (m, H_{c,c'}), 8.24 (m, H_{k,k'}), 7.77 (m, H_{b'}), 7.73 (m, H_b), 7.57 (bs, H_g), 7.50 (m, H_a), 7.44 (m, H_{a,j}), 7.38 (bs, H_j), 7.27 (bs, H_{g'}), 5.88 (bs, H_f), 4.46 (bs, H_f), 3.45 (s, H_h), 2.26 (bs, encapsulated 1-fluoroadamantane), 1.76 (bs, encapsulated 1-fluoroadamantane), 1.70 (bs, encapsulated 1-fluoroadamantane), 1.58 (m, encapsulated 1-fluoroadamantane). ¹³C{¹H} NMR (125 MHz, D₂O) δ_C = 175.4, 174.2, 164.8, 158.7, 156.4, 146.9, 144.1, 140.3, 131.6, 130.1, 127.4, 125.0, 122.7, 120.7, 43.1 (encapsulated 1-fluoroadamantane), 38.4, 35.2 (encapsulated 1-fluoroadamantane), 31.8 (encapsulated 1-fluoroadamantane). ¹⁹F{¹H} NMR (471 MHz, D₂O, referenced to TFA in a (CD₃)₂CO capillary): δ_F = -111.83 (**2**[SO₄]), -111.97 (**2**[SO₄]), -112.25 (**2**[SO₄]), -112.39 (**2**[SO₄]), -120.23 (encapsulated 1-fluoroadamantane).

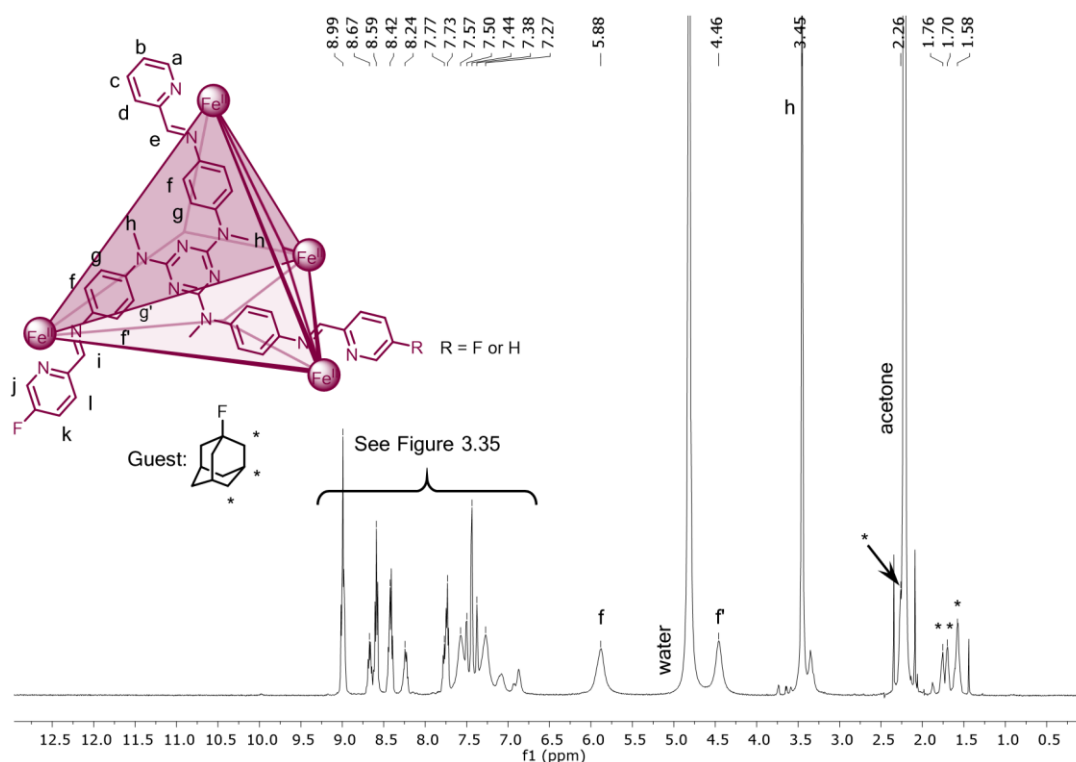


Figure 3.34 ¹H NMR spectrum of 1-fluoroadamantane \subset **2**[SO₄] in D₂O.

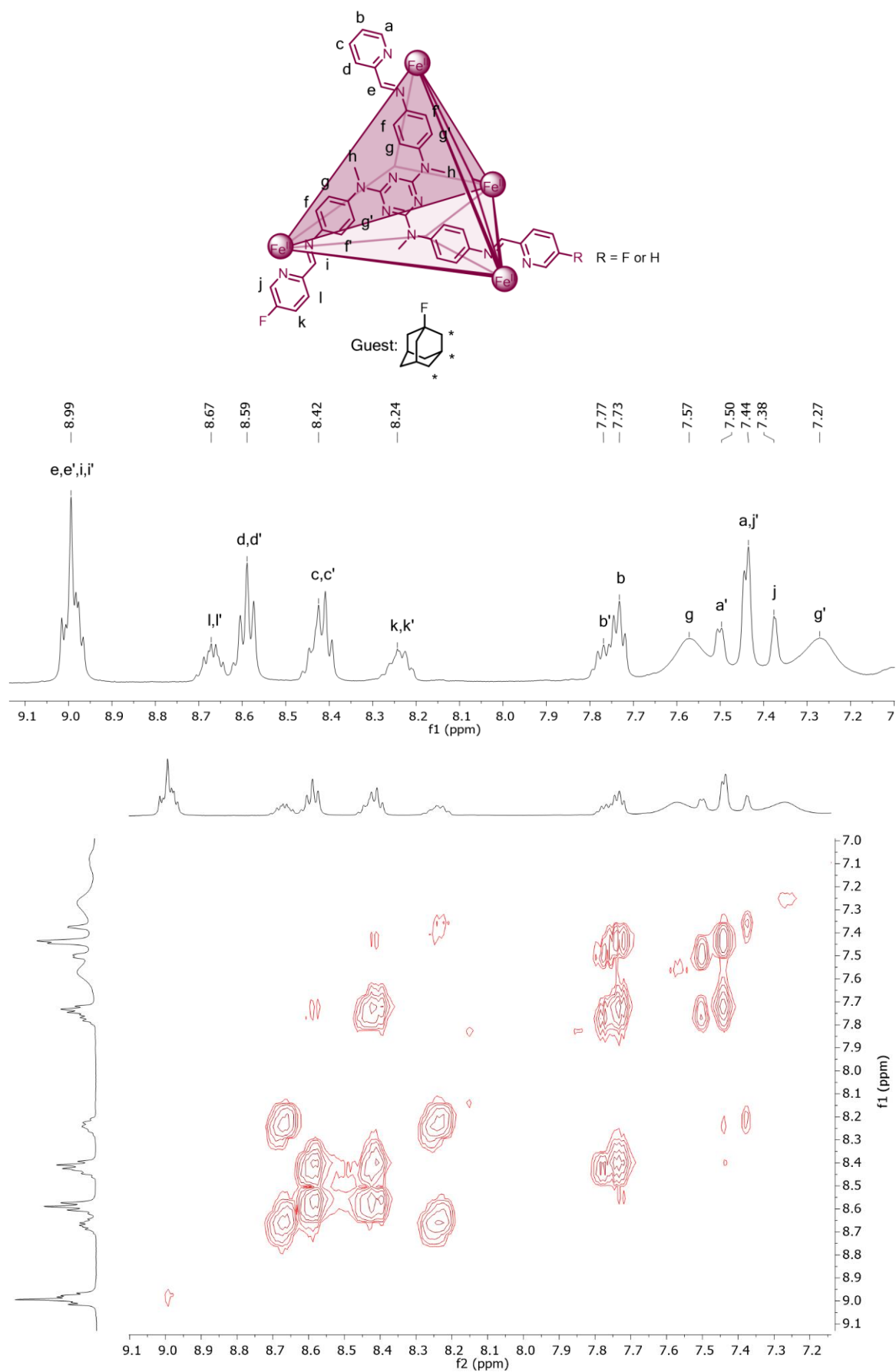


Figure 3.35 ¹H COSY NMR spectrum of 1-fluoroadamantane c 2[SO₄] in D₂O.

Chapter 3. Phase Transfer of an Fe^{II}₄L₄ Cage and Encapsulated Cargo

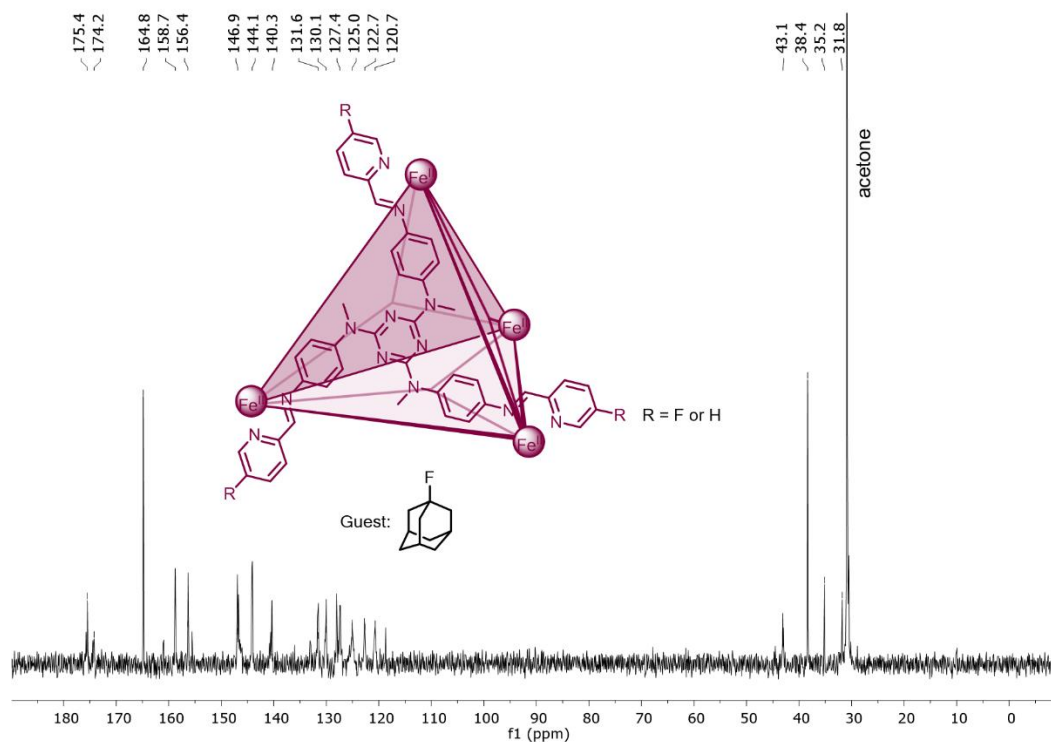


Figure 3.36 ¹³C NMR spectrum of 1-fluoroadamantane c 2[SO₄] in D₂O.

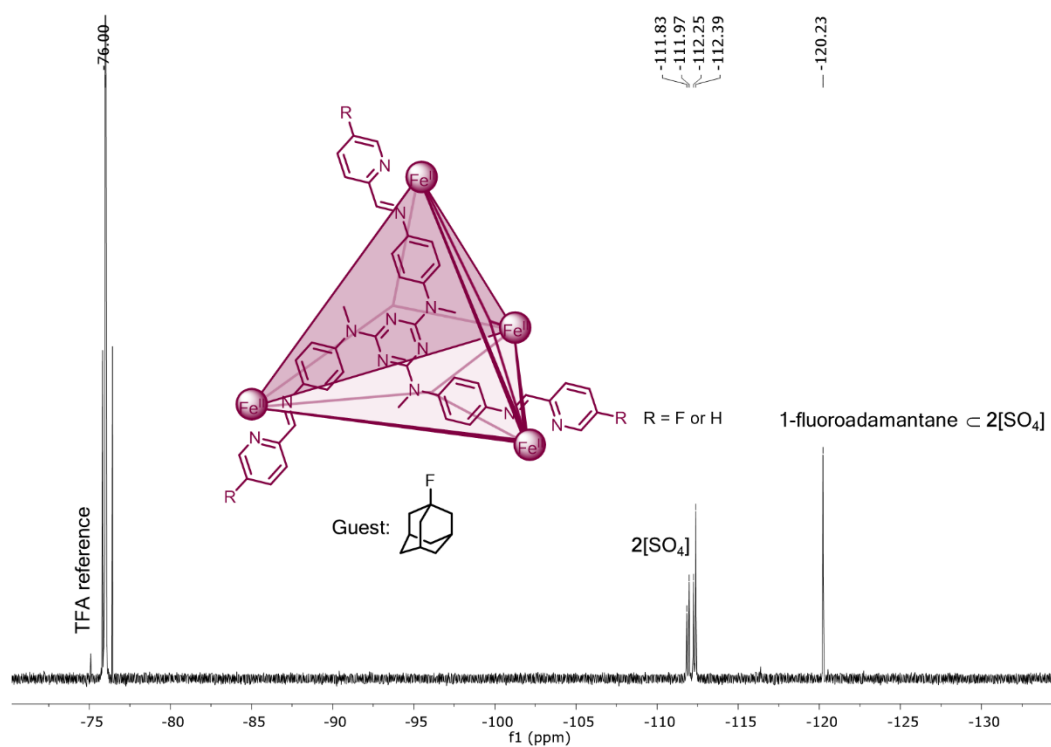


Figure 3.37 ¹⁹F NMR spectrum of 1-fluoroadamantane c 2[SO₄] in D₂O.

1-Fluorobenzene \subset $[\text{Me}_4\text{N}]\mathbf{3}$

This cage was prepared according to a previously reported procedure. ^1H NMR signals are in agreement with the values reported in the literature.⁴³ ^1H NMR (500 MHz, D_2O): $\delta_{\text{H}} = 10.85$ (bs, H_{e}), 9.30 (bs, $\text{H}_{\text{e}'}$), 9.19 (bs, H_{d}), 8.77 (bs, H_{a}), 8.69 (bs, $\text{H}_{\text{d}'}$), 8.35 (bs, H_{c}), 8.27 (bs, $\text{H}_{\text{b,c}'}$), 7.75 (bs, H_{b}), 7.51 (bs, $\text{H}_{\text{a}'}$), 7.25 (bs, H_{g}), 7.14 (bs, $\text{H}_{\text{g}'}$), 6.43 (bs, $\text{H}_{\text{h,h}'}$), 6.03 (bs, H_{f}), 5.82 (bs, H_{f}), 3.17 (bs, H_{i}). $^{19}\text{F}\{^1\text{H}\}$ NMR (471 MHz, D_2O , referenced to TFA in a $(\text{CD}_3)_2\text{CO}$ capillary): $\delta_{\text{F}} = -106.39$ (encapsulated 1-fluorobenzene), -113.76 (free 1-fluorobenzene).

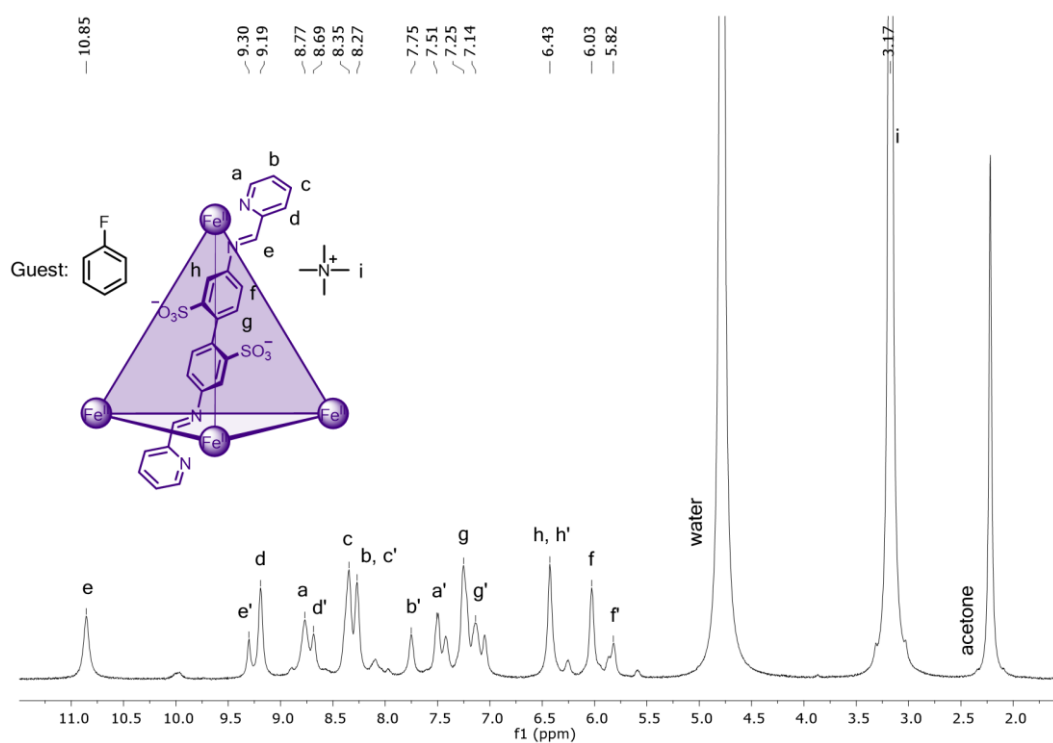


Figure 3.38 ^1H NMR spectrum of 1-fluorobenzene \subset $[\text{Me}_4\text{N}]\mathbf{3}$ in D_2O .

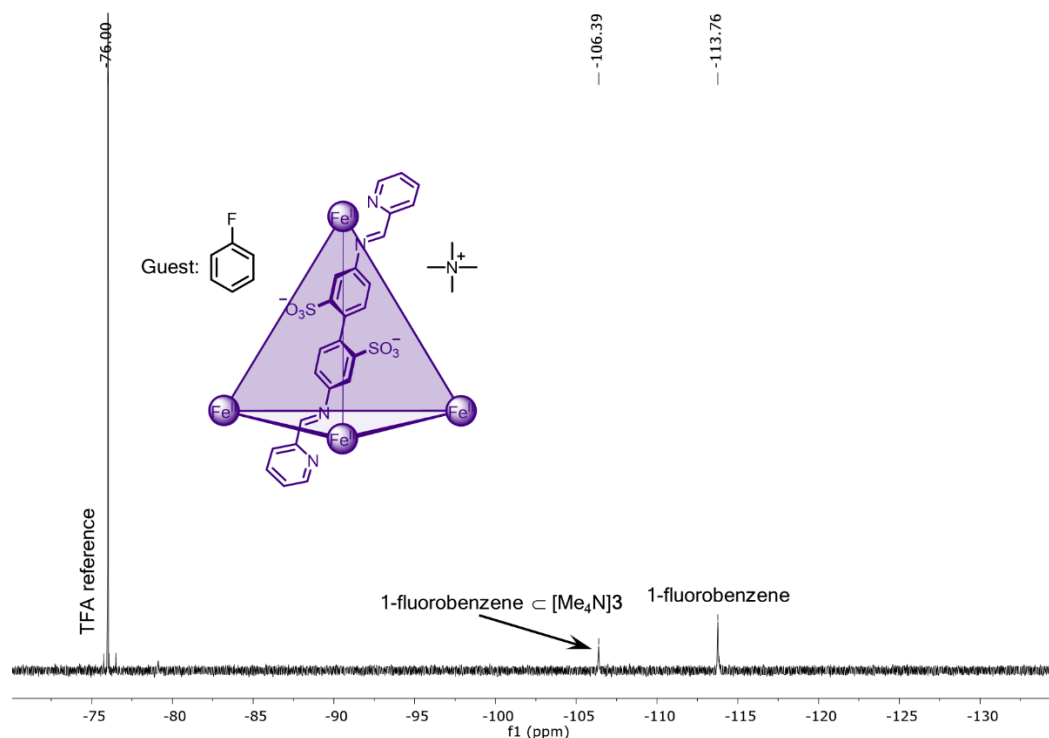


Figure 3.39 ^{19}F NMR spectrum of 1-fluorobenzene \subset $[\text{Me}_4\text{N}]\mathbf{3}$ in D_2O .

1-Hexyl-3-methylimidazolium tetrafluoroborate ([hmim][BF₄])

This ionic liquid was synthesised by modifying a procedure previously described in the literature.⁴⁴ 1-Hexyl-3-methylimidazolium chloride (5.0 g, 25 mmol) was dissolved in a minimum amount of water. Separately, sodium tetrafluoroborate (3.3 g, 30 mmol) was dissolved in a minimum amount of water. The aqueous solution of sodium tetrafluoroborate was added dropwise to the aqueous solution of 1-hexyl-3-methylimidazolium chloride. A second, denser liquid phase immediately began to form, and the reaction mixture was stirred for 24 hours. The aqueous layer was then decanted off. The ionic liquid layer was then washed with water (2 mL portions) until the addition of an aqueous silver nitrate solution to the wash gave no precipitation of silver chloride. ^1H and ^{13}C NMR signals matched the values reported in the literature.⁴⁴ ^1H NMR (500 MHz, CDCl_3): $\delta_{\text{H}} = 8.67$ (s, 1H, H_b), 7.37 (s, 1H, H_d), 7.33 (s, 1H, H_c), 4.12 (t, $J = 7.4$ Hz, 2H, H_e), 3.89 (s, 3H, H_a), 1.82 (m, 2H, H_f), 1.25 (m, 6H, H_{g,h,i}), 0.82 (t, $J = 6.9$ Hz, 3H, H_j). $^{13}\text{C}\{^1\text{H}\}$ NMR (125 MHz, CDCl_3): $\delta_{\text{C}} = 135.8$, 123.7, 122.2, 49.8, 35.9, 30.8, 29.8, 25.6, 22.1, 13.7. $^{19}\text{F}\{^1\text{H}\}$ NMR (471 MHz, neat, locked and referenced to TFA in a $(\text{CD}_3)_2\text{CO}$ capillary): $\delta_{\text{F}} = -149.99$, -150.05 . Elemental analysis (%) calcd for $\text{C}_{10}\text{H}_{19}\text{BF}_4\text{N}_2$: C, 47.27; H, 7.54; N, 11.03; Cl, 0.00; found: C, 47.07; H, 7.73; N, 11.00; Cl, <0.01.

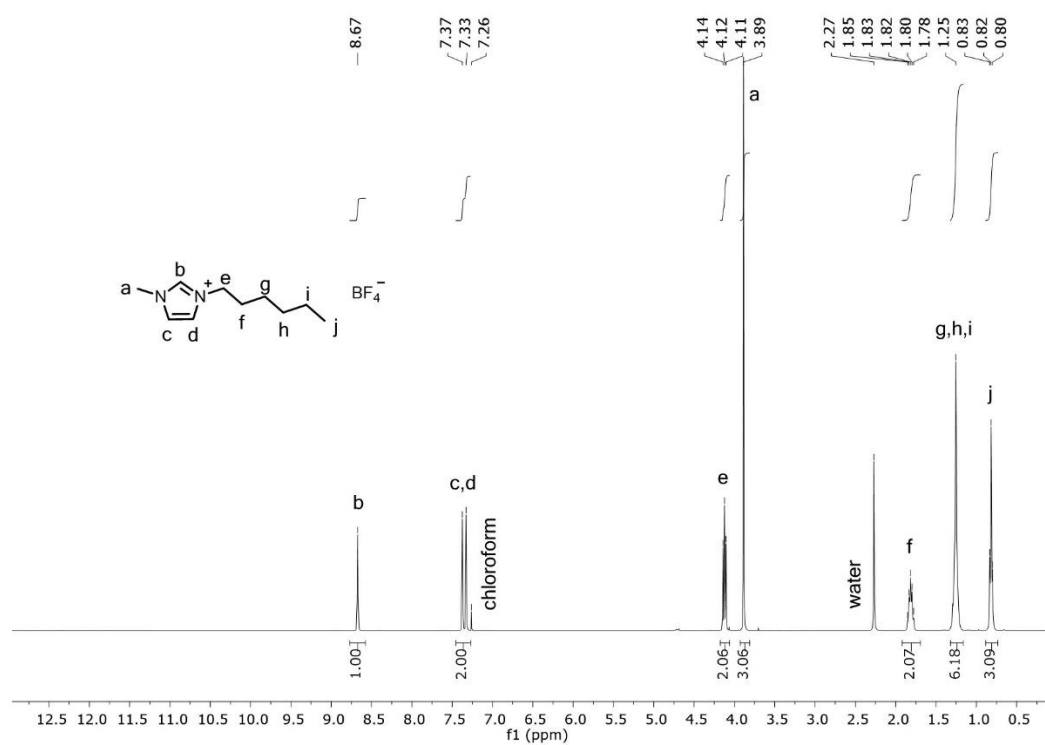


Figure 3.40 ^1H NMR spectrum of 1-hexyl-3-methylimidazolium tetrafluoroborate in CDCl_3 .

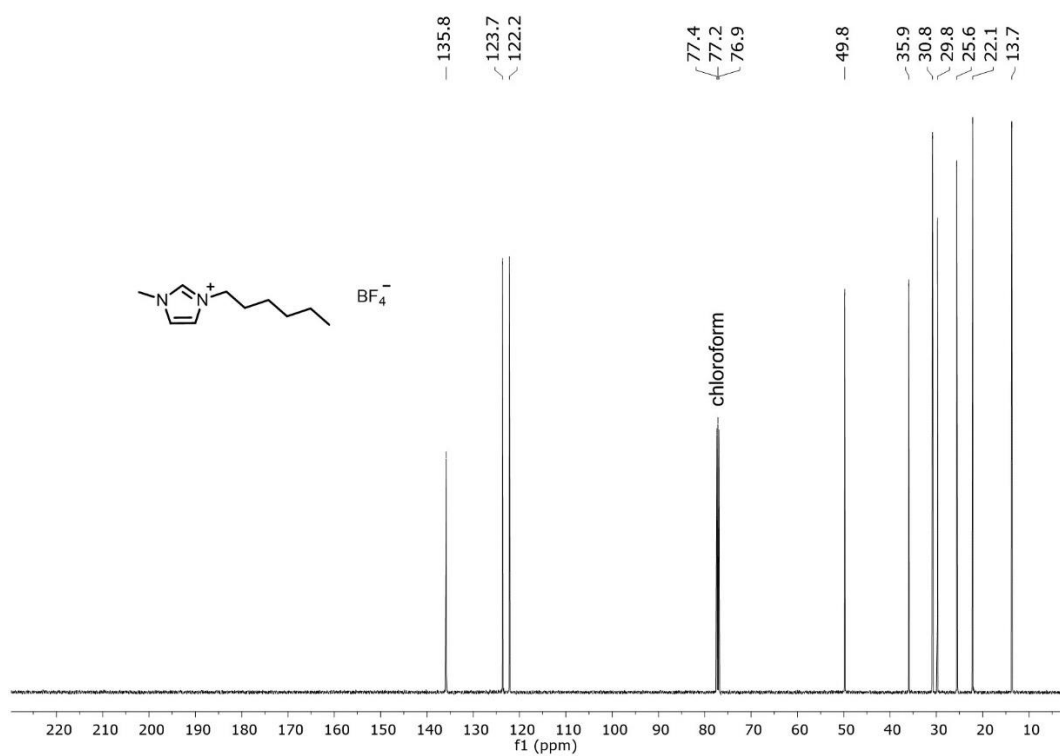


Figure 3.41 ^{13}C NMR spectrum of 1-hexyl-3-methylimidazolium tetrafluoroborate in CDCl_3 .

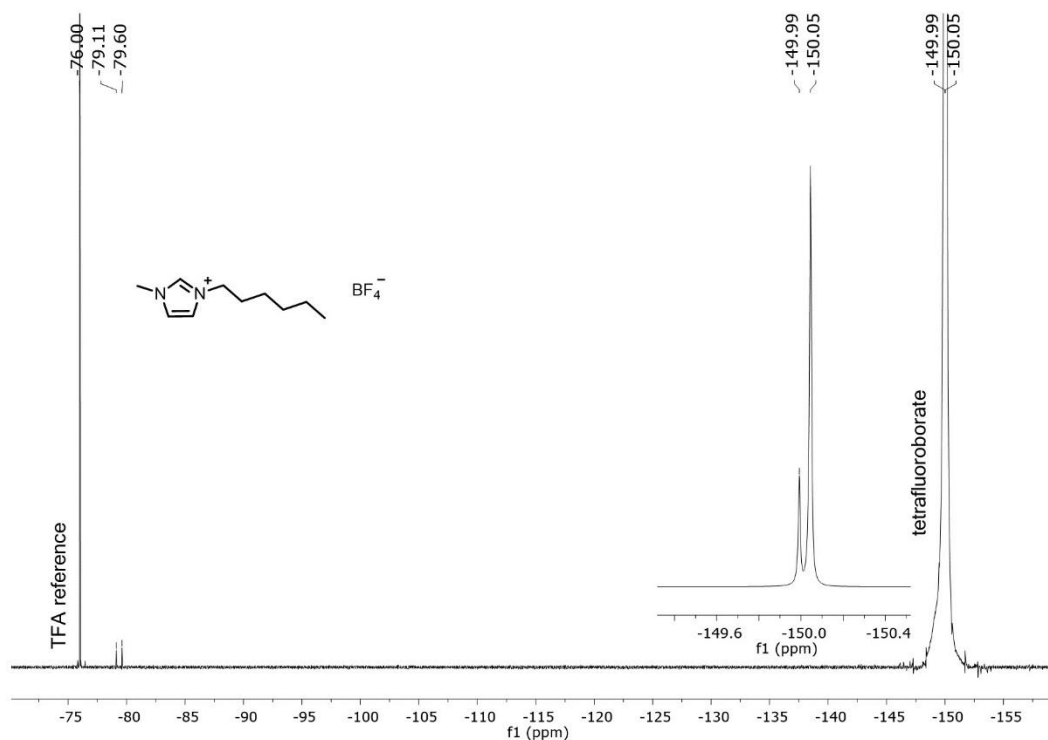


Figure 3.42 ¹⁹F NMR spectrum of 1-hexyl-3-methylimidazolium tetrafluoroborate in CDCl₃.

1-Ethyl-3-methylimidazolium triflimide ([emim][NTf₂])

This ionic liquid was synthesised by modifying a procedure previously described in the literature.⁴⁵ 3-Ethyl-1-methylimidazolium ethyl sulfate (5.00 g, 21.2 mmol) was dissolved in water (5 mL). Separately, lithium triflimide (7.28 g, 25.4 mmol) was dissolved in water (5 mL). The aqueous solution of lithium triflimide was added dropwise to the aqueous solution of 3-ethyl-1-methylimidazolium ethyl sulfate, and the reaction mixture was stirred for an additional 24 hours. The product, 3-ethyl-1-methylimidazolium triflimide, formed as a separate, colourless layer and was washed with water (3 x 5 mL). ¹H and ¹³C NMR signals are in agreement with the values reported in the literature.⁴⁶ ¹H NMR (400 MHz, CD₃OD): δ_H = 8.84 (s, 1H, H_b), 7.60 (s, 1H, H_d), 7.52 (s, 1H, H_c), 4.25 (q, *J* = 7.4 Hz, 2H, H_e), 3.91 (s, 3H, H_a), 1.52 (t, *J* = 7.4 Hz, 3H, H_f). ¹³C{¹H} NMR (100 MHz, CD₃OD): δ_C = 137.1, 124.8, 123.1, 121.0, 45.9, 36.4, 15.3. ¹⁹F{¹H} NMR (471 MHz, neat, locked and referenced to TFA in a (CD₃)₂CO capillary): δ_F = -80.34. Elemental analysis (%) calcd for C₈H₁₁F₆N₃O₄S₂: C, 24.56; H, 2.83; N, 10.74, Cl, 0.00; found: C, 24.59; H, 2.76; N, 10.67; Cl, <0.004.

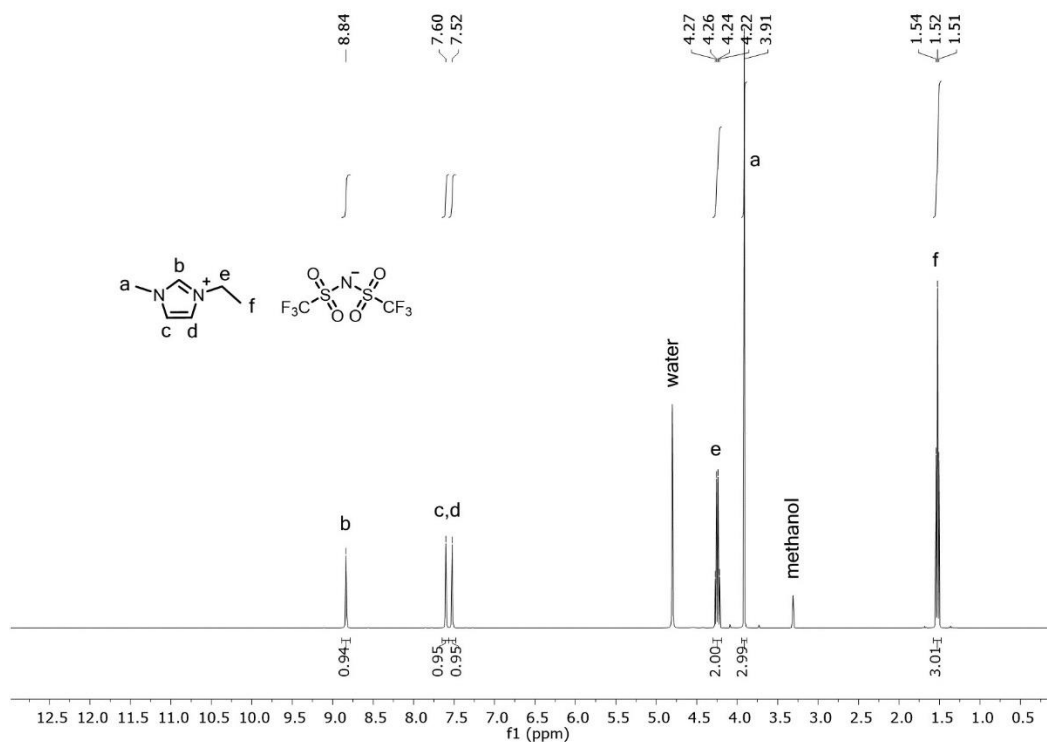


Figure 3.43 ^1H NMR spectrum of 1-ethyl-3-methylimidazolium triflimide in CD_3OD .

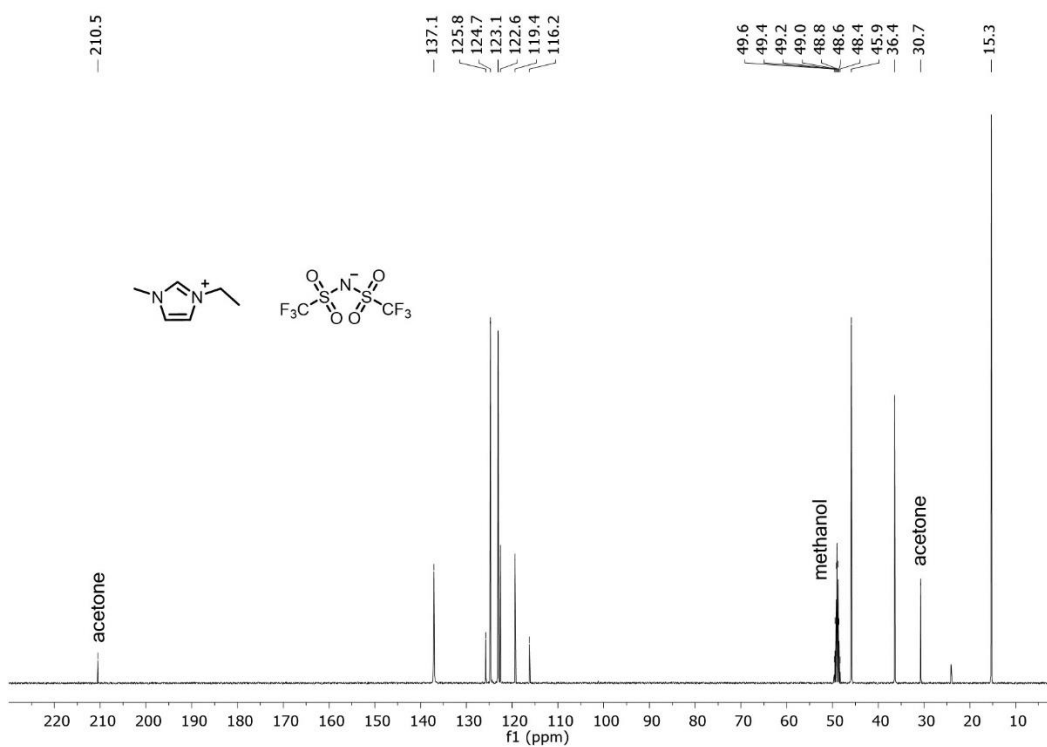


Figure 3.44 ^{13}C NMR spectrum of 1-ethyl-3-methylimidazolium triflimide in CD_3OD .

Chapter 3. Phase Transfer of an Fe^{II}L₄ Cage and Encapsulated Cargo

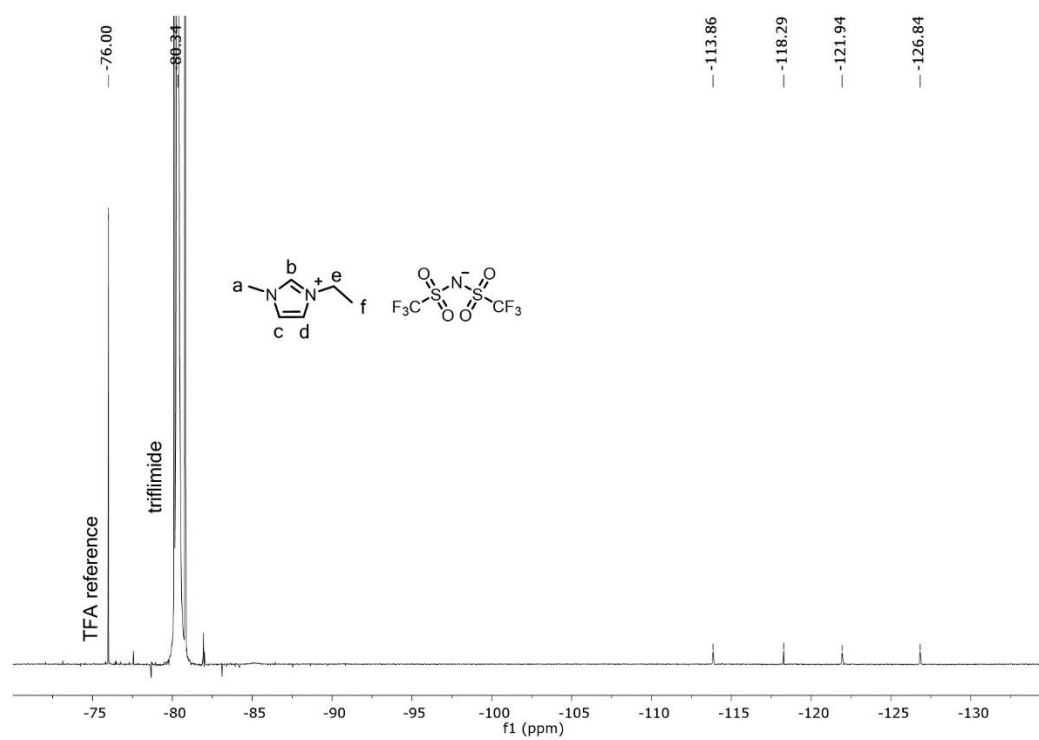


Figure 3.45 ¹⁹F NMR spectrum of 1-ethyl-3-methylimidazolium triflimide in CD₃OD.

3.5 References

- (1) Grommet, A. B.; Nitschke, J. R. *J. Am. Chem. Soc.* **2017**, *139*, 2176.
- (2) Hashim, M. I.; Hsu, C.-W.; Le, H. T. M.; Miljanić, O. Š. *Synlett* **2016**, 27 (13), 1907.
- (3) Wang, Q. Q.; Day, V. W.; Bowman-James, K. *J. Am. Chem. Soc.* **2013**, *135* (1), 392.
- (4) Collins, M. S.; Carnes, M. E.; Nell, B. P.; Zakharov, L. N.; Johnson, D. W. *Nat Commun* **2016**, *7*, 11052.
- (5) Wu, N. W.; Rebek, J. *J. Am. Chem. Soc.* **2016**, *138* (24), 7512.
- (6) Zhang, G.; Presly, O.; White, F.; Oppel, I. M.; Mastalerz, M. *Angew. Chem. Int. Ed.* **2014**, *53* (20), 5126.
- (7) Pandurangan, K.; Kitchen, J. A.; Blasco, S.; Boyle, E. M.; Fitzpatrick, B.; Feeney, M.; Kruger, P. E.; Gunnlaugsson, T. *Angew. Chem. Int. Ed.* **2015**, *54* (15), 4566.
- (8) Bruns, C. J.; Fujita, D.; Hoshino, M.; Sato, S.; Stoddart, J. F.; Fujita, M. *J. Am. Chem. Soc.* **2014**, *136* (34), 12027.
- (9) Rizzuto, F. J.; Wu, W. Y.; Ronson, T. K.; Nitschke, J. R. *Angew. Chem. Int. Ed.* **2016**, *55* (28), 7958.
- (10) Yi, S.; Brega, V.; Captain, B.; Kaifer, A. E. *Chem. Commun.* **2012**, 48 (83), 10295.
- (11) Zhou, X.-P.; Wu, Y.; Li, D. *J. Am. Chem. Soc.* **2013**, *135* (43), 16062.
- (12) Custelcean, R. *Chem. Soc. Rev.* **2014**, *43* (6), 1813.
- (13) Evans, N. H.; Beer, P. D. *Angew. Chem. Int. Ed.* **2014**, *53* (44), 11716.
- (14) Freye, S.; Michel, R.; Stalke, D.; Pawliczek, M.; Frauendorf, H.; Clever, G. H. *J. Am. Chem. Soc.* **2013**, *135* (23), 8476.
- (15) Kieffer, M.; Pilgrim, B. S.; Ronson, T. K.; Roberts, D. A.; Aleksanyan, M.; Nitschke, J. R. *J. Am. Chem. Soc.* **2016**, *138* (21), 6813.
- (16) Löffler, S.; Lubben, J.; Krause, L.; Stalke, D.; Dittrich, B.; Clever, G. H. *J. Am. Chem. Soc.* **2015**, *137* (3), 1060.
- (17) Luo, D.; Zhou, X. P.; Li, D. *Inorg. Chem.* **2015**, *54* (22), 10822.
- (18) Luo, D.; Zhou, X. I.-P.; Li, D. *Angew. Chem. Int. Ed.* **2015**, *54*, 6190.
- (19) Nakamura, T.; Ube, H.; Miyake, R.; Shionoya, M. *J. Am. Chem. Soc.* **2013**, *135* (50), 18790.
- (20) Samanta, D.; Mukherjee, P. S. *Chem. Eur. J.* **2014**, *20* (39), 12483.
- (21) Wu, J.-Y.; Zhong, M.-S.; Chiang, M.-H.; Bhattacharya, D.; Lee, Y.-W.; Lai, L.-L. *Chem. Eur. J.* **2016**, *22* (21), 7238.
- (22) Zhu, R.; Lübben, J.; Dittrich, B.; Clever, G. H. *Angew. Chem. Int. Ed.* **2015**, *54* (9),

- 2796.
- (23) Bolliger, J. L.; Ronson, T. K.; Ogawa, M.; Nitschke, J. R. *J. Am. Chem. Soc.* **2014**, *136* (41), 14545.
- (24) Chifotides, H. T.; Dunbar, K. R. *Acc. Chem. Res.* **2013**, *46* (4), 894.
- (25) Yan, X.; Wang, M.; Cook, T. R.; Zhang, M.; Saha, M. L.; Zhou, Z.; Li, X.; Huang, F.; Stang, P. J. *J. Am. Chem. Soc.* **2016**, *138* (13), 4580.
- (26) Forsyth, S. A.; Pringle, J. M.; MacFarlane, D. R. *Aust. J. Chem.* **2004**, *57* (2), 113.
- (27) Hagiwara, R.; Ito, Y. *J. Fluor. Chem.* **2000**, *105* (2), 221.
- (28) Hallett, J. P.; Welton, T. *Chem. Rev.* **2011**, *111* (5), 3508.
- (29) Herchl, R.; Waser, M. *Tetrahedron* **2014**, *70* (11), 1935.
- (30) Serguchev, Y. A.; Ponomarenko, M. V.; Ignat'ev, N. V. *J. Fluor. Chem.* **2016**, *185*, 1.
- (31) Freire, M. G.; Santos, L. M. N. B. F.; Fernandes, A. M.; Coutinho, J. A. P.; Marrucho, I. M. *Fluid Phase Equilib.* **2007**, *261* (1–2), 449.
- (32) Ranke, J.; Othman, A.; Fan, P.; Muller, A. *Int. J. Mol. Sci.* **2009**, *10* (3), 1271.
- (33) Mal, P.; Schultz, D.; Beyeh, K.; Rissanen, K.; Nitschke, J. R. *Angew. Chem. Int. Ed.* **2008**, *47* (43), 8297.
- (34) Kewley, A.; Stephenson, A.; Chen, L.; Briggs, M. E.; Hasell, T.; Cooper, A. I. *Chem. Mater.* **2015**, *27* (9), 3207.
- (35) Slater, A. G.; Cooper, A. I. *Science* **2015**, *348* (6238), 988.
- (36) Zhang, G.; Mastalerz, M. *Chem. Soc. Rev.* **2014**, *43* (6), 1934.
- (37) Sholl, D. S.; Lively, R. P. *Nature* **2016**, *532* (7600), 435.
- (38) Huerta, E.; Serapian, S. A.; Santos, E.; Cequier, E.; Bo, C.; de Mendoza, J. *Chem. Eur. J.* **2016**, *22* (38), 13496.
- (39) Otte, M. *ACS Catal.* **2016**, 6491.
- (40) Otte, M.; Kuijpers, P. F.; Troepner, O.; Ivanovič-Burmazovič, I.; Reek, J. N. H.; De Bruin, B. *Chem. Eur. J.* **2013**, *19* (31), 10170.
- (41) Turega, S.; Whitehead, M.; Hall, B. R.; Meijer, A. J. H. M.; Hunter, C. A.; Ward, M. D. *Inorg. Chem.* **2013**, *52* (2), 1122.
- (42) Voloshin, Y.; Belaya, I.; Krämer, R. *The Encapsulation Phenomenon: Synthesis, Reactivity and Applications of Caged Ions and Molecules*; Springer International Publishing: Switzerland, 2016.
- (43) Smulders, M. M. J.; Zarra, S.; Nitschke, J. R. *J. Am. Chem. Soc.* **2013**, *135* (18), 7039.
- (44) Bravo, J. L.; López, I.; Cintas, P.; Silvero, G.; Arévalo, M. J. *Ultrason. Sonochem.* **2006**, *13* (5), 408.

- (45) Shimojo, K.; Nakashima, K.; Kamiya, N.; Goto, M. *Biomacromolecules* **2006**, 7, 2.
- (46) Dubois, P.; Marchand, G.; Fouillet, Y.; Berthier, J.; Douki, T.; Hassine, F.; Gmouh, S.; Vaultier, M. *Anal. Chem.* **2006**, 78 (14), 4909.

Chapter 4:

Reversible Phase Transfer of Cages by Anion Exchange

*As discussed in Chapter 3, coordination cages can selectively encapsulate guests based on their size and shape, making these cage structures promising scaffolds for performing size-selective separations. Specifically, we have proposed phase transfer of host-guest complexes as a method by which to address current separations problems. Here we demonstrate that three different coordination cages – $Fe^{II}_4L_6$ **1**, $Fe^{II}_4L_4$ **2**, and $Fe^{II}_8L_{12}$ **3** – undergo anion exchange to transfer reversibly between water and ethyl acetate layers. This process was monitored both by UV-Vis spectrophotometry and slice-selective 1H NMR, which indicates no significant degradation of the three cages even after crossing the phase boundary more than 10 times. Furthermore, we designed a system that achieves sequential phase transfer of individual cage species within a mixture. With the development of this technology, we grow closer to using supramolecular phase transfer for industrially relevant separations.*

4.1 Introduction

Having introduced in Chapter 3 the idea of using coordination cages to transport molecular cargo between immiscible liquid phases, we now report fully reversible phase transfer of three different cages between water and ethyl acetate (EtOAc). Fundamentally, this result represents a new way by which a supramolecular architecture can shuttle reversibly between different physical compartments,^{1,2} with the potential for carrying a molecular cargo bound selectively according to its size, shape, and chemical functionality. The technology developed in this chapter represents a significant advancement over our previous system, in which we demonstrated that a cage and its cargo transported irreversibly from water to an ionic liquid layer upon exchange of the cage counterions from sulfate ($[SO_4]$) to tetrafluoroborate ($[BF_4]$) or triflimide ($[NTf_2]$).³ While the cargo \subset cage complex could be manipulated back into the original water layer, this process required several additional steps. The present work thus represents the first example of fully reversible phase transfer of coordination cages between two immiscible liquid phases. Furthermore, we demonstrate that this general technique enables

phase transfer of three different coordination cages: **1**,⁴ **2**,⁵ and **3**⁶ (Figure 4.1), which were self-assembled from twofold, threefold, and fourfold amine ligands, respectively.

In addition to many examples in which anions^{7,8} template the formation of^{9–11} or are encapsulated by coordination cages,^{12,13} counterions are also known to strongly influence the solubility preferences of coordination cages. When cages **1**, **2**, and **3** are paired with sulfate counterions, they are soluble in water despite the relatively poor aqueous solubility of their individual subcomponents. Paired with more hydrophobic anions such as tetrakis(pentafluorophenyl)borate, triflate, or triflimide, however, they are insoluble in water but are soluble in organic solvents such as acetonitrile. This feature allows the design of a system in which these cationic cages can be transported between immiscible liquid phases. Upon addition of hydrophobic anions tetrakis(pentafluorophenyl)borate ([BArF₅]) or tetrakis[3,5-bis(trifluoromethyl)phenyl]borate ([BAr(CF₃)₂]) to a biphasic system composed of EtOAc and a cage in water, the cages were observed to undergo an anion exchange from **1**[SO₄] / **2**[SO₄] / **3**[SO₄] to **1**[A] / **2**[A] / **3**[A] ([A] ≡ [BArF₅] or [BAr(CF₃)₂]) (Figure 4.1). This anion exchange rendered the cages insoluble in water and soluble in EtOAc, thus triggering phase transfer. Conversely, upon the addition of sulfate to a biphasic system composed of water and **1**[A] / **2**[A] / **3**[A] in EtOAc, the cages underwent an anion exchange to **1**[SO₄] / **2**[SO₄] / **3**[SO₄] and transferred back to the water phase.

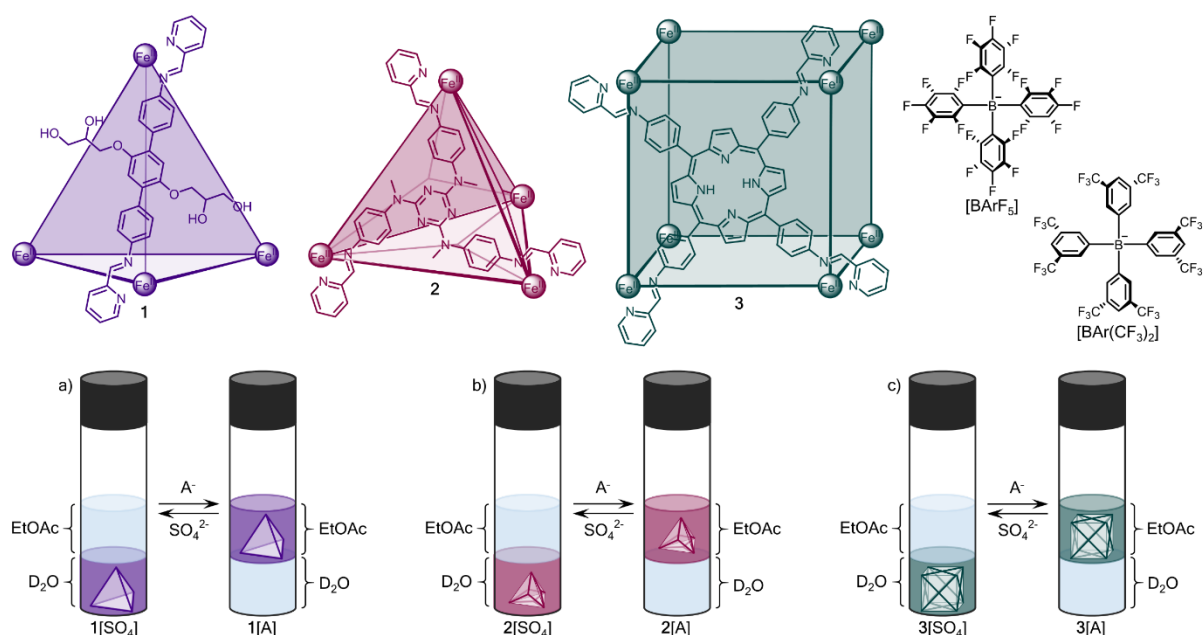


Figure 4.1 Reversible phase transfer of cage **1** (a), cage **2** (b), or cage **3** (c) between water and EtOAc upon the addition of a hydrophobic anion ([BArF₅] or [BAr(CF₃)₂]) or a hydrophilic anion ([SO₄]).

4.2 Results and Discussion

4.2.1 Stability of cages 1, 2, and 3 in water and EtOAc

UV-Vis measurements were conducted to determine the stability of cages **1**, **2**, and **3** in water (with $[\text{SO}_4]$) or EtOAc (with $[\text{BArF}_5]$ or $[\text{BAr}(\text{CF}_3)_2]$) over 60 minutes at low concentrations (5 – 30 μM). To gauge the stability of cages **1** $[\text{SO}_4]$, **2** $[\text{SO}_4]$, or **3** $[\text{SO}_4]$ in water, solutions of cages **1** $[\text{SO}_4]$, **2** $[\text{SO}_4]$, or **3** $[\text{SO}_4]$ in water were prepared, and UV-Vis spectra of these samples were recorded every 5 minutes over 60 minutes, the maximum length of time required for a full experiment as described in Chapter 4.2.2. To gauge the stability of cages **1** $[\text{BArF}_5]$, **1** $[\text{BAr}(\text{CF}_3)_2]$, **2** $[\text{BArF}_5]$, **2** $[\text{BAr}(\text{CF}_3)_2]$, **3** $[\text{BArF}_5]$, and **3** $[\text{BAr}(\text{CF}_3)_2]$ in EtOAc, samples were prepared by adding a minimum amount of $[\text{Li}][\text{BArF}_5]$ or $[\text{Na}][\text{BAr}(\text{CF}_3)_2]$ to a biphasic system of EtOAc (4 mL) and water (4 mL) until complete phase transfer of the cages from water into EtOAc was observed. UV-Vis spectra of these samples were recorded every 5 minutes over 60 minutes. The table below summarises the proportion of cage intact after 60 minutes; the data can be found in Chapter 4.4.4.

Table 4.1 Proportion of cages intact in water and EtOAc after 60 minutes

Cage:	$[\text{SO}_4]$ / Water	$[\text{BArF}_5]$ / EtOAc	$[\text{BAr}(\text{CF}_3)_2]$ / EtOAc
1	95.6%	100%	99.0%
2	98.8%	84.4%	52.3%
3	99.5%	100%	87.9%

Cage **1** was observed to be relatively stable in water and EtOAc, regardless of the counterion. In general, cages **2** and **3** were observed to be more stable in water than in EtOAc. Furthermore, cages **2** and **3** were observed to be more stable in EtOAc with $[\text{BArF}_5]$ than with $[\text{BAr}(\text{CF}_3)_2]$.

4.2.2 Determination of the minimum anion equivalents necessary for cage transport

In order to determine the minimum equivalents of $[\text{BArF}_5]$ or $[\text{BAr}(\text{CF}_3)_2]$ necessary to achieve quantitative transfer of cages **1**, **2**, or **3** from water to EtOAc, UV-Vis spectrophotometry was used to measure the absorption spectra of the water and EtOAc layers after the addition of the hydrophobic anions. In an effort to minimise errors due to EtOAc evaporation and/or decomposition of the cages in the EtOAc layer, both of which accumulate over time, parallel

experiments were set up such that different equivalents of anion were added to individual experiments within each set.

Before each experiment, stock solutions of cage (30 μM cage **1**[SO₄] in water; 30 μM cage **2**[SO₄] in water; 5 μM cage **3**[SO₄] in water) and anion (4 mM [Li][BArF₅] in EtOAc; 4 mM [Na][BAr(CF₃)₂] in EtOAc; 4 mM [ⁿBu₄N][SO₄] in water) were prepared in advance. For experiments in which cages were transported from water to EtOAc, cage stock solution (4 mL) was combined with the appropriate volume of [BArF₅] or [BAr(CF₃)₂] stock solution – the total volume of the experiment was then adjusted to 8 mL with EtOAc. All parallel experiments were simultaneously inverted 10 times and were left to settle a short time. Aliquots (3 mL) from each of the EtOAc layers were added to a quartz cuvette with a 1 cm path length and a screw cap with a PTFE seal. In order to minimise error from decomposition, the UV-Vis spectra from aliquots with the lowest cage concentration were collected before samples with higher cage concentration. Aliquots (3 mL) from each of the water layers were then analysed in a similar manner as aliquots from the EtOAc layers. Because EtOAc is more soluble in water than *vice versa*, a dilution factor was incorporated into the “corrected” concentration of each phase. This data can be found in Chapter 4.4.5.

The data acquired from each layer was then fitted to a standard function that defines symmetrical sigmoidal curves (Equation 4.1), in which L is the asymptotic limit of maximum transport (*e.g.* 100%), d is the asymptotic limit of minimum transport (*e.g.* 0%), r is the steepness of the curve, and t_m is the inflection point. Data was fitted to a logistic model using loglet.com by not excluding “zero” data points and leaving all constants (L , d , r , and t_m) unspecified. We define the intersection of the two curves (from water and EtOAc) as the point at which 50% of complete phase transfer is achieved; twice this value thus gives the anion equivalents required for complete phase transfer.

$$y = \frac{L-d}{1+e^{-r(t-t_m)}} + d \quad \text{Equation 4.1}$$

The UV-Vis results, as represented in Figure 4.2, indicate that the rates (proportion of cages transported *vs.* anion equivalents added) at which cages **1**, **2**, and **3** transferred from water to EtOAc were dependent on 1) the identity of the cage and 2) the identity of the hydrophobic anion. Roughly twice the equivalents of [BAr(CF₃)₂] than [BArF₅] were required to achieve complete cage transfer. Furthermore, tetrahedral cage **2** required fewer equivalents of anion

([BArF₅] = 7.6 equiv; [BAr(CF₃)₂] = 12 equiv) to approach complete transport than tetrahedral cage **1** ([BArF₅] = 13 equiv; [BAr(CF₃)₂] = 25 equiv), and cubic cage **3** required more anion equivalents ([BArF₅] = 28 equiv; [BAr(CF₃)₂] = 49 equiv) than either of the tetrahedral cages.

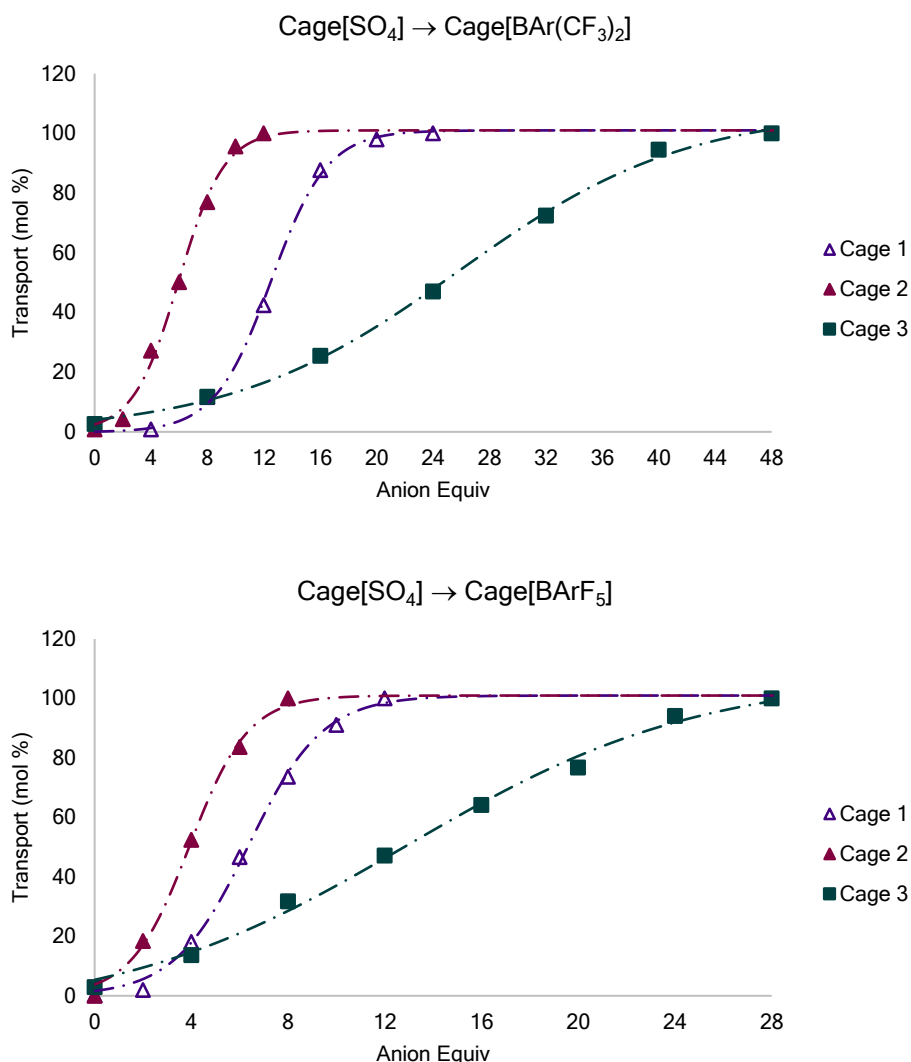


Figure 4.2 Graphical representation of the amount of cage transferred from water to EtOAc vs. number of [A] equivalents added to the system. [A] ≡ [BAr(CF₃)₂] or [Li][BArF₅]. Data obtained from measuring the UV-Vis spectrum of the EtOAc layer.

Likewise, in order to determine the minimum equivalents of [SO₄] required to achieve quantitative transfer of cages from EtOAc to water, we used a similar procedure as described above, in which parallel experiments were employed within each set, and the resulting data were fitted to sigmoidal curves. Samples were prepared with a total volume of 8 mL as previously described. The appropriate volume of [ⁿBu₄N][SO₄] stock solution was then added

to each of the parallel experiments, making the total volume of the experiments greater than 8 mL and thus necessitating an additional dilution factor for the calculation of the “corrected” concentration of the water layers. The UV-Vis spectra were collected as previously described for the water to EtOAc cage transport experiments. The data was also processed as previously described. This data can be found in Chapter 4.4.5.

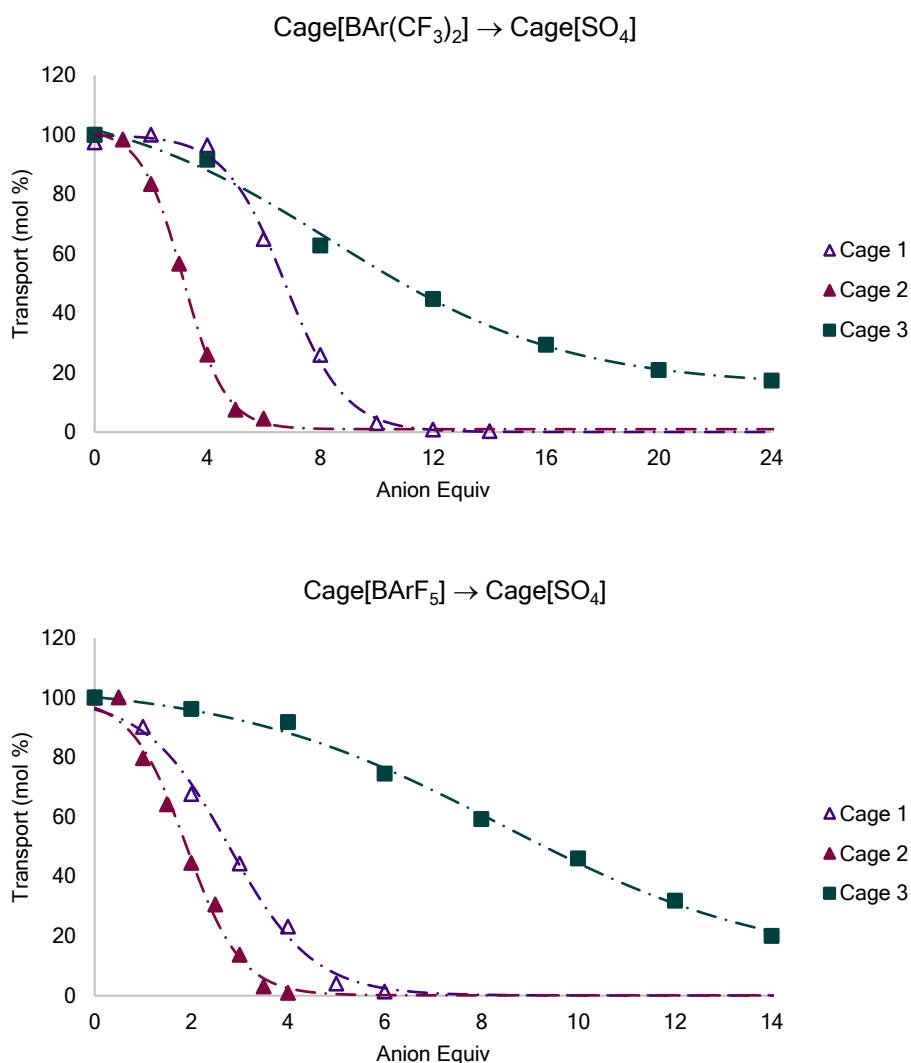


Figure 4.3 Proportion of cage transferred from EtOAc to water upon the addition of [ⁿBu₄N][SO₄].

For cages **1** and **2**, each anion exchange required approximately half the equivalents of [SO₄] to achieve complete transport into water as [A] equivalents were required to achieve cage transport into EtOAc; the curves representing cage transfer into water (Figure 4.3) thus mirror the corresponding curves representing cage transfer into EtOAc. More specifically, the transformations 2[BArF₅] → 2[SO₄] and 2[BAr(CF₃)₂] → 2[SO₄] required 3.6 equiv and 6.2

equiv, respectively, to achieve complete transport back to water. And the transformations $1[\text{BArF}_5] \rightarrow 1[\text{SO}_4]$ and $1[\text{BAr}(\text{CF}_3)_2] \rightarrow 1[\text{SO}_4]$ required 5.4 equiv and 13 equiv, respectively.

As can be seen in Figure 4.3, however, the EtOAc layer was never observed to become colourless as $3[\text{BArF}_5] \rightarrow 3[\text{SO}_4]$ or $3[\text{BAr}(\text{CF}_3)_2] \rightarrow 3[\text{SO}_4]$ and the cages transferred out of EtOAc into the water layer. To investigate the identity of the species remaining in the EtOAc layer after phase transfer of the cage, these experiments were performed at a higher concentration so that ^1H NMR could be used to observe the EtOAc layer. Two NMR samples of cage $3[\text{SO}_4]$ in D_2O were prepared (0.5 mL, 0.5 mM). EtOAc (0.5 mL), followed by $[\text{BArF}_5]$ (28 equiv) or $[\text{BAr}(\text{CF}_3)_2]$ (49 equiv) was then added to both NMR samples, and the samples were inverted 20 times and allowed to settle. In both samples, complete transfer of cage **3** to the EtOAc layer was observed. To the sample containing cage $3[\text{BArF}_5]$, 14 equiv of $[\text{SO}_4]$ were added; to the sample containing cage $3[\text{BAr}(\text{CF}_3)_2]$, 25 equiv $[\text{SO}_4]$ was added. Both samples were inverted 20 times and allowed to settle; the water layer containing cage $3[\text{SO}_4]$ was removed from both samples, and the ^1H NMR spectra of the remaining yellow EtOAc layers was collected. Aromatic peaks corresponding to the cage or the cage subcomponents were not found in either spectra. This result suggests that, if the yellow colour in the EtOAc is the result of cage decomposition, the decomposition products must be highly coloured and very dilute. While the residual yellow colour in the EtOAc layer thus distorts the shape of the sigmoidal curves obtained from the UV-Vis data, the species in the EtOAc layer do not significantly impact cage transport at relatively high concentrations (0.5 mM cage).

After determining the minimum anion equivalents necessary to achieve reversible transfer of cages between water and EtOAc, we sought to establish the capability of these systems to remain robust over multiple phase transfer cycles, as described in Chapter 4.2.3.

4.2.3 Slice-selective ^1H NMR to monitor phase transfer cycles

A brief explanation of slice-selective NMR

In Chapters 2 and 3, we separated and subsequently recombined different layers within multiphasic systems for analysis by NMR. Because this procedure is experimentally tedious, we decided to use slice-selective ^1H NMR, a spectroscopic technique reported in the literature,^{14,15} to measure 1D ^1H NMR spectra from different locations within the biphasic

NMR samples in this chapter. When a pulsed field gradient is applied along the z -axis of an NMR sample, the external field gradient (B_g) can be described in terms of the location along the z -axis of the NMR sample (z) according to equation 4.2, in which B_0 is the field strength of the spectrometer (*e.g.* 500 MHz) and G_z is the strength of the gradient (*e.g.* 50%).

$$B_g(z) = B_0 + G_z z \quad \text{Equation 4.2}$$

As can be seen in Figure 4.4, B_g can be used to determine the electromagnetic frequency required to bring nuclei at locations z_1 and z_2 into resonance with the external magnetic field. Varying the pulse bandwidth and frequency thus changes the width and location, respectively, of the irradiated “slice” within the NMR sample. Furthermore multiple 1D NMR spectra can be collected along the z -axis of an NMR sample to create a pseudo-2D NMR spectrum that describes chemical shift *vs.* intensity *vs.* location within the NMR sample.

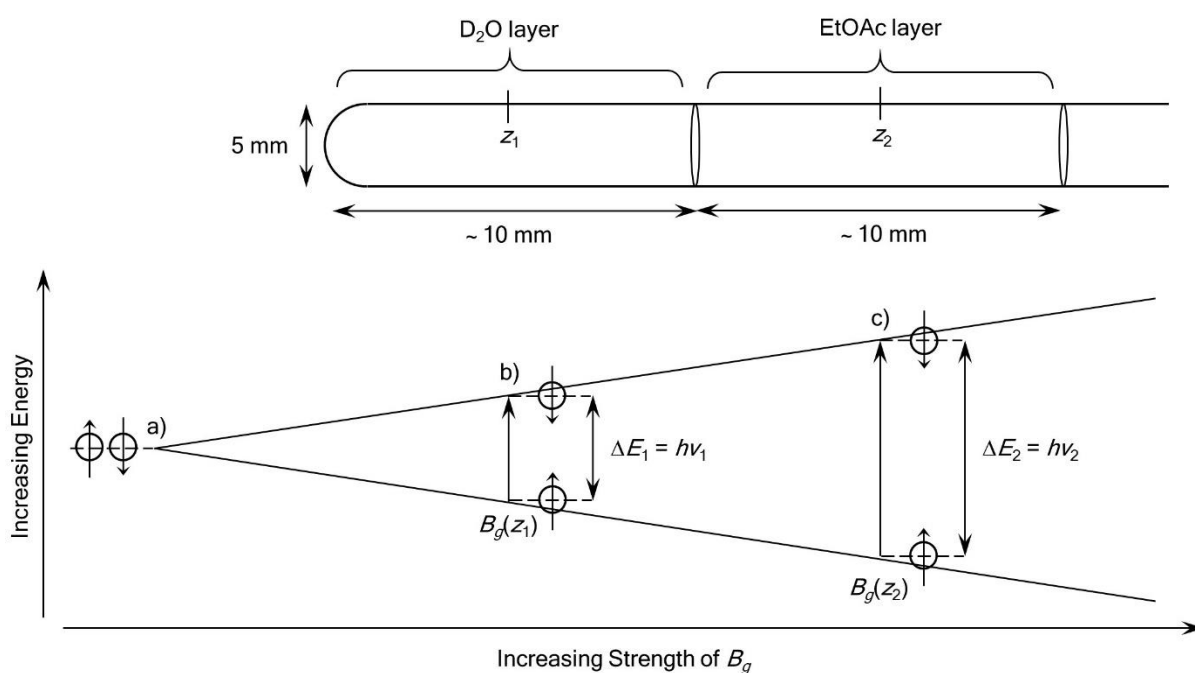


Figure 4.4 Graphical representation of a pulsed field gradient aligned along the z -axis of a biphasic NMR sample, with water and EtOAc layers. a) When no external magnetic field is present, $\Delta E = 0$ between opposite nuclear spins. b) At position z_1 along the NMR sample, the external magnetic field is equivalent to $B_g(z_1)$; the energy difference between opposite nuclear spins is equivalent to ΔE_1 , and the electromagnetic frequency required to excite the nuclei at z_1 is equivalent to ν_1 . c) Same as b), but the strength of the magnetic field $B_g(z_2)$, and the energy/pulse frequency required to excite the nuclei at z_2 (ΔE_2 and ν_2 , respectively) reflect the different location (z_2) along the z -axis of the NMR sample.

In this chapter, we were thus able to measure the ^1H NMR spectrum from 1 mm slices centred in the water or EtOAc phases by applying a pulsed field gradient and selecting pulses of the most appropriate bandwidth and frequency. Using this technique, we were able to track the cages as they were transported across the phase interface between water and EtOAc more than 10 times.

General procedure

A 5 mm NMR tube with 0.38 mm wall thickness was used for the following slice-selective ^1H NMR experiments. NMR tubes with thicker walls were found to be less suitable for these experiments because the wall thickness significantly reduced the volume of sample in each 1 mm slice. A solution of cage **1**[SO₄] (200 μL ; 1 mM in D₂O), **2**[SO₄] (200 μL ; 2 mM in D₂O), or **3**[SO₄] (200 μL ; 0.5 mM) was combined with EtOAc (200 μL , nondeuterated). The resulting biphasic system was inverted 20 times.

Using the depth gauge for the instrument, the sample was positioned such that the interface would be located as near as possible to the mid-point of the probe's transmit/receive coils. The sample was locked to D₂O and tuned to the ^1H nucleus, but the sample was left unshimmed. A pseudo-2D slice-selective ^1H NMR experiment was then run with the number of scans (ns) = 1, G_z = 50%, and B_0 = 500 MHz. A representative spectrum can be found in Figure 4.5. The peaks in the 2D spectrum represent the chemical shift of the signal vs. the signal intensity vs. the location of the 1D "slice" along the NMR tube. In the D₂O layer, relatively small peaks from residual H₂O and dissolved EtOAc can be observed. In the EtOAc layer, relatively large peaks from the non-deuterated solvent can be observed. The curvature of the peaks along the direction of y-axis of the 2D spectrum (corresponding to the location of the "slice" along the NMR tube) results from the inhomogeneity of the magnetic field – this effect is insignificant, however, on the millimetre scale.

By toggling through the multi-display mode, the slice with the sharpest, most intense solvent peaks from each layer was chosen, and the *spoffs1* (offset) values intrinsic to those two slices were recorded. Since the experiment was run with $ns = 1$, the cage peaks in the water layer were observed to be very small in the pseudo-2D spectrum. Two new 1D slice-selective ^1H NMR experiments were created (one experiment for each layer), and the best *spoffs1* values recorded from the 2D experiment were used for the 1D experiments. The 1D slice-selective

NMR experiments were then run with $ns = 64$ or 128 , depending on the concentration of the sample.

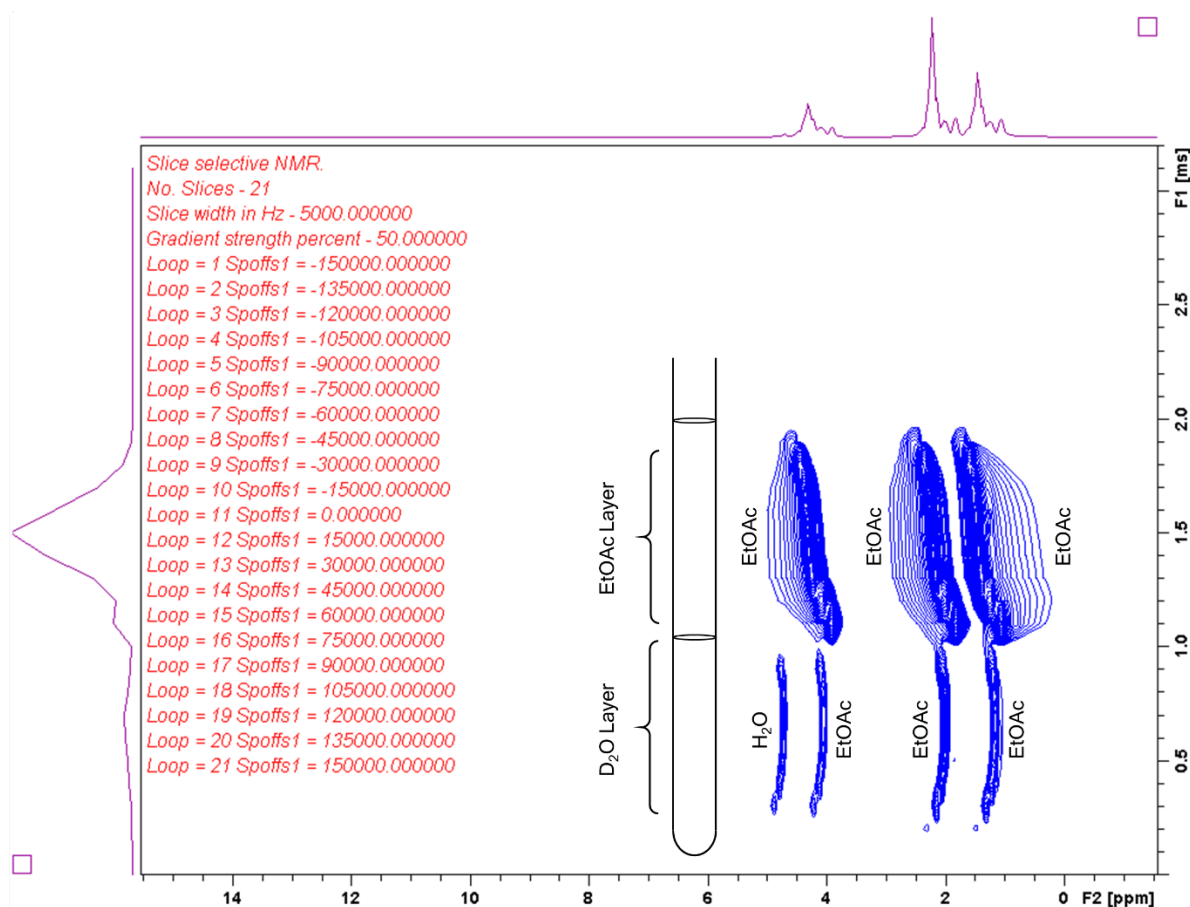


Figure 4.5 Representative pseudo-2D slice-selective ^1H NMR spectrum of a biphasic $\text{D}_2\text{O}/\text{EtOAc}$ NMR sample.

Before each series of slice-selective ^1H NMR experiments, stock solutions of [A] in EtOAc and $[\text{SO}_4]$ in D_2O were prepared such that $10 \mu\text{L}$ of the stock solution would contain the appropriate amount of [A] or $[\text{SO}_4]$. As summarised in Table 4.2, the amount of [A] required for complete transfer of the cage from D_2O to EtOAc was determined using the UV-Vis results described in Chapter 4.2.2; the amount of $[\text{SO}_4]$ used to transfer the cage from EtOAc to D_2O was equal to half the amount of [A].

After collecting an initial 1D slice-selective ^1H NMR spectrum from each layer in the NMR sample, $[\text{BArF}_5]$ or $[\text{BAr}(\text{CF}_3)_2]$ was added to the sample to trigger phase transfer of the cage from the D_2O to the EtOAc layer. The NMR sample was inverted 20 times before repeating the procedure described previously for running the initial slice-selective ^1H NMR experiments. After collecting the 1D slice-selective ^1H NMR spectra from both the D_2O and EtOAc layers, $[\text{SO}_4]$ was added to the sample trigger phase transfer of the cage from EtOAc back to D_2O .

Table 4.2 Summary of anion equivalents added

Cage:	[SO ₄] ⇌ [BAr(CF ₃) ₂]		[SO ₄] ⇌ [BArF ₅]	
	[BAr(CF ₃) ₂] (equiv):	[SO ₄] (equiv):	[BArF ₅] (equiv):	[SO ₄] (equiv)
1	25	13	13	6.5
2	12	6	7.6	3.8
3	49	25	28	14

The procedure described above was repeated until the cage had crossed the phase boundary 11 times. Notably, no subcomponent peaks were observed to appear over time in either layer, indicating that no significant cage decomposition occurred for any combination of cage and counterion after transferring across the D₂O/EtOAc interface 11 times. During the course of the experiment, the interface between the two layers would move up the NMR tube as the bottom layer was diluted by the addition of [SO₄] stock solution. Periodically repeating the pseudo-2D slice-selective ¹H NMR experiment was thus necessary so that the *spoffs1* value for the 1D experiments could be adjusted to reflect the correct position of each layer.

Phase transfer cycles: $\mathbf{1}[\text{SO}_4] \rightleftharpoons \mathbf{1}[\text{BAR}(\text{CF}_3)_2]$

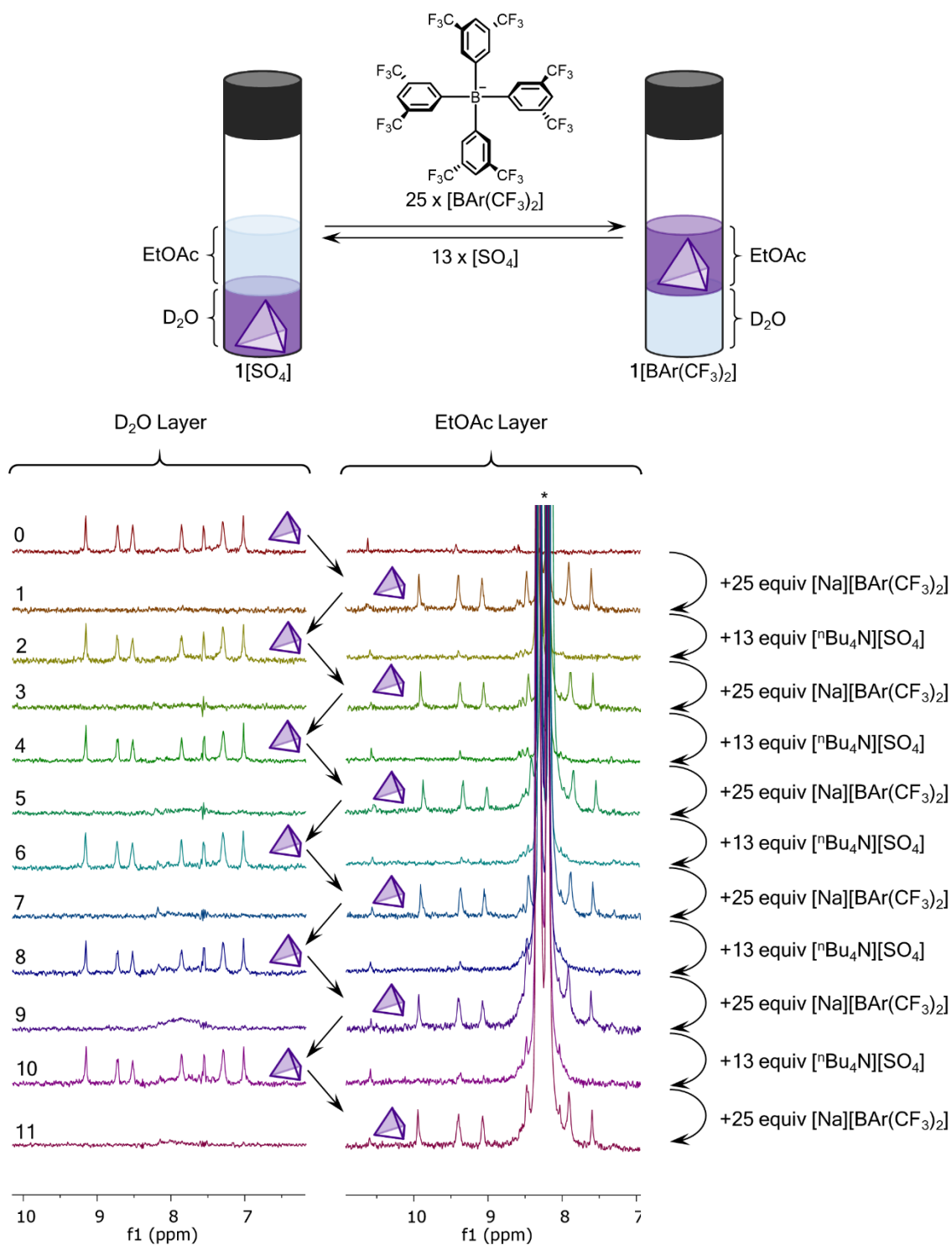


Figure 4.6 ^1H NMR spectra in D_2O (left) or EtOAc (right) depicting the transformation $\mathbf{1}[\text{SO}_4] \rightleftharpoons \mathbf{1}[\text{BAR}(\text{CF}_3)_2]$ as $[\text{BAR}(\text{CF}_3)_2]$ (25 equiv) or $[\text{SO}_4]$ (13 equiv) were added to drive phase transfer. * $[\text{BAR}(\text{CF}_3)_2]$

Phase transfer cycles: $1[\text{SO}_4] \rightleftharpoons 1[\text{BArF}_5]$

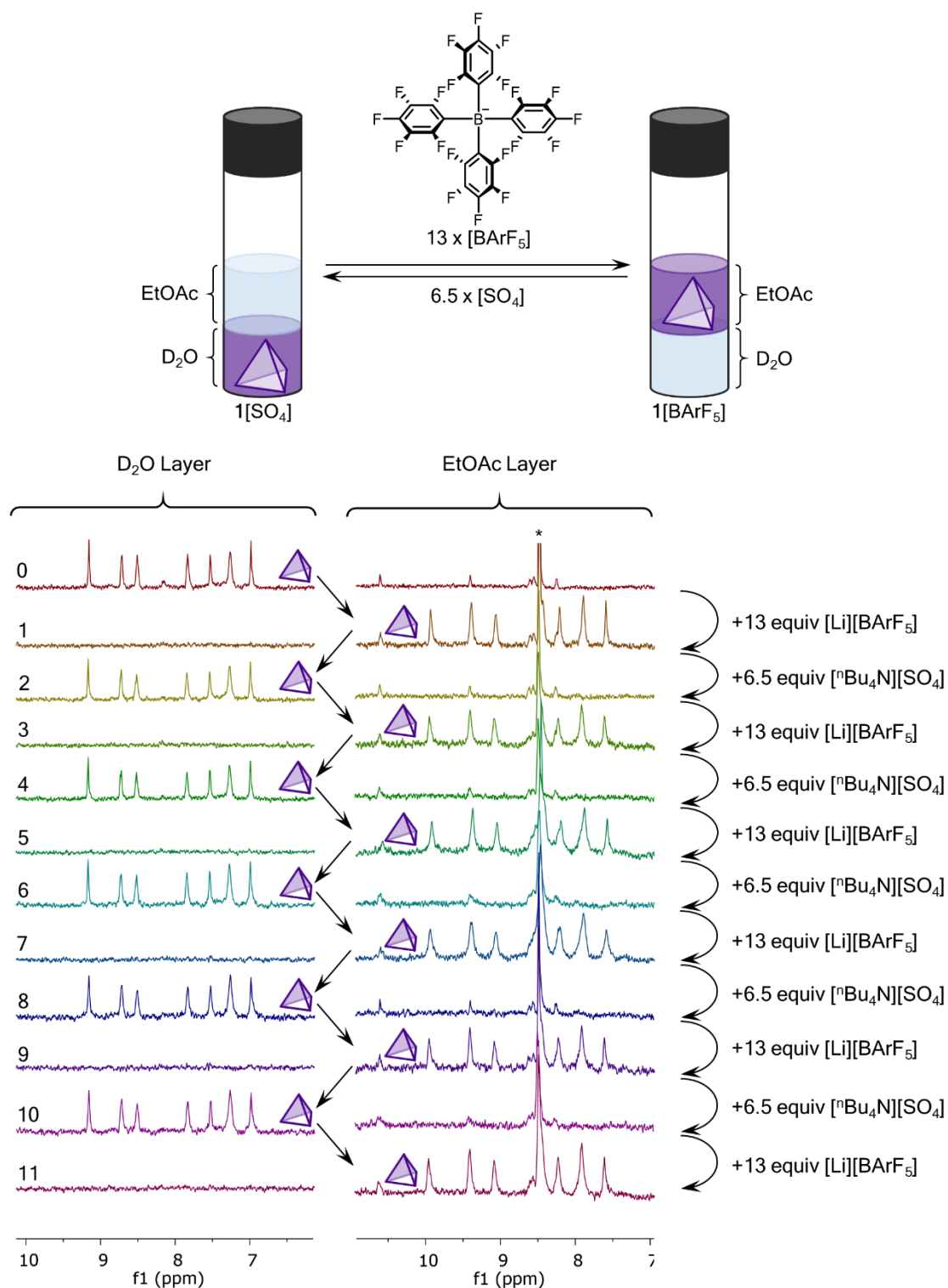


Figure 4.7 ^1H NMR spectra in D_2O (left) or EtOAc (right) depicting the transformation $1[\text{SO}_4] \rightleftharpoons 1[\text{BArF}_5]$ as $[\text{BArF}_5]$ (13 equiv) or $[\text{SO}_4]$ (6.5 equiv) were added to drive phase transfer. *Impurity in commercial EtOAc.

Phase transfer cycles: $2[\text{SO}_4] \rightleftharpoons 2[\text{BAr}(\text{CF}_3)_2]$

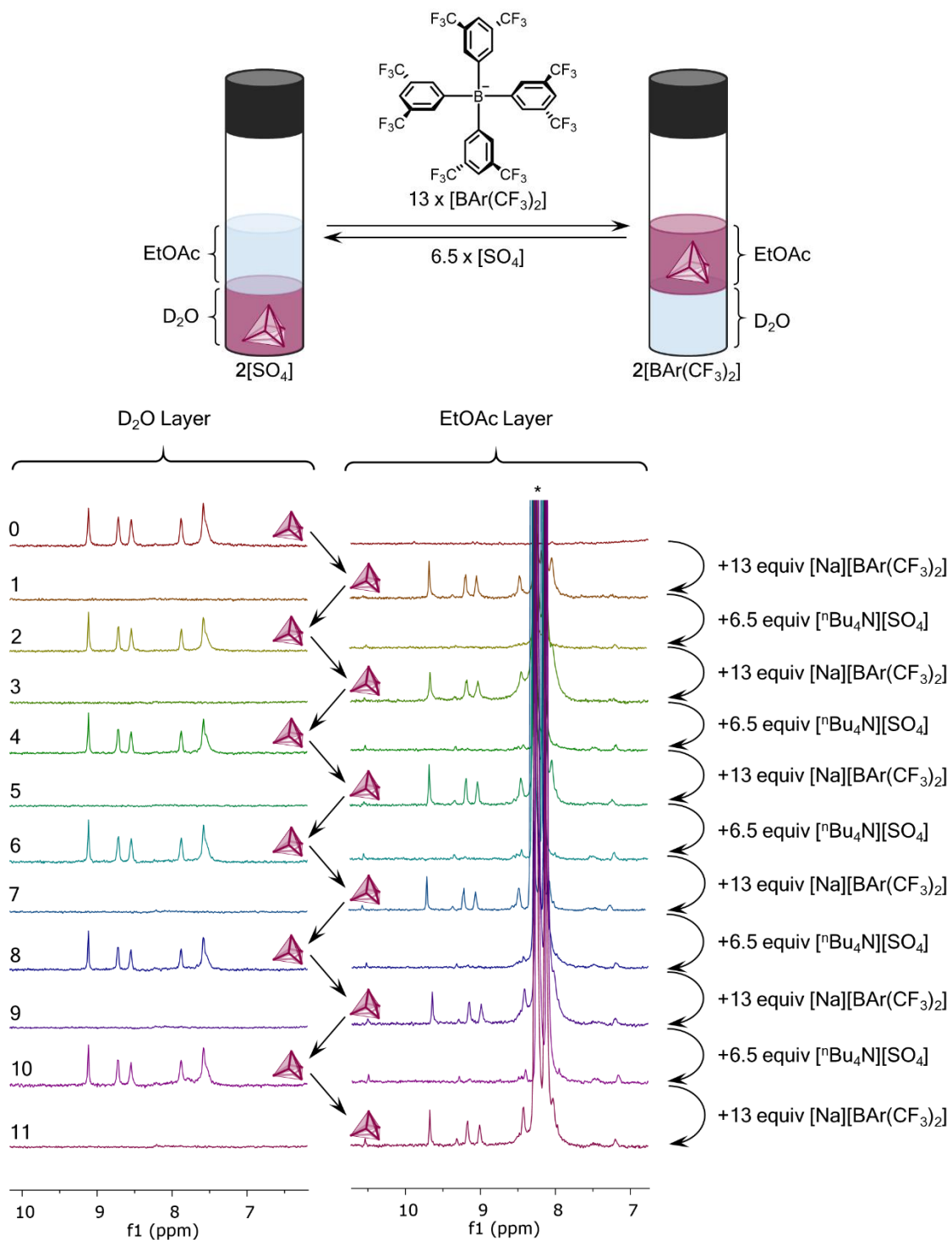


Figure 4.8 ^1H NMR spectra in D₂O (left) or EtOAc (right) depicting the transformation $2[\text{SO}_4] \rightleftharpoons 2[\text{BAr}(\text{CF}_3)_2]$ as $[\text{BAr}(\text{CF}_3)_2]$ (12 equiv) or $[\text{SO}_4]$ (6 equiv) were added to drive phase transfer. * $[\text{BAr}(\text{CF}_3)_2]$

Phase transfer cycles: $2[\text{SO}_4] \rightleftharpoons 2[\text{BArF}_5]$

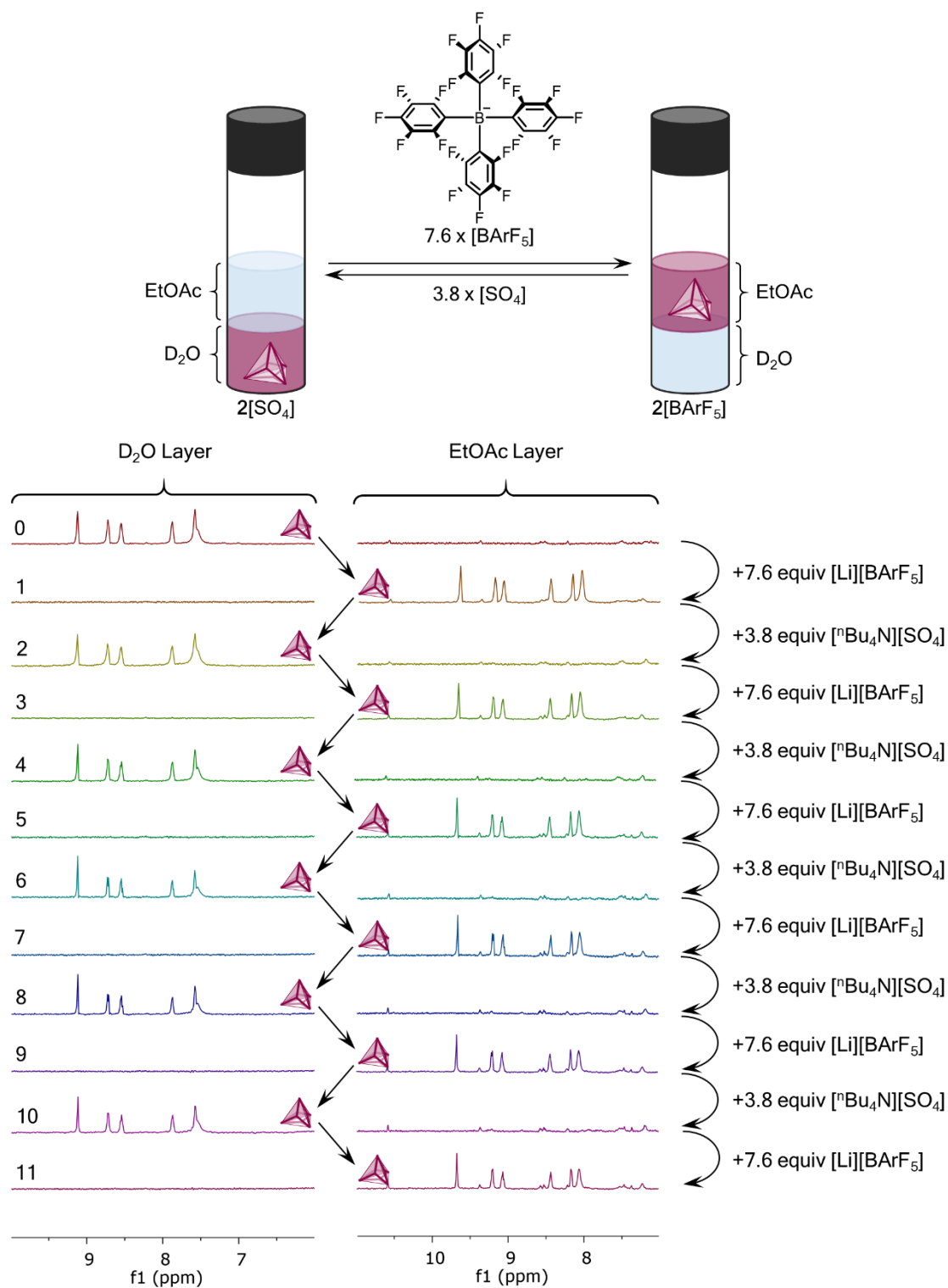


Figure 4.9 ¹H NMR spectra in D₂O (left) or EtOAc (right) depicting the transformation $2[\text{SO}_4] \rightleftharpoons 2[\text{BArF}_5]$ as [BArF₅] (7.6 equiv) or [SO₄] (3.8 equiv) were added to drive phase transfer.

Phase transfer cycles: $3[\text{SO}_4] \rightleftharpoons 3[\text{BAr}(\text{CF}_3)_2]$

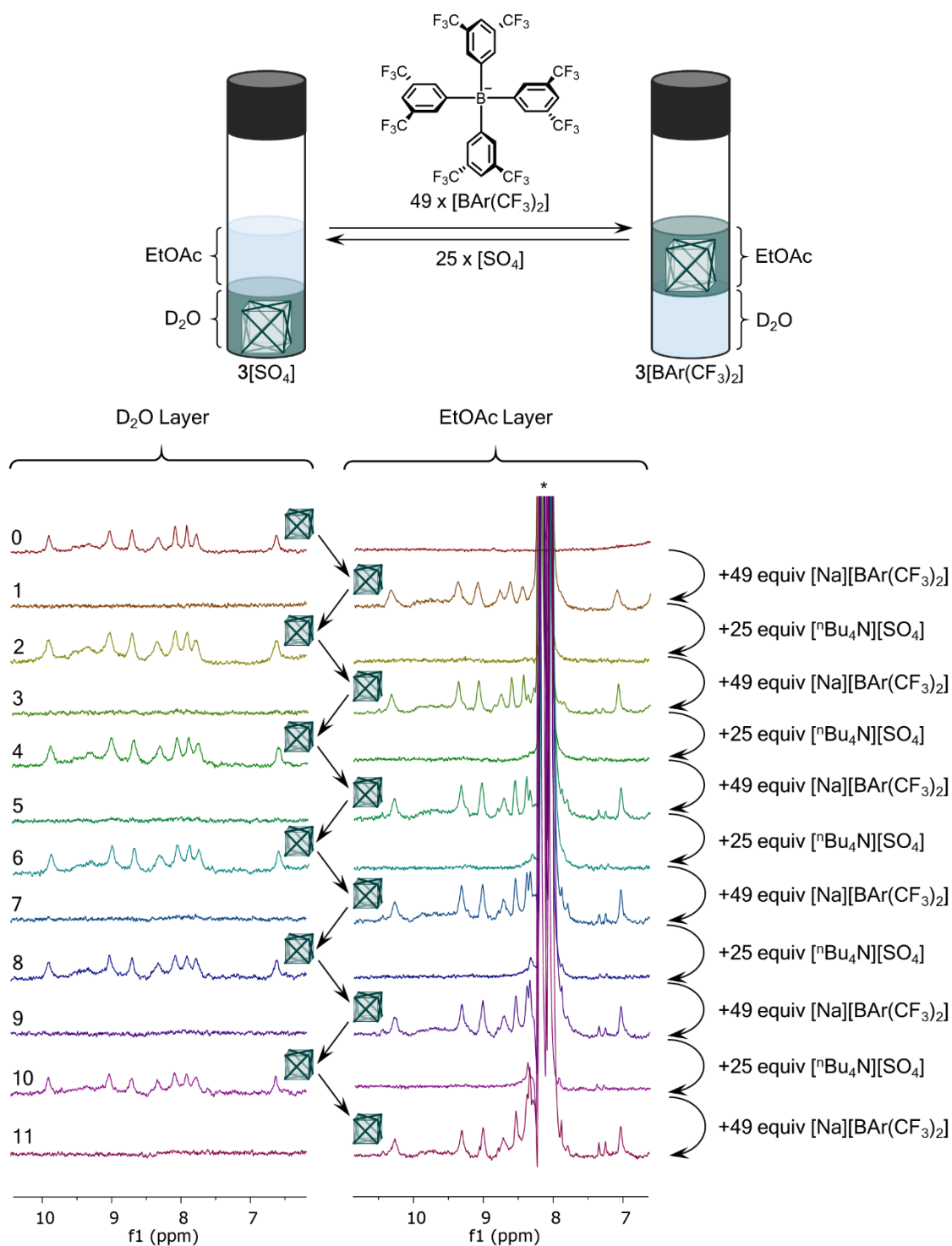


Figure 4.10 ^1H NMR spectra in D_2O (left) or EtOAc (right) depicting the transformation $3[\text{SO}_4] \rightleftharpoons 3[\text{BAr}(\text{CF}_3)_2]$ as $[\text{BAr}(\text{CF}_3)_2]$ (49 equiv) or $[\text{SO}_4]$ (25 equiv) were added to drive phase transfer. * $[\text{BAr}(\text{CF}_3)_2]$

Phase transfer cycles: $3[\text{SO}_4] \rightleftharpoons 3[\text{BARF}_5]$

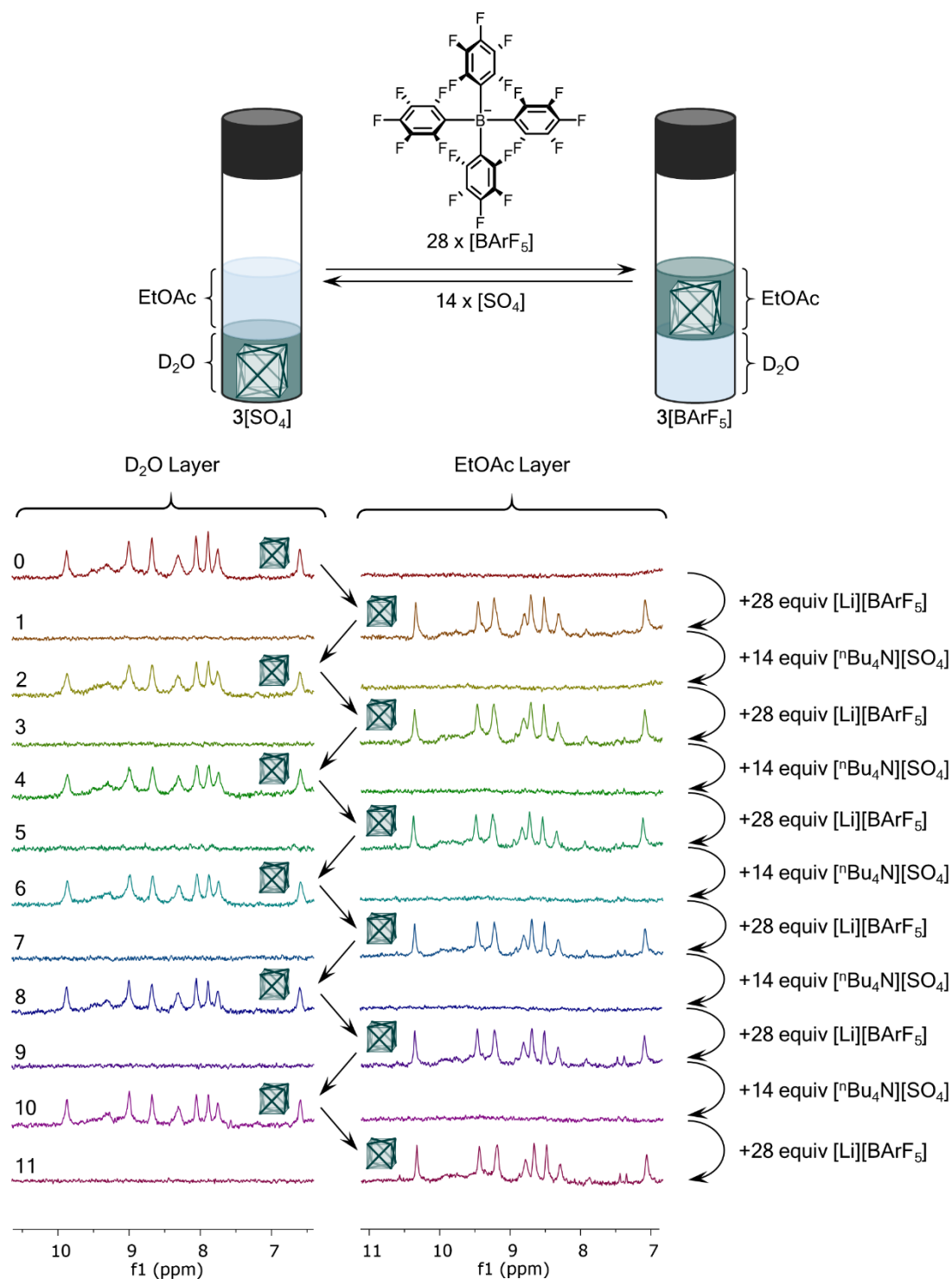


Figure 4.11 ^1H NMR spectra in D_2O (left) or EtOAc (right) depicting the transformation $3[\text{SO}_4] \rightleftharpoons 3[\text{BARF}_5]$ as $[\text{BARF}_5]$ (28 equiv) or $[\text{SO}_4]$ (14 equiv) were added to drive phase transfer.

4.2.4 Sequential phase transfer of coordination cages

Because the cages chosen for this study have different affinities for anions, we designed a system that achieves sequential phase transfer of individual cage species within a water/EtOAc biphasic system containing mixtures of two cages: cages **1** and **2**, cages **1** and **3**, and cages **2** and **3**.

As in Chapter 4.2.3, a 5 mm NMR tube with 0.38 mm wall thickness was used for the following slice-selective ^1H NMR experiments. For each mixture of two cages, each cage was present in 0.5 mM concentration, in a 200 μL D_2O solution. Each mixture was combined with EtOAc (200 μL , nondeuterated), and the resulting biphasic system was inverted 20 times. Slice-selective ^1H NMR was then performed on both water and EtOAc layers, as described in Chapter 4.2.3. For the mixture of cages **1** and **2**, slice-selective ^1H NMR was then used to monitor both layers as 7.6 equiv $[\text{BArF}_5]$ were added sequentially to the system until both cages transferred from the water to the EtOAc phase. This data can be found at the end of this section. While the signals in the ^1H NMR data are too small and broad to accurately integrate the signals from cage **1** vs. cage **2**, cage **2** could clearly be observed transporting from the aqueous mixture into the EtOAc layer before cage **1**, with good separation between cage **1** and cage **2** after a total of 15.2 equiv $[\text{BArF}_5]$ had been added to the system. This trend, in which cage **2** required fewer anion equivalents than cage **1** to achieve complete transport from water to EtOAc, is consistent with the trend observed by UV-Vis in Chapter 4.2.2.

For the mixture of cages **1** and **3**, slice-selective ^1H NMR was used to monitor both layers as 14 equiv $[\text{BArF}_5]$ were added sequentially to the system until both cages transferred from the water to the EtOAc phase. The data can be found at the end of this section. Notably, the order in which the two cages were observed to transport from water to EtOAc did not follow the order established in Chapter 4.2.2: upon the addition of $[\text{BArF}_5]$ to the system, cage **3** was observed to transport into the EtOAc layer before being joined by cage **2**. Given that cage **3** required more equivalents of $[\text{BArF}_5]$ and $[\text{SO}_4]$ than cage **2** to achieve complete transport in our UV-Vis investigations, our observation that cage **3** transferred between layers before cage **2** is perhaps counterintuitive. Because cage **3** carries twice the positive charge as cage **2** (+16 vs. +8, respectively), however, we hypothesise that cage **3** has a higher affinity for anions than cage **2**, thus explaining how cage **3** was able to successfully outcompete cage **2** for $[\text{BArF}_5]$ counteranions in this combined system. As with the phase transfer of individual cages, this

process is fully reversible. Upon the sequential addition of 7 equiv [SO₄] to the system, cage **2** was observed to transport into the water layer before being joined by **3**.

For the mixture of cages **2** and **3**, slice-selective ¹H NMR was used to monitor both layers as 14 equiv [BArF₅] were added sequentially to the system until both cages transferred from the water to the EtOAc phase. The data can be found at the end of this section. As in the mixture of cages **1** and **3**, cubic cage **3** (+16 charge) was clearly observed to transport from the aqueous mixture into the EtOAc layer before tetrahedral cage **2** (+8 charge).

Sequential phase transfer of cages 1 and 2

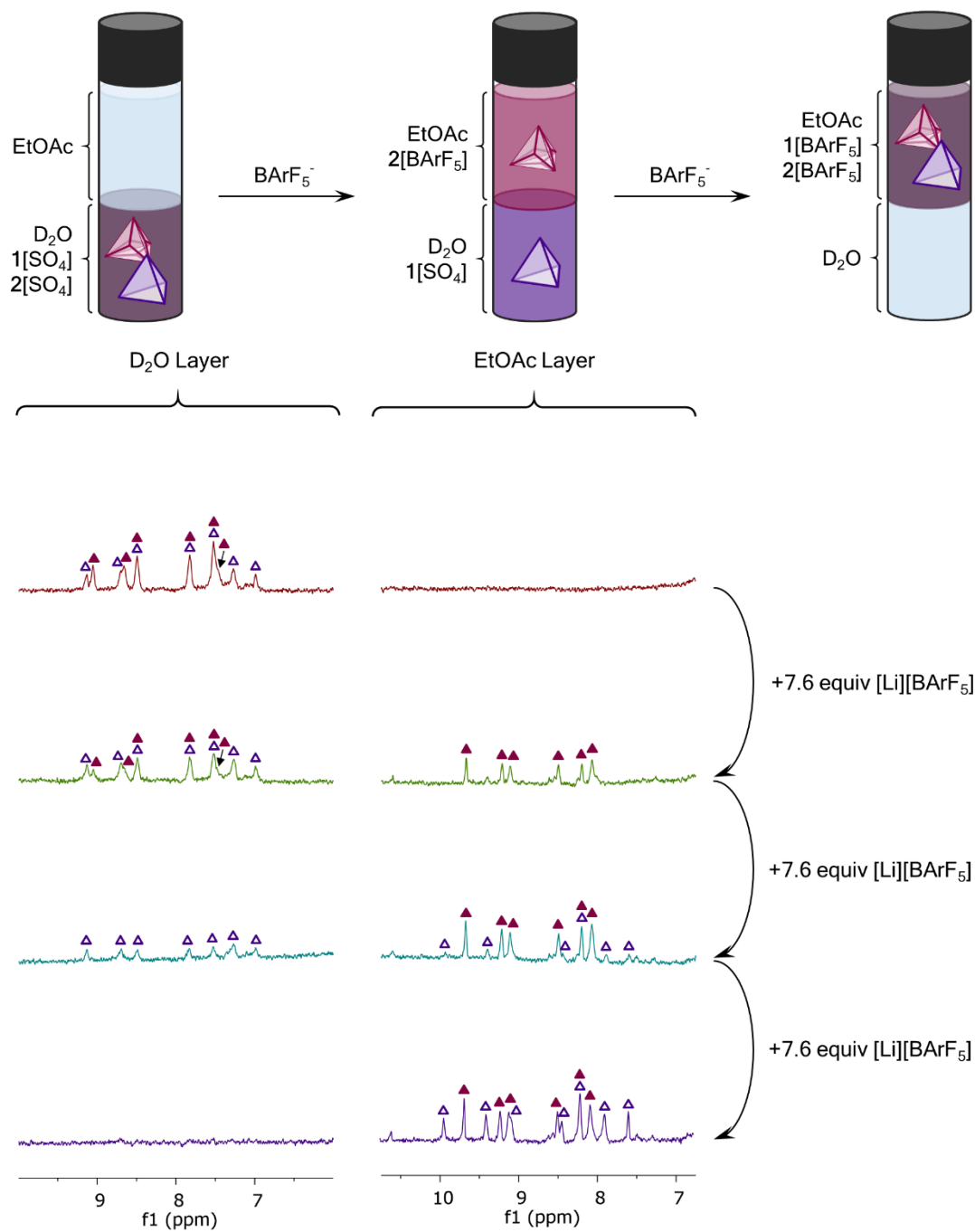


Figure 4.12 ¹H NMR spectra in D₂O (left) or EtOAc (right) monitoring the phase transfer of cages **1** and **2** from water into EtOAc upon the sequential addition of [BArF₅⁻] (7.6 equiv).

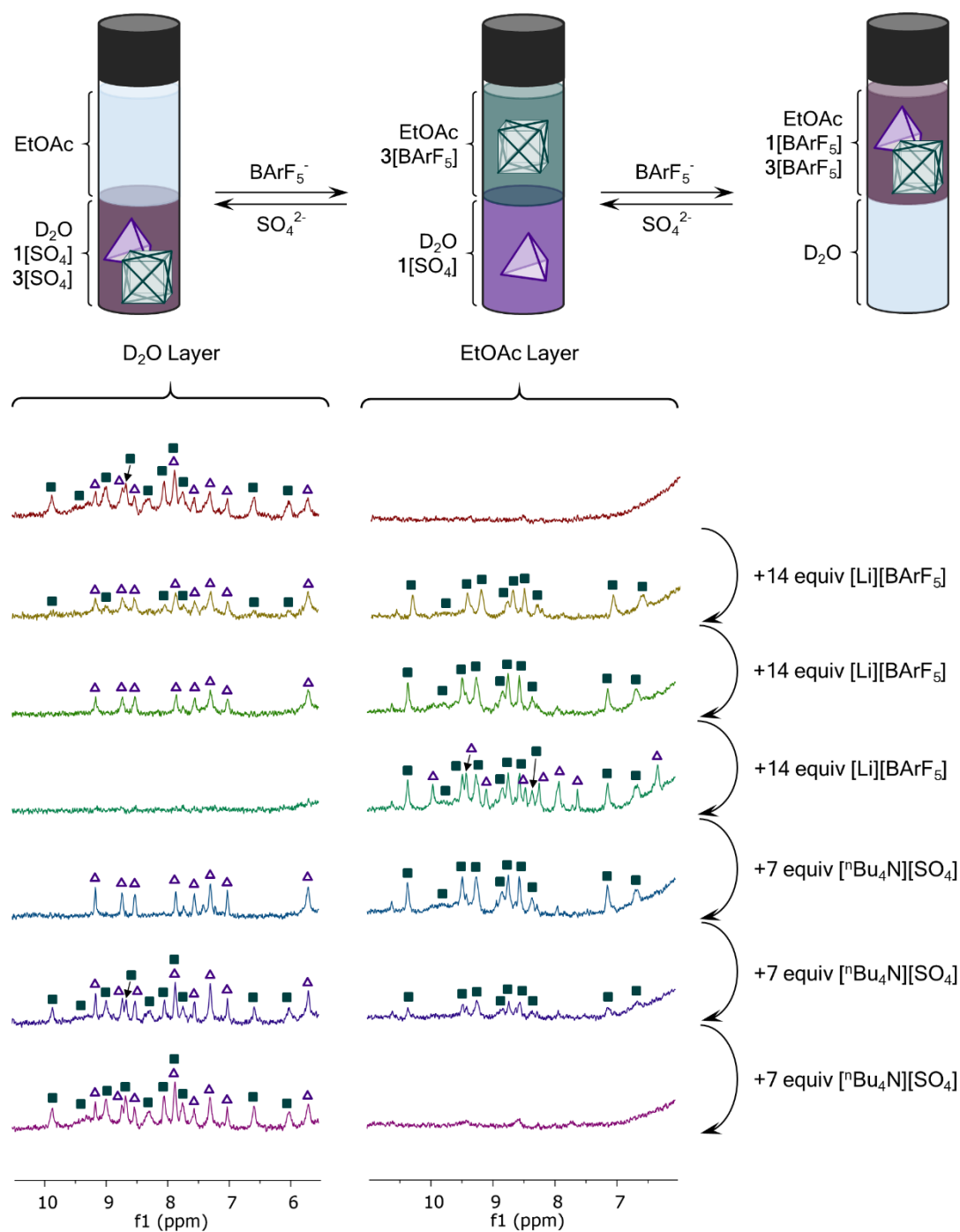
Sequential phase transfer of cages **1** and **3**

Figure 4.13 1H NMR spectra in D_2O (left) or EtOAc (right) monitoring the phase transfer of cages **1** and **3** from water into EtOAc upon the sequential addition of $[BArF_5]$ (14 equiv). This process was observed to be reversible upon the sequential addition of $[SO_4]$ (7 equiv).

Sequential phase transfer of cages 2 and 3

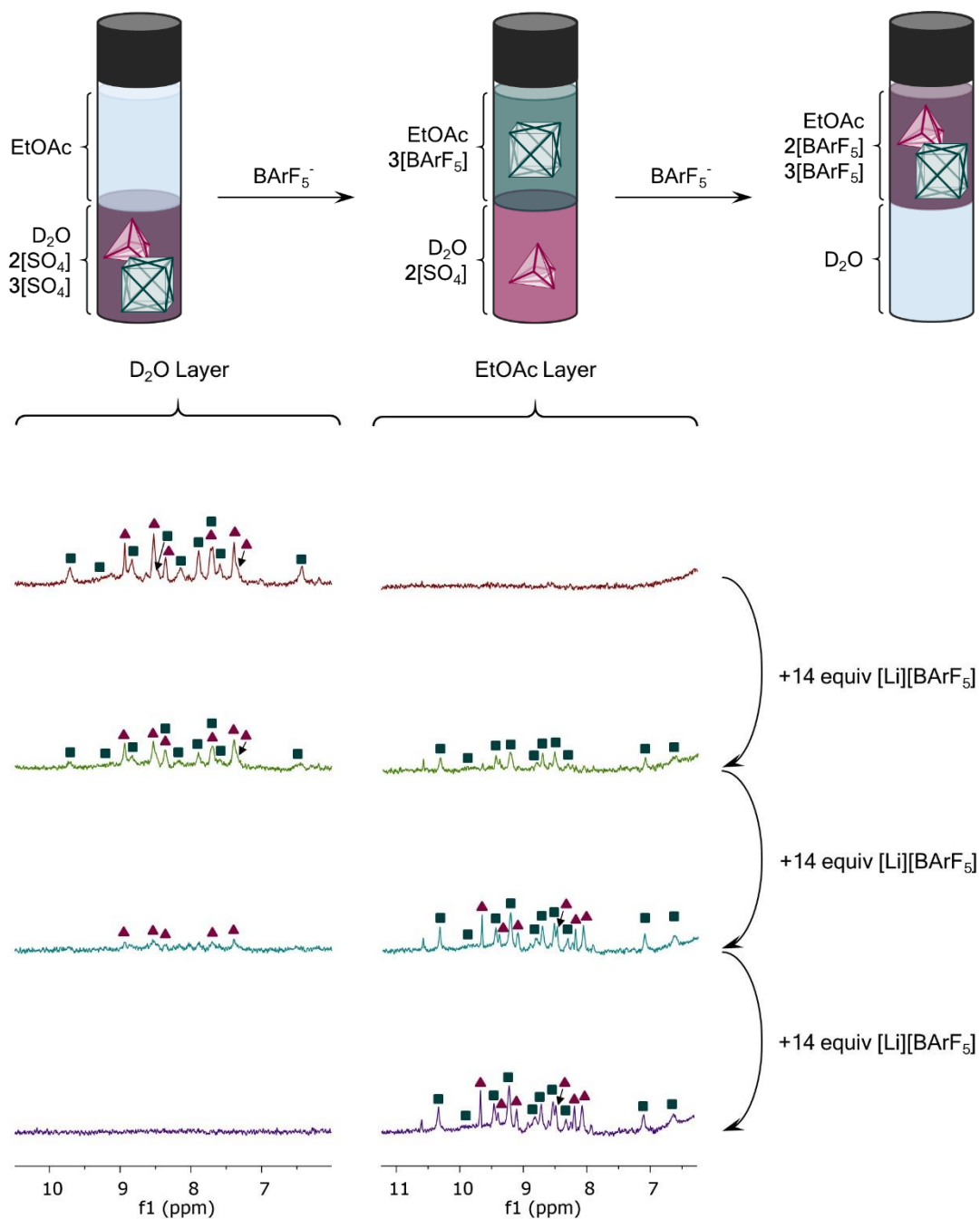


Figure 4.14 ¹H NMR spectra in D₂O (left) or EtOAc (right) monitoring the phase transfer of cages 2 and 3 from water into EtOAc upon the sequential addition of [BARF₅]⁻ (14 equiv).

4.3 Conclusions and Future Work

We hypothesise that patterns observed above, both in our preliminary UV-Vis studies and in the sequential transport system, are the result of a complex relationship between the affinity of cages for counterions, the solvation enthalpy associated with the cationic cage, and the solvation enthalpy associated with the counterions. The cubic cage **3**, for example, has twice the positive charge of the tetrahedral cages **1**, and **2**. We would thus expect cage **3** to have stronger affinity for anions than cages **1** and **2**. While cages **1** and **2** both have the same charge, cage **1** contains pendent glycerol groups that assist its solvation in water – more hydrophobic anions are thus required to transport the cage into EtOAc. Cage **2** incorporates no such solubilising groups, thus enabling the cage to readily undergo anion exchange and phase transfer into EtOAc.

The results in this chapter demonstrate that three different coordination cages can be reversibly transported between immiscible liquid phases by exchanging their counterions. We expect this technology to be extensible to cages already reported in the literature,^{16–22} many of which are capable of size-selective guest encapsulation.^{23–26} Due to time restraints, we were unable to finish several experiments and analyses that would add value to the results discussed in this chapter. We are currently in the process of completing the sequential phase transfer experiments. Specifically, we will perform the sequential phase transfer of cages **1** and **2** and cages **2** and **3** again, adding [SO₄] after the phase transfer to EtOAc is complete to observe the sequential transfer of these cages from EtOAc back to water. We are also in the process of completing sequential phase transfer experiments with mixtures of cages containing molecular cargo. Furthermore, we are developing a mathematical model to thermodynamically describe the reversible phase transfer of cages by anion exchange. In addition to potentially serving a useful function^{27,28} – transporting guest molecules between separate physical compartments –^{29–32} phase transfer of cages *via* anion exchange also provides a window through which to compare the affinity of cages for their counterions. Furthermore, by exploiting both the solvent affinity and the anion affinity of cages with different guest-binding properties, we anticipate that cages with different guests may be directed into different physical compartments. Building upon this technology, we envisage that supramolecular capsules will contribute towards solving current separations problems.

4.4 Experimental

4.4.1 General

Reagents and solvents were purchased and used as supplied unless otherwise noted. D₂O and CH₃CN for cage syntheses were degassed by 3-4 evacuation/N₂ fill cycles prior to use. ¹H NMR spectra were recorded either at 500 MHz on a Bruker AVIII HD Smart Probe spectrometer or at 400 MHz on a Bruker Avance III HD Smart Probe spectrometer. ¹³C{¹H} NMR spectra were recorded at 125 MHz on a Bruker 500 MHz AVIII HD Smart Probe spectrometer, at 125 MHz on a Bruker 500 MHz DCH Cryoprobe spectrometer, or at 100 MHz on a Bruker 400 MHz Avance III HD Smart Probe spectrometer. ¹H chemical shifts (δ_{H}) are expressed in parts per million (ppm) and reported relative to the internal standard acetonitrile ($\delta_{\text{H}} = 2.06$ ppm) or *tert*-butanol ($\delta_{\text{H}} = 1.24$ ppm) in D₂O, or relative to the external standard dextran sulfate sodium salt (DSS) ($\delta_{\text{H}} = 0.00$ ppm) in a D₂O capillary. ¹³C chemical shifts (δ_{C}) are expressed in ppm and reported relative to the resonance of the carbons in CH₃CN ($\delta_{\text{C}} = 119.68$ ppm and 1.47 ppm), *tert*-butanol (70.36 ppm and 30.29 ppm), or tetrahydrofuran (THF) ($\delta_{\text{C}} = 68.68$ ppm and 25.67 ppm) in D₂O. All measurements were carried out at 298 K. Abbreviations used in the description of NMR data are as follows: bs, broad singlet; bm, broad multiplet; s, singlet; d, doublet; t, triplet. Coupling constants (*J*) are given in Hz. UV-Vis spectra were taken on an Agilent Technologies Cary Series UV-Vis-NIR spectrophotometer.

4.4.2 Self-assembly of cages 1, 2, and 3

In this section, the preparation and characterisation of cages **1**, **2**, and **3** are described. Because the ¹H NMR signals from cages **1**, **2**, and **3** shift slightly depending on whether the cages are 1) dissolved in D₂O in the absence of an EtOAc layer, 2) dissolved in D₂O in the presence of an EtOAc layer, or 3) dissolved in EtOAc, the characterisation data for all three cages in all three different environments are presented in this section. After taking the ¹H NMR, ¹³C NMR, and ¹H COSY of cage[SO₄] in D₂O, an equal volume of EtOAc was added to the sample. The sample was then inverted and allowed to settle before collecting the ¹H NMR and ¹H COSY of the water layer. Finally, a minimum amount of solid Li[BArF₅] was added to achieve complete transport of the cages from water to EtOAc. The water layer was removed, and the ¹H NMR and ¹H COSY spectra were collected of the remaining EtOAc layer.

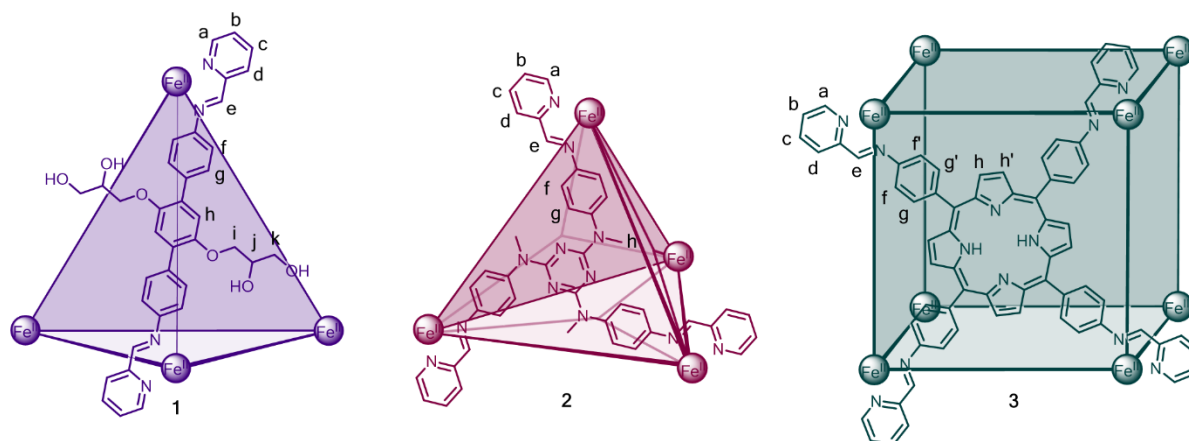


Figure 4.15 Cages 1, 2, and 3 with proton designations.

Cage 1[SO₄] in D₂O

This compound was synthesised according to a procedure previously described in the literature.⁴ In a glovebox, (2R,2'R)-3,3'-((4,4''-diamino-[1,1':4',1''-terphenyl]-2',5'-diyl)bis(oxy))bis(propane-1,2-diol) (prepared by Dr Jeanne Bolliger) (13.2 mg, 3.00 x 10⁻² mmol), 2-formylpyridine (6.43 μL, 6.00 x 10⁻² mmol), and iron (II) sulfate heptahydrate (5.56 mg, 2.00 x 10⁻² mmol) were combined with D₂O (5 mL). The resulting purple solution was stirred for 12 hours to give a 1 mM stock solution, which was used without further purification. ¹H NMR (500 MHz, D₂O, 298K, referenced to DSS): δ_H = 9.08 (bs, 12H, H_e), 8.64 (unresolved d, 12H, H_d), 8.46 (unresolved dd, 12H, H_c), 7.79 (unresolved dd, 12H, H_b), 7.50 (unresolved d, 12H, H_a), 7.27 (bs, 24H, H_g), 6.99 (bs, 12H, H_h), 5.67 (bs, 24H, H_f), 3.98 (bs, 24H, H_i), 3.85 (bs, 12H, H_j), 3.54 (bs, 24H, H_k); ¹³C{¹H} NMR (125 MHz, D₂O, 298K, referenced to THF): δ_C = 175.3, 159.2, 156.5, 150.3, 150.2, 140.7, 139.3, 131.8, 131.4, 131.0, 130.3, 122.2, 116.3, 71.0, 70.5, 63.7.

Chapter 4. Reversible Phase Transfer of Cages by Anion Exchange

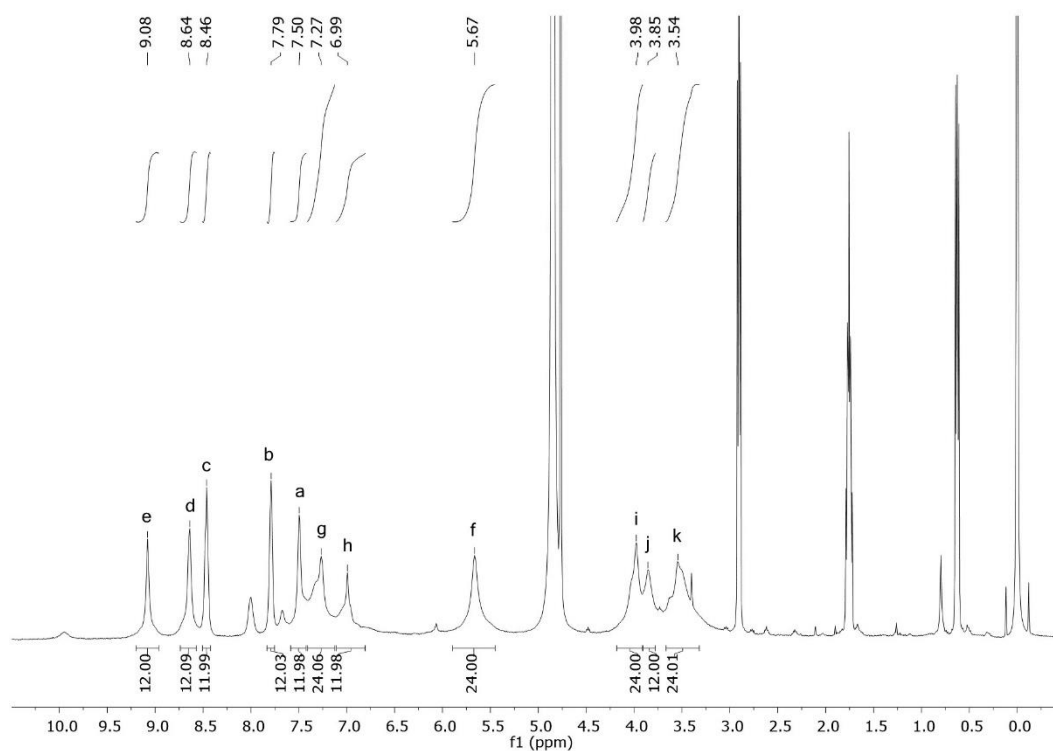


Figure 4.16 ^1H NMR (500 MHz, D_2O , 298 K, referenced to DSS) of $\mathbf{1}[\text{SO}_4]$.

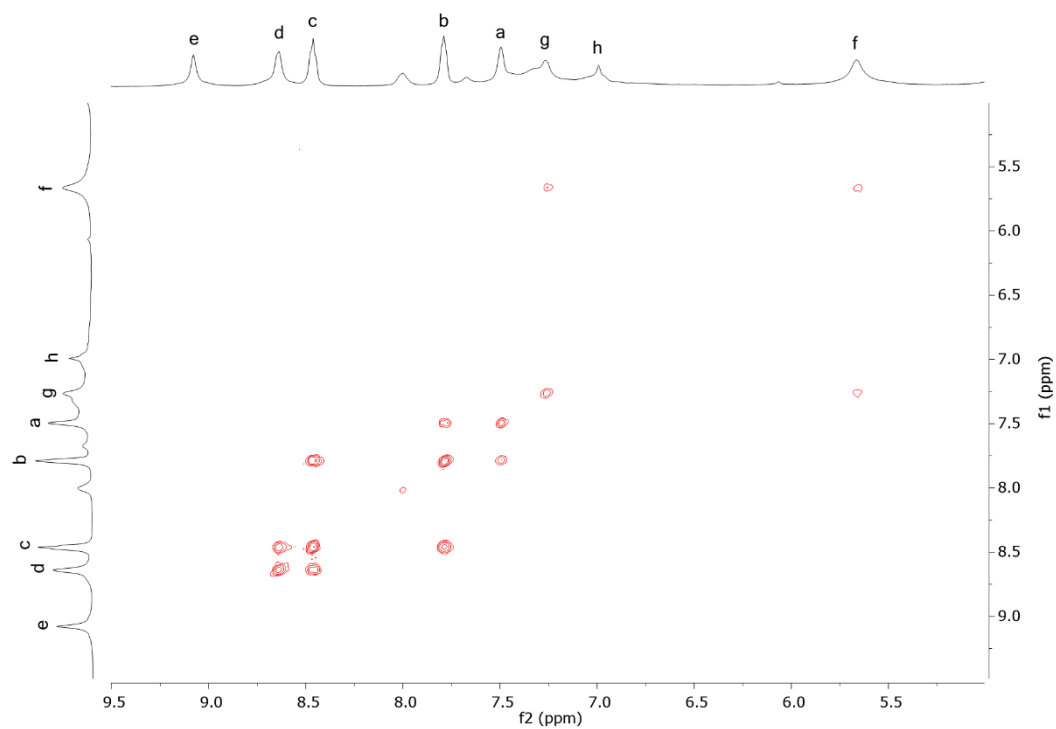


Figure 4.17 ^1H COSY (500 MHz, D_2O , 298 K, referenced to DSS) of $\mathbf{1}[\text{SO}_4]$.

Cage 1[SO₄] in D₂O, with EtOAc layer

¹H NMR (500 MHz, D₂O, 298K, referenced to DSS): $\delta_{\text{H}} = 9.14$ (bs, 12H, H_e), 8.70 (unresolved d, 12H, H_d), 8.51 (unresolved dd, 12H, H_c), 7.84 (unresolved dd, 12H, H_b), 7.53 (unresolved d, 12H, H_a), 7.28 (bs, 24H, H_g), 7.00 (bs, 12H, H_h), 5.68 (bs, 24H, H_f). ¹H NMR peaks corresponding to H_i, H_j, and H_k are obscured by large signals from EtOAc.

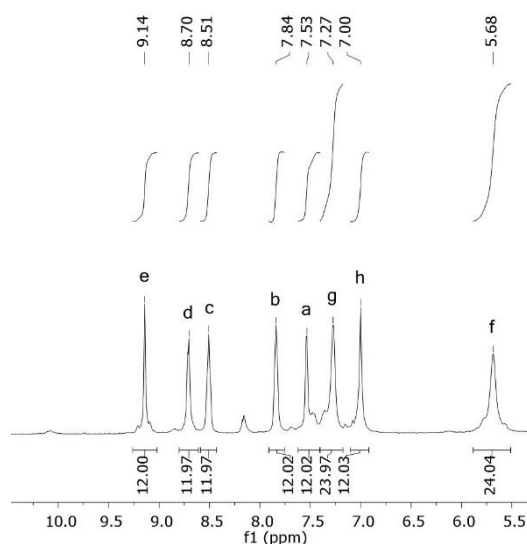


Figure 4.18 ¹H NMR (500 MHz, D₂O, 298 K, referenced to DSS) of **1**[SO₄], in the presence of an EtOAc layer.

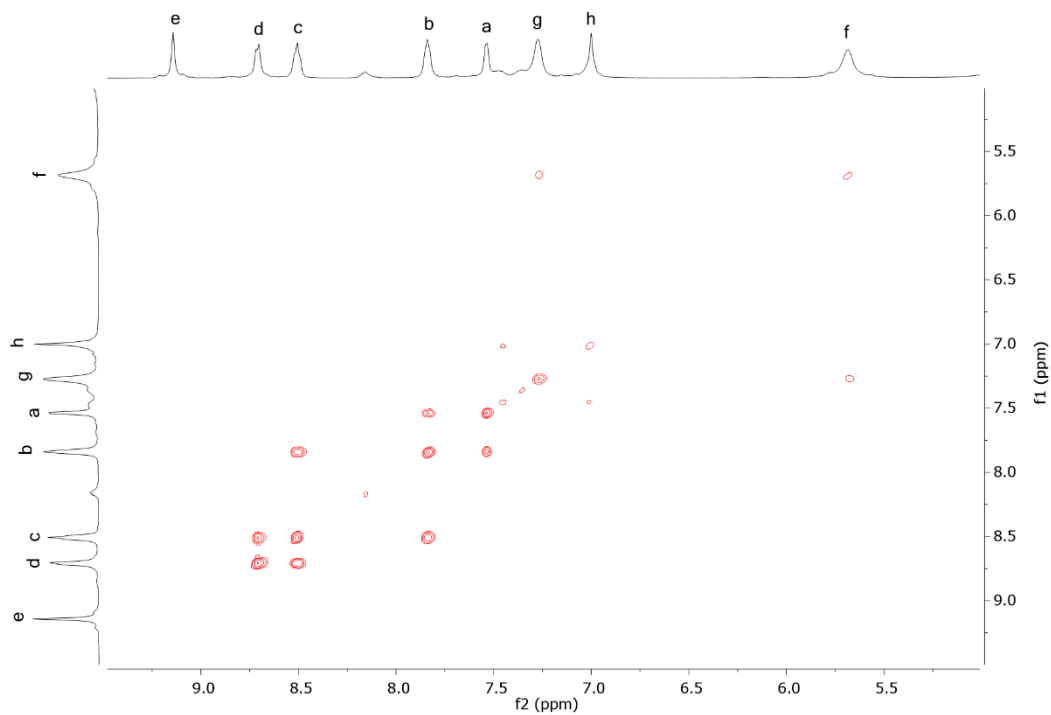


Figure 4.19 ¹H COSY (500 MHz, D₂O, 298 K, referenced to DSS) of **1**[SO₄], in the presence of an EtOAc layer.

Cage 1[BArF₅] in EtOAc

¹H NMR (500 MHz, EtOAc, 298 K, locked to a D₂O capillary, referenced to DSS): δ_H = 9.93 (s, 12H, H_e), 9.39 (d, *J* = 7.2 Hz, 12H, H_d), 9.07 (t, *J* = 7.5 Hz, 12H, H_c), 8.43 (t, *J* = 5.9 Hz, 12H, H_b), 8.21 (d, *J* = 4.1 Hz, 12H, H_a), 7.89 (d, *J* = 6.9 Hz, 24H, H_g), 7.58 (s, 12H, H_h), 6.29 (d, *J* = 6.1 Hz, 24H, H_f). ¹H NMR peaks corresponding to H_i, H_j, and H_k are obscured by large signals from EtOAc.

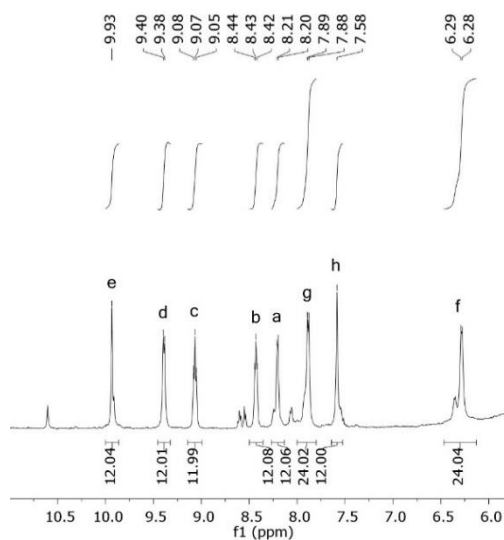


Figure 4.20 ¹H NMR (500 MHz, EtOAc, 298 K, locked to a D₂O capillary, referenced to DSS) of **1**[BArF₅].

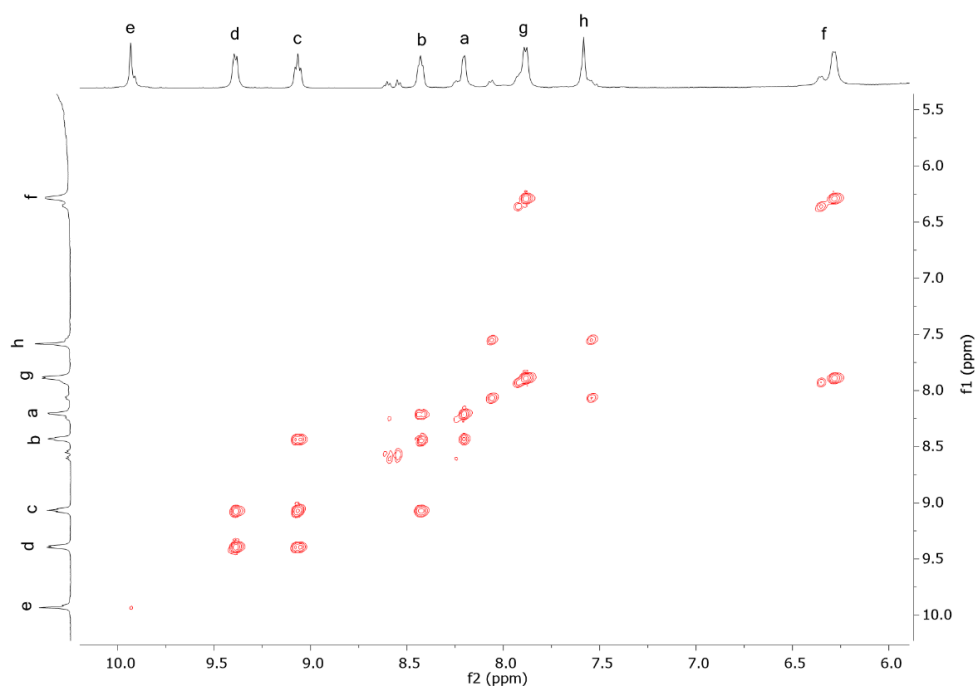


Figure 4.21 ¹H COSY (500 MHz, EtOAc, 298 K, locked to a D₂O capillary, referenced to DSS) of **1**[BArF₅].

Cage 2[SO₄] in D₂O

This compound was synthesised by modifying a procedure previously described in the literature.³ In a glovebox, N₂,N₄,N₆-tris(4-aminophenyl)-N₂,N₄,N₆-trimethyl-1,3,5-triazine-2,4,6-triamine (35.3 mg, 8.00×10^{-2} mmol), 2-formylpyridine (22.8 μ L, 24.0×10^{-2} mmol), and iron (II) sulfate heptahydrate (22.2 mg, 8.00×10^{-2} mmol) were combined with acetonitrile (5 mL) and D₂O (5 mL). The resulting purple solution was stirred for 12 hours; the acetonitrile was then removed, and the total volume of the solution was adjusted to 10 mL with D₂O to give a 2 mM stock solution, which was used without further purification. Note that complete removal of solvent will cause partial decomposition of the cage. ¹H NMR (500 MHz, D₂O, 298 K, referenced to acetonitrile): $\delta_{\text{H}} = 9.02$ (s, 12H, H_e), 8.61 (d, $J = 7.8$ Hz, 12H, H_d), 8.43 (t, $J = 7.8$ Hz, 12H, H_c), 7.76 (t, $J = 6.7$ Hz, 12H, H_b), 7.47 (d, $J = 5.6$ Hz, 12H, H_a), 7.44 (bs, 24H, H_g), 5.26 (bs, H_f), 3.47 and 3.46 (s, 36H, H_h from **1**[SO₄] and H_h from 2-formylpyridine \subset **1**[SO₄]). ¹³C{¹H} NMR (125 MHz, D₂O, 298 K, referenced to acetonitrile): $\delta_{\text{C}} = 175.8, 165.3, 159.1, 156.7, 151.0$ (encapsulated 2-formylpyridine), 147.2, 144.7, 140.7, 139.8 (encapsulated 2-formylpyridine), 131.9, 130.4, 126.2, 122.2, 38.6.

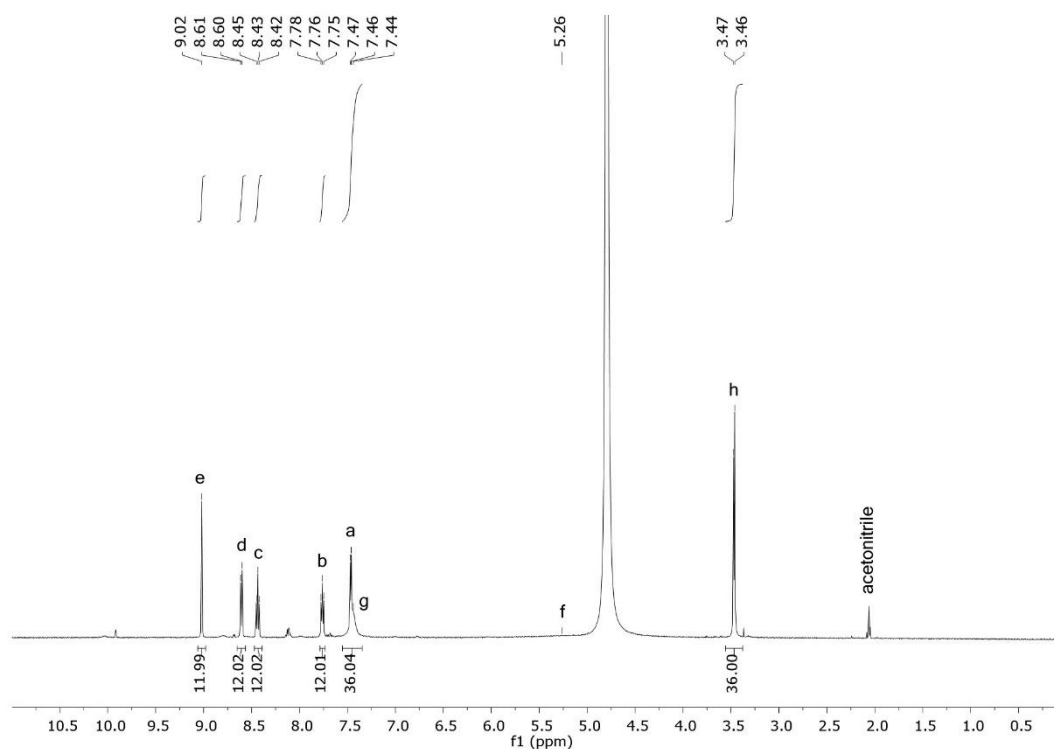


Figure 4.22 ¹H NMR (500 MHz, D₂O, 298 K, referenced to acetonitrile) of **2**[SO₄].

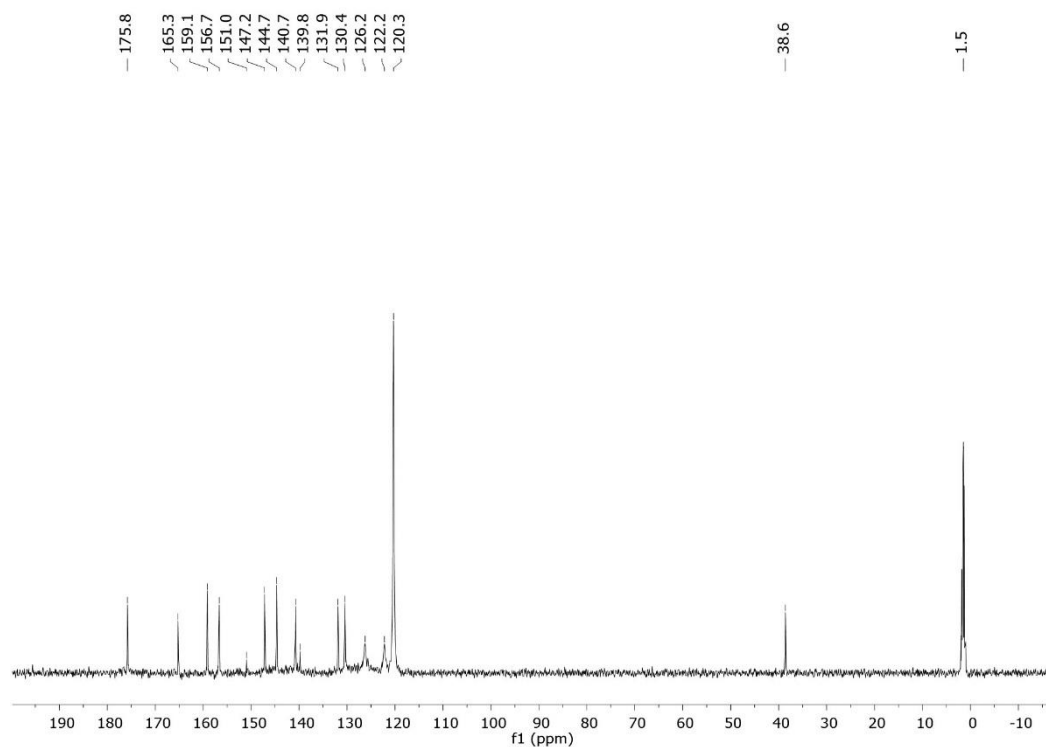


Figure 4.23 $^{13}\text{C}\{^1\text{H}\}$ NMR (125 MHz, D_2O , 298 K, referenced to acetonitrile) of $2[\text{SO}_4]$.

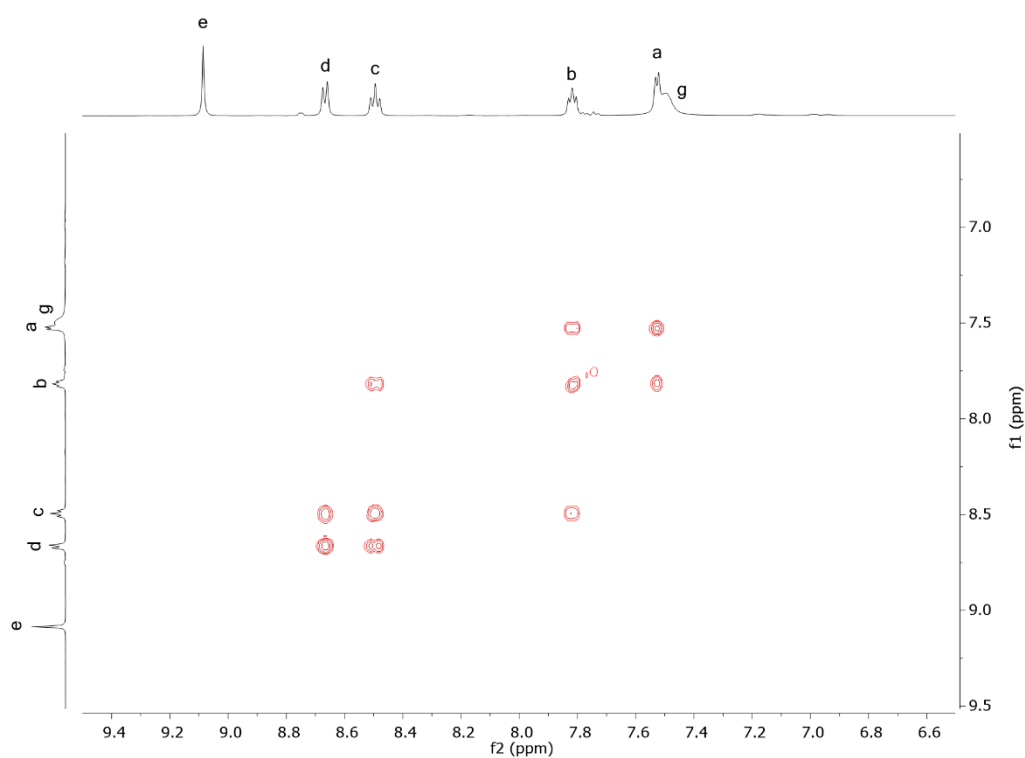


Figure 4.24 ^1H COSY (500 MHz, D_2O , 298 K, referenced to DSS) of $2[\text{SO}_4]$.

Cage 2[SO₄] in D₂O, with EtOAc layer

¹H NMR (500 MHz, D₂O, 298K, referenced to DSS): $\delta_{\text{H}} = 9.12$ (s, 12H, H_e), 8.72 (d, $J = 7.7$ Hz, 12H, H_d), 8.54 (t, $J = 7.8$ Hz, 12H, H_c), 7.87 (t, $J = 7.7$ Hz, 12H, H_b), 7.58 (d, $J = 5.4$ Hz, 12H, H_a), 7.54 (bs, 24H, H_g), 5.65 (bs, H_f), 3.54 (s, 36H, H_h).

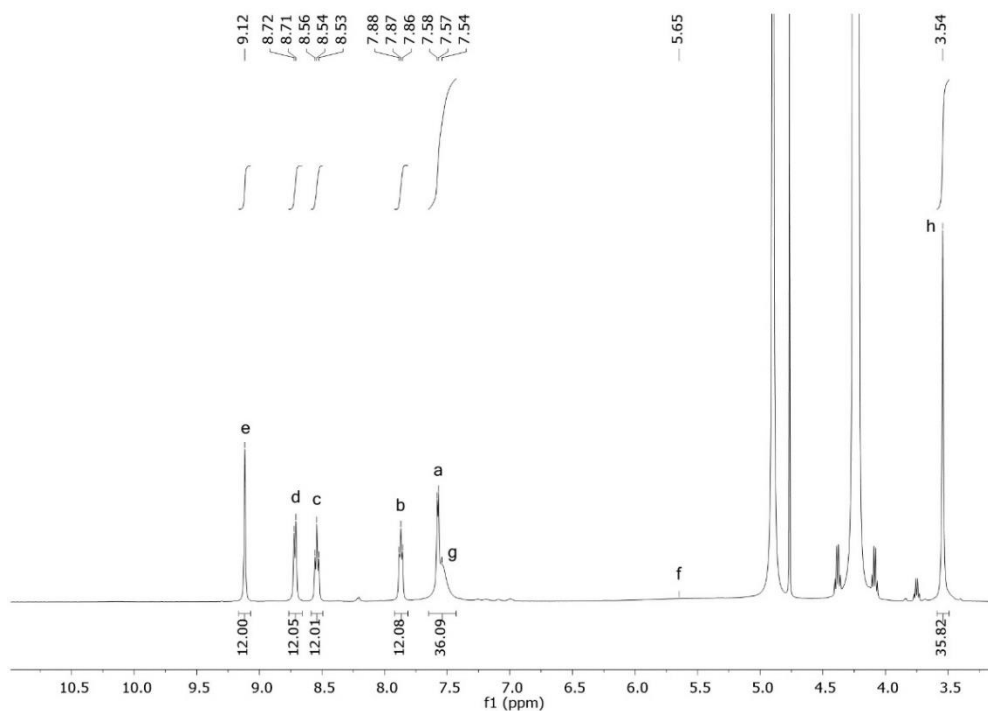


Figure 4.25 ¹H NMR (500 MHz, D₂O, 298 K, referenced to DSS) of 2[SO₄], in the presence of an EtOAc layer.

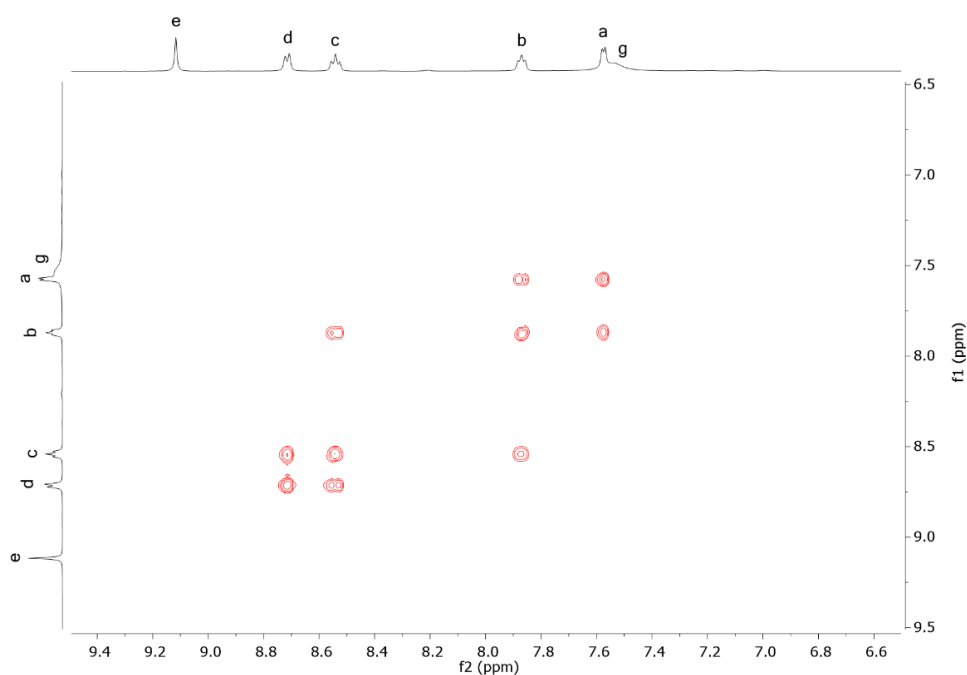


Figure 4.26 ¹H COSY (500 MHz, D₂O, 298 K, referenced to DSS) of 2[SO₄], in the presence of an EtOAc layer.

Cage 2[BArF₅] in EtOAc

¹H NMR (500 MHz, EtOAc, 298K, locked to a D₂O capillary, referenced to DSS): δ_H = 9.67 (s, 12H, H_e), 9.22 (unresolved d, 12H, H_d), 9.10 (unresolved t, 12H, H_c), 8.48 (unresolved t, 12H, H_b), 8.20 (unresolved d, 12H, H_a), 8.07 (bs, 24H, H_g), 5.84 (bs, H_f). The ¹H NMR peak corresponding to H_h is obscured by large signals from EtOAc.

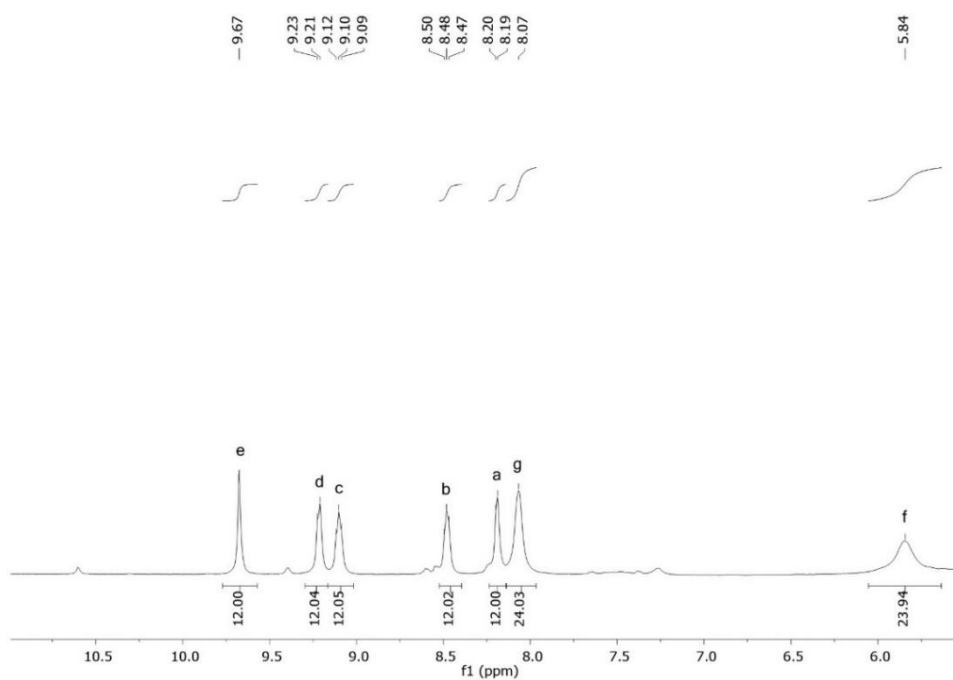


Figure 4.27 ¹H NMR (500 MHz, EtOAc, 298 K, locked to a D₂O capillary, referenced to DSS) of **2**[BArF₅].

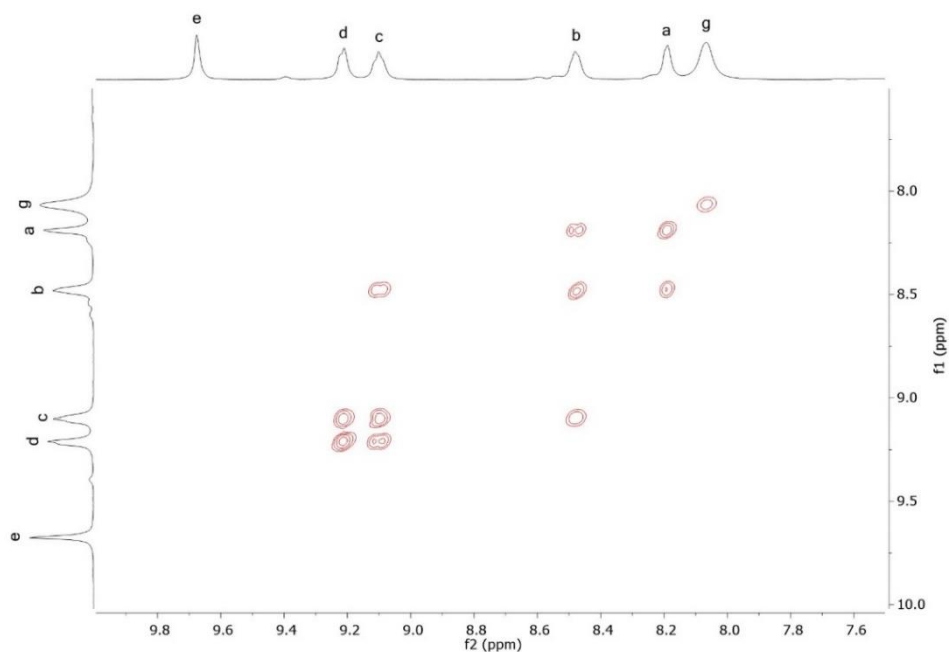


Figure 4.28 ¹H COSY (500 MHz, EtOAc, 298 K, locked to a D₂O capillary, referenced to DSS) of **2**[BArF₅].

Cage 3[SO₄] in D₂O

This compound was prepared by Dr Edmundo Guzman-Percastegui by modifying a procedure previously described in the literature.⁶ In a Schlenk flask, 5,10,15,20-tetrakis(4-aminophenyl)-21H, 23H-porphine (35.0 mg, 0.05 mmol, 6 equiv), 2-formylpyridine (19.5 μ L, 0.20 mmol, 24 equiv), and iron (II) triflate (25.0 mg, 0.07 mmol, 8 equiv) were combined with anhydrous DMF (1.5 mL). The mixture was degassed by three evacuation/nitrogen fill cycles and heated at 70°C overnight. The crude material was purified by precipitation with diethyl ether yielding **3**[OTf] as a purple solid. The NMR and ESI-MS data fully correspond to those previously obtained. Then, **3**[OTf] was dissolved in CH₃CN (1.5 mL) and tetrabutylammonium sulfate solution 50wt% in H₂O (1.5 equivalents relative to cage) was added, the mixture was centrifuged, and the precipitate was washed thoroughly with CH₃CN:H₂O (9:1). Note that the pH of the tetrabutylammonium sulfate solution must be near neutral for successful conversion of cage **3**[OTf] to **3**[SO₄]. Cage **3**[SO₄] was obtained as a dark red solid, and the product was dissolved in D₂O to give a 1 mM stock solution. ¹H NMR (400 MHz, D₂O, 298 K, referenced to *tert*-butanol): $\delta_{\text{H}} = 9.78$ (bs, 24H, H_e), 9.52 – 9.38 (bm, 48H, H_h/H_{h'}), 8.86 (bs, 24H, H_d), 8.53 (bs, 24H, bs, H_c), 8.27 (bs, 24H, H_{g'}), 7.90 (bs, 24H, H_b), 7.75 (bs, 48H, H_a/H_g), 6.50 (bs, 24H, H_f), 5.95 (bs, 24H, H_f). ¹³C{¹H} NMR (125 MHz, D₂O, referenced to *tert*-butanol): $\delta_{\text{C}} = 176.6, 159.2, 156.6, 150.9, 142.1, 140.6, 136.1, 131.9, 130.4, 125.6, 121.1, 120.7, 119.4$.

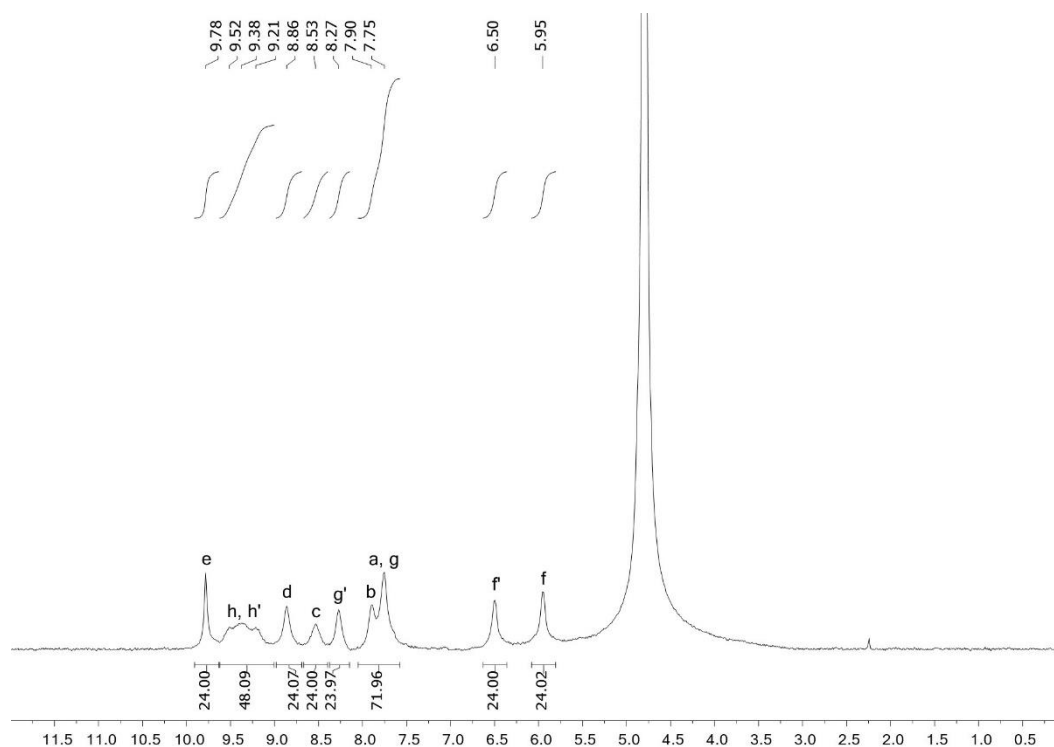


Figure 4.29 ¹H NMR (500 MHz, D₂O, 298 K, referenced to *tert*-butanol) of **3**[SO₄].

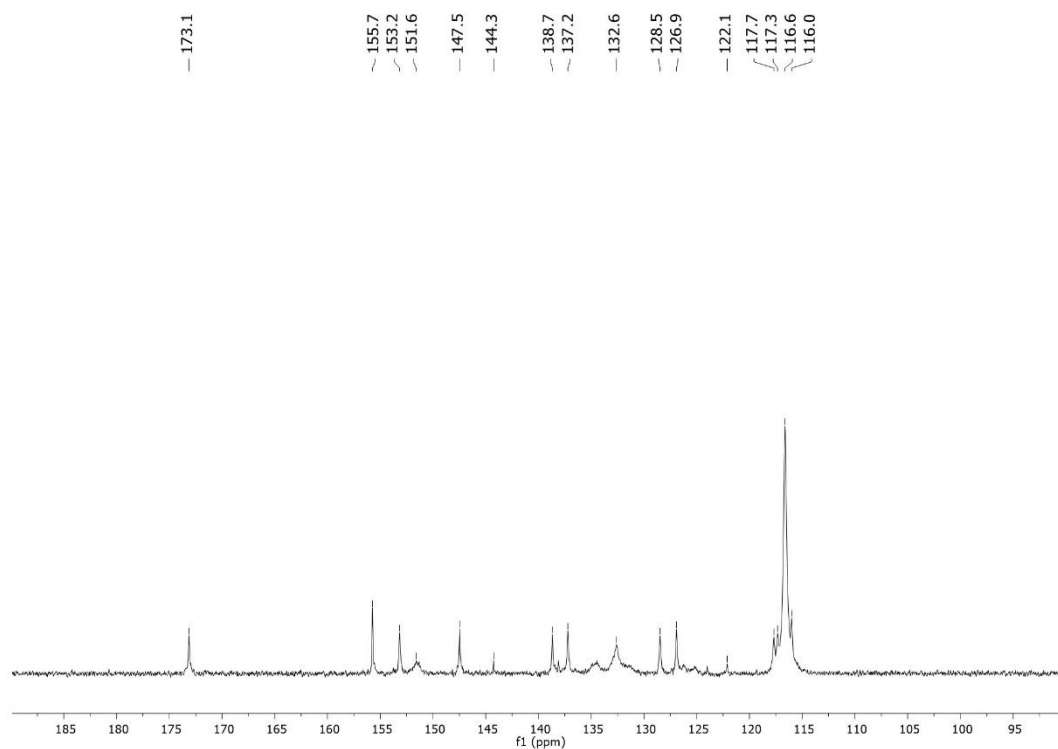


Figure 4.30 $^{13}\text{C}\{^1\text{H}\}$ NMR (125 MHz, D_2O , 298 K, referenced to *tert*-butanol) of $3[\text{SO}_4]$.

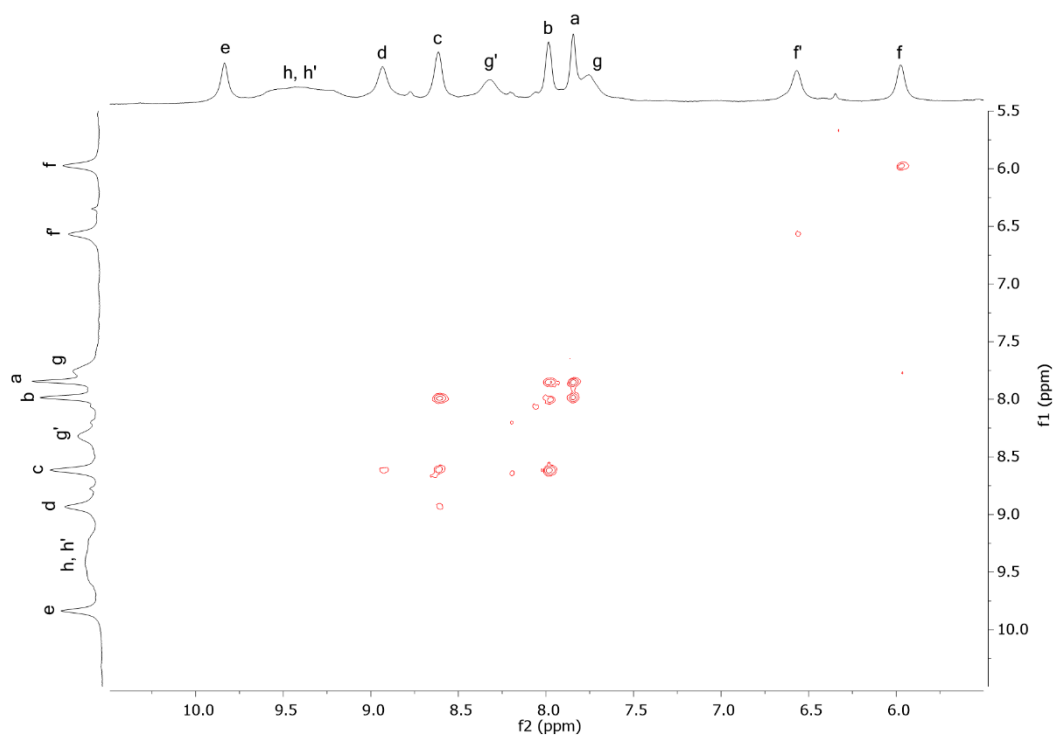


Figure 4.31 ^1H COSY (500 MHz, D_2O , 298 K, referenced to *tert*-butanol) of $3[\text{SO}_4]$.

Cage 3[SO₄] in D₂O, with EtOAc layer

¹H NMR (500 MHz, D₂O, 298K, referenced to DSS): $\delta_{\text{H}} = 9.87$ (bs, 24H, H_e), 9.49 – 9.30 (bm, 48H, H_h/H_{h'}), 9.00 (bs, 24H, H_d), 8.67 (bs, 24H, H_c), 8.30 (bs, 24H, H_{g'}), 8.05 (bs, 24H, H_b), 7.88 (bs, 24H, H_a), 7.74 (bs, 24H, H_g), 6.59 (bs, 24H, H_f), 6.02 (bs, 24H, H_f).

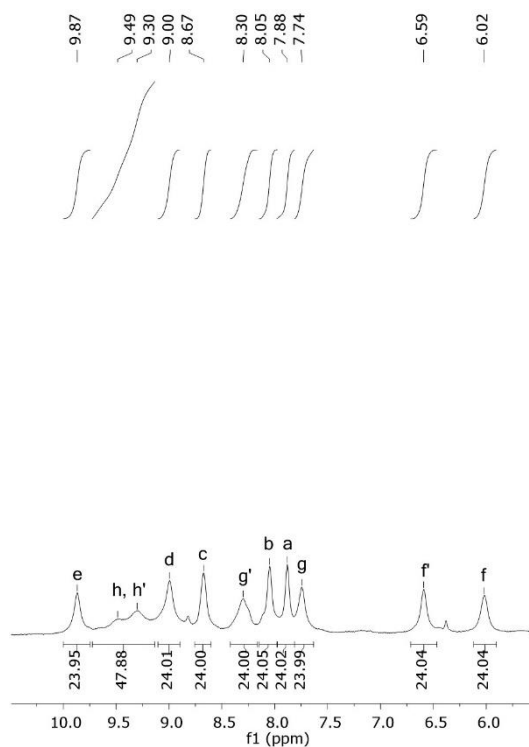


Figure 4.32 ¹H NMR (500 MHz, D₂O, 298 K, referenced to DSS) of **3**[SO₄], in the presence of an EtOAc layer.

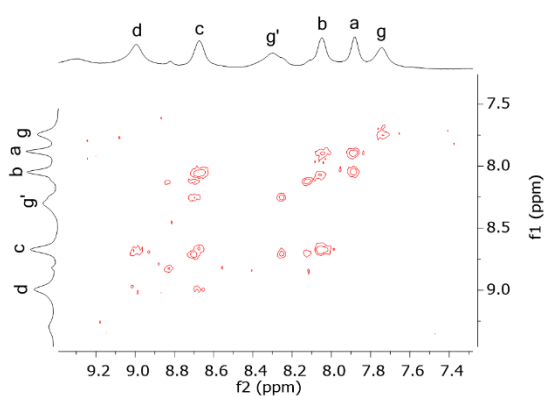


Figure 4.33 ¹H COSY (500 MHz, D₂O, 298 K, referenced to DSS) of **3**[SO₄], in the presence of an EtOAc layer.

Cage 3[BARF₅] in EtOAc

¹H NMR (500 MHz, EtOAc, 298K, locked to a D₂O capillary, referenced to DSS): δ_H = 10.33 (bs, 24H, H_e), 9.94 – 9.77 (bm, 48H, H_h/H_{h'}), 9.45 (bs, 24H, H_d), 9.23 (bs, 24H, H_c), 8.80 (bs, 24H, H_{g'}), 8.71 (bs, 24H, H_b), 8.52 (bs, 24H, H_a), 8.32 (bs, 24H, H_g), 7.10 (bs, 24H, H_f), 6.62 (bs, 24H, H_f).

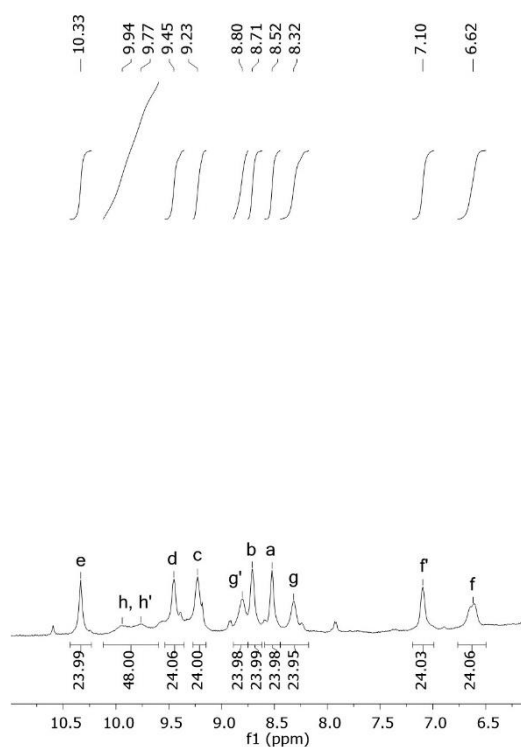


Figure 4.34 ¹H NMR (500 MHz, EtOAc, 298 K, locked to a D₂O capillary, referenced to DSS) of 3[BARF₅].

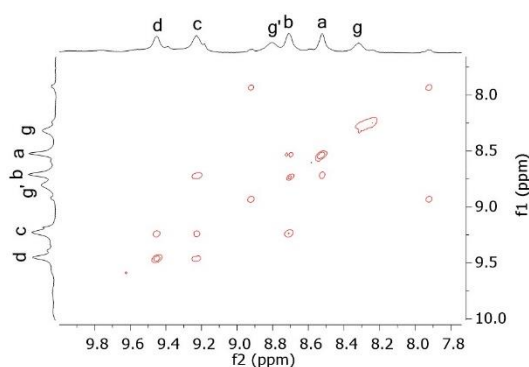


Figure 4.35 ¹H COSY (500 MHz, EtOAc, 298 K, locked to a D₂O capillary, referenced to DSS) of 3[BARF₅].

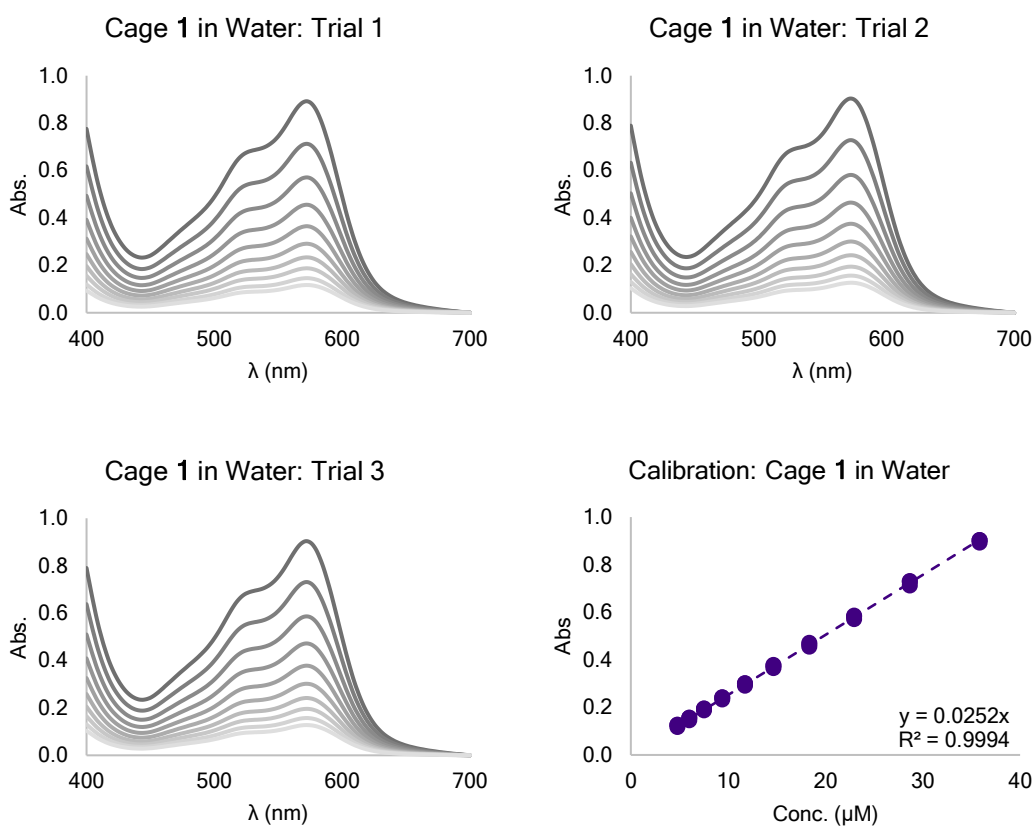
4.4.3 UV-Vis calibration data

General procedure

To prepare the calibration curves for cages **1**[SO₄], **2**[SO₄], or **3**[SO₄] in water, a stock solution was prepared in a 5 mL volumetric flask. The stock solution was diluted by 4/5, and the UV-Vis spectrum was recorded after each dilution (Sections S5.2, S5.4, and S5.6). Because solvent effects may have a small effect on the absorbance of the cages, the calibration curves for cages **1**[BArF₅], **2**[BArF₅], and **3**[BArF₅] in EtOAc were also recorded. To a biphasic system of EtOAc (2 mL) and cage **1**[SO₄], **2**[SO₄], or **3**[SO₄] in water (2 mL), a minimum amount of [Li][BArF₅] was added to achieve complete phase transfer of the cages into EtOAc. The EtOAc layer was then removed into a 5 mL volumetric flask, and the water layer was washed with EtOAc (3 x 0.75 mL). The EtOAc washes were combined with the initial EtOAc layer, and the volume of the solution was adjusted to 5 mL with EtOAc. This stock solution was diluted by 4/5, and the UV-Vis spectrum was recorded after each dilution (Sections S5.3, S5.5, and S5.7). We assumed that the phase transfer of cage **1**, **2**, or **3** from water to EtOAc was quantitative and that there was no significant decomposition of the cage in EtOAc.

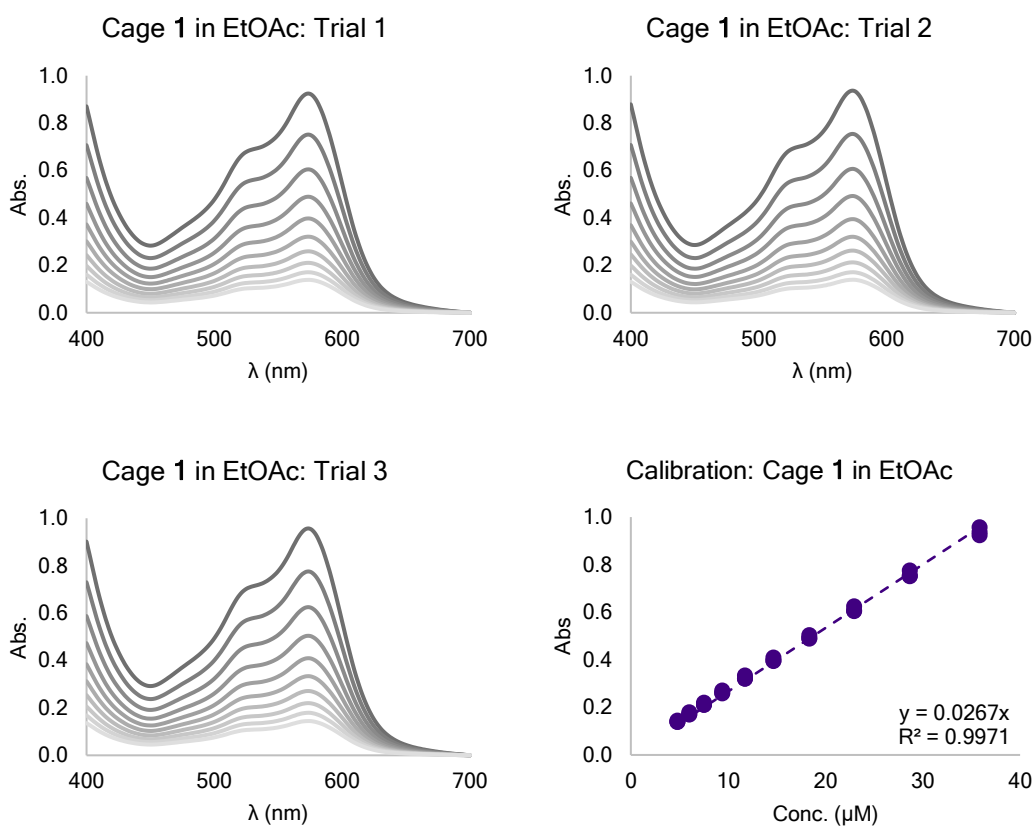
Calibration of cage **1** in water**Table 4.3** Summary of calibration data for cage **1** in water

Conc (μM):	Abs at λ_{572} (1):	Abs at λ_{572} (2):	Abs at λ_{572} (3):
35.8	0.892	0.904	0.903
28.7	0.713	0.728	0.731
22.9	0.571	0.581	0.586
18.4	0.456	0.465	0.472
14.7	0.365	0.375	0.378
11.7	0.291	0.301	0.302
9.40	0.234	0.243	0.242
7.52	0.188	0.194	0.196
6.01	0.146	0.157	0.157
4.81	0.117	0.127	0.128

**Figure 4.36** Raw UV-Vis data and calibration curve for cage **1** in water. $y = 0.0252x$

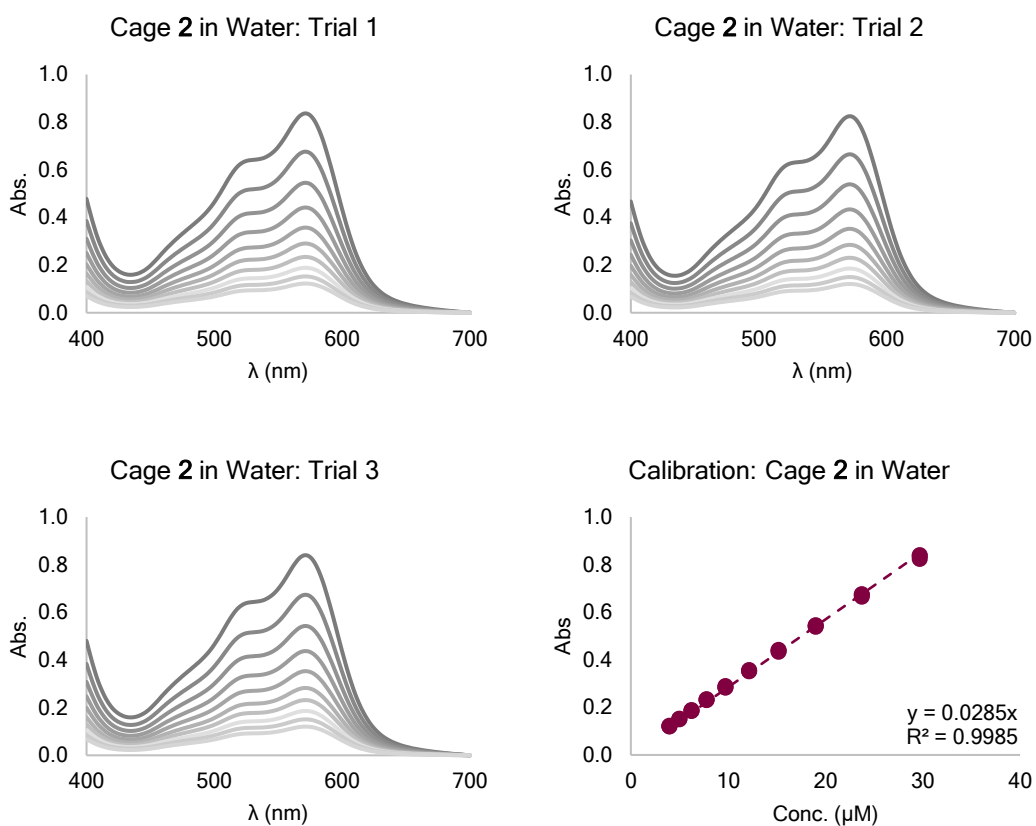
Calibration of cage **1** in EtOAc**Table 4.4** Summary of calibration data for cage **1** in EtOAc

Conc (μM):	Abs at λ_{574} (1):	Abs at λ_{574} (2):	Abs at λ_{574} (3):
35.8	0.924	0.937	0.957
28.7	0.751	0.754	0.776
22.9	0.605	0.607	0.625
18.4	0.489	0.492	0.504
14.7	0.398	0.395	0.410
11.7	0.321	0.321	0.334
9.40	0.259	0.262	0.271
7.52	0.210	0.212	0.220
6.01	0.171	0.171	0.180
4.81	0.139	0.139	0.145

**Figure 3.37** Raw UV-Vis data and calibration curve for cage **1** in EtOAc. $y = 0.0267x$

*Calibration of cage 2 in water***Table 4.5** Summary of calibration data for cage 2 in water

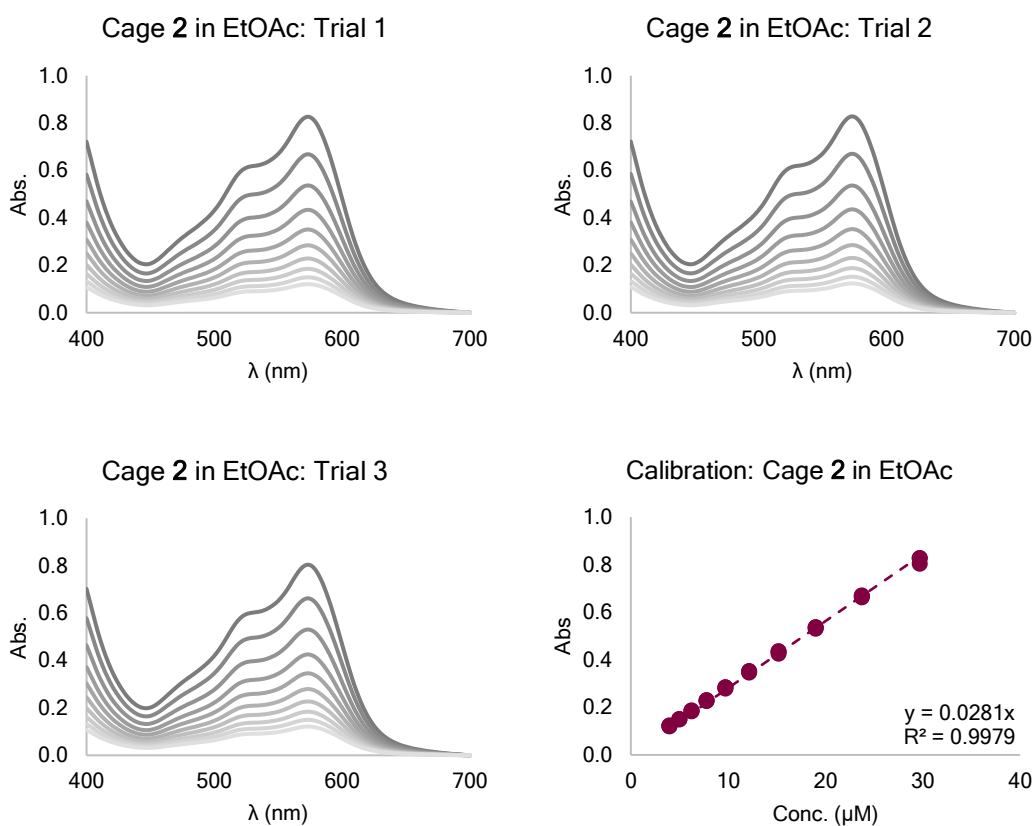
Conc (μM):	Abs at λ_{571} (1):	Abs at λ_{571} (2):	Abs at λ_{571} (3):
29.7	0.837	0.825	0.840
23.8	0.676	0.665	0.674
19.0	0.545	0.539	0.543
15.2	0.442	0.434	0.437
12.2	0.357	0.352	0.353
9.73	0.291	0.285	0.283
7.78	0.234	0.231	0.232
6.23	0.189	0.185	0.186
4.98	0.152	0.150	0.151
3.99	0.122	0.121	0.120

**Figure 4.38** Raw UV-Vis data and calibration curve for cage 2 in water. $y = 0.0285x$

Calibration of cage 2 in EtOAc

Table 4.6 Summary of calibration data for cage 2 in EtOAc

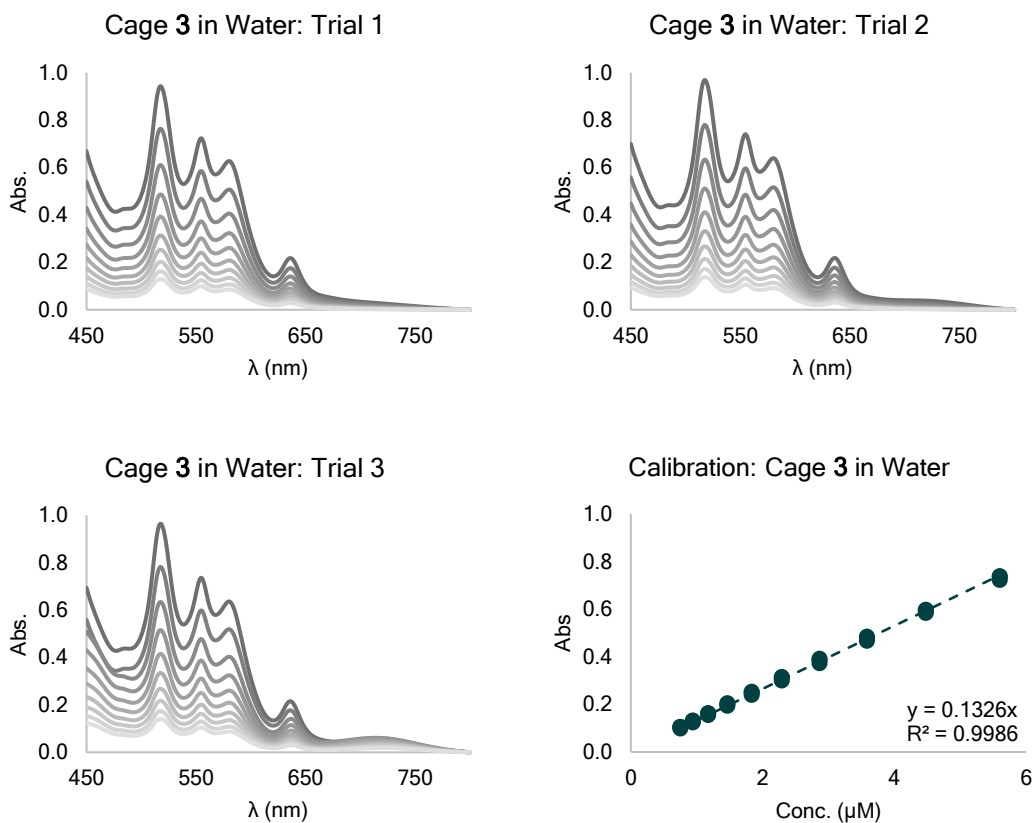
Conc (μM):	Abs at λ_{573} (1):	Abs at λ_{573} (2):	Abs at λ_{573} (3):
29.7	0.827	0.828	0.804
23.8	0.668	0.671	0.662
19.0	0.537	0.537	0.531
15.2	0.434	0.436	0.426
12.2	0.351	0.353	0.346
9.73	0.284	0.285	0.280
7.78	0.229	0.231	0.227
6.23	0.185	0.188	0.184
4.98	0.149	0.152	0.150
3.99	0.121	0.124	0.122

Figure 4.39 Raw UV-Vis data and calibration curve for cage 2 in EtOAc. $y = 0.0281x$

Calibration of cage 3 in water

Table 4.7 Summary of calibration data for cage 3 in water

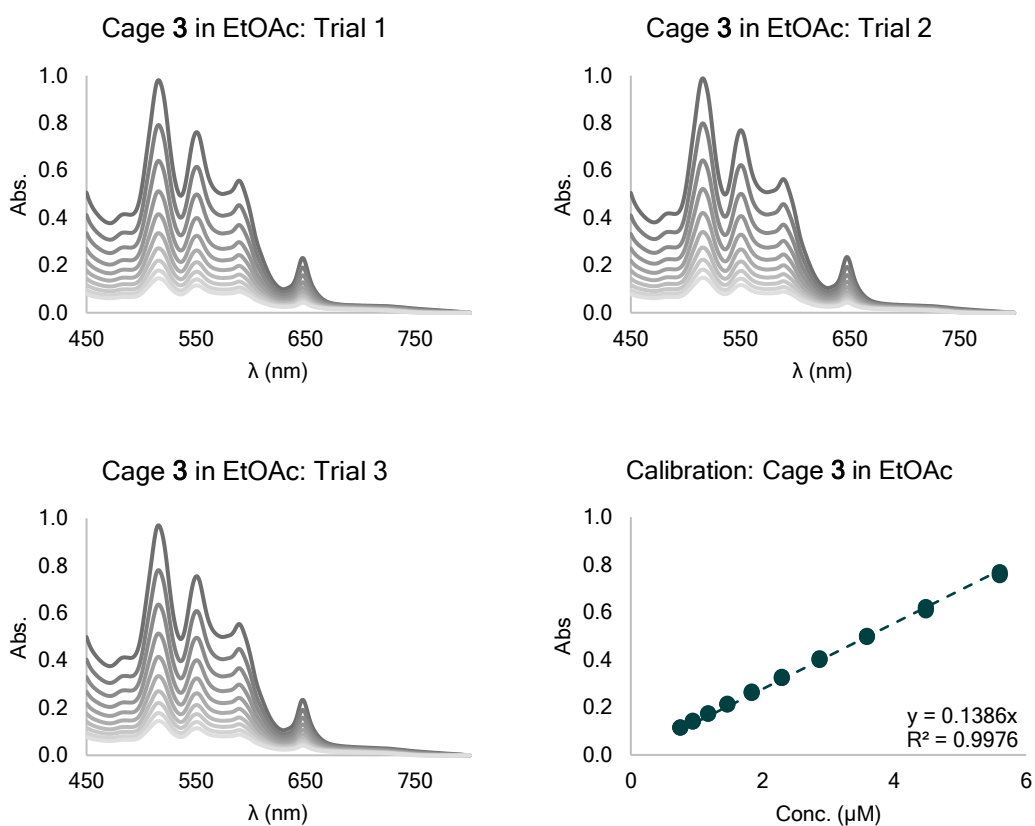
Conc (μM):	Abs at λ_{555} (1):	Abs at λ_{555} (2):	Abs at λ_{555} (3):
5.60	0.723	0.740	0.736
4.48	0.585	0.596	0.598
3.58	0.468	0.485	0.479
2.87	0.373	0.392	0.387
2.29	0.301	0.315	0.311
1.84	0.240	0.254	0.250
1.468	0.194	0.205	0.201
1.174	0.155	0.164	0.162
0.940	0.124	0.132	0.130
0.752	0.099	0.105	0.105

Figure 4.40 Raw UV-Vis data and calibration curve for cage 3 in water. $y = 0.133x$

Calibration of cage 3 in EtOAc

Table 4.8 Summary of calibration data for cage 3 in EtOAc

Conc (μM):	Abs at λ_{551} (1):	Abs at λ_{551} (2):	Abs at λ_{551} (3):
5.60	0.761	0.769	0.755
4.48	0.615	0.622	0.608
3.58	0.499	0.501	0.496
2.87	0.399	0.407	0.401
2.29	0.324	0.329	0.324
1.84	0.263	0.267	0.261
1.468	0.213	0.216	0.212
1.174	0.173	0.176	0.174
0.940	0.14	0.144	0.14
0.752	0.115	0.117	0.115

Figure 4.41 Raw UV-Vis data and calibration curve for cage 3 in EtOAc. $y = 0.139x$

4.4.4 Stability of cages 1, 2, and 3 by UV-Vis

*Stability of cage 1***Table 4.9** Summary of UV-Vis data for stability of **1**[SO₄] in water

Time (min):	Abs at λ_{572} :	Conc (μM):	Cage Proportion (%):
0	0.777	30.8	100
5	0.770	30.6	99.1
10	0.765	30.3	98.4
15	0.761	30.2	97.8
20	0.757	30.1	97.4
25	0.755	29.9	97.1
30	0.752	29.9	96.8
35	0.751	29.8	96.6
40	0.749	29.7	96.3
45	0.747	29.7	96.1
50	0.746	29.6	95.9
55	0.745	29.5	95.8
60	0.743	29.5	95.6

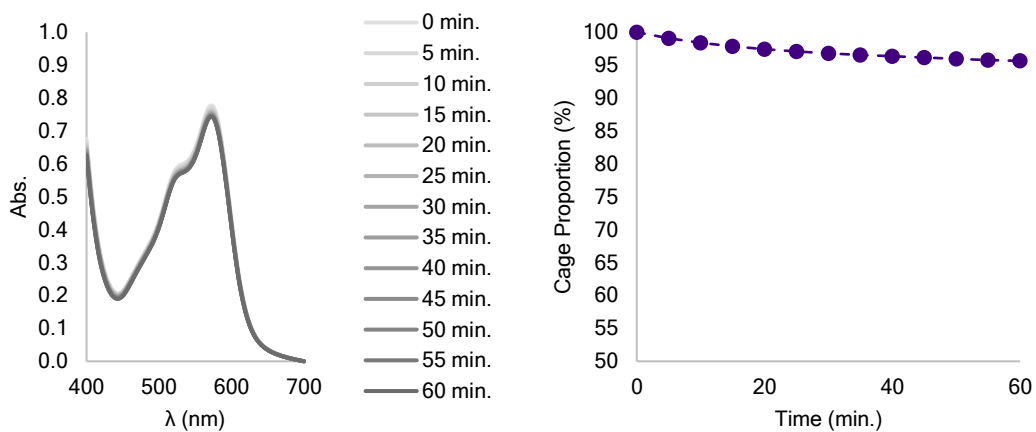
**Figure 4.42** Stability of cage **1**[SO₄] in water over 60 minutes.

Table 4.10 Summary of UV-Vis data for stability of **1**[BAr(CF₃)₂] in EtOAc

Time (min):	Abs at λ_{574} :	Conc (μM):	Cage Proportion (%):
0	0.403	15.1	100
5	0.402	15.0	99.7
10	0.402	15.0	99.7
15	0.401	15.0	99.6
20	0.401	15.0	99.5
25	0.401	15.0	99.5
30	0.400	15.0	99.4
35	0.400	15.0	99.3
40	0.400	15.0	99.3
45	0.400	15.0	99.2
50	0.399	15.0	99.2
55	0.399	14.9	99.1
60	0.399	14.9	99.0

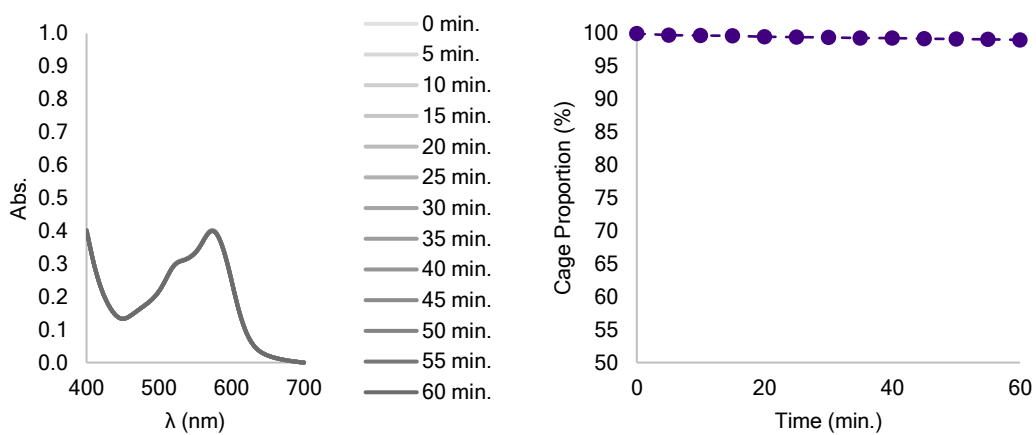
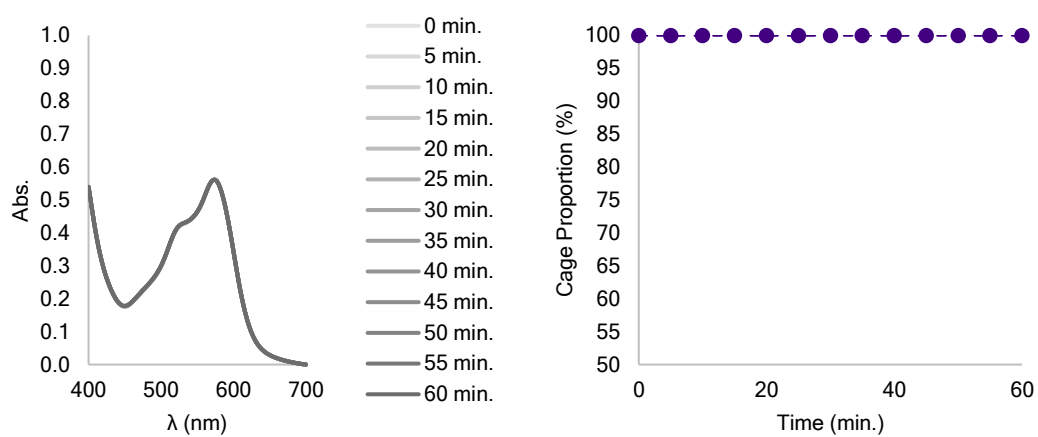
**Figure 4.43** Stability of cage **1**[BAr(CF₃)₂] in EtOAc over 60 minutes.

Table 4.11 Summary of UV-Vis data for stability of **1**[BArF₅] in EtOAc

Time (min):	Abs at λ_{574} :	Conc (μM):	Cage Proportion (%):
0	0.559	20.9	100
5	0.560	21.0	100
10	0.560	21.0	100
15	0.560	21.0	100
20	0.561	21.0	100
25	0.561	21.0	100
30	0.561	21.0	100
35	0.561	21.0	100
40	0.561	21.0	100
45	0.561	21.0	100
50	0.561	21.0	100
55	0.561	21.0	100
60	0.561	21.0	100

**Figure 4.44** Stability of cage **1**[BArF₅] in EtOAc over 60 minutes.

Stability of cage 2

Table 4.12 Summary of UV-Vis data for stability of 2[SO₄] in water

Time (min):	Abs at λ_{571} :	Conc (μM):	Cage Proportion (%):
0	0.497	17.4	100
5	0.496	17.4	99.8
10	0.496	17.4	99.8
15	0.495	17.4	99.6
20	0.495	17.4	99.6
25	0.494	17.3	99.4
30	0.493	17.3	99.2
35	0.493	17.3	99.2
40	0.492	17.3	99.0
45	0.492	17.3	99.0
50	0.492	17.3	99.0
55	0.491	17.2	98.8
60	0.491	17.2	98.8

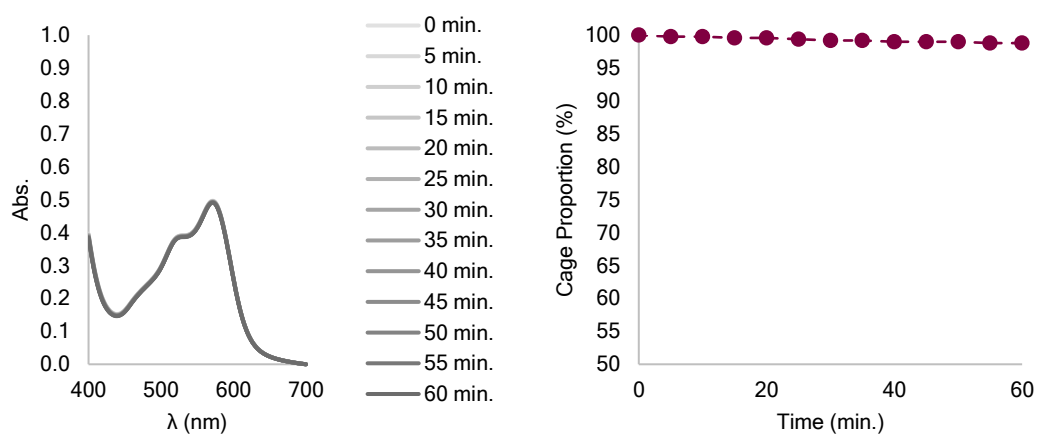
Figure 4.45 Stability of cage 2[SO₄] in water over 60 minutes.

Table 4.13 Summary of UV-Vis data for stability of **2**[BAr(CF₃)₂] in EtOAc

Time (min):	Abs at λ_{573} :	Conc (μM):	Cage Proportion (%):
0	0.369	13.1	100
5	0.351	12.5	95.1
10	0.329	11.7	89.2
15	0.309	11.0	83.7
20	0.291	10.4	78.9
25	0.275	9.79	74.5
30	0.260	9.25	70.5
35	0.246	8.75	66.7
40	0.234	8.33	63.4
45	0.222	7.90	60.2
50	0.212	7.54	57.5
55	0.202	7.19	54.7
60	0.193	6.87	52.3

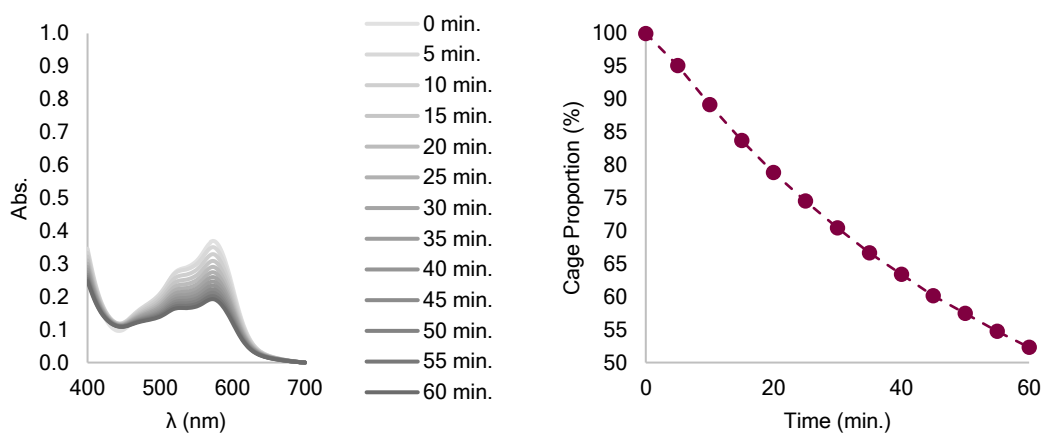
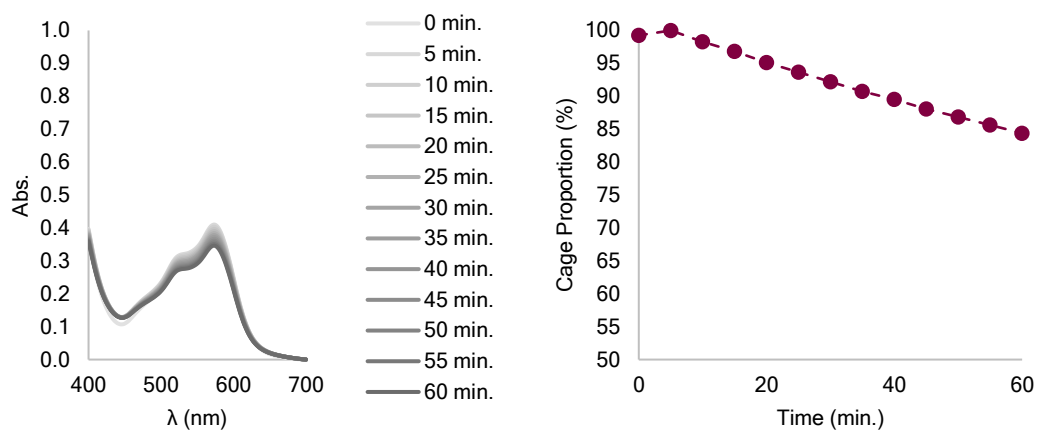
**Figure 4.46** Stability of cage **2**[BAr(CF₃)₂] in EtOAc over 60 minutes.

Table 4.14 Summary of UV-Vis data for stability of 2[BArF₅] in EtOAc

Time (min):	Abs at λ_{573} :	Conc (μM):	Cage Proportion (%):
0	0.407	14.5	99.3
5	0.410	14.6	100
10	0.403	14.3	98.3
15	0.397	14.1	96.8
20	0.390	13.9	95.1
25	0.384	13.7	93.7
30	0.378	13.5	92.2
35	0.372	13.2	90.7
40	0.367	13.1	89.5
45	0.361	12.8	88.0
50	0.356	12.7	86.8
55	0.351	12.5	85.6
60	0.346	12.3	84.4

**Figure 4.47** Stability of cage 2[BArF₅] in EtOAc over 60 minutes.

*Stability of cage 3***Table 4.15** Summary of UV-Vis data for stability of 3[SO₄] in water

Time (min):	Abs at λ_{555} :	Conc (μM):	Cage Proportion (%):
0	0.560	19.6	100
5	0.560	19.6	100
10	0.559	19.6	99.8
15	0.558	19.6	99.6
20	0.558	19.6	99.6
25	0.558	19.6	99.6
30	0.558	19.6	99.6
35	0.558	19.6	99.6
40	0.558	19.6	99.6
45	0.557	19.5	99.5
50	0.557	19.5	99.5
55	0.557	19.5	99.5
60	0.557	19.5	99.5

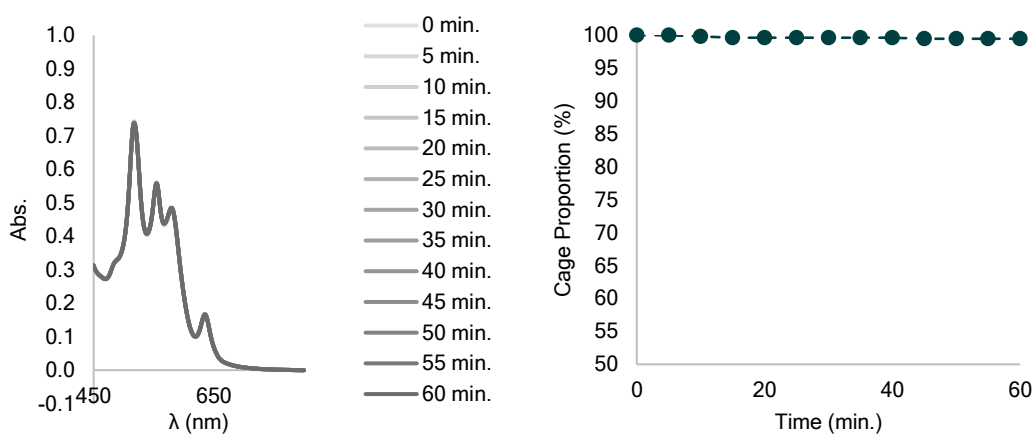
**Figure 4.48** Stability of cage 3[SO₄] in water over 60 minutes.

Table 4.16 Summary of UV-Vis data for stability of 3[BAr(CF₃)₂] in EtOAc

Time (min):	Abs at λ_{551} :	Conc (μM):	Cage Proportion (%):
0	0.646	4.66	100.0
5	0.625	4.51	96.7
10	0.621	4.48	96.1
15	0.617	4.45	95.5
20	0.612	4.42	94.7
25	0.608	4.39	94.1
30	0.603	4.35	93.3
35	0.599	4.32	92.7
40	0.594	4.29	92.0
45	0.589	4.25	91.2
50	0.583	4.21	90.2
55	0.575	4.15	89.0
60	0.568	4.10	87.9

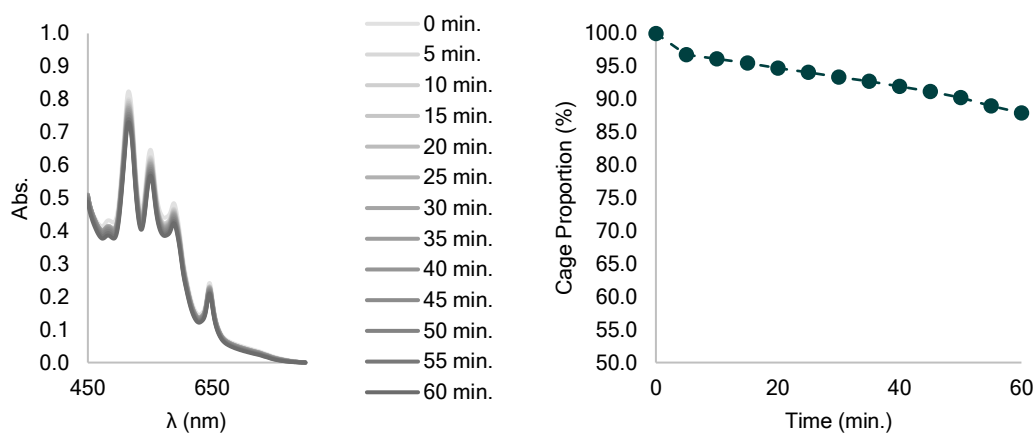
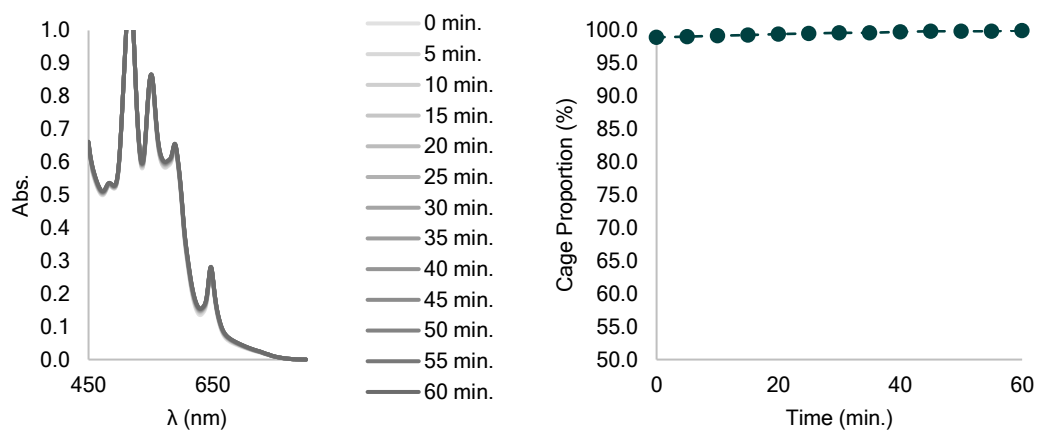
**Figure 4.49** Stability of cage 3[BAr(CF₃)₂] in EtOAc over 60 minutes.

Table 4.17 Summary of UV-Vis data for stability of 3[BArF₅] in EtOAc

Time (min):	Abs at λ_{551} :	Conc (μM):	Cage Proportion (%):
0	0.858	6.19	99.0
5	0.859	6.20	99.1
10	0.860	6.20	99.2
15	0.861	6.21	99.3
20	0.862	6.22	99.4
25	0.863	6.23	99.5
30	0.864	6.23	99.7
35	0.864	6.23	99.7
40	0.865	6.24	99.8
45	0.866	6.25	99.9
50	0.866	6.25	99.9
55	0.866	6.25	99.9
60	0.867	6.26	100

**Figure 4.50** Stability of cage 3[BArF₅] in EtOAc over 60 minutes.

4.4.5 Anion titrations

Phase transfer: $\mathbf{1}[\text{SO}_4] \rightleftharpoons \mathbf{1}[\text{BAr}(\text{CF}_3)_2]$

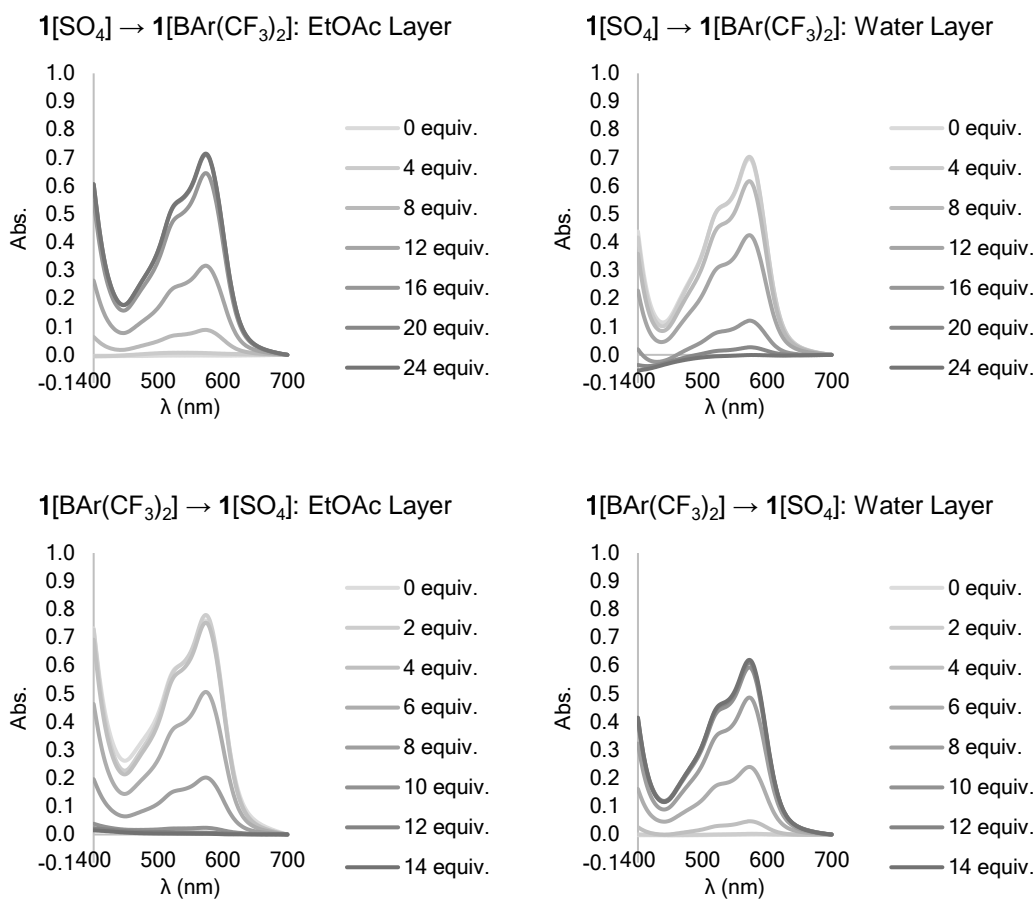


Figure 4.51 Raw UV-Vis spectrophotometry data from the EtOAc and water layers during the transformations $\mathbf{1}[\text{SO}_4] \rightarrow \mathbf{1}[\text{BAr}(\text{CF}_3)_2]$ and $\mathbf{1}[\text{BAr}(\text{CF}_3)_2] \rightarrow \mathbf{1}[\text{SO}_4]$.

Table 4.18 Summary of UV-Vis data for $1[\text{SO}_4] \rightarrow 1[\text{BAr}(\text{CF}_3)_2]$

Layer:	Anion Equiv:	Abs (H_2O , λ_{572}) (EtOAc, λ_{574}):	Conc. (μM):	Dilution Factor:	Corrected Conc. (μM):	Cage Proportion (%):
EtOAc	0	-2.56×10^{-3}	-0.0958	3.75	-0.0898	-0.327
EtOAc	4	6.41×10^{-3}	0.240	3.81	0.229	0.832
EtOAc	8	8.87×10^{-2}	3.32	3.87	3.21	11.7
EtOAc	12	3.17×10^{-1}	11.9	3.93	11.7	42.4
EtOAc	16	6.45×10^{-1}	24.2	3.99	24.1	87.7
EtOAc	20	7.10×10^{-1}	26.6	4.05	26.9	97.9
EtOAc	24	7.15×10^{-1}	26.8	4.11	27.5	100
H_2O	0	7.03×10^{-1}	27.8	4.25	29.5	100
H_2O	4	6.97×10^{-1}	27.5	4.25	29.3	99.1
H_2O	8	6.17×10^{-1}	24.4	4.25	25.9	87.7
H_2O	12	4.25×10^{-1}	16.8	4.25	17.8	60.4
H_2O	16	1.21×10^{-1}	4.80	4.25	5.10	17.3
H_2O	20	2.69×10^{-2}	1.06	4.25	1.13	3.82
H_2O	24	-7.41×10^{-4}	-0.0293	4.25	-0.0311	-0.105

Table 4.19 Constants for fitted logistic curves

Layer:	d :	L :	r :	t_m :	R^2 :
EtOAc	-0.121	101	0.501	12.5	0.994
H_2O	-0.0752	99.9	-0.460	12.8	0.988

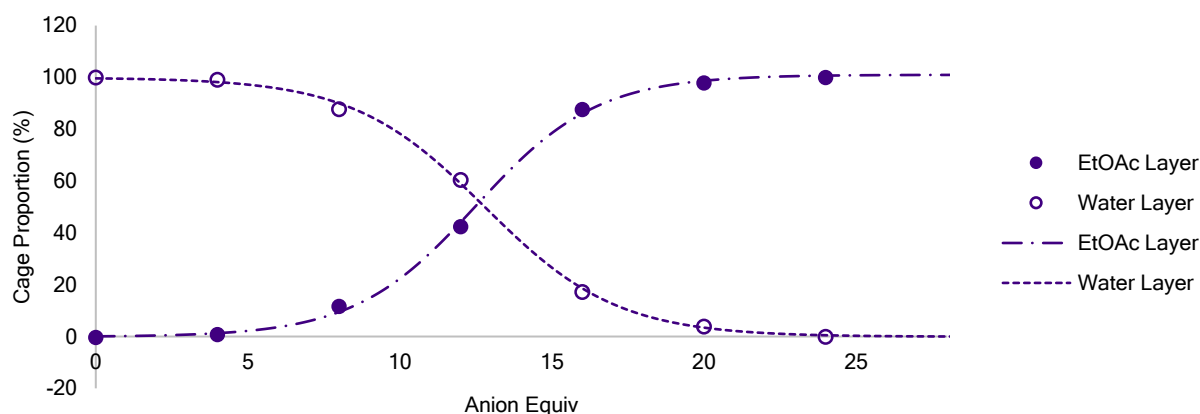
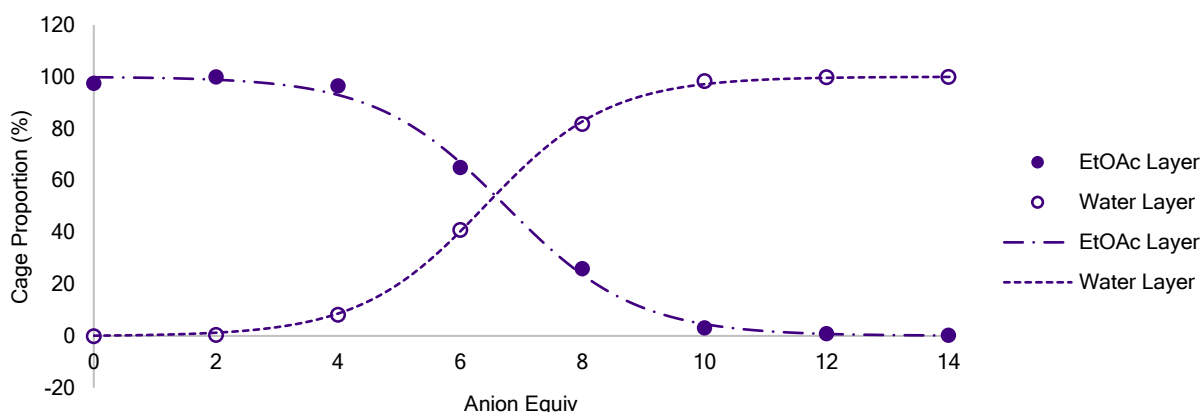
**Figure 4.52** Phase transfer of cage **1** from water to EtOAc upon anion exchange ($1[\text{SO}_4] \rightarrow 1[\text{BAr}(\text{CF}_3)_2]$). The intersection of the two fitted curves is at 13 anion equiv; 25 anion equiv were thus required for complete transport.

Table 4.20 Summary of UV-Vis data for $1[\text{BAr}(\text{CF}_3)_2] \rightarrow 1[\text{SO}_4]$

Layer:	Anion Equiv:	Abs (H_2O , λ_{572}) (EtOAc, λ_{574}):	Conc. (μM):	Dilution Factor:	Corrected Conc. (μM):	Cage Proportion (%):
EtOAc	0	7.60×10^{-1}	28.5	3.75	26.7	97.5
EtOAc	2	7.80×10^{-1}	29.2	3.75	27.4	100
EtOAc	4	7.52×10^{-1}	28.2	3.75	26.4	96.5
EtOAc	6	5.06×10^{-1}	19.0	3.75	17.8	64.9
EtOAc	8	2.02×10^{-1}	7.58	3.75	7.11	26.0
EtOAc	10	2.39×10^{-2}	0.894	3.75	0.838	3.06
EtOAc	12	6.52×10^{-3}	0.244	3.75	0.229	0.836
EtOAc	14	2.43×10^{-3}	0.0912	3.75	0.0855	0.312
H_2O	0	-5.69×10^{-4}	-0.0225	4.67	-0.0263	-0.101
H_2O	2	2.48×10^{-3}	0.0982	4.61	0.113	0.434
H_2O	4	4.71×10^{-2}	1.86	4.55	2.12	8.13
H_2O	6	2.40×10^{-1}	9.48	4.49	10.6	40.9
H_2O	8	4.86×10^{-1}	19.2	4.43	21.3	81.8
H_2O	10	5.93×10^{-1}	23.5	4.37	25.6	98.4
H_2O	12	6.10×10^{-1}	24.1	4.31	26.0	99.8
H_2O	14	6.20×10^{-1}	24.5	4.25	26.0	100

Table 4.21 Constants for fitted logistic curves

Layer:	a :	L :	r :	t_m :	R^2 :
EtOAc	0.0511	100	-0.939	6.75	0.997
H_2O	-0.0940	100	0.979	6.40	0.995

**Figure 4.53** Phase transfer of cage **1** from EtOAc to water upon anion exchange ($1[\text{BAr}(\text{CF}_3)_2] \rightarrow 1[\text{SO}_4]$). The intersection of the two fitted curves is at 6.6 anion equiv; 13 anion equiv were thus required for complete transport.

Phase transfer: $1[SO_4] \rightleftharpoons 1[BArF_5]$

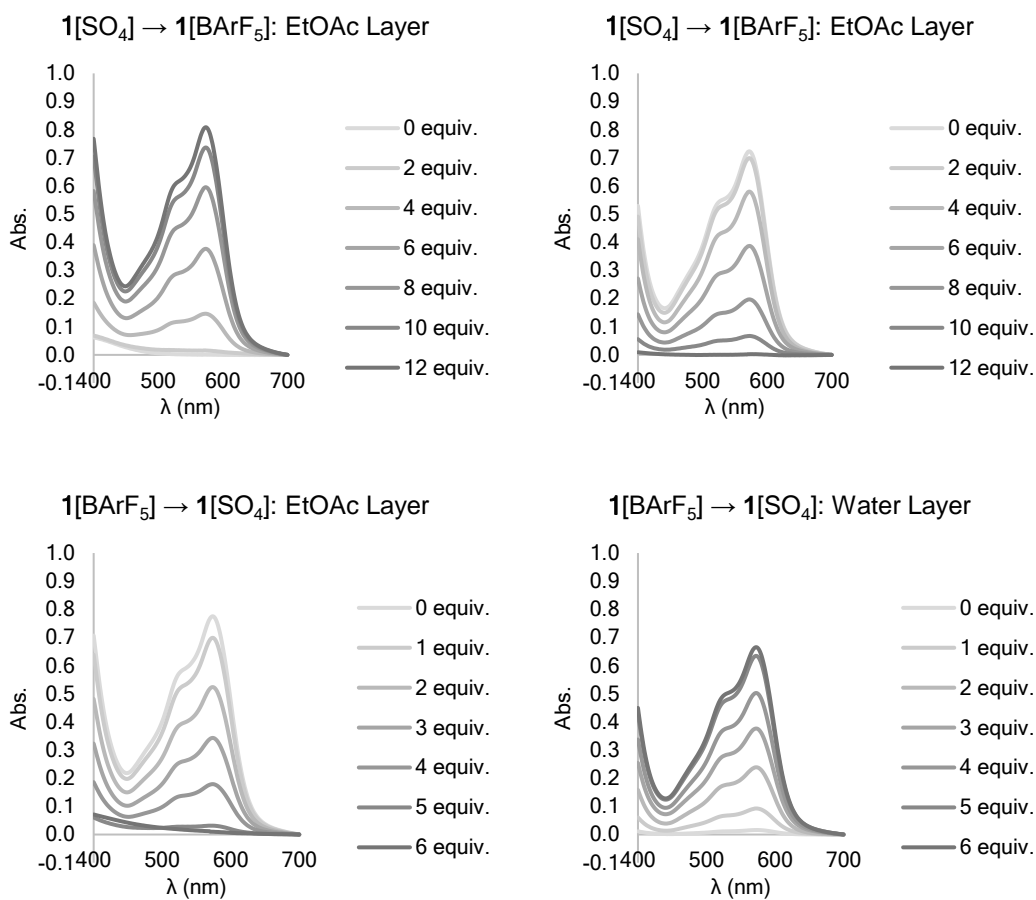


Figure 4.54 Raw UV-Vis spectrophotometry data from the EtOAc and water layers during the transformations $1[SO_4] \rightarrow 1[BArF_5]$ and $1[BArF_5] \rightarrow 1[SO_4]$.

Table 4.22 Summary of UV-Vis data for $1[\text{SO}_4] \rightarrow 1[\text{BArF}_5]$

Layer:	Anion Equiv:	Abs (H_2O , λ_{572}) (EtOAc, λ_{574}):	Conc. (μM):	Dilution Factor:	Corrected Conc. (μM):	Cage Proportion (%):
EtOAc	0	9.03×10^{-4}	0.0338	3.75	0.0317	0.112
EtOAc	2	1.56×10^{-2}	0.585	3.75	0.548	1.93
EtOAc	4	1.46×10^{-1}	5.47	3.75	5.13	18.1
EtOAc	6	3.77×10^{-1}	14.1	3.75	13.2	46.6
EtOAc	8	5.95×10^{-1}	22.3	3.75	20.9	73.6
EtOAc	10	7.37×10^{-1}	27.6	3.75	25.9	91.1
EtOAc	12	8.09×10^{-1}	30.3	3.75	28.4	100
H_2O	0	7.23×10^{-1}	28.6	4.25	30.4	100
H_2O	2	6.99×10^{-1}	27.6	4.25	29.3	96.7
H_2O	4	5.80×10^{-1}	22.9	4.25	24.3	80.2
H_2O	6	3.87×10^{-1}	15.3	4.25	16.2	53.5
H_2O	8	1.97×10^{-1}	7.79	4.25	8.27	27.3
H_2O	10	6.71×10^{-2}	2.65	4.25	2.82	9.29
H_2O	12	2.23×10^{-3}	0.0880	4.25	0.0935	0.308

Table 4.23 Constants for fitted logistic curves

Layer:	a :	L :	r :	t_m :	R^2 :
EtOAc	0.0374	101	0.651	6.36	0.967
H_2O	0.0146	100	-0.635	6.31	0.956

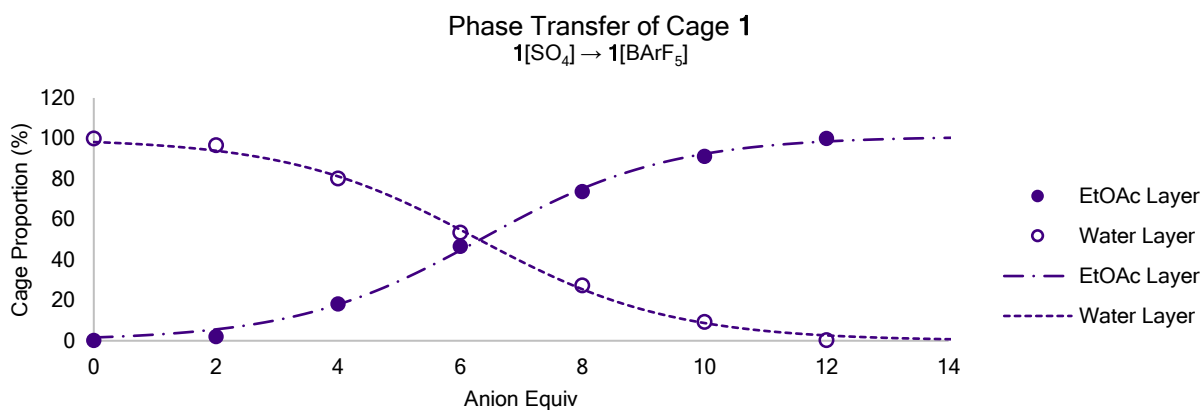
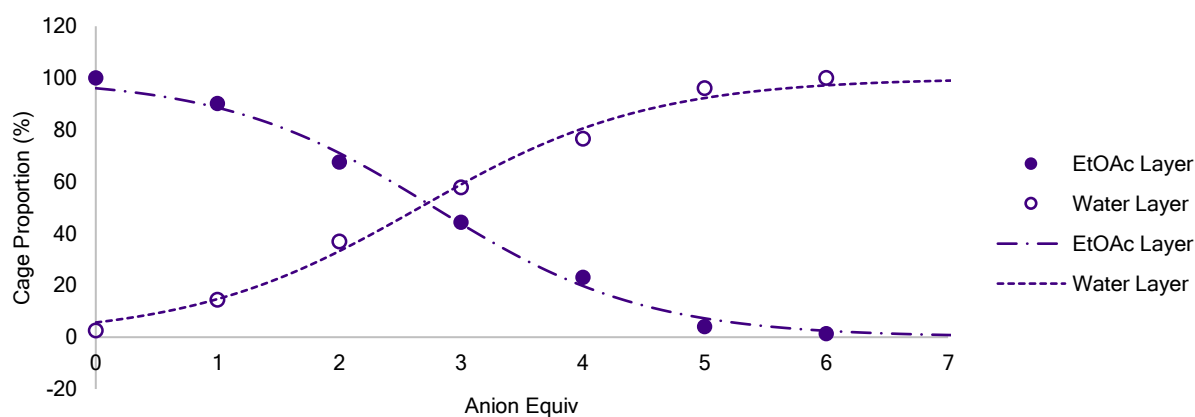
**Figure 4.55** Phase transfer of cage 1 from water to EtOAc upon anion exchange ($1[\text{SO}_4] \rightarrow 1[\text{BArF}_5]$). The intersection of the two fitted curves is at 6.3 anion equiv; 13 anion equiv were thus required for complete transport.

Table 4.24 Summary of UV-Vis data for $1[\text{BARF}_5] \rightarrow 1[\text{SO}_4]$

Layer:	Anion Equiv:	Abs (H_2O , λ_{572}) (EtOAc, λ_{574}):	Conc. (μM):	Dilution Factor:	Corrected Conc. (μM):	Cage Proportion (%):
EtOAc	0	7.75×10^{-1}	29.0	3.75	27.2	100.0
EtOAc	1	6.99×10^{-1}	26.2	3.75	24.5	90.1
EtOAc	2	5.24×10^{-1}	19.6	3.75	18.4	67.6
EtOAc	3	3.43×10^{-1}	12.8	3.75	12.0	44.3
EtOAc	4	1.79×10^{-1}	6.70	3.75	6.28	23.1
EtOAc	5	3.14×10^{-2}	1.18	3.75	1.10	4.06
EtOAc	6	9.95×10^{-3}	0.373	3.75	0.349	1.28
H_2O	0	1.61×10^{-2}	0.634	4.46	0.707	2.51
H_2O	1	9.26×10^{-2}	3.66	4.43	4.05	14.4
H_2O	2	2.39×10^{-1}	9.44	4.4	10.4	36.9
H_2O	3	3.76×10^{-1}	14.9	4.37	16.3	57.8
H_2O	4	5.03×10^{-1}	19.9	4.34	21.6	76.6
H_2O	5	6.34×10^{-1}	25.1	4.31	27.0	96.0
H_2O	6	6.65×10^{-1}	26.3	4.28	28.1	100.0

Table 4.25 Constants for fitted logistic curves

Layer:	d :	L :	r :	t_m :	R^2 :
EtOAc	0.0656	100	-1.15	2.78	0.989
H_2O	0.0486	100	1.06	2.66	0.979

**Figure 4.56** Phase transfer of cage **1** from EtOAc to water upon anion exchange ($1[\text{BARF}_5] \rightarrow 1[\text{SO}_4]$). The intersection of the two fitted curves is at 2.7 anion equiv; 5.4 anion equiv were thus required for complete transport.

Phase transfer: $2[SO_4] \rightleftharpoons 2[BAr(CF_3)_2]$

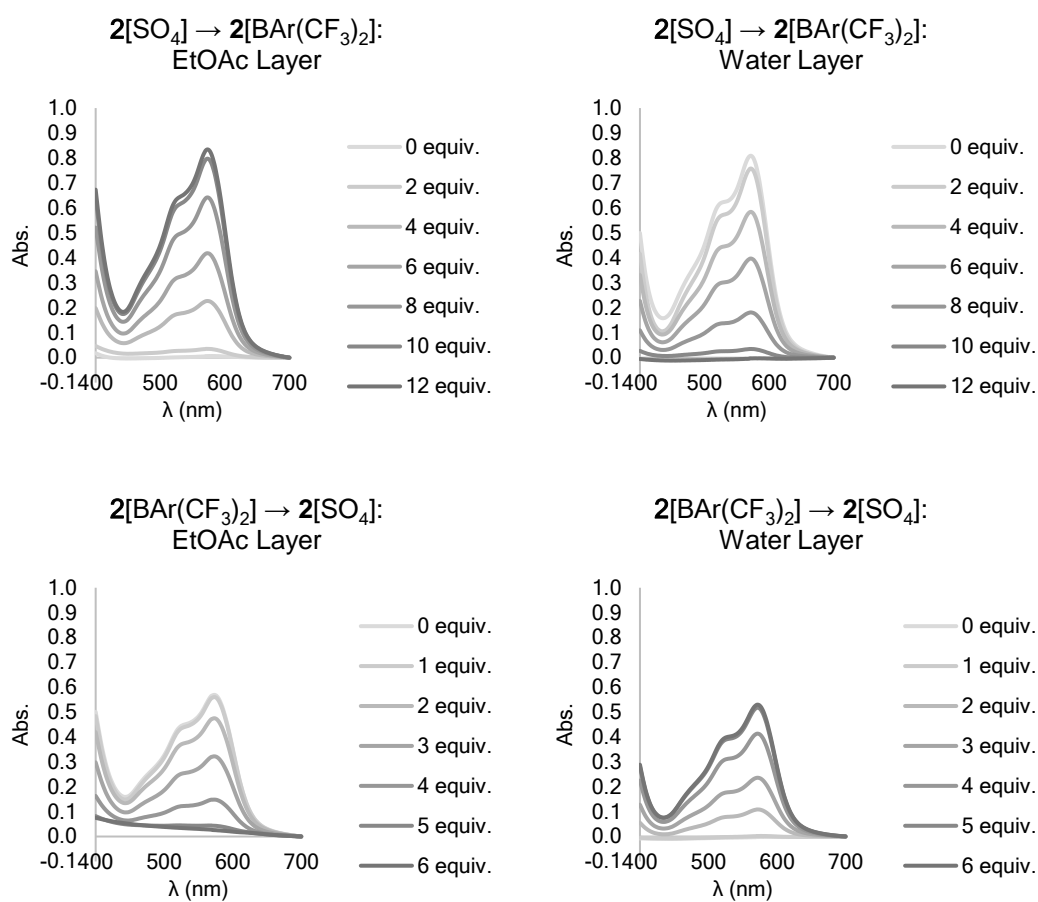


Figure 4.57 Raw UV-Vis spectrophotometry data from the EtOAc and water layers during the transformations $2[SO_4] \rightarrow 2[BAr(CF_3)_2]$ and $2[BAr(CF_3)_2] \rightarrow 2[SO_4]$.

Table 4.26 Summary of UV-Vis data for $2[\text{SO}_4] \rightarrow 2[\text{BAr}(\text{CF}_3)_2]$

Layer:	Anion Equiv:	Abs (H_2O , λ_{571}) (EtOAc, λ_{573}):	Conc. (μM):	Dilution Factor:	Corrected Conc. (μM):	Cage Proportion (%):
EtOAc	0	6.42×10^{-3}	0.228	3.75	0.214	0.769
EtOAc	2	3.51×10^{-2}	1.25	3.75	1.17	4.21
EtOAc	4	2.27×10^{-1}	8.08	3.75	7.57	27.2
EtOAc	6	4.18×10^{-1}	14.9	3.75	14.0	50.2
EtOAc	8	6.42×10^{-1}	22.8	3.75	21.4	77.0
EtOAc	10	7.97×10^{-1}	28.4	3.75	26.6	95.6
EtOAc	12	8.34×10^{-1}	29.7	3.75	27.8	100
H_2O	0	8.09×10^{-1}	28.4	4.25	30.2	100
H_2O	2	7.58×10^{-1}	26.6	4.25	28.2	93.7
H_2O	4	5.84×10^{-1}	20.5	4.25	21.8	72.2
H_2O	6	3.97×10^{-1}	13.9	4.25	14.8	49.1
H_2O	8	1.81×10^{-1}	6.36	4.25	6.75	22.4
H_2O	10	3.48×10^{-2}	1.22	4.25	1.30	4.30
H_2O	12	-2.79×10^{-3}	-0.0979	4.25	-0.104	-0.345

Table 4.27 Constants for fitted logistic curves

Layer:	a :	L :	r :	t_m :	R^2 :
EtOAc	0.0677	101	0.622	5.96	0.991
H_2O	-0.316	100	-0.621	5.85	0.990

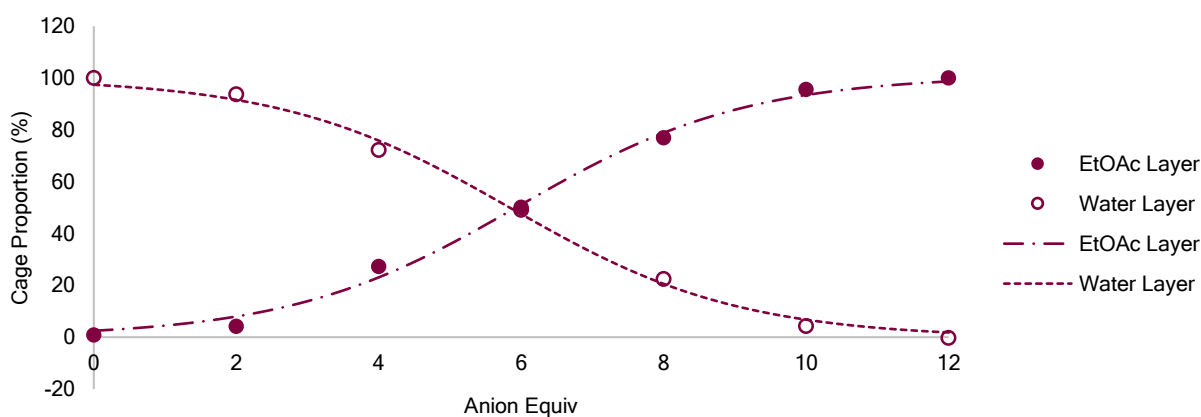
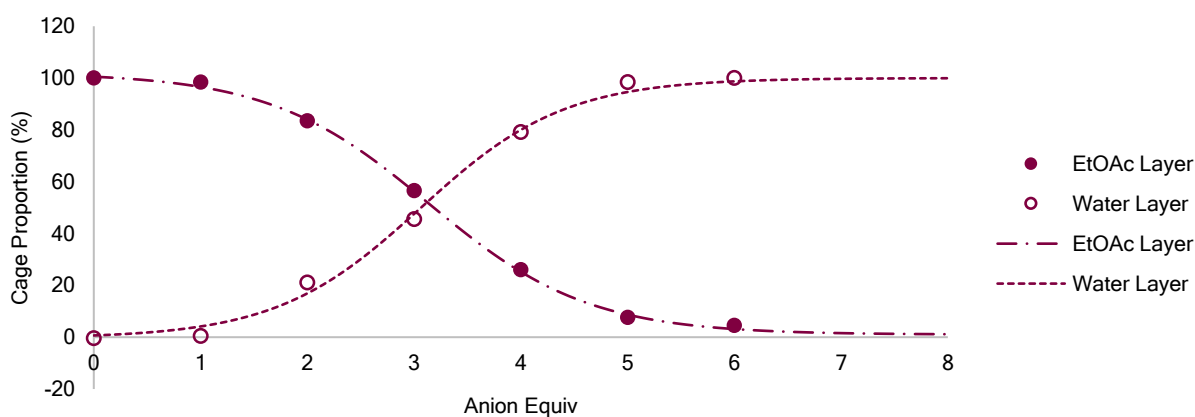
**Figure 4.58** Phase transfer of cage **2** from water to EtOAc upon anion exchange ($2[\text{SO}_4] \rightarrow 2[\text{BAr}(\text{CF}_3)_2]$). The intersection of the two fitted curves is at 5.9 anion equiv; 12 anion equiv were thus required for complete transport.

Table 4.28 Summary of UV-Vis data for $2[\text{BAr}(\text{CF}_3)_2] \rightarrow 2[\text{SO}_4]$

Layer:	Anion Equiv:	Abs (H_2O , λ_{571}) (EtOAc, λ_{573}):	Conc. (μM):	Dilution Factor:	Corrected Conc. (μM):	Cage Proportion (%):
EtOAc	0	5.69×10^{-1}	20.3	3.75	19.0	100.0
EtOAc	1	5.60×10^{-1}	19.9	3.75	18.7	98.4
EtOAc	2	4.75×10^{-1}	16.9	3.75	15.9	83.5
EtOAc	3	3.22×10^{-1}	11.5	3.75	10.8	56.6
EtOAc	4	1.48×10^{-1}	5.28	3.75	4.95	26.0
EtOAc	5	4.32×10^{-2}	1.54	3.75	1.44	7.59
EtOAc	6	2.58×10^{-2}	0.918	3.75	0.861	4.53
H_2O	0	-2.04×10^{-3}	-0.0717	4.46	-0.0800	-0.402
H_2O	1	2.11×10^{-3}	0.0740	4.43	0.0819	0.412
H_2O	2	1.09×10^{-1}	3.82	4.4	4.20	21.1
H_2O	3	2.36×10^{-1}	8.29	4.37	9.05	45.5
H_2O	4	4.13×10^{-1}	14.5	4.34	15.7	79.1
H_2O	5	5.18×10^{-1}	18.2	4.31	19.6	98.4
H_2O	6	5.30×10^{-1}	18.6	4.28	19.9	100

Table 4.29 Constants for fitted logistic curves

Layer:	d :	L :	r :	t_m :	R^2 :
EtOAc	1.00	102	-1.34	3.14	0.989
H_2O	-0.400	100	1.48	3.06	0.966

**Figure 4.59** Phase transfer of cage **2** from EtOAc to water upon anion exchange ($2[\text{BAr}(\text{CF}_3)_2] \rightarrow 2[\text{SO}_4]$). The intersection of the two fitted curves is at 3.1 anion equiv; 6.2 anion equiv were thus required for complete transport.

Phase transfer: $2[\text{SO}_4] \rightleftharpoons 2[\text{BArF}_5]$

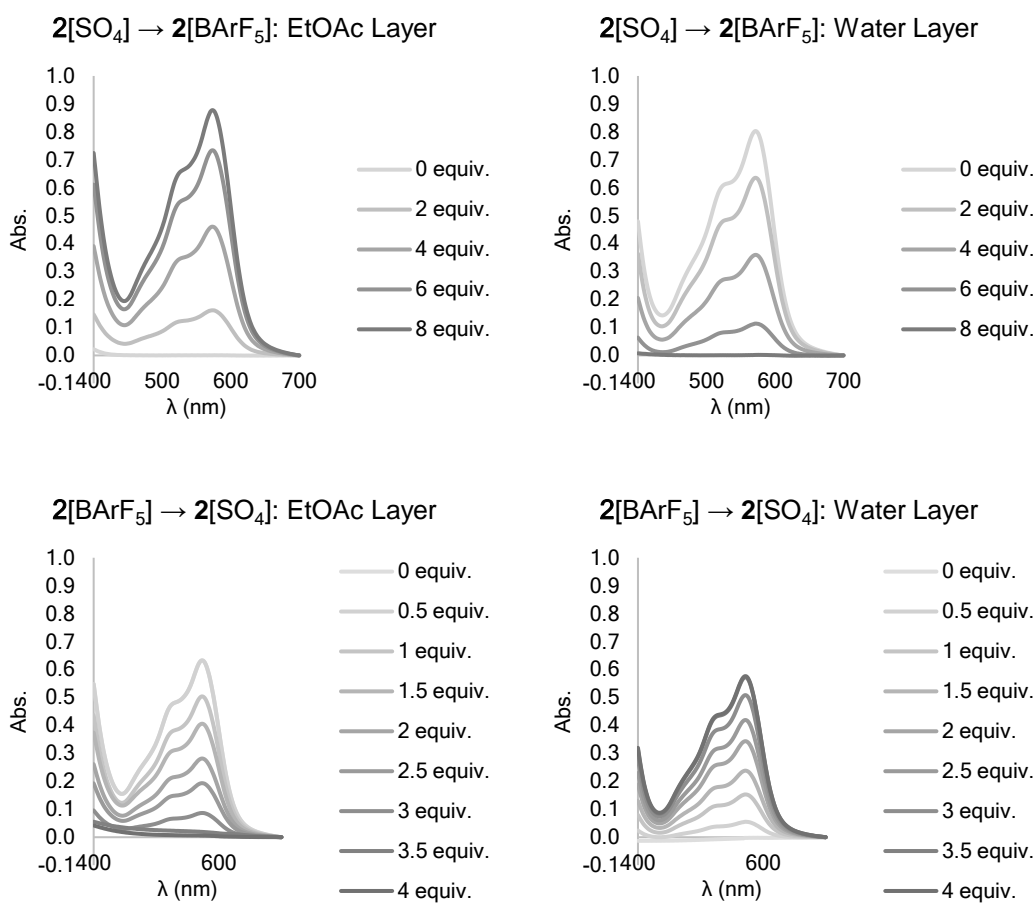


Figure 4.60 Raw UV-Vis spectrophotometry data from the EtOAc and water layers during the transformations $2[\text{SO}_4] \rightarrow 2[\text{BArF}_5]$ and $2[\text{BArF}_5] \rightarrow 2[\text{SO}_4]$.

Table 4.30 Summary of UV-Vis data for $2[\text{SO}_4] \rightarrow 2[\text{BArF}_5]$

Layer:	Anion Equiv:	Abs (H_2O , λ_{571}) (EtOAc, λ_{573}):	Conc. (μM):	Dilution Factor:	Corrected Conc. (μM):	Cage Proportion (%):
EtOAc	0	4.19×10^{-4}	0.0149	3.75	0.0140	0.0478
EtOAc	2	1.61×10^{-1}	5.74	3.75	5.39	18.4
EtOAc	4	4.61×10^{-1}	16.4	3.75	15.4	52.5
EtOAc	6	7.34×10^{-1}	26.1	3.75	24.5	83.6
EtOAc	8	8.77×10^{-1}	31.2	3.75	29.3	100
H_2O	0	8.03×10^{-1}	28.2	4.25	29.9	100
H_2O	2	6.35×10^{-1}	22.3	4.25	23.7	79.2
H_2O	4	3.60×10^{-1}	12.6	4.25	13.4	44.8
H_2O	6	1.14×10^{-1}	3.99	4.25	4.24	14.2
H_2O	8	1.75×10^{-3}	0.0615	4.25	0.0653	0.218

Table 4.31 Constants for fitted logistic curves

Layer:	a :	L :	r :	t_m :	R^2 :
EtOAc	0.00682	101	0.825	3.93	0.915
H_2O	0.0159	100	-0.843	3.74	0.924

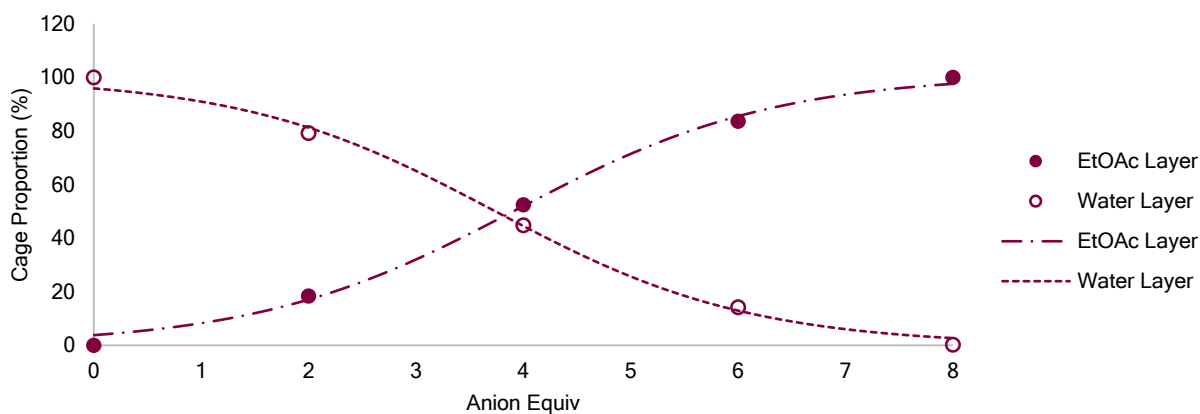
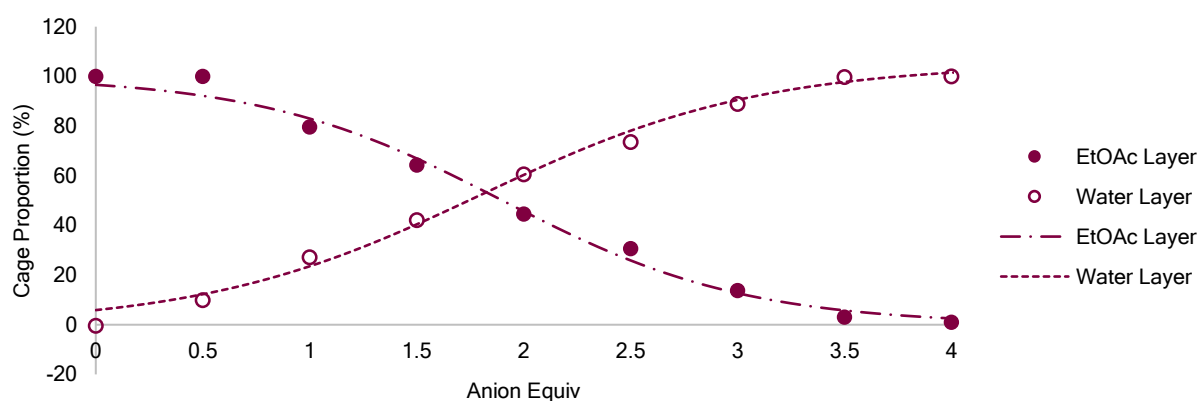
**Figure 4.61** Phase transfer of cage 2 from water to EtOAc upon anion exchange ($2[\text{SO}_4] \rightarrow 2[\text{BArF}_5]$). The intersection of the two fitted curves is at 3.8 anion equiv; 7.6 anion equiv were thus required for complete transport.

Table 4.32 Summary of UV-Vis data for $2[\text{BARF}_5] \rightarrow 2[\text{SO}_4]$

Layer:	Anion Equiv:	Abs (H ₂ O, λ_{571}) (EtOAc, λ_{573}):	Conc. (μM):	Dilution Factor:	Corrected Conc. (μM):	Cage Proportion (%):
EtOAc	0	6.33×10^{-1}	22.5	3.75	21.1	100
EtOAc	0.5	6.33×10^{-1}	22.5	3.75	21.1	100
EtOAc	1	5.04×10^{-1}	17.9	3.75	16.8	79.6
EtOAc	1.5	4.06×10^{-1}	14.4	3.75	13.5	64.2
EtOAc	2	2.82×10^{-1}	10.0	3.75	9.39	44.5
EtOAc	2.5	1.93×10^{-1}	6.88	3.75	6.45	30.6
EtOAc	3	8.67×10^{-2}	3.08	3.75	2.89	13.7
EtOAc	3.5	1.90×10^{-2}	0.677	3.75	0.635	3.01
EtOAc	4	5.88×10^{-3}	0.209	3.75	0.196	0.930
H ₂ O	0	-2.46×10^{-3}	-0.0865	4.37	-0.0945	-0.440
H ₂ O	0.5	5.53×10^{-2}	1.94	4.355	2.11	9.83
H ₂ O	1	1.53×10^{-1}	5.37	4.34	5.83	27.1
H ₂ O	1.5	2.38×10^{-1}	8.36	4.325	9.03	42.1
H ₂ O	2	3.43×10^{-1}	12.1	4.31	13.0	60.4
H ₂ O	2.5	4.19×10^{-1}	14.7	4.295	15.8	73.5
H ₂ O	3	5.08×10^{-1}	17.8	4.28	19.1	88.8
H ₂ O	3.5	5.72×10^{-1}	20.1	4.265	21.4	99.7
H ₂ O	4	5.76×10^{-1}	20.2	4.25	21.5	100

Table 4.33 Constants for fitted logistic curves

Layer:	d :	L :	r :	t_m :	R^2 :
EtOAc	0.123	100	-1.76	1.90	0.971
H ₂ O	-0.421	105	1.53	1.80	0.984

**Figure 4.62** Phase transfer of cage **2** from EtOAc to water upon anion exchange ($2[\text{BARF}_5] \rightarrow 2[\text{SO}_4]$). The intersection of the two fitted curves is at 1.8 anion equiv; 3.6 anion equiv were thus required for complete transport.

Phase transfer: $3[\text{SO}_4] \rightleftharpoons 3[\text{BAr}(\text{CF}_3)_2]$

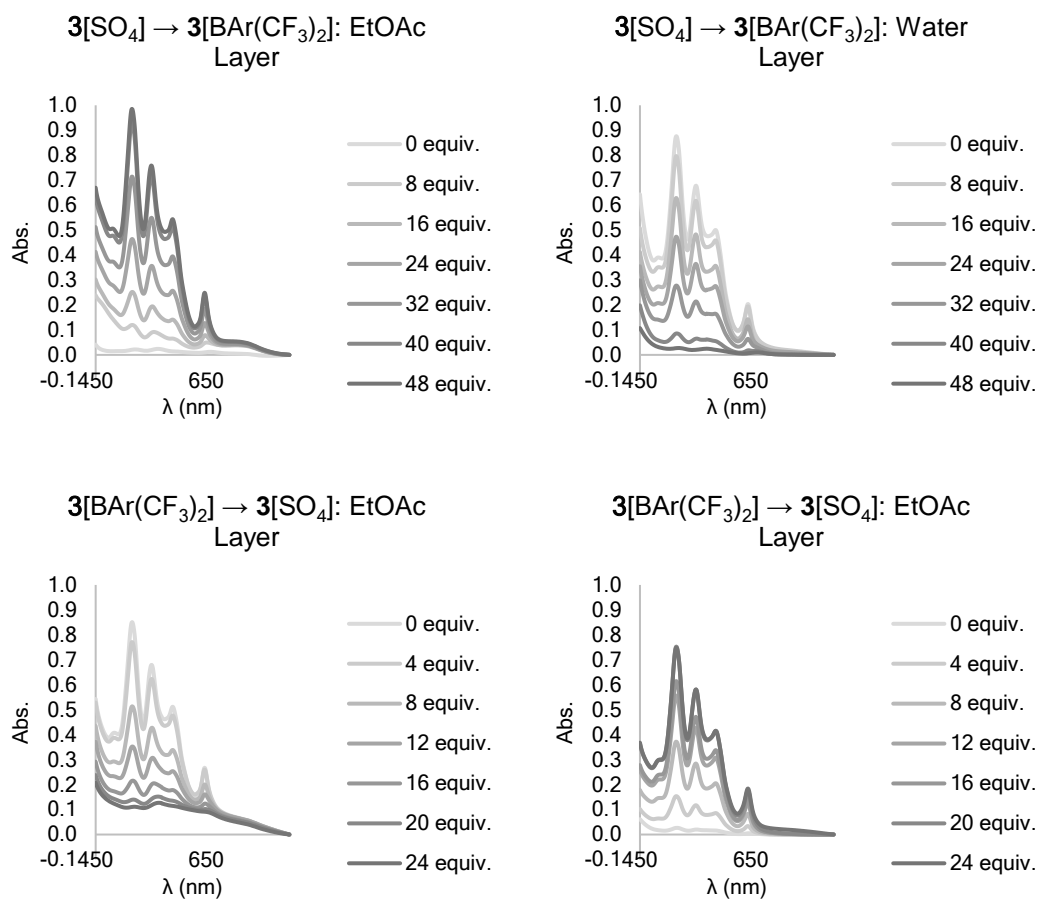


Figure 4.63 Raw UV-Vis spectrophotometry data from the EtOAc and water layers during the transformations $3[\text{SO}_4] \rightarrow 3[\text{BAr}(\text{CF}_3)_2]$ and $3[\text{BAr}(\text{CF}_3)_2] \rightarrow 3[\text{SO}_4]$.

Table 4.34 Summary of UV-Vis data for $3[\text{SO}_4] \rightarrow 3[\text{BAr}(\text{CF}_3)_2]$

Layer:	Anion Equiv:	Abs (H_2O , λ_{555}) (EtOAc, λ_{551}):	Conc. (μM):	Dilution Factor:	Corrected Conc. (μM):	Cage Proportion (%):
EtOAc	0	1.96×10^{-2}	0.141	3.75	0.133	2.58
EtOAc	8	8.88×10^{-2}	0.641	3.75	0.601	11.7
EtOAc	16	1.93×10^{-1}	1.40	3.75	1.31	25.5
EtOAc	24	3.57×10^{-1}	2.57	3.75	2.41	47.0
EtOAc	32	5.49×10^{-1}	3.96	3.75	3.72	72.4
EtOAc	40	7.17×10^{-1}	5.17	3.75	4.85	94.5
EtOAc	48	7.58×10^{-1}	5.47	3.75	5.13	100
H_2O	0	6.78×10^{-1}	5.11	4.25	5.43	100
H_2O	8	6.18×10^{-1}	4.66	4.25	4.95	91.1
H_2O	16	4.83×10^{-1}	3.64	4.25	3.87	71.2
H_2O	24	3.65×10^{-1}	2.75	4.25	2.92	53.8
H_2O	32	2.14×10^{-1}	1.61	4.25	1.71	31.6
H_2O	40	6.47×10^{-2}	0.488	4.25	0.519	9.55
H_2O	48	2.04×10^{-2}	0.153	4.25	0.163	3.00

Table 4.35 Constants for fitted logistic curves

Layer:	d :	L :	r :	t_m :	R^2 :
EtOAc	-0.313	108	0.123	25.8.5	0.992
H_2O	0.0673	100	-0.130	24.8	0.991

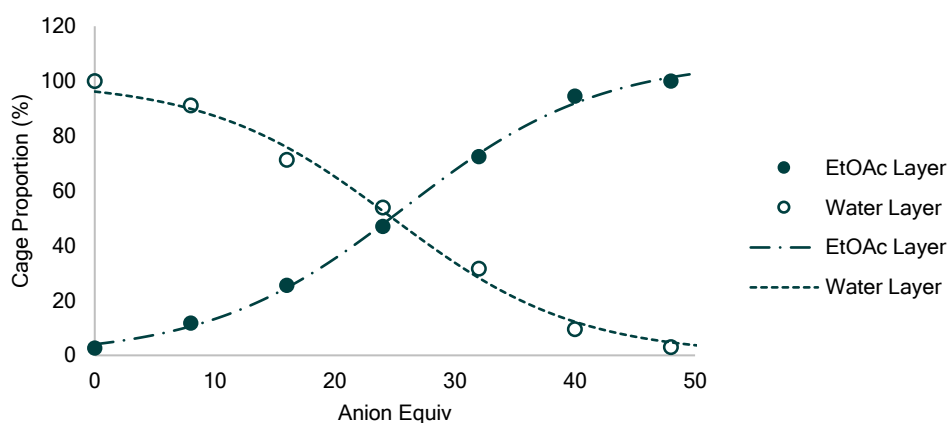
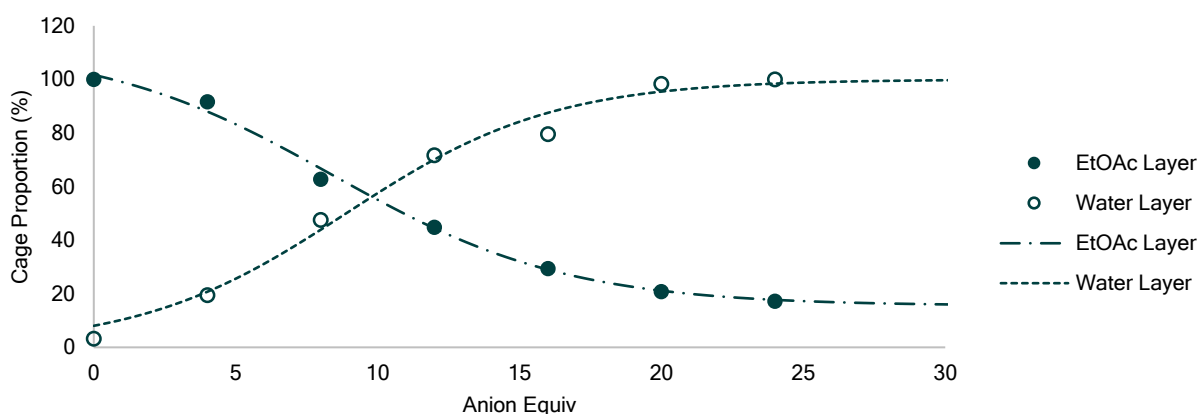
**Figure 4.64** Phase transfer of cage **3** from water to EtOAc upon anion exchange ($3[\text{SO}_4] \rightarrow 3[\text{BAr}(\text{CF}_3)_2]$). The intersection of the two fitted curves is at 25 anion equiv; 49 anion equiv were thus required for complete transport.

Table 4.36 Summary of UV-Vis data for $3[\text{BAr}(\text{CF}_3)_2] \rightarrow 3[\text{SO}_4]$

Layer:	Anion Equiv:	Abs (H_2O , λ_{555}) (EtOAc, λ_{551}):	Conc. (μM):	Dilution Factor:	Corrected Conc. (μM):	Cage Proportion (%):
EtOAc	0	6.80×10^{-1}	4.91	3.75	4.60	100.0
EtOAc	4	6.23×10^{-1}	4.50	3.75	4.22	91.7
EtOAc	8	4.27×10^{-1}	3.08	3.75	2.89	62.8
EtOAc	12	3.05×10^{-1}	2.20	3.75	2.06	44.8
EtOAc	16	2.00×10^{-1}	1.44	3.75	1.35	29.4
EtOAc	20	1.42×10^{-1}	1.02	3.75	0.96	20.9
EtOAc	24	1.18×10^{-1}	0.848	3.75	0.80	17.3
H_2O	0	1.99×10^{-2}	0.150	4.25	0.159	3.29
H_2O	4	1.17×10^{-1}	0.884	4.27	0.944	19.5
H_2O	8	2.84×10^{-1}	2.15	4.29	2.30	47.6
H_2O	12	4.27×10^{-1}	3.22	4.31	3.47	71.8
H_2O	16	4.72×10^{-1}	3.56	4.33	3.85	79.6
H_2O	20	5.80×10^{-1}	4.38	4.35	4.76	98.4
H_2O	24	5.82×10^{-1}	4.39	4.41	4.84	100.0

Table 4.37 Constants for fitted logistic curves

Layer:	d :	L :	r :	t_m :	R^2 :
EtOAc	15.5	113	-0.241	8.42	0.996
H_2O	0.00	100	0.274	8.89	0.958

**Figure 4.65** Phase transfer of cage **3** from EtOAc to water upon anion exchange ($3[\text{BAr}(\text{CF}_3)_2] \rightarrow 3[\text{SO}_4]$). The intersection of the two fitted curves is at 9.8 anion equiv; 20 anion equiv were thus required for complete transport.

Phase transfer: $3[\text{SO}_4] \rightleftharpoons 3[\text{BArF}_5]$

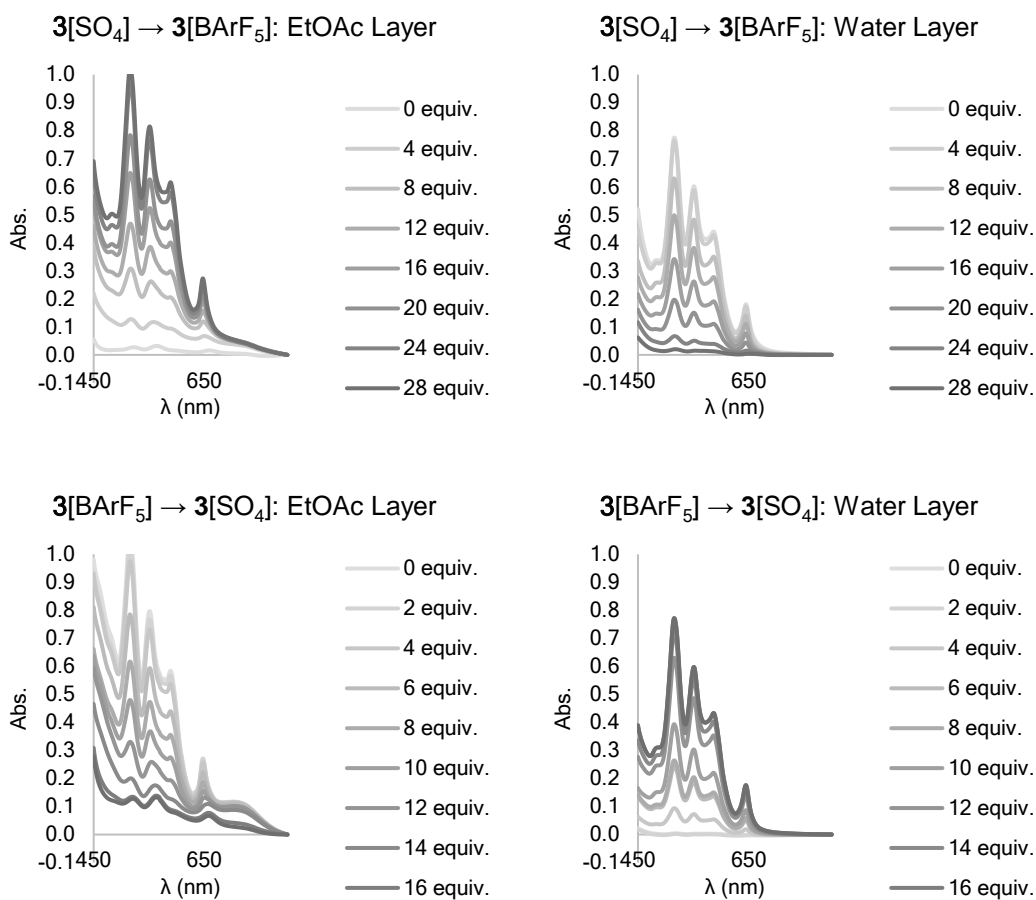


Figure 4.66 Raw UV-Vis spectrophotometry data from the EtOAc and water layers during the transformations $3[\text{SO}_4] \rightarrow 3[\text{BArF}_5]$ and $3[\text{BArF}_5] \rightarrow 3[\text{SO}_4]$.

Table 4.38 Summary of UV-Vis data for $3[\text{SO}_4] \rightarrow 3[\text{BArF}_5]$

Layer:	Anion Equiv:	Abs (H_2O , λ_{555}) (EtOAc, λ_{551}):	Conc. (μM):	Dilution Factor:	Corrected Conc. (μM):	Cage Proportion (%):
EtOAc	0	2.40×10^{-2}	0.173	3.75	0.162	2.95
EtOAc	4	1.12×10^{-1}	0.807	3.75	0.756	13.7
EtOAc	8	2.59×10^{-1}	1.87	3.75	1.75	31.8
EtOAc	12	3.84×10^{-1}	2.77	3.75	2.60	47.1
EtOAc	16	5.23×10^{-1}	3.78	3.75	3.54	64.2
EtOAc	20	6.26×10^{-1}	4.52	3.75	4.23	76.8
EtOAc	24	7.67×10^{-1}	5.53	3.75	5.19	94.1
EtOAc	28	8.15×10^{-1}	5.88	3.75	5.51	100.0
H_2O	0	6.02×10^{-1}	4.54	4.25	4.82	100.0
H_2O	4	5.88×10^{-1}	4.43	4.25	4.71	97.7
H_2O	8	4.83×10^{-1}	3.64	4.25	3.87	80.3
H_2O	12	3.82×10^{-1}	2.88	4.25	3.06	63.5
H_2O	16	2.62×10^{-1}	1.98	4.25	2.10	43.5
H_2O	20	1.50×10^{-1}	1.13	4.25	1.21	25.0
H_2O	24	5.07×10^{-2}	0.382	4.25	0.406	8.42
H_2O	28	1.48×10^{-2}	0.112	4.25	0.119	2.47

Table 4.39 Constants for fitted logistic curves

Layer:	a :	L :	r :	t_m :	R^2 :
EtOAc	-7.00	108	0.164	12.9	0.995
H_2O	0.165	105	-0.223	14.1	0.988

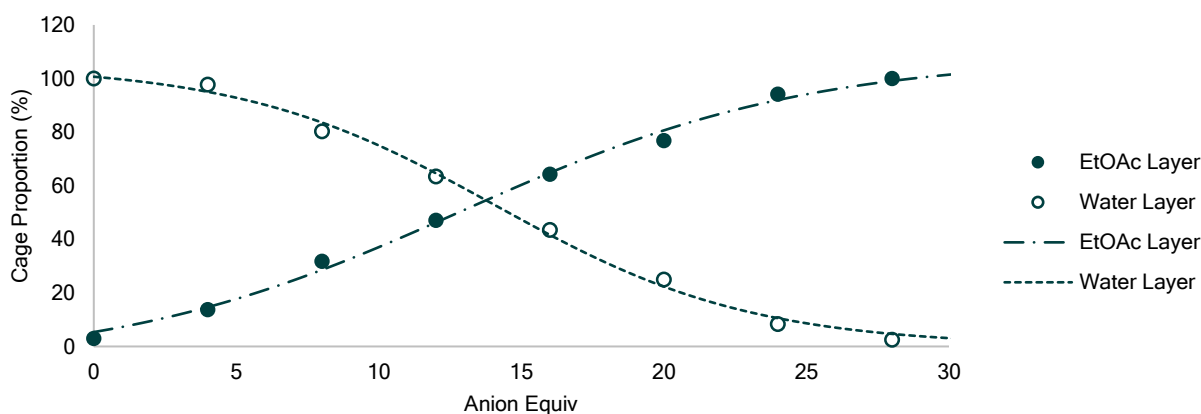
**Figure 4.67** Phase transfer of cage **3** from water to EtOAc upon anion exchange ($3[\text{SO}_4] \rightarrow 3[\text{BArF}_5]$). The intersection of the two fitted curves is at 14 anion equiv; 28 anion equiv were thus required for complete transport.

Table 4.40 Summary of UV-Vis data for $3[\text{BARF}_5] \rightarrow 3[\text{SO}_4]$

Layer:	Anion Equiv:	Abs (H_2O , λ_{555}) (EtOAc, λ_{551}):	Conc. (μM):	Dilution Factor:	Corrected Conc. (μM):	Cage Proportion (%):
EtOAc	0	7.97×10^{-1}	5.75	3.75	5.39	100.0
EtOAc	2	7.67×10^{-1}	5.53	3.75	5.19	96.2
EtOAc	4	7.31×10^{-1}	5.28	3.75	4.95	91.7
EtOAc	6	5.93×10^{-1}	4.28	3.75	4.01	74.4
EtOAc	8	4.73×10^{-1}	3.41	3.75	3.20	59.3
EtOAc	10	3.67×10^{-1}	2.65	3.75	2.48	46.0
EtOAc	12	2.54×10^{-1}	1.83	3.75	1.72	31.9
EtOAc	14	1.60×10^{-1}	1.15	3.75	1.08	20.1
EtOAc	16	1.16×10^{-1}	0.839	3.75	0.787	14.6
EtOAc	18	1.10×10^{-1}	0.797	3.75	0.747	13.9
H_2O	0	2.75×10^{-3}	0.0207	4.25	0.0220	0.451
H_2O	2	5.82×10^{-4}	0.00439	4.26	0.00467	0.0957
H_2O	4	7.27×10^{-2}	0.548	4.27	0.585	12.0
H_2O	6	1.87×10^{-1}	1.41	4.28	1.51	30.9
H_2O	8	2.05×10^{-1}	1.54	4.29	1.65	33.9
H_2O	10	3.04×10^{-1}	2.29	4.3	2.46	50.4
H_2O	12	4.87×10^{-1}	3.67	4.31	3.95	81.0
H_2O	14	5.57×10^{-1}	4.20	4.32	4.54	92.9
H_2O	16	5.98×10^{-1}	4.51	4.33	4.88	100.0
H_2O	18	5.95×10^{-1}	4.49	4.34	4.87	99.7

Table 4.41 Constants for fitted logistic curves

Layer:	α :	L :	r :	t_m :	R^2 :
EtOAc	9.71	105	-0.349	8.41	0.993
H_2O	0.0171	107	0.384	9.63	0.861

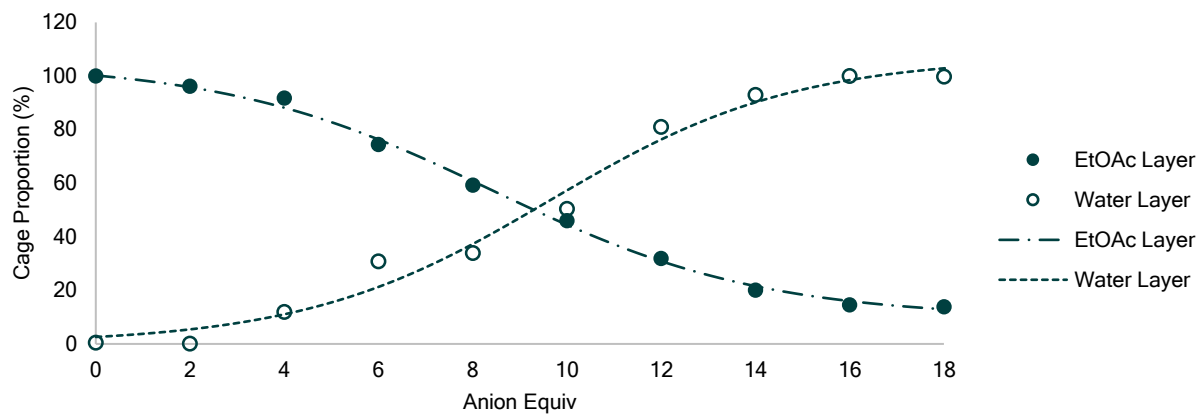


Figure 4.68 Phase transfer of cage **3** from EtOAc to water upon anion exchange ($3[\text{BARF}_5] \rightarrow 3[\text{SO}_4]$). The intersection of the two fitted curves is at 9.3 anion equiv; 19 anion equiv were thus required for complete transport.

4.5 References

- (1) Lister, F. G. A.; Le Bailly, B. A. F.; Webb, S. J.; Clayden, J. *Nat. Chem.* **2017**, *9* (5), 420.
- (2) Langton, M. J.; Keymeulen, F.; Ciaccia, M.; Williams, N. H.; Hunter, C. A. *Nat. Chem.* **2017**, *9* (5), 426.
- (3) Grommet, A. B.; Nitschke, J. R. *J. Am. Chem. Soc.* **2017**, *139*, 2176.
- (4) Bolliger, J. L.; Belenguer, A. M.; Nitschke, J. R. *Angew. Chem. Int. Ed.* **2013**, *52* (31), 7958.
- (5) Bolliger, J. L.; Ronson, T. K.; Ogawa, M.; Nitschke, J. R. *J. Am. Chem. Soc.* **2014**, *136* (41), 14545.
- (6) Percástegui, E. G.; Mosquera, J.; Nitschke, J. R. *Angew. Chem. Int. Ed.* **2017**, *56* (31), 9136.
- (7) Chifotides, H. T.; Dunbar, K. R. *Acc. Chem. Res.* **2013**, *46* (4), 894.
- (8) Yeung, M. C. L.; Chu, B. W. K.; Yam, V. W. W. *ChemistryOpen* **2014**, *3* (5), 172.
- (9) Yi, S.; Brega, V.; Captain, B.; Kaifer, A. E. *Chem. Commun.* **2012**, *48* (83), 10295.
- (10) Klein, C.; Gütz, C.; Bogner, M.; Topić, F.; Rissanen, K.; Lützen, A. *Angew. Chem. Int. Ed.* **2014**, *53* (14), 3739.
- (11) Wang, W.; Wang, Y.-X.; Yang, H.-B. *Chem. Soc. Rev.* **2016**, *45* (9), 2656.
- (12) Sommer, F.; Marcus, Y.; Kubik, S. *ACS Omega* **2017**, *2* (7), 3669.
- (13) Clever, G. H.; Punt, P. *Acc. Chem. Res.* **2017**, *50* (9), 2233.
- (14) Niklas, T.; Stalke, D.; John, M. *Chem. Commun.* **2015**, *51* (7), 1275.
- (15) Pöppler, A. C.; Frischkorn, S.; Stalke, D.; John, M. *ChemPhysChem* **2013**, *14* (13), 3103.
- (16) Holloway, L. R.; Bogie, P. M.; Hooley, R. J. *Dalt. Trans.* **2017**, *46* (43), 14719.
- (17) Young, M. C.; Holloway, L. R.; Johnson, A. M.; Hooley, R. J. *Angew. Chem. Int. Ed.* **2014**, *53* (37), 9832.
- (18) Kang, S. O.; Johnson, T. S.; Day, V. W.; Bowman-James, K. *Supramol. Chem.* **2017**, *278* (December), 1.
- (19) Chen, L.-J.; Yang, H.-B.; Shionoya, M. *Chem. Soc. Rev.* **2017**, *46* (9), 2555.
- (20) Van Craen, D.; Rath, W. H.; Huth, M.; Kemp, L.; Räuber, C.; Wollschläger, J. M.; Schalley, C. A.; Valkonen, A.; Rissanen, K.; Albrecht, M. *J. Am. Chem. Soc.* **2017**, *jacs.7b10098*.
- (21) Beaudoin, D.; Rominger, F.; Mastalerz, M. *Angew. Chem. Int. Ed.* **2017**, *56* (5), 1244.

- (22) Bhat, I. A.; Jain, R.; Siddiqui, M. M.; Saini, D. K.; Mukherjee, P. S. *Inorg. Chem.* **2017**, *56* (9), 5352.
- (23) Löffler, S.; Wuttke, A.; Zhang, B.; Holstein, J. J.; Mata, R. A.; Clever, G. H. *Chem. Commun.* **2017**, *53* (i), 11933.
- (24) Huerta, E.; Serapian, S. A.; Santos, E.; Cequier, E.; Bo, C.; de Mendoza, J. *Chem. Eur. J.* **2016**, *22* (38), 13496.
- (25) Lu, X.; Isaacs, L. *Angew. Chem. Int. Ed.* **2016**, *55* (28), 8076.
- (26) Yamashina, M.; Akita, M.; Hasegawa, T.; Hayashi, S.; Yoshizawa, M. *Sci. Adv.* **2017**, *3*, 2.
- (27) Zhang, G.; Mastalerz, M. *Chem. Soc. Rev.* **2014**, *43* (6), 1934.
- (28) Clever, G. H.; Kawamura, W.; Shionoya, M. *Inorg. Chem.* **2011**, *50* (11), 4689.
- (29) Cohen, E.; Weissman, H.; Shimoni, E.; Kaplan-Ashiri, I.; Werle, K.; Wohlleben, W.; Rybtchinski, B. *Angew. Chem. Int. Ed.* **2017**, *56* (8), 2203.
- (30) Gale, P. A.; Davis, J. T.; Quesada, R. *Chem. Soc. Rev.* **2017**, *46* (9), 2497.
- (31) Williams, N. J.; Bryanstev, V. S.; Custelcean, R.; Seipp, C. A.; Moyer, B. A. *Supramol. Chem.* **2016**, *28* (1–2), 176.
- (32) Benz, S.; Macchione, M.; Verolet, Q.; Mareda, J.; Sakai, N.; Matile, S. *J. Am. Chem. Soc.* **2016**, *138* (29), 9093.